(2)

OFFICE OF NAVAL RESEARCH

FINAL REPORT

on the Project Entitled

(Part 1)

"AMORPHOUS FAST ION CONDUCTING SYSTEMS"

and

(Part 2)

"STRUCTURE AND PROPERTIES OF MID AND FAR IR TRANSMITTING MATERIALS"

Performed Under

Grant No. N00014-84-K-0289

by

C. A. Angell

Department of Chemistry

Arizona State University

During the Period April 1984 to October 31, 1991

INDEX

Statement A per telecon Robert Nowak
ONR/Code 1113/
Arlingon,VA 22217-5000

NWW 7/30/92

"Amorphous Fast Ion Conducting Systems" (Part 1)
and
"Structure and Properties of Mid and Far IR Transmitting Materials" (Part 2)

INTRODUCTION

The research supported under contract No. N00014-84-K-0289 was commenced in 1984 with the aim of developing understanding of solid electrolyte systems, of which those selected for particular study were the fast ion-conducting glassy systems. Since work in this laboratory in this general area was already being supported by the Department of Energy, a specialization was selected for the ONR program. This specialization involved the study of mechanical manifestations of the same fast ion jumping process responsible for the fast ion conduction. At the commencement of research, very little information was available on fast ion conducting systems with respect to mechanical relaxation although considerable information was available for the classical alkali silicate and borate glasses. Our program was to utilize the rheovibron instrument already in our laboratory to study the mechanical loss in fast ion glasses over the whole temperature range from the glass transition temperature down to and beyond the region in which electrical relaxation had been earlier observed.

While this was the principal focus of research in the years 1984-1987, the program later took a new turn in order to include the study of the popular "salt-in-polymer" electrolytes which had not been investigated in our laboratory under any previous program. This seemed appropriate in view of the detailed knowledge of liquid relaxation processes developed in this group over many years under fundamental research support, coupled with the fact that the migration mechanism for ions in polymer systems is essentially liquid-like in nature. This work continued until 1989

when the study of fast ion conducting systems was discontinued by the ONR Chemistry Division.

The research effort under this contract was, however, continued under a separate program in which optical materials were the focus of interest, and this laboratory's expertise in the study of fluoride glasses was to be used to advantage. Under the new direction, we developed computer simulation methods for calculating the vibrational spectra of fluoride crystals and glasses based on expertise in computer simulation developed in this laboratory over a long period (It was, in fact, this laboratory which published the first simulation work on fluoride glasses). Under this new direction we also took up the study of some chalcogenide systems previously investigated under an ONR Physics Division grant which had been joint with Prof. S. M. Lindsay of Arizona State University to which institute the principal investigator moved in 1989. The details of the research accomplishments are summarized in the next section in which reference will be made to the published documents at appropriate points. The overall impact of this research can be measured by the number of invitations to present keynote or plenary lectures at international conferences which have resulted. These will be mentioned in the following accomplishments sections. Partly as a result of the work supported by ONR, the P.I. has been honored by being the successful nominee of the George Morey award of the American Ceramic Society Glass Division in 1990 and the Neville Mott award from the Journal of Non-Crystalline Solids in 1992.

ACCOMPLISHMENTS

1. Mechanical Relaxation and Relation to Electrical Relaxation in Fast Ion-Conducting Glasses

An earlier accomplishment under this grant was the identification of glassforming composition ranges in extremely simple molten salt mixtures, mainly those containing only alkali metal and group 1b cations and monovalent anions, e.g. AgCl-CSI. The conductivity of these systems at room temperature was the highest measured to date although the systems were actually above their glass transition temperatures under ambient temperatures. The discovery was reported in Materials Research Bulletin (see the first entry in the Bibliography following). The correlation of mechanical relaxation with electrical relaxation times in these systems was reported in Bib. No. 2, and a broader report on this type of system was made at the Lake Tahoe 7th International Conference on Solid State Ionics in 1986, see Bib. No. 3. At this conference, a plenary lecture on the subject of recent developments in fast ion-transporting glassy and polymer systems was given and acknowledged our ONR support, see Bib. No. 4. At this conference, we also described a new type of fast ion conductor based on plastic crystal principles, see Bib. No. 5. Similar acknowledgements were given for the preparation of a state of the art review invited for a workshop in Bangalore, India, in 1986, see Bib. No. 6.

The importance of the problem of correlating mechanical and electrical relaxation phenomenon was recognized by an invitation to make the subject a topic in a special issue of *Materials Chemistry and Physic* devoted to glassy fast ion conductors under the special editorship of T. Minami in 1989, see Bib. No. 7. The last experimental contribution made under this ONR-supported work was the study of the effect of

pressure on the fast ion-conduction process in silver ion-conducting systems reported in bibliography No. 8. A review was solicited by the editor of *Chemical Reviews* for a special issue dealing with the dynamics of processes in condensed matter in 1990, see Bib. No. 10.

2. Salt/Polymer Fast Ion-Conducting Systems

Our first excursion into the polymer/salt systems commenced in collaboration with Prof. L. M. Torell of Chalmers University of Technology in Sweden, when we took the concept of the decoupling index (which we had used as a figure of merit in discussion of fast ion conduction in glasses) and applied it to the case of salt/polymer systems. The essential point was the salt/polymer systems worked for a completely different reason than that underlying the success of fast ion-conducting glass systems and indeed had decoupling indexes in the opposite sense from them. This exposition became the opening article in the proceedings of the First International Conference on Polymer Electrolytes held in St. Andrews, Scotland, in 1987 and published in the *British Polymer Journal* in 1988 (see Bib. No. 11). This work was followed by a letter to *Journal of Physical Chemistry* analyzing the comparisons of salt and polymer systems in a different light and listed here as Bib. No. 12. Our final contribution in the salt/polymer arena is the paper listed as Bib. No. 13 in which a more detailed study of the conductivity and viscosity of two model salt/polymer systems was given, relating the observations to the spectroscopic ion-pairing studies performed in Prof. Torell's laboratory in Sweden. We note that though ONR support of this research was withdrawn in 1988, its continuation under D.O.E. auspices has resulted in the development of a new and unusual type of rubbery solid electrolyte which is being patented at this time.

3. Structure and Relaxation in Optical Materials

Under the final phase of this contract, research effort was diverted to the study of glassy systems suitable as infrared transmitting materials. The work consisted of two parts, one dealing with the visible-range-transparent fluoride glasses, and the other with the visibly-opaque but infrared-transparent systems based on chalcogenide mixtures. The first type of glassy system was investigated primarily by computer simulation techniques, a paper discussing "structural motifs" in zirconium fluoride-containing glasses being given by the author and student, Carol Phifer, at the Japanese 4th International Symposium on Fluoride Glasses in 1990. This work was followed by two papers, one of which gave a detailed analysis, based on experimental findings including new experimental results on certain fluoride crystals, which allowed one to systematically assess all of the structural features affecting the IR and Raman absorption frequencies in fluoride crystals and glasses. Such an analysis, which was made largely at the initiative of student Carol C. Phifer (now at Sandia Labs) was urgently necessary in order to resolve some of the misconceptions and consequent structural misinterpretations which had been made by other authors over the previous decade. A final work was the publication of a study of vibrational spectra in fluoride glasses and included an investigation of beryllium fluoride subjected to very large pressures which collapsed the structure from a tetrahedral network to an octahedrally-coordinated structure. It is presented here as Bib. No. 16.

The final phase of this work, in which the important chalcogenide glasses were subjected to experimental study and theoretical analysis using the concept of rigidity percolation due to Phillips and Thorpe, is documented by Bib. Nos. 17-20. In the first of these, it was demonstrated in a *Physical Review* Letter that the simple three-component system Ge-As-Se exhibited most of the phenomena common to the whole

field of glassforming systems and that these could be "tuned in" by relatively minor changes of composition. The key to this behavior is the random cross-linking of Se chains which takes the system up to and through the rigidity percolation threshold. Subsequent studies (Bib. Nos. 18-20) showed that not only the "fragility" (i.e. viscosity vs. temperature) behavior correlates with the connectivity through the Phillips-Thorpe analysis, but so also does the "departure from exponential relaxation" which has been receiving so much attention from the glass community in recent years, under the stimulus of K. L. Ngai of the NRL. These correlations have since been expanded to embrace most glassforming systems and are making a major contribution to the systemization of phenomenology in glassforming systems.

CONCLUSIONS

Significant and well-recognized contributions in three distinct areas of Energy and Glass science have been made during the 10-year tenure of ONR support. These contributions in the fields of fast ion-conducting glasses, polymer salt electrolytes and infrared optical materials have resulted in a number of conference lecture honors and scientific honors culminating in the recently announced Neville Mott award for 1992. It may be concluded that the ONR funding of this work has been justified.

BIBLIOGRAPHY

A. Mechanical Relaxation and Relation to Electrical Relaxation in Fast Ion-Conducting Glasses

1. "Silver Alkali Halide Glasses and a Vitreous Analog of the $RbAg_4I_5$ Superionic Conductor," Changle Liu, H. G. K. Sundar and C. A. Angell, Mat Res. Bull., **20**, 525 (1985)

2. "Mechanical Relaxation by Mobile Ions Cu^+ and Ag^+ in Fast Ion Conducting Glasses," Changle Liu and C. A. Angell, J. de Physique Colloque, **C10**, Suppl. No. 12, 46, 493-496 (1985)

3. "All Halide Superionic Glasses," Changle Liu, H. G. K. Sundar and C. A. Angell, Sol. State Ionics, **18 & 19**, 442 (1986).

4. "Recent Developments in Fast Ion Transport in Glassy and Amorphous Materials," C. A. Angell, Solid State Ionics, **18 & 19**, 72 (1986) (text of plenary lecture).

5. "Ambient Temperature Plastic Crystal Fast Ion Con-ductors (PLICFICS)" E. I. Cooper and C. A. Angell, Solid State Ionics, **18 & 19**, 570 (1986).

6. "Glassy Solids and dc Conductivity in the Liquid and Glassy States," C. A. Angell, in *Materials for Solid State Batteries*, ed. by B. V. R. Chowdari and S. Radhakrishna, p. 31-40, (1986).

7. "Correlation of Mechanical and Electrical Relaxation Phenomena in Superionic Glasses," C. A. Angell, Mat. Chem. Phys., **23**, 143, (1989)

8. "Effect of Pressure on Conductivity in Liquid and Glassy States of a Superionic Conducting Glass," C. A. Angell and J. Zhou, Solid State Ionics, **34**, 243 (1989).

9. "Fast Ion Conduction in Glass; the New Solid Electrolytes," C. A. Angell, Proc. Workshop on Application of Glasses, Bangalore, India, Nov. 1988, eds K. J. Rao, A. R. Cooper, and H. Jain, World Scientific Pub., Singapore, 1989, p. 245.

10. "Dynamic Processes in Ionic Glasses." C. A. Angell, Chem. Rev., **90**, 523 (1990).

B. Salt/Polymer Fast Ion-Conducting Systems

11. "Ion-Matrix Coupling in Polymer Electrolytes from Relaxation Time Studies," L. M. Torell and C. A. Angell, Polymer J. (Proc. 1st International Conference on Polymer Electrolytes), British Polymer Journal, **20**, 173 (1988).

12. "Contrasting Conductance/Viscosity Relations in Glassy and Polymer 'Solid' Electrolytes", M. McLin and C. A. Angell, J. Phys. Chem. (Letters Section), **92**, 2083 (1988).

13. "Ion-Pairing Effects on Viscosity/Conductance Rela-tions in Raman-Characterized Polymer Electrolytes: $LiClO_4$ and $NaCF_3SO_3$ in PPG(4000)", M. C. McLin and C. A. Angell, J. Phys. Chem., **95**, 9464 (1991).

C. Structure and Relaxation in Optical Materials

14. "Structural Motifs in Fluoride Glasses and Their Influence on Liquid and Glassy State Properties," C. A. Angell and C. C. Phifer, Mat. Sci. Forum, **32-33**, 373, (1988).

15. "Effects of Coordination Environment on the Zr-F Symmetric Stretching Frequency of Fluorozirconate Glasses, Crystals and Melts," Carol C. Phifer, David J. Gostola, John Kieffer and C. Austen Angell, J. Chem. Phys., **94**, 3440 (1991).

16. "Vibrational Spectra in Fluoride Crystals and Glasses (Ba/Zr/F and BeF_2) at Normal and High Pressures", B. Boulard, C. A. Angell, J. Kieffer, and C. C. Phifer, J. Non-Cryst. Sol., **140**, 350 (1992).

17. "Fragility of Ge-As-Se Glassforming Liquids in Relation to Rigidity Percolation and the Kauzmann Paradox," M. Tatsumisago, B. L Halfpap, J. L. Green, S. M. Lindsay, and C. A. Angell, Phys. Rev. Lett., **64**, 1549, (1990).

18. "Correlations of the Non-exponentiality and State Dependence of Mechanical Relaxations with Bond Connectivity in Ge-As-Se Supercooled Liquids," Roland Böhmer and C.A. Angell, Phys. Rev. B., **45**, 10091 (1992)..

19. "Elastic and Viscoelastic Properties of Amorphous Selenium: Possible Identification of the Elusive Phase Transition," R. Böhmer and C. A. Angell (submitted to Phys. Rev. B).

20. "Connectivity, Fragility, and Non-exponentiality of Mechanical Relaxations, in Covalently Bonded Glassformers," R. Böhmer and C. A. Angell, Proc. 6th European Conference on Internal Friction and Ultrasonic Attenuation, Cracow, September 1991 (in press)

APPENDICES (FOLLOWING)

Mat. Res. Bull., Vol. 20, pp. 525-530, 1985. Printed in the USA.
0025-5408/85 $3.00 + .00

SILVER ALKALI HALIDE GLASSES AND A VITREOUS ANALOG OF THE $RbAg_4I_5$ SUPERIONIC CONDUCTOR

C. Liu, H. G. K. Sundar and C. A. Angell
Department of Chemistry
Purdue University
West Lafayette, Indiana 47907

(Received March 6, 1985; Communicated by R. A. Huggins)

ABSTRACT

We report the existence of silver halide-rich glasses of a type not previously recognized. These contain only monovalent halides and represent perhaps the simplest ionic glasses yet realized. Despite the lack of the usual oxyanion matrix the new glasses show room temperature conductances which equal or exceed those of the best Ag^+ glasses yet reported. Cu^+ analogues have also been prepared. At the high conducting extreme apparently lies a vitreous state analog of the well-known crystalline conductor $RbAg_4I_5$. A crystalline analog of the latter FIC, $CsAg_4(I_{0.45}Cl_{0.55})_5$ forms metastably on careful devitrification of the glass. Like its prototype, it has a very high conductivity and exhibits a sharp C_p anomaly at low temperatures, -77°C, in the vicinity of which the activation energy for conductance changes abruptly.

Introduction

Most of the halide-containing fast ion conducting glasses prepared to date have been based on the incorporation of the halide into a matrix of some oxyanion glass containing a high charge radius species such as B[III] (1), P[V] (2), As[V] (3,4), Se[VI] (5), Mo[VI] (6) or W[VI] (7). The one instance in which an alternative route-based on mixing of a large mole fraction of LiI with a glass-forming diluent of "weaker" cations—was attempted, met with complete failure (8). It might have been expected from the latter experience that the mixing of Ag^+ cations—which are quite acid in the Lewis sense—with large alkali cations would likewise result in the locking up of Ag^+ as complexes with a consequent diminution of conductivity. However, at least at high AgX contents, this proves not to be the case as we show in the present paper.

We report here a selection of results from a quite extensive study of the properties of glasses formed when molten mixtures of silver halides and alkali

halides are quenched to room temperature or below. The conductivities of some of these are exceptionally high although the content of AgI itself never exceeds 50 mol%. Initial experiments showed that glass formation in quaternary systems of the type AgCl-AgI-RbCl-CsCl, and their Cu^+ analogs is extensive. To isolate the principal features of these systems we focus attention on the ternary system AgCl-AgI-CsCl.

The glass-forming region for ternary AgCl-AgI-CsCl glasses formed by quenching 2-3 gm melt samples between metal blocks is shown in Figure 1(a). The mixtures made up from pure compounds fuse easily (the ternary eutectic in AgX-rich compositions lies at ~173°C) in pyrex glass tubes to give melts of very high fluidity. DSC scans of representative glasses are exemplified in Figure 1(b). These show that T_g increases rapidly with increasing X_{CsCl} at constant X_{AgX}, and weakly with increasing X_{AgI} at constant X_{CsCl}, as shown in Figure 1(c). The latter result is a little surprising since anion mass and electric field intensity factors would lead to the opposite expectation. Ease of glass formation and stability against recrystallization are given by the indexes, $(T_c-T_g)/T_g$ marked in Figure 1.

Glasses in the center of the glass-forming region are almost colorless, and are quite resistant to photolytic discoloration (yellowing). They remain far-IR transparent in thick sections to below 400 cm^{-1}. Thus, the optical window is the widest yet reported in the IR visible range.

D.C. conductivities σ were determined by complex impedance plots of data in the frequency range 0.012-100 kHz obtained using a GenRad 1689 impedance bridge programmed by a HP 9836 microcomputer to both scan in frequency and set temperature, averaging 20 readings at each frequency to improve precision as described elsewhere (9). One of the samples was measured in standard disc form. Silver paint electrodes were used because T_g was too low for electrode sputtering to be achieved without devitrification. For the best conductors such samples were unsatisfactory. In these cases the disc sample obtained by quenching was cut when $T \approx T_g \approx$ R.T. to yield a strip sample on which copper foil electrodes were wrapped as indicated in Figure 2 insert, and secured by clamping between plexiglass plates. The cell constant for such samples was

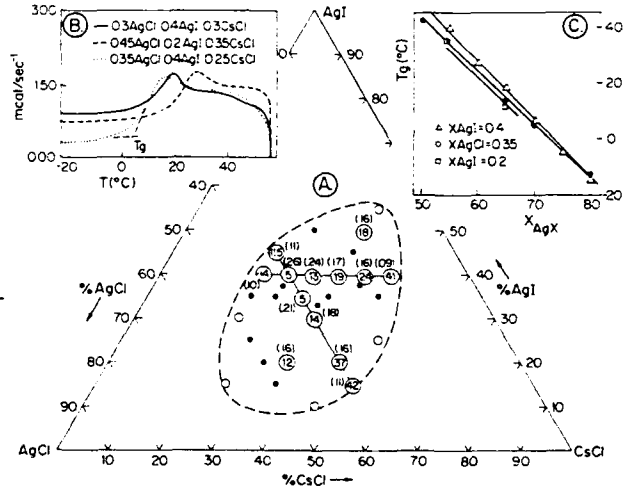

FIG. 1

Glass-forming domain in the ternary system AgI-AgCl-CsCl. Stabilities of glasses at compositions marked T_g (T_g in °C) are indicated by $(T_c-T_g)/T_g$ (all T in K) are given in brackets.
Insert (a) shows DSC scans typical of glasses in the system. Insert (b) shows the variation of T_g with Ag halide content for two fixed AgI contents and one fixed AgCl content.

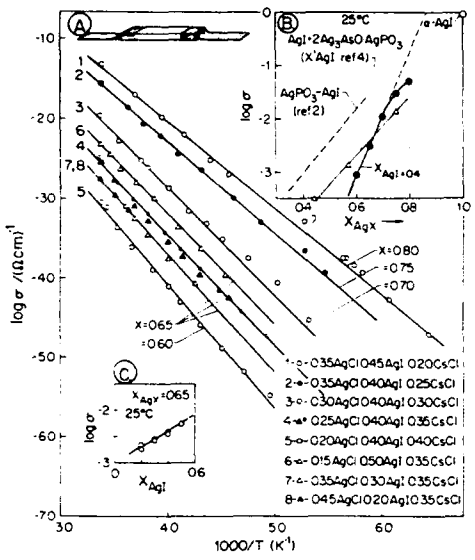

FIG. 2

Arrhenius plots of various glasses in the AgI-AgCl-CsCl system. Glass transition temperatures are marked on the plots.
Insert (a) sample + electrode configuration used for high-conducting samples.
Insert (b) AgX-dependence of room temperature conductivity, compared with data on AgI + $AgPO_3$ (2) and AgI + $AgPO_3$ + 1/3(Ag_3AsO_4) glasses (4).
Insert (c) anion dependence of $\sigma_{25°C}$ at fixed X_{AgX}.

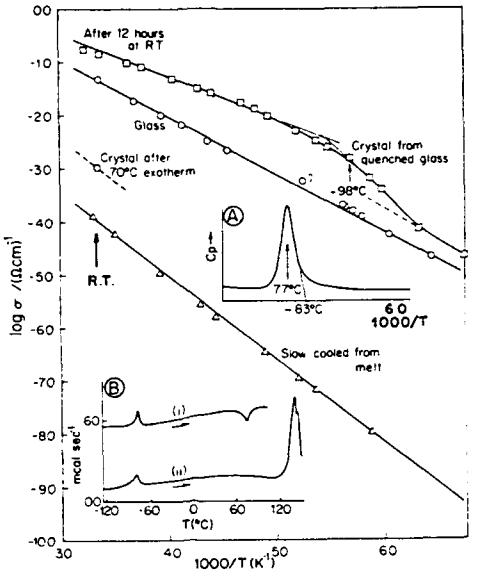

FIG. 3

Effect of devitrification of $CsAg_4(0.45Cl.55I)_5$ glass on conductivity and thermal behavior: upper curve is for first devitrification product described under insert (a).
Insert (a) DSC scan (vs. 1/T as for logσ), for the transparent crystalline sample produced by crystallization at 25°C of a sample initially fast quenched to far below its T_g.
Insert (b): curve (i): DSC scan on linear T scale showing exothermic change at 70°C to low conductivity phase. Curve (ii) shows that low T anomaly remains in low σ phase.

larger by a factor of ~100 for the disc configuration.

Conductivity Results

The results for different compositions are shown as an Arrhenius function of temperature in Figure 2. Problems with electrode contact, sample geometries, and the possibility of undetectable submicroscopic partial devitrification products during room temperature handling (at higher AgX contents), combine to diminish the data precision in comparison with our usual capabilities. For the highest-conducting glass, X = 0.80 in Figure 2, the complex impedance plots for temperatures in the vicinity of 200 K were abnormal and unsatisfactory for σ determination , possibly due to microphase behavior related to the order-disorder anomalies seen in the crystallized samples (see below). No data are reported for this range, though σ values from higher and lower temperatures are compatible. Despite such experimental problems, the overall pattern of behavior for the system is clear. Arrhenius plots are consistent

with a single-valued pre-exponent $A_\sigma = 10^{2.2}$ in the expression

$$\sigma = A_\sigma \exp(-E_a/RT) \quad (1)$$

as seen in earlier work (10), though best fit plots of the present data would show some scatter about this value. The activation energies E_a depend mainly on CsCl content, and the smallest value observed is 21 kJ mol^{-1}. The composition dependence of the d.c. conductivity at 25°C as a function of total silver halide content (but constant $X_{AgI} = 0.40$) is shown as insert (b). Comparison is made with data from the 'classic' system AgI + $AgPO_3$ (2), and data from the recently reported wide composition range AgI-$AgPO_3$-1/3(Ag_3AsO_4) glasses (4).

Discussion

We first comment on the anion dependence of the conductivity, since all fast Ag^+-conducting glass systems have previously involved only AgI. Figure 2 insert (b) shows that a 25°C conductivity $4.7 \times 10^{-2}\Omega^{-1}cm^{-1}$ above the best on record (11) can be achieved with a 'glass' (12) containing only 40 mol% AgI provided additional Ag^+ is present as chloride. Furthermore, the rate at which σ is increasing with total AgX, at constant X_{AgI}, is such that the 25°C conductivity of pure α-AgI (extrapolated from above 149°C) would be exceeded while X_{AgX} is well below 1.0. Actually, the conductivity seems to be saturating near $X_{AgX} = 0.8$. Presumably the explanation for such behavior is not to be sought in the existence of α-AgI-like clusters as has seemed the best interpretation of previous AgI-containing glasses (3-5,13,14). We should note, however, that the conductivity at constant X_{AgX}, is favored by increase of I^-/Cl^- [Figure 2 insert (c)].

The nature of the vitreous state substructure responsible for the high conductivity is strongly suggested by the results of devitrification studies shown in Figure 3. Here the conductivity of the glass obtained by quenching melts of composition 0.2 CsCl-0.35 AgCl-0.45 AgI [i.e. ~$CsAg_4(ICl)_{5/2}$] to the low temperature vitreous state (with pause at ambient temperature to cut a strip sample) are compared with the conductivities of their possible devitrification products. If the quenched glass is devitrified slowly at room temperature, a transparent crystalline product is obtained. The transparency is presumably due to a homogeneous nucleation process which, due to the slow growth rate, produces such a high concentration of crystallites that none approach the 1 μm size needed to scatter light. The crystallization at RT is accompanied by a half order of magnitude increase in conductivity, see Figure 3, to a value which is stable at least on the time scale of days.

This crystallized material has two features of interest. The first is a region in the logσ vs T^{-1} plot around -100°C where a rapid but continuous increase in activation energy, which is reproducible, occurs on cooling. The second is the appearance, in a DSC scan, of a sharp heat capacity spike in the same temperature range. This is shown in Figure 3 inserts displaced to -77°C: its position and magnitude seem to depend somewhat on history. Similar features are found in the behavior of the much-studied and utilized $RbAg_4I_5$ FIC around -64°C, and at lower temperatures in analog compounds (15,16). It may be concluded that this first devitrification product which, by the Ostwald step rule, is the crystalline structure most similar in energy and topology to the glass, is a mixed (and disordered) anion analogue of the same structure.

That this high conductivity crystalline structure is metastable is shown by the effect of heating the sample to $T \geq 70$°C. DSC studies [Figure 3 insert, curve (i)] show a further exothermic event, which could be a further

crystallization/decomposition or even mere grain-coarsening, and which yields a product with a much lower condcutivity (by two orders of magnitude at R.T.). This product, however, still possesses a low temperature transition [starting at -84°C on either heating or cooling—see Figure 3, insert (b)] but sample fracturing prevented characterization of the conductivity in this lower temperature region. A further product of even lower conductivity which lacks any trace of the -77°C transition, is obtained by relatively slow cooling of the melt. Conductivity data for this material are shown in Figure 3, lower curve, which exhibitis no anomalies. It presumably contains free AgI partly substituted with Cl^- because of a large transition during heating is found starting at 130°C (c.f. β-AgI <—> αAgI at 147°C). The crystal chemistry of this system is evidently complex and we have not pursued it.

We conclude that the high conductivities of the glasses produced in this study are due to the development, with increasing X_{AgX}, of $RbAg_4I_5$-like topologies, in which Ag^+ ions move easily through tetrahedral halide channels possessing many equivalent Ag^+ sites.

Results for analogous Cu^+-containing systems, which have glass transition temperatures uniformly higher by some 40°C, will be reported separately.

Acknowledgment

This work was supported by the Office of Naval Research under Contract No. N84KO289.

References

1. A. Magistris, G. Chiodelli and A. Schiraldi, Electrochimica Acta 24, 203 (1979).

2. J. P. Malugani, A. Wasniewski, M. Doreau and G. Robert, Mat. Res. Bull. 13, 42 (1978).

3. R. J. Grant, M. D. Ingram, L. D. S. Juner and C. A. Vincent, J. Phys. Chem. 82, 2838 (1978).

4. S. W. Martin and A. Schiraldi, J. Phys. Chem. 89, (April 25, 1985) in press.

5. T. Minami, J. Non-Cryst. Solids 56, 15 (1983).

6. A. Magistris and G. Chiodelli, Electrochem. Acta 26, 1241 (1981).

7. T. Takahashi, S. Ikeda and O. Yamamoto, J. Electrochem. Soc. 120, 647 (1973).

8. E. I. Cooper and C. A. Angell, Solid State Ionics 9-10, 617 (1983).

9. S. W. Martin and C. A. Angell, J. Non-Cryst. Solids (to be published).

10. C. Liu and C. A. Angell, Solid State Ionics 13, 105 (1984).

11. T. Minami, Kreidl Symposium review paper, J. Non-Cryst. Sol. 68 (1985) in press.

12. At 25°C the best conductors are, in fact, somewhat above their T_g, hence σ values strictly refer to supercooled liquid properties. However, in superionic glasses, unlike the general case, there is little change in

temperature dependence of σ at T_g [M. D. Ingram, C. A. Vincent, and A. R. Wandless, J. Non-Cryst. Solids 53, 73 (1982)] so the comparisons with other glasses at R.T. remain valid.

13. L. M. Torell and L. Borgesson, Physics Lett. 107A, 190 (1985).

14. J. P. Malugani and R. Mercier, Solid State Ionics 13, 0000 (1984).

15. R. A. Vargas, M. B. Salamon, and C. P. Flynn, Phys. Rev. B 17(1), 269 (1977).

16. "Physics of Superionic Conductors," ed. M. B. Salamon, pp. 65, 120 & 185. Springer Verlag, Berlin, Chapter 3, S. M. Shapiro and F. Reidinger, p. 65; Chapter 5, M. J. Delaney and S. Ushioda, p. 120.

JOURNAL DE PHYSIQUE
Colloque C10, supplément au n°12, Tome 46, décembre 1985 page C10-493

MECHANICAL RELAXATION BY MOBILE IONS (Cu^+ AND Ag^+) IN FAST ION CONDUCTING GLASSES

C. LIU AND C.A. ANGELL

Department of Chemistry, Purdue University, West Lafayette, IN 47907, U.S.A.

Abstract - The dissipation of mechanical energy in glasses of the "fast ion conductor" type ($AgI-AgPO_3$, $AgI-AgBO_2$ and $AgCl-CsI$) has been studied using a Rheovibron mechanical analyzer in the temperature range -190 to 200°C. In most cases a single loss peak at low temperature is found for fixed-frequency scans. The peak temperature almost coincides with that for electrical conductivity relaxation but is much broader. The loss magnitude does not correlate with peak temperature but depends on glass constitution. Where loss is small, the relaxation time follows Arrhenius Law with $\tau_o = 1/2\pi f_o$, where f_o is found from far IR spectra. For large loss glasses, important non-Arrhenius behavior is found.

INTRODUCTION

Although the technological need for solid electrolytes has led to an explosive increase in the number of conductivity studies in crystalline and vitreous ionic materials, there has been relatively little attention given to the response of the mobile ions to mechanical, as opposed to electrical, stresses. Apart from classic studies focussed on normal oxide glasses, there has only been the ultrasonics study of Carini and colleagues on $AgI-Ag_2O-B_2O_3$ glasses /1/. This is unfortunate because the mechanical response is qualitatively different from the electrical response insofar as the real part of the modulus remains finite at low frequencies. An electrical stress acting on the same ions will be completely dissipated by the unimpeded motion of the ions across the sample. Furthermore, the mechanical response is a secondary relaxation, the primary relaxation being that which leads to the glass transition.

For the classical (weakly-conducting) glasses, the investigation of mobile ion motion is tedious because of the small magnitude of the loss. For fast ion conductors, on the other hand, the losses are much greater, and less-sensitive instruments such as a Rheovibron (Toyo Instruments Inc.) may be employed with a resultant increase in rate of data acquisition of at least one order of magnitude.

In this report we describe essential features of the mechanical response of three types of fast ion conductors over wide temperature ranges.

EXPERIMENTAL SECTION

The principles of the measurement are illustrated in Fig. 1. Two sample configurations are in common use. The first utilizes a fiber which is held between stainless steel jaws connected to the frequency generating and stress/strain detecting elements of the Rheovibron. A sinusoidal strain α_1 is applied, and the lag of the stress α_2 behind the strain is recorded as the loss tangent illustrated in the lower part of the figure. The second, from which the same information can be acquired, uses the

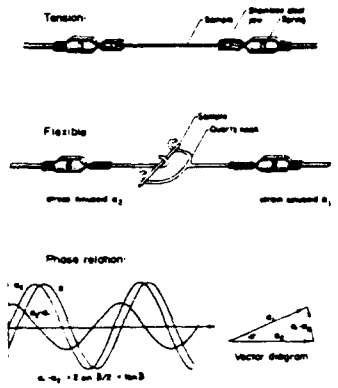

Fig. 1 - Principles of measurement.

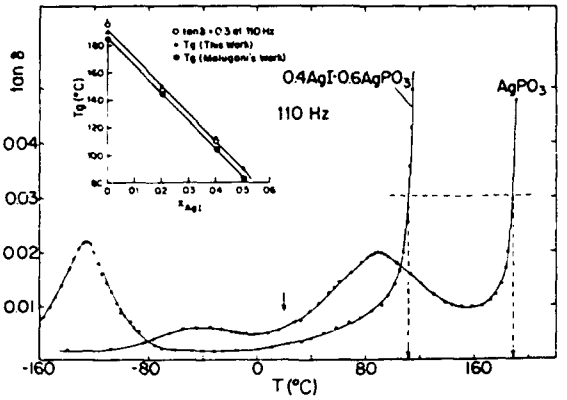

Fig. 2 - Loss scans for AgI-$AgPO_3$ glasses.

flexure configuration illustrated in the center section of Fig. 1. The jaw/sample assembly is enclosed in a variable temperature metal block, and the loss tangent and dynamic modulus at constant frequency are read at frequent intervals during a slow temperature scan from -200 to + 200°C (as needed).

RESULTS

Complete scans, from the low temperature regime where the "mobile ion" loss is recorded, up to the high temperature limit where the viscoelastic relaxation occurs (large loss with sample stretching) is illustrated in Fig. 2. Two compositions in the system $AgPO_3$- AgI are represented. The agreement of the viscoelastic loss temperature with the usual (DSC) glass temperature T_g, is shown in the insert. Details of the low temperature peak of interest to this work are shown in Fig. 3. Some data for the system $Cu_2O \cdot P_2O_5$-Cu(I or Cl) are shown in Fig. 4.

The storage and loss data are combined to give the real and imaginary parts of the tensile modulus, E' and E" respectively, in Fig. 5. Results are shown for two frequencies, although the frequency dependence of the response is only clearly seen in the imaginary part.

Comparison with electrical responses is made in Fig. 6 for a composition in the AgI-$AgPO_3$ system using an inverse temperature scale to cast the data in a form similar to that obtained for frequency scans at constant temperature. The latter are shown, in the insert, for the electrical modulus, M" ($M^* = 1/\varepsilon^*$). Fig. 6 brings out the important fact that, while both responses show maxima in their loss curves at

Fig. 3 - Loss "spectra" due to mobile ions in AgI-PO_3 glasses.

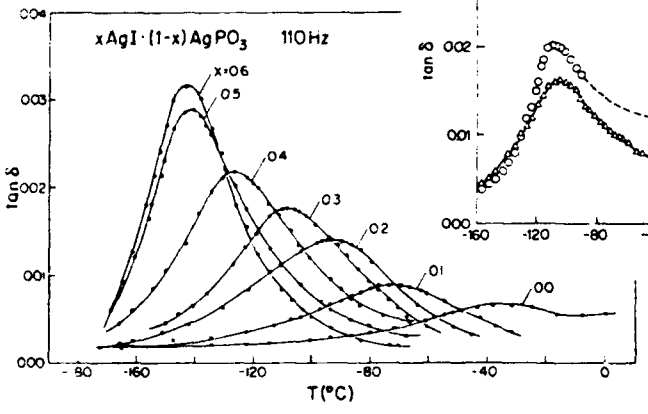

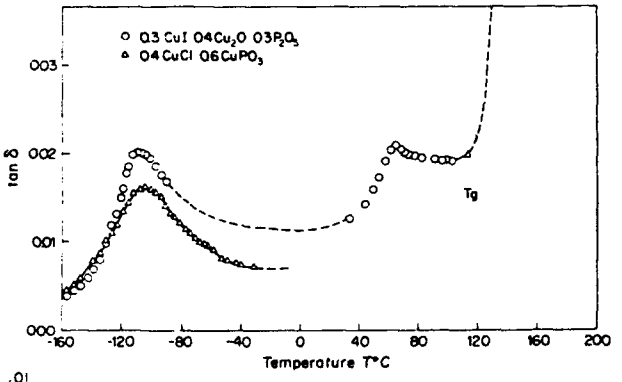

Fig. 4 - Loss vs. T for some CuI-Cu phosphate glasses.

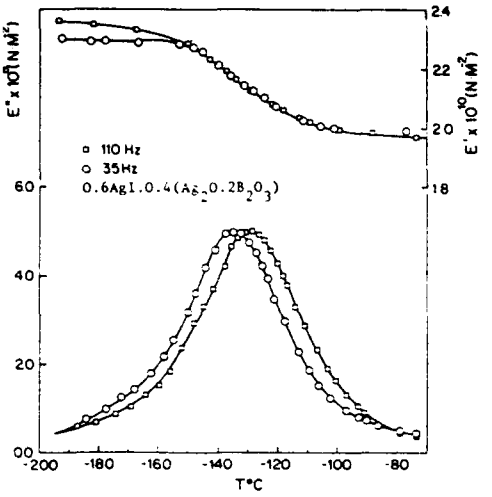

Fig. 5 - Real and imaginary parts of complex tensile modulus. (E' is discrepant at 35 Hz). Sample is 0.6 $AgI.0.4(Ag_2O.2B_2O_3)$.

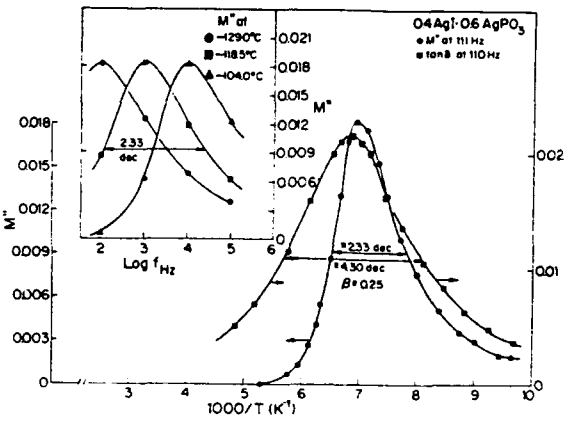

Fig. 6 - Comparison of electrical and mechanical loss moduli plotted vs. 1/T to give same shape as isothermal spectra shown in insert.

approximately the same temperature (i.e. the most probable relaxation time is not very different) the mechanical response is much broader, particularly on the high temperature (low frequency) side. Indeed, there are temperatures at which the electrical loss has almost vanished while the mechanical loss is still half its maximum value. The electrical relaxation is described by $\theta(t) = \exp-[(t/\tau)^{\beta}]$ with $\beta = 0.45$

A comparison of loss peaks amongst systems of different constitution, including the recently developed all-halide glasses of the type AgI-AgCl-CsCl, is made in Fig. 7. This figure brings out the important point that systems of comparable relaxation time may have very different loss magnitudes (implying that different fractional modulus changes are not correlated with the ionic mobility).

DISCUSSION

The outstanding features of the present findings are (1) the magnitude of the loss in some but not all cases compared to previous glass studies, (2) the fact that most probable times for electrical and mechanical relaxation are closely similar while the spectral widths are very different and (3) the fact that despite the different widths (which could be taken to indicate different activation energy distributions /1/) the activation energies for the two types of relaxation are indistinguishable. We discuss these in turn.

Data for a single system, e.g. $AgI-AgPO_3$, Fig. 3, would suggest that the loss, which is proportional to the fractional change in modulus due to relaxation, scales with the log of the relaxation time. However, the new data for the all-halide system show this is not so. Thus, attention must be redirected from the mobility of the silver ions towards the nature of the matrix within which they move. We note there are no asymmetric anions in the case of the halide glass while there are triangular (BO_3) groups in the very lossy borate compared with tetrahedral (PO_4) groups in the phosphate glass.

In considering the meaning of the much greater spectral width for mechanical compared with electrical relaxation we note again the qualitative difference between the two responses. Given time, the electrical response completely relaxes an applied stress, i.e. there is no zero-frequency electrical modulus. By contrast, the mechanical response relaxes the modulus to a zero-frequency value just 5-15% less than the high frequency value. Furthermore, the mechanical relaxation, unlike the electrical, is secondary in nature, the primary relaxation having been that which is observed at the glass transition. The electrical relaxation is well described by the Fourier transform of the Kohlrausch-Williams-Watts (KWW) relation $\theta(t) = \exp-[(t/\tau)^{\beta}]$, with β

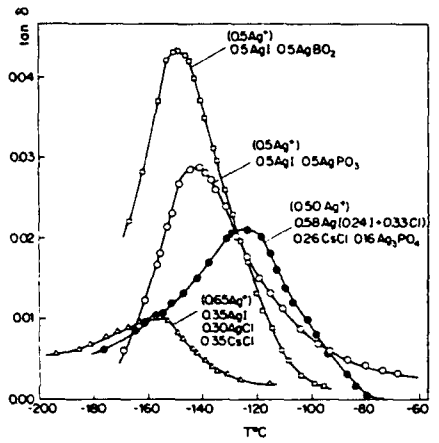

Fig. 7 - Comparison of loss peaks for different glasses.

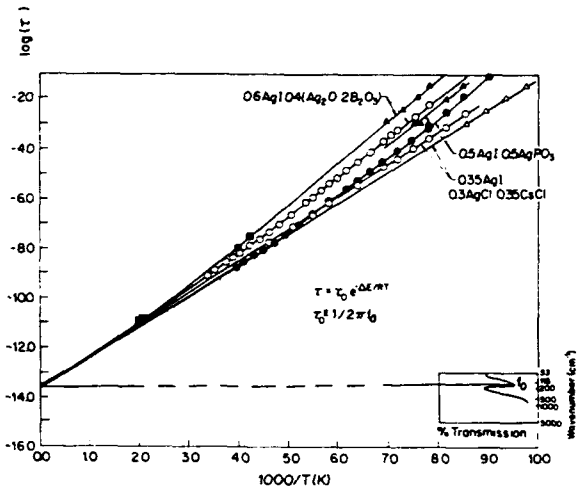

Fig. 8 - Electrical and mechanical relaxation times and relation to IR spectrum.

in the range 0.45-0.50 for all cases. The adequacy of the KWW form for the mechanical spectra has not yet been properly evaluated due to lack of sufficient measuring frequency range and precision. However, should this form be appropriate, then the peak halfwidths imply β values as small as 0.2 which will have to be rationalized by theory. Comparable widths in 1/T have been found in the ultrasonic range /1/, though, by GHz frequencies, a remarkable narrowing to give single relaxation time behavior has very recently been observed /2/.

Finally, we examine the temperature dependence of the relaxation process. The relaxation times $1/2\pi f$ are plotted vs. the 1/T values at which the loss maxima are found, in Fig. 8, for all the Ag^+ systems discussed in this paper. Fig. 8 shows that the least lossy glass exhibits Arrhenius behavior for both conductivity and mechanical relaxations with a simple extrapolation to the Ag^+ quasi-lattice "rattling" time ($1/2\pi f_o$) observable in the far IR (Fig. 8 insert). The more lossy glasses show regions of non-Arrhenius behavior. For the borate glass, extended-range mechanical relaxation studies /1,2/ permit characterization down to $\tau = 10^{-11}$sec , see Fig. 8. These data support extrapolations of the nonlinear Arrhenius plots to the same far IR frequency. These results are analyzed in more detail elsewhere /3/.

ACKNOWLEDGMENTS

Supported by ONR Grant No. N84k0289 and NSF-MRL Grant No. DMR 8316988.

REFERENCES

/1/ (a) Carini, G., Cutroni, M., Federico, M. and Galli, G., Solid State Comm. 44 (1982) 1427.
(b) Carini, G., Cutroni, M., Federico, M, Galli, G. and Tripodo, G., J. Non-Cryst. Solids 56 (1983) 393.
/2/ Borgesson, L., Martin, S. W., Torell, L. M. and Angell, C. A., Phys. Rev. Lett. (submitted).
/3/ Liu, Changle and Angell, C. A., J. Non-Cryst. Solids (submitted).

Solid State Ionics 18 & 19 (1986) 442-448
North-Holland, Amsterdam

ALL-HALIDE SUPERIONIC GLASSES

Changle LIU, H.G.K. SUNDAR and C.A. ANGELL

Department of Chemistry, Purdue University, West Lafayette, IN 47907, USA

To date all the highest-conducting Ag^+ and alkali cation glasses have involved admixture of a halide, usually the iodide, with some oxyanion salt of the same cation. In this paper we report cases where the oxyanion can be omitted. Instead, a second cation (Cs^+ or Rb^+) is introduced to provide, together with a mixture of anions, the immobile quasi-lattice through which the mobile cations, Ag+ or Cu+, can migrate. The materials are evidently vitreous state analogs of the well-known superionic crystals $CsAg_4I_5$ and $RbCu_4I_5$. In these new systems, conductivities at 25°C can reach record values. Glass transition temperatures, however, are lower than for oxyanion- containing glasses of the same conductivity. Since they contain only heavy monovalent ions, the far IR transparency of the new glasses is unprecedented. The characteristics of stress relaxation for both electrical and mechanical stresses are studied and are compared with those of the oxyanion + halide glasses. The all-halide glasses show less exponential relaxation (broader distributions of relaxation times) despite equivalence of all Ag^+.They nevertheless show smaller deviations from the Arrhenius law in their temperature dependences.

1. INTRODUCTION

This laboratory recently reported the existence and characteristics of fast ion conducting glasses in which no oxyanions or other complex species are present.[1] The glasses contained only monovalent cations and anions, the anions being chloride and iodide and the cations being silver and cesium. Although these glasses are generally characterized by low glass transition temperatures, they are of interest (a) because of their simple constitution, (b) because those richest in silver salts give the highest electrical conductivity so far measured at room temperature, and (c) because, in contrast to previous Ag oxysalt + Ag halide systems, it is reasonable to suppose **all** the Ag^+ ions present to be equally mobile. Comparison of properties with those of the oxysalt-halide glasses may therefore throw light on those features of the behavior which are related to mixed mobility properties.

In the present article we extend the study of glasses of all-halide type to the Cu^+ analogs, and examine the a.c. conductivity as well as the d.c. conductivity characteristics. We will also introduce comparisons with mechanical relaxation studies, and with the known properties of oxyanion-based silver halide glasses.

2. EXPERIMENTAL

Chemicals used were all high purity substances obtained from Merck, and Alfa, and Chemical Cos.The lowest purity level was 99.8% for CuCl. Glassforming regions in the various tertiary and

0 167-2738/86/$ 03.50

quaternary systems, e.g., AgCl-AgI-CsCl, CuCl-CuI-RbCl, and CuCl-CuI-RbCl-KCl, were identified by quenching weighed mixtures melted in Pyrex glass tubes at 500 - 600°C, between cold metal plates. In favorable cases thick pellets of glass could be formed by natural cooling on the metal plate.

Discs formed by quenching were coated on each side with a standard area of silver paint, and their electrical conductivities were determined using a standard two terminal arrangement. The temperature range -170°C to room temperature, was covered by allowing slow temperature rise from an initial liquid nitrogen environment in a Dewar flask, readings over the frequency range 12-100,000 Hz being taken automatically by a computer controlled GENRAD digibridge model 1689 in the manner described by Martin and Angell.[2] For the highest temperature ranges the conductivities were too high for the (low cell constant) disc arrangement to be satisfactory. For these cases linear strip samples were cut from the discs, and copper foil electrodes pressed in contact at the ends as indicated in the inset to Fig. 4. d.c. conductivities were determined using the complex impedance plots shown in Fig. 1. The diagram shows the extreme temperature ranges of data obtained with linear strip samples.

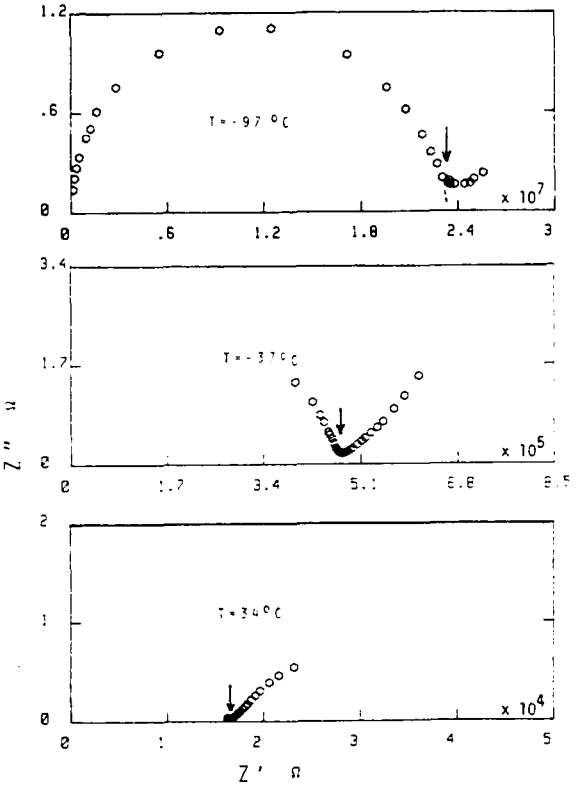

Fig. 1. Complex impedance plots for linear strip sample of AgI-AgCl-CsCl glass at various temperatures showing definition of σ_{dc}.

For the disc configuration samples, in which fringing effects are absent, the real and imaginary parts of the complex impedance contain information on the kinetics of electrical relaxation in the bulk vitreous material. The relaxation of electrical stress in vitreous media is not exponential, and the departure from exponentiality is currently generating considerable interest among chemical physicists.[3] Since the present system shows greater departures from exponential relaxation than ever previously observed for ionic conduction processes we present some of the data in form suitable for further analysis in Fig. 2. Fig. 2 shows the real and imaginary parts of the complex electrical modulus, $M^* = M' + iM''$, $= 1/\epsilon^*$ We discuss these data further below.

To obtain some information on the relaxation of mechanical stresses at frequencies overlapping those of the electrical measurements, linear strip samples cut from the initial discs were mounted in a stirrup configuration illustrated in Fig. 7 below and subjected to sinusoidal flexural deformations using a Toyo Instruments Rheovibron. The instrument reads out the ratio of the imaginary to real parts of the complex tensile modulus E^* as the loss tangent, tan δ. This can be determined continuously during slow temperature rise from -160°C. Results for the present and previous[4,5] systems show that tan δ for fast-ion conducting glasses rises to a maximum value at some temperature determined by the chemical constitution of the glass, before going off scale as T approaches T_g.

To determine the attempt frequency for the fundamental barrier crossing step involved in the

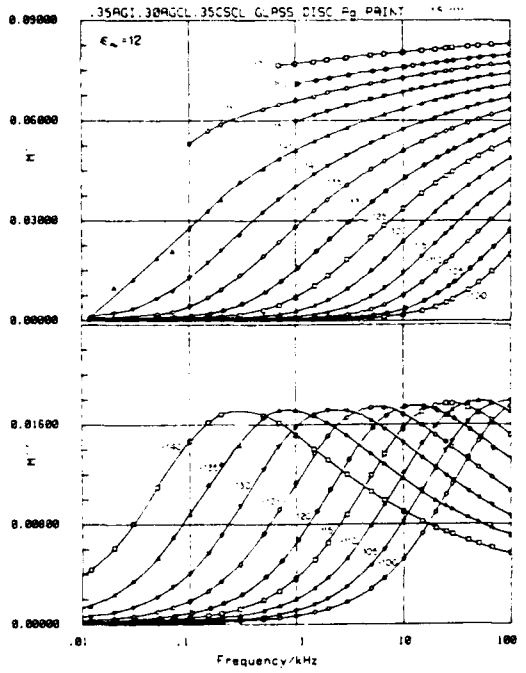

Fig. 2. Real and imaginary parts of the complex electrical modulus 0.35AgI0.30AgCl0.35CsCl, glass obtained using disc sample.

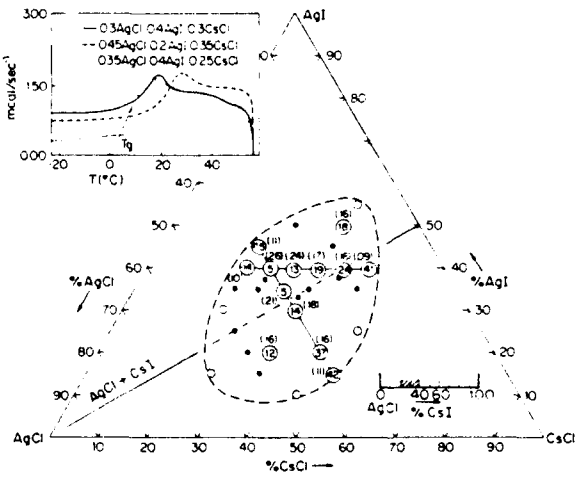

Fig. 3(a). Glassforming composition region and glass transition temperatures in AgCl-AgI-CsCl ternary systems. DSC scans are shown above for some cases.

relaxation processes, and to evaluate the IR transparency, infrared spectra were obtained using a Perkin Elmer Model 567 for the range $> 200\ cm^{-1}$. Far IR spectra have been obtained on AgI - $AgPO_3$ and CuI - $CuPO_3$ glasses, but not, so far, on the all-halide glasses due to difficulties associated with the low T_g values.

3. RESULTS AND DISCUSSION

The glassforming regions for several Ag^+ and Cu^+- based ternary and quaternary systems are shown in Fig. 3. Glasses high in CuCl have particularly low glass temperatures, which may be raised by $PbCl_2$ additions. The T_g values for glasses rich in RbCl or CsCl are quite high , comparable with those observed in mixed Ca^{2+}/K^+ nitrate glasses[6]. Note that a line of glasses across the middle of the ternary system AgCl-AgI-CsCl corresponds to compositions in the simple binary system AgCl-CsI. A number of compositions that we have studied in detail correspond to compositions in this binary system and will be referred to as such in the text and figures.

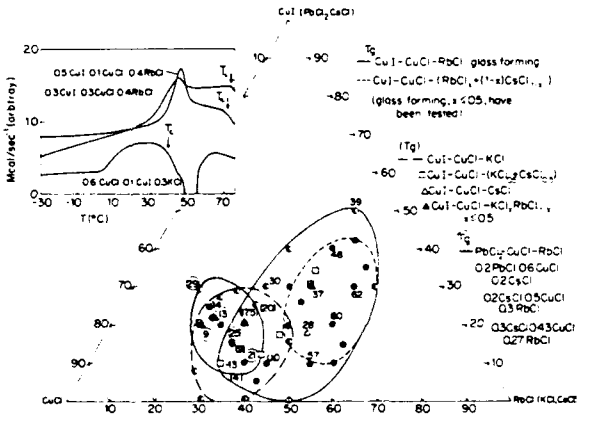

Fig. 3(b). Glassforming composition regions and glass transition temperatures for four types of CuCl-based halide glass systems. For key to T_g identification, see legend. Half-filled symbols indicate mixed glass and crystal from quench.

The d.c. conductivities for various compositions in the Ag^+-containing and Cu^+-containing glasses of Fig. 3 have been extracted from Figure 1 type data representations and are shown in Figs. 4 and 5 respectively. Not surprisingly, the highest conductivities are obtained with the highest Ag^+ and Cu^+ contents. For the silver systems, the trend with composition at constant AgCl, or constant AgI, contents respectively, are shown in the inset.

The conductivities for the silver halides are extremely high. Comparisons with the best silver ion-conducting glasses known from previous work[7,8] are made in the inset to Fig. 4. Unfortunately, these remarkable conductivities are obtained at the expense of rather low glass transition temperatures. Data on systems in which the all-halide glasses are incorporated progressively in oxyanion matrices (by analogy with the previously studied AgI-$AgPO_3$, and AgI-$AgBO_2$ systems) will be described in separate publications.[9]

The conductivities of the Cu^+ halide glasses at low temperatures are considerably greater than those of the best Cu^+-conducting glasses previously reported[10] (CuI + $CuPO_3$). However, due to their low glass transition temperatures, the highest-conducting compositions cannot be studied at room temperature.

Fig. 5 contains, as the highest- conducting sample, an interesting material obtained by controlled crystallization of an initially glassy material containing 14% $PbCl_2$. The glass itself has a low glass transition temperature, 10°C, and crystallization occurs over a period of 2 hrs at room temperature. The material produced, however, retains its transparent character though the conductivity increases considerably as a consequence of the crystallization. This material also retains considerable mechanical strength and is immune to attack by atmospheric moisture. It is potentially a very interesting material for both conductivity and infrared transmission purposes.

Turning now to the spectroscopic characteristics of the electrical response we note that in Fig. 2 the full width at half-height, FWHH, is much greater than

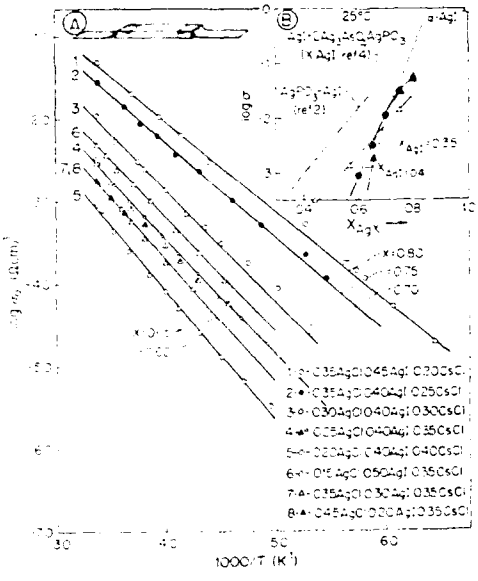

Fig. 4. Arrhenius plot of conductivity for AgCl - AgI - CsCl glasses. Insert: composition dependence of ambient temperature conductivity.

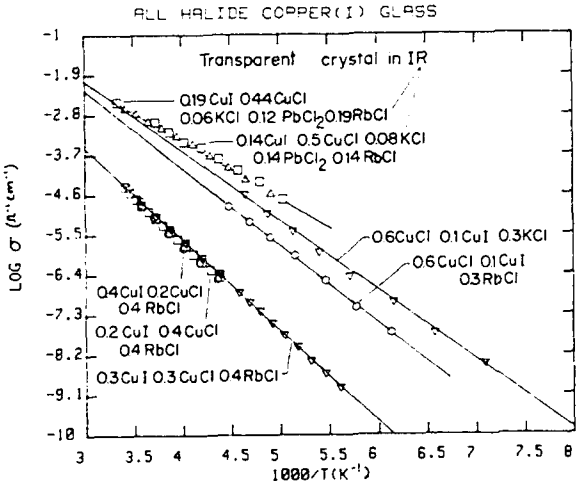

Fig. 5. Arrhenius plot of CuCl - based glasses. Note that the highest - conducting case is a devitrified metastable crystal containing $PbCl_2$.

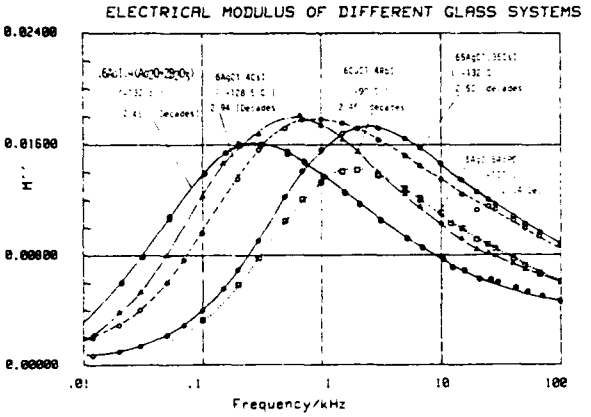

Fig. 6. Comparison of electrical loss spectra for various AgCl-CsI, AgI -Ag oxyanion glasses and CuCl-CuI-RbCl. FWHHs marked on diagram.

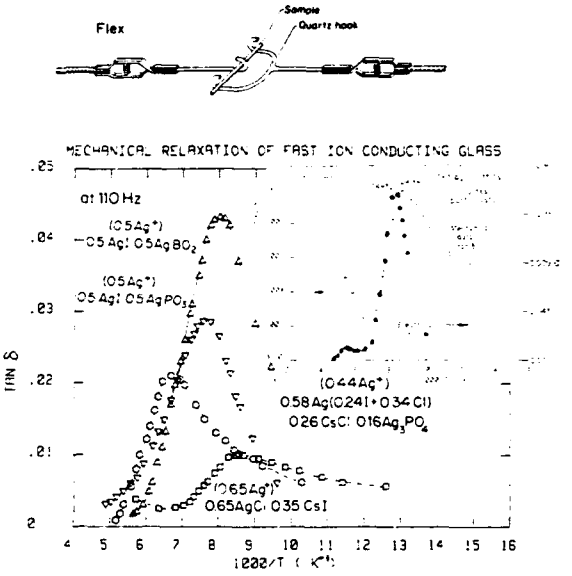

Fig. 7. Tan δ plots at 110 Hz vs 1/T (to give frequency spectrum form). Insert: Comparison of electrical and mechanical loss scans at 100 Hz.

for Debye relaxation, as is almost always the case for ionic conduction in glasses. The FWHHs we observe, however, are exceptional. We compare M" spectra for several glasses of the present and previous study in Fig. 6 and note the existence of FWHHs generally greater than two decades and approaching three decades in the case of 0.6AgCl 0.4CsI. This implies a value of the exponent β in the Kohlrausch-Williams-Watts relaxation expression[11,12]

$$\phi(t) = e^{-(t/\tau)^{\beta}} \qquad (1)$$

of 0.36, the smallest yet recorded for electrical relaxation. We find also a weak tendency to broaden as temperature decreases for a given glass, the opposite behavior from that found in silicate glasses.[13] The breadth of the spectra in these exceptionally high conductivity glasses continues a trend noted in a recent study by Martin and Angell[2] which correlates decreasing β with increasing conductivity at fixed temperature.

It is of interest to compare the electrical relaxation with that observed for mechanical stresses. Note that where an electrical stress (instantaneous field created by placing opposite charges on either side of a sample) will be completely dissipated by movement of ions across the sample, a mechanical stress will not. Rather a deformation to a limiting value characteristic of the stressed state will occur. Since the mechanical measurements are limited in their frequency range we present the observations as scans in temperature at fixed frequency. They are shown in Fig. 7 plotted vs 1/T so that the same form as in Fig. 3 will be obtained. (This is rigorous if the FWHH is constant with T, and the Arrhenius Law is obeyed, as is approximately true in the present case). We include data for other Ag^+ - containing systems with different oxyanions, for comparison. Data for Cu^+ - containing oxyanion glasses showing similar features are published elsewhere.[5]

It is notable that the all-halide glasses, besides having their loss peaks at the lowest temperatures (expected from their higher conductivities), have spectra very much broadened at low temperatures. This indicates the presence of a high density of fast-relaxing modes, and is the opposite of what might have been expected of a system in which all silver ions

may be presumed equivalent. Certainly this finding must raise much doubt about the possibility of attributing spectral width in oxysalt-halide glasses to populations of different intrinsic mobility[14]. Because of the equivalence of form, a FWHH in 1/T can be converted to an approximate FWHH in frequency. The value implied is an extraordinary 8 decades. A comparison with the electrical relaxation is made in the insert to Fig. 7 where electrical modulus M" data are shown scanned in temperatures at fixed frequency. The mechanical spectrum is strikingly broader at lower temperatures (high frequency) implying mechanically excitable modes which have no dipole moment associated with them. It is probable that this sample has suffered partial crystallisation during preparation. Therefore some spectral distortion could be due to nucleus-matrix surface modes and further study will be needed to decide whether the exceptional behavior observed is intrinsic to the glass. The width of the more crystallisation - resistant mixed system $AgPO_3$+ (halide glass) seen in Fig. 6, suggests that it is. In this case, unusual behavior may be expected in the cryogenic range where anomalous specific heat and thermal conductivity properties are generally found.

Some interesting features are observed in the electrical modulus behavior in partially crystallised samples. Fig. 7 (insert) shows the presence of a bump at low 1/T corresponding to a second and slower electrical relaxation such as may be seen in electrolyte solutions[15]. This phenomenon will be analysed in more detail in a separate publication[9].

Finally, we combine all the relaxation time data available for these glasses into a single Arrhenius plot (Fig. 8) to show how both mechanical and electrical relaxations have a common origin in the quasi-lattice vibrational modes seen in the Far IR. In the case of the all-halide glass the absorption centered at ≃100 cm^{-1} (which causes the IR cut-off for thick sections at ≃300 cm^{-1} shown in the insert) is the only IR absorption, in contrast to the case of the oxyanion - containing glasses. An example of extended range mechanical relaxation data covering 10 orders of magnitude (for an AgI-[$Ag_2O \cdot 2B_2O_3$] glass) is included for comparison (see Borgesson and Torell, this proceedings). Although the M" spectra are the broadest yet observed, the relaxation times show very little of the deviation from Arrhenius behavior seen frequently for the iodide - oxyanion glasses[16].

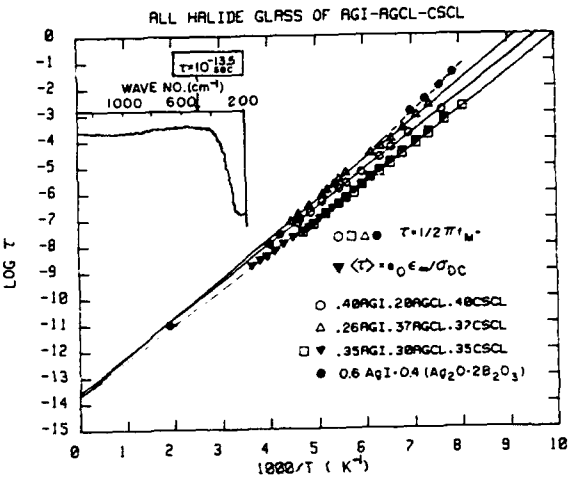

Fig. 8. Arrhenius plot of electrical and mechanical relaxation times, showing extrapolation to infra-red absorption frequency. Included are mechanical data for an AgI-$Ag_2O \cdot 2B_2O_3$ glass.

An advantage of the all-halide systems is that they are non-corrosive and low-melting hence lend themselves to precision measurements in the mobile liquid state. We are currently extending the study of the dynamics of these systems to temperatures where the limiting high conductivity will be closely approached in order to complete the "map" presented in Fig. 8 and in addition, to show how the decoupling of electrical and primary structural relaxation occurs as T_g is approached from the liquid state.

ACKNOWLEDGEMENTS

This work has been supported primarily by the Office of Naval Research under Contract No. N84K0289. The work on $PbCl_2$-containing systems was performed under the auspices of the Department of Energy under Grant No. DE-FG02-84ER45102.

REFERENCES

1. C. Liu, H.G.K. Sundar and C.A. Angell, Mat. Res. Bull. **20.** (1985) 525.
2. S. W. Martin and C.A. Angell, J. Non-Cryst. Sol. (to be published)
3. "Relaxation in Complex Systems", Eds. K.L. Ngai and G.B. Wright, Nat. Tech. Inf. Service (U.S. Dept. of Commerce) 1984, pp. 3-11.
4. C. Liu and C.A. Angell, J. Non. Cryst. Sol. (in press).
5. C. Liu and C.A. Angell, J. de Physique, (in press).
6. K.J. Rao. C.A. Angell and D.B. Helphrey. Phys. Chem. Glasses **14** (1973) 26.
7. S.W.Martin and A. Schiraldi,J.Phys. Chem.. **89** (1985) 2070.
8. a) T. Minami, T. Shimizu and M. Tanaka, Sol. State Ionics B 9/10 (1983) 77. b) T. Minami J. Non. Cryst. Sol. (in press).
9. Changle Liu and C.A.Angell, (to be published)
10. Liu and C.A. Angell, Sol. State Ionics, **13** (1984) 105.
11. R. Kohlrausch, Ann. Phys. (Leipzig) **12** (1847) 393.
12. G. Williams and D.C. Watts. Trans Faraday Soc., **66** (1970) 80.
13. L. P. Boesch and C. T. Moynihan, J. Non-Cryst. Sol. **17** (1975) 44.
14. G.Carini, M.Cutroni, M.Federico, G.Galli and G.Tripodo, J. Non-Cryst. Sol. **56** (1983) 393.
15. F.S. Howells and C.T. Moynihan, Bull. Chem. Soc. Jap **57** (1984) 6521.
16. M.D.Ingram, C.A.Vincent, and A.R.Wandless,J. Non-Cryst. Sol. **53** (1982) 3.

Solid State Ionics 18 & 19 (1986) 72-88
North-Holland, Amsterdam

RECENT DEVELOPMENTS IN FAST ION TRANSPORT IN GLASSY AND AMORPHOUS MATERIALS

C. A. ANGELL

Department of Chemistry, Purdue University, West Lafayette, IN 47907, USA

We review new developments in the expanding phenomenology of amorphous solid electrolytes. We consider separately (a) the vitreous materials in which the charge carriers are highly decoupled from the supporting matrix, and (b) the polymer-electrolyte solutions, in which the charge carriers are coupled to, and move cooperatively with, a locally fluid (though globally elastic) matrix. To these we add briefly some observations on orientationally amorphous solids (plastic crystals in their interesting temperature range) which show some potential for combining the best features of both (a) and (b) above.

In the vitreous cases, new methods of preparation, including vapor deposition and sol-gel processes, are allowing exploration of compositions in previously inaccessible regions - also of new vitreous "states" within known composition regions. Use of new heavy element oxide chalcogenide matrixes has revealed some new and pleasing fast-conducting compositions. Among conventionally prepared glasses, the highest conductivities are still obtained with Ag^{+} and Cu^{+} containing glasses. New Ag^{+} glasses containing only halide anions yield $\sigma_{25^{\circ}C} = 4{\cdot}7 \times 10^{-2}\ \Omega^{-1}\ cm^{-1}$, even higher than for the AgI + oxyanion-containing record-holders. Fast anion-conducting (F^{-}, Cl^{-}), and possibly fast divalent cation-conducting, (Pb^{2+}) glasses have been developed.

We emphasize the importance of studying the fast ion motions by mechanical response, in addition to electrical response, measurements. Data on several systems are now available from low frequency tensile, ultrasonic, and hypersonic (Brillouin light scattering) techniques covering in all ten decades of frequency. These show that the mechanical response has the same average time constant as the electrical response, and the same activation energy but quite different spectral widths (relaxation time distributions). Furthermore, the greatest widths are found for a case where only one "type" of Ag^{+} is present suggesting that the spectral widths do not simply reflect the mobile ion site distributions. Of importance is the observation that the change in mechanical modulus due to relaxation of the fast ions decreases with increasing temperature. This seems incompatible with the weak electrolyte models, which require the displaceable ion concentration to increase with increasing temperature.

In the polymer electrolyte solution field, new polymeric solvents with more flexible backbones, hence lower "local" viscosities at ambient temperatures, have been developed. The "solid" electrolytes based on these show behavior which is predictable from models developed for ordinary concentrated electrolyte solutions.Comparisons are made with the properties of low temperature "plicfics".

1. INTRODUCTION

In reviewing developments in the field of amorphous solid electrolytes two years ago[1] I distinguished two distinct classes of substances which were under investigation. The distinction, illustrated in Fig. 1, lay in the position of the glass transition temperature T_g of the material relative to the temperature range of intended application e.g. ambient to 100°C.

The only materials which can be used below their T_g, obviously, are those in which a fraction of the charged species in the material can move independently of those species whose motions are being frozen out at T_g. If the conductivity were to be determined by species whose motions are being frozen at T_g, then

0 167-2738/86/S 03.50

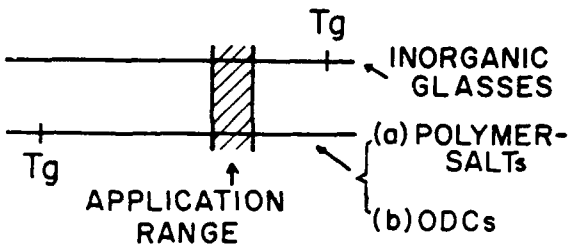

Figure 1.
Classes of amorphous fast ion conductors distinguished by relation Of T_g to temperature range of application. (ODC ≡ orientationally disordered crystal).

it is easily shown that the conductivity could not be greater than $10^{-14}\Omega^{-1}cm^{-1}$ at T_g* , and would become rapidly smaller at lower temperatures. Since T_g stands as the temperature above which amorphous solids can flow, a conducting glass ceases to be a "solid" electrolyte above T_g unless it has special structural features such as semi-infinite polymer chains, or a centre-of-mass ordered lattice structure (as in the case of "glassy crystal" materials). If a conducting material has either of the latter characteristics, then its possiblitities as a component of a solid state ionic system are greatly expanded since its d.c. conductivity is no longer dependent on the decoupling of ion and matrix motions. An ideal system would combine a decoupling of motions of the constituent particles, with a resistance to flow above T_g. So far such a material has not been clearly identified.

The extent to which the conducting ion motions are decoupled from those of the surrounding matrix can be described by a decoupling index defined by the relation of the structural relaxation time τ_s to the conductivity relaxation time τ_σ. The latter can be obtained directly fom the d.c. conductivity,

$$\tau_\sigma \simeq \epsilon_\infty e_o/\sigma_{dc} \simeq 9\times10^{-13}/\sigma_{dc}\text{sec} \qquad (1)$$

($\epsilon_o = 8.5 \times 10^{-14}$ Fcm^{-1}, $\epsilon_\infty \simeq 12$: for details see ref. 1), while τ_s is 200 sec at T_g[2,3] and is usually not known at other temperatures. The best vitreous conductors have R_τ values of order 10^{13} at T_g. For cases in which τ_s is known for $T > T_g$, the decoupling index is found to decrease with $T > T_g$ approaching unity in the highly fluid state (see Fig. 1 of ref. 1). The conductivity at **ambient** temperatures in decoupled systems depends jointly on the decoupling index, and on the interval of temperatures between T_g and ambient. For equal R_τ, the ambient temperature conductivity will always be greater for the glass with T_g closest to ambient. In **coupled** systems, the ambient temperature conductivity depends on the interval of temperature (ambient - T_g, and on the 'fragility' of the solution[4] (which determines the $d\sigma/dt$ characteristics).

In this review I will discuss first, and in most detail, the glassy (decoupled) systems, noting new vitreous electrolyte preparation methods, and new systems, followed by new investigations of the conductance mechanism. I will then put these in perspective by overviewing development in the polymer-electrolyte solutions (coupled systems) and PLICFIC (coupling characteristics not yet clarified) research areas.

So much new work has been done that any review will necessarily fall short of noting all the important developments. The author apologises to investigators whose work has escaped his attention through ignorance or inadvertance. In general, we have not referenced FIC studies prior to the '83 Grenoble SSI Congress. It is also the prerogative of a plenary speaker to emphasize those developments with which he is most familiar, viz., those from his own laboratory, and this imbalance should be borne in mind by the critical reader.

2 GLASSY SOLID ELECTROLYTES (Sub-T_g materials)

2.1 New Preparation Methods

Most glasses are formed by cooling the liquid melt to the glassy state at some moderately fast cool-

* We know this from the combination of Stokes-Einstein and Nernst-Einstein equations which shows $\sigma \propto$ viscosity^{-1}, and the viscosity increases by 15 orders of magnitude between the temperature of "normal" viscosity, where $\sigma \simeq 1\ \Omega^{-1}cm^{-1}$, and T_g.

ing rate. Compositions which may be explored for superionic properties by conventional means are therefore limited by the resistance to crystallization of the supercooled liquid. Although very wide ranges of composition can in some cases be covered using ordinary melt-quenching techniques, the indications of wide composition range studies are that the composition of maximum conductivity usually falls outside the normal glass-forming composition region. This finding focuses attention on means of accessing the most favorable composition range by unconventional methods.

Three methods of extending the normal composition range of glass formation are currently being applied. The first of these simply speeds up the rate of cooling from the liquid state by use of techniques of various sophistications, and, in its most recent application by Minami and colleagues[6-9], has produced vitreous forms of even such high-melting and stable compounds as lithium orthosilicate. It is argued that this requires quenching rates of $10^9 Ks^{-1}$. The remaining two methods avoid the liquid state entirely, in one case by using vapor phase techniques to condense thin films, and in the other producing the glass by a sol-gel process.[10]

Fast quenching methods for producing glasses have been in vogue since the early work on metallic glasses, but have only been applied to the fast ion conduction problem rather recently. Twin roller techniques pioneered for this application by Nassau and colleagues[11] have now been combined with a fast-melting technique using a thermal imaging device by Tatsumisago et al,[6] who have used it to prepare interesting glasses involving mixtures of orthoborate and orthosilicate ions which show a conductivity maximum (mixed anion effect). Glass transitions for Li_2O-SiO_2 glasses up to and including the orthosilicate composition have been determined for the vitrified products, and show systematic variations, T_g falling to 190 °C for the orthosilicate[6]. Lithium silicates have also been roller quenched by Tomazawa and coworkers[12].

With such techniques available, the range of compositions which **cannot** now be vitrified is enormously reduced. Glasses nominally beyond the orthoborate composition have been produced by Kasper et al[13], in the system Na_2O-B_2O_3 though in this case glass formation was assisted by the presence of carbonate anions residual from the starting materials. Also, a wide range of Li_2O-BaO-Nb_2O_5 have been prepared by the roller quenching technique, and studied by Tsumisago et al[7,8].

Several workers have bypassed the liquid state by choosing evaporation or spluttering type methods to obtain glass formation. Such methods are of interest because of the very thin films which are automatically produced. This method of amorphous solid electrolyte preparation was described at the last SSI Congress by Levasseur and co-workers[14], and new work has been reported by Ito et al[15] and by Minami and Kaneko[16]. Ito et al produced Li_2O-B_2O_3 films up to 85 mole percent Li_2O and observed continuous increases in conductivity with increasing Li_2O up to 80% - Li_2O. Interestingly enough, the conductivities at chosen temperatures, e.g. *150°C, fell below rather* than above the values for normally prepared glasses of the same composition in overlapping composition ranges[24]. This contrasts with the agreement of bulk and thin film conductivities found by Levasseur et al[14]. Minami and Kaneko[17], on the other hand, found increased conductivities for flash evaporated films in the systems AgI-Ag_2MoO_4 and AgI-Ag_2O-B_2O_3. Radio-frequency sputtered films were found to be amorphous to x-ray diffraction but the transport number of Ag^+ was only 0.9. They concluded that flash-evaporation was the most promising technique for amorphous film preparation important for thin film batteries.

Finally we note that attempts are being made to produce alkali-conducting glasses by the popular sol-gel technique. Initial results have been reported by Ravaine and colleagues[10], who have also reported a new family of organically modified silicates which are also alkali ion conductors[18]. The application of such

techniques to yield a wide range of unconventional and perhaps exceptional amorphous materials is awaited with interest.

2.2 New Systems

Rather than extending the composition range of glass formation in known systems, various workers have investigated, and reported, novel systems which are glassforming at normal cooling rates. Some of these have interesting, and in some cases exceptional, ionic conductivities. A wide range of conventionally prepared glasses has been reviewed by Minami[19], who has himself contributed new systems based on the logical extension of previous studies incorporating chalcogenide elements into the glass structure. Data for such new systems as $AgI\text{-}Ag_2Se\text{-}P_2Se_5$ are compared with previously reported glasses in Fig. 2 which is taken from Minami's paper and modified by addition of new systems to be mentioned below. An extensive study, achieving near record conductances but seeing no mixed anion effect, in $AgI\text{-}Ag_2O\text{-}As_2O_5\text{-}P_2O_5$ has been reported by Martin and Schiraldi[20]; they also offer a theoretical account of their observations. Further work on $LiI\text{-}Li_2S\text{-}B_2S_3$[21], and $Li_2S\text{-}SiS_2$ based glasses[22] has been reported. As pointed out by Souquet in an earlier review[23], the silicon-containing glasses always have the higher conductivities at constant molar ratio of other components. A rationalization for this observation in micro-structural terms has now been offered by and Martin and Angell[24]. An interesting mixed anion effect has been observed in $AgI\text{-}Ag_2SeO_4\text{-}Ag_2MoO_4$[25].

A new type of system in which conventional glass-forming species such as P(V), Si(IV), and B(III) are omitted, and which contain none of the usual oxyanions (MoO_4^{2-}, etc.) has been described by Liu et al for the case of Ag^{+}[26] and Cu^{+}[27] ion conductors. The latter are being reported for the first time at this congress. Liu et al show that the vitreous analogs of well-known crystalline conductors such as $RbAg_4I_5$ and $RbCu_4I_5$ can be produced if the anion constituents are mixed. Although these materials have very low glass transition temperatures relative to the oxyanion-containing systems, their conductivities at ambient temperatures are exceptionally high. Data for one of these are included in Fig. (2a) for comparision. Thin films of these glasses can be devitrified to

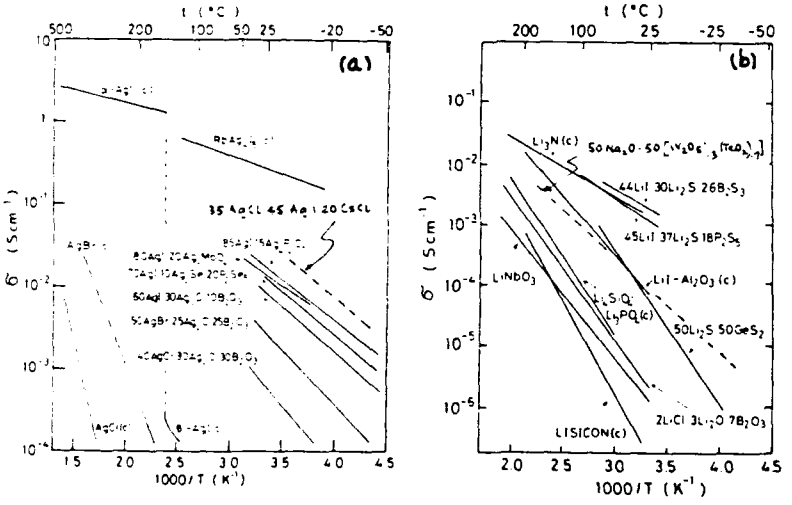

Figure 2.
Arrhenius plot of conductivities of various Ag^{+} and Li^{+} conducting systems (after Minami[19]) including two recent high conducting systems (one of them an Na^{+} conductor.) See dashed lines.

produce materials of even higher conductivity, sometimes with improvements in mechanical and moisture-resistance properties[26].

Among **sodium ion** conductors, it has been found that even in conventional oxide type glassy systems, conductivities of the order $10^{-3}\Omega^{-1}cm^{-1}$ at room temperature can be obtained. Kim, working in the author's laboratory[28], has found that with heavy element oxides, TeO_2 and V_2O_5 as mixed glass formers, the system $50\ Na_2O \cdot 50\ [(TeO_2)_{0.7}(V_2O_5)_{0.3}]$ yields the conductivities included in part (b) of Fig. 2 (for comparison with the best Li^+ conductors). Further improvements with additions of sulfide and halide ions might be anticipated. These glasses are mixed ionic electronic conductors in which ionic conductance dominates at high alkali contents, see Section 2.6).

At the time of the last congress no attempts had been made to find glasses in which **divalent** cations are mobile (in the way Pb^{2+} ,for instance, is mobile in β- alumina[29] and Zn^{2+} is mobile in Li_2SO_4[30]). In the interim, two attempts to rectify this situation have been made, both of which are being reported at this congress. Johnson[31] has now described a very low conductivity in PbO - B_2O_3 - PbI_2 glasses, while Sundar, Martin and the author[32] have found quite high conductivity and low activation energy in $Pb(PO_3)_2$ - $PbBr_2$ glasses of high $PbBr_2$ content. The activation energy is only 2/3 that of the anionic crystal conductor $PbBr_2$. However Pb^{2+} mobility has not yet been confirmed. Sundar et al concluded that at least in the $PbCl_2$-$Pb(PO_3)_2$ glasses the conductivity was probably mainly anionic, in which case these glasses had almost the best anionic conductivity yet reported. (σ (200°C) = > $1 \times 10^{-5}\ \Omega^{-1}\ cm^{-1}$ compared with previous high values of $3 \times 10^{-6}\ \Omega^{-1}\ cm^{-1}$ for PbF_2-PbO-SiO_2[33a] and most recently $2 \times 10^{-5}\ \Omega^{-1}\ cm^{-1}$ for a fluorosilicate glass studied by Shelby[33b]. A substantial improvement in **anionic** conduction has since been achieved by Kulkarni[34] working in this laboratory, by using high PbF_2 content glasses. A glass with $85PbF_2 \cdot 5\ MnF_2 \cdot 10\ Al(PO_3)_3$ shows a conductivity of $1.1 \times 10^{-4}\ \Omega^{-1}\ cm^{-1}$ at 200°C.

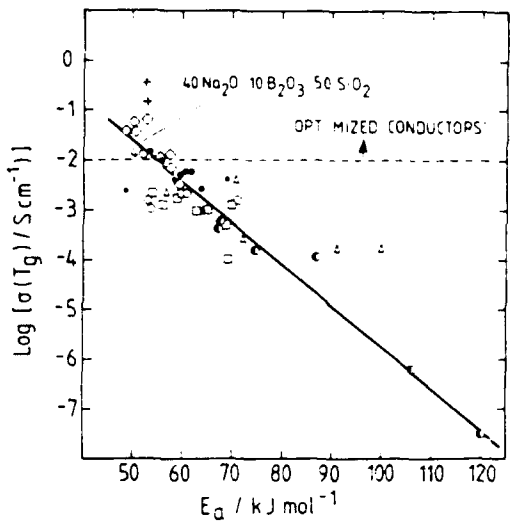

Figure 3.
Correlation of conductivity at T_g with activation energy for a variety of glasses.(After Hunter and Ingram[35].

2.3 Mode Decoupling

With the new data in hand we are now in a position to examine the question of decoupling of cationic and matrix modes which occurs in the *liquid state* and which is essential for the existence of fast ion conducting glasses. Fig. 3, reproduced from the work of Hunter and Ingram[35], shows how the conductivity measured at T_g varies systematically with the observed activation energy for conductivity. Since the relaxation time for the total structure is ≃200s at T_g we can use Eq. 1 to assess the decoupling index for these glasses and for additional cases for which new data have now been presented. Table 1 lists the conductivities at 25°C and at T_g, the conductivity relaxation time τ_σ at T_g, and the decoupling index, R_τ, for a representative selection of systems.

We see that the the highest values of R_τ are obtained in glasses high in familiar oxide glassformer content (B_2O_3 and SiO_2). The meaning of this high decoupling ratio is illustrated most succinctly in Fig. 4 also taken from a work of Ingram[36] which plots the conductivity of FIC AgI-silver borate glass on the same scale as the conductivity for a familiar molten salt, KNO_3, and compares these with the data for a

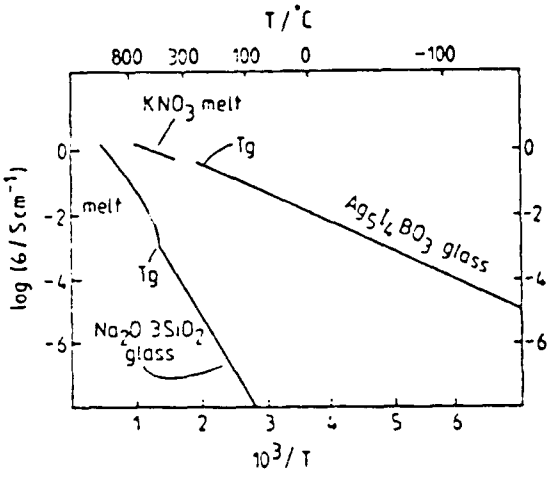

Figure 4.
Comparison of Ag^+ fast ion conducting glass with liquid state conductivity of a common molten salt, KNO_3 and behavior of a classic glass system (Ingram[36]).

standard sodium silicate glass. The point to observe is that in the FIC there is no suggestion that the silver ions have become aware of the cooperative processes which are leading the matrix (within which they move) into the typical non-Arrhenius regime in which rapidly increasing relaxation times lead to vitrification at temperatures not far below the onset of cooperative relaxation. The precise reason the silver borate and NaSiglass quasi-lattices provide a supporting structure for such low barrier pathways is at this time still not clear.

The other point to be reiterated is that the most decoupled systems are not necessarily or even often the best ambient temperature conductors. The AgI - Ag_2O - B_2O_3 and NaSiglass cases which head the decoupling index list in Table 1 are poorer conductors at 25°C then the best of the all-halide glasses. This is a direct consequence of the higher glass transition temperatures of the former.

It may be possible to gain some insight into this problem through studies at constant glass composition in which the glass transition temperature is changed by the application of pressure on the liquid before passing into the glassy state. Several studies of the effect of pressure **on the glass, after** it has been formed at normal pressure, have been reported, but then this tests a different aspect of the problem. The latter measurements show interesting and contrary characteristics. In some cases, increase of the pressure decreases the conductivity (Li_2O - B_2O_3[37], and low temperature AgI-Ag_2MoO_4[38]) while the latter glass at ambient temperatures shows an initial increase and a

Table 1. Decoupling indexes $R_\tau = \tau_S/\tau_\sigma$ for various fast ion conducting glasses at their T_g.

No.	System	σ_{25} Ω^{-1} cm^{-1}	T_g K	σ_{T_g} Ω^{-1} cm^{-1}	$\tau_\sigma(T_g)$ sec.	$R_\tau(T_g)$
1	75 AgI · 25 Ag_2MoO_4	$13{\cdot}6\times10^{-3}$	325	2.8×10^{-2}	3.8×10^{-11}	5.3×10^{12}
2	73 AgI·20 Ag_2MoO_4· 7 $Ag_2Mo_2O_7$	22.4×10^{-4}	344	9.08×10^{-2}	11.7×10^{-12}	1.7×10^{13}
3	20 AgI·80 (Ag_2O·B_2O_3)	1.5×10^{-5}	603	2.2×10^{-2}	4.73×10^{-11}	$4{\cdot}23\times10^{12}$
4	80 AgI·20(Ag_2O·B_2O_3)	3.1×10^{-2}	483	$38{\cdot}0\times10^{-2}$	$2{\cdot}8\times10^{-12}$	$7{\cdot}15\times10^{13}$
5	66.7 AgI 25 Ag_2O $8{\cdot}3P_2O_5$:(AgI-Ag orthophosphate)	1.5×10^{-2}	323	$2{\cdot}47\times10^{-2}$	$4{\cdot}30\times10^{-11}$	$4\cdot\times10^{12}$
6	65 AgI·23·3 Ag_2O 11.7 P_2O_5 (AgI-Ag pyrophosphate)	2.0×10^{-2}	321	$2{\cdot}96\times10^{-2}$	$3{\cdot}59\times10^{-11}$	$5{\cdot}57\times10^{12}$
7	50 AgI·25 Ag_2O·25 P_2O_5 (AgI-Ag metaphosphate)	5.0×10^{-3}	337	$1{\cdot}25\times10^{-2}$	$8\cdot\times10^{-11}$	$2{\cdot}35\times10^{12}$
8	35 AgCl·45 AgI·20 CsCl	$4{\cdot}7\times10^{-2}$	259	$1{\cdot}26\times10^{-2}$	$8{\cdot}44\times10^{-11}$	$2{\cdot}37\times10^{12}$
9	36 GeS_2·24 Li_2S·40 LiI	1.0×10^{-4}	499	$18{\cdot}51\times10^{-2}$	$5{\cdot}74\times10^{-12}$	$3{\cdot}48\ 10^{13}$
10	NaSiglass ($Na_{3.75}Zr_{1.1}Si_{2.75}P_{0.25}O_{10.2}$)	1.9×10^{-3}	1035	$5{\cdot}2\times10^{-1}$	$1{\cdot}53\times10^{-12}$	$1{\cdot}30\times10^{14}$

maximum[39].

Hunter and Ingram[35] have shown that the activation energy for conductance, which they correlate with the conductivity at T_g, Fig. 3, can be predicted with good reliability from the optical basicity of the glass which in turn can be calculated from tabulated quantities for the constituent elements (electronegativities, polarisabilities). The more basic the glass, the lower is E_a. This offers another, and suprisingly non-structural, approach to understanding the FIC problem.

2.4 Structure-Related Studies

The outstanding structural questions which we must seek to resolve may be classed as follows: **short range order** where we seek to understand local coordination characteristics and, in particular, whether or not distinct environments for mobile and immobile cations can be distinguished; **intermediate range order** where information on second and third nearest neighbor relationships is sought; and finally, **clustering or microheterogeneity,** where a tendency of multicomponent glasses to contain distinct microregions of the α-AgI, or Li-halide type structures is suspected, and is in urgent need of verification.

To answer the first question, techniques such as x-ray and neutron diffraction, vibrational spectroscopy, nuclear magnetic resonance, EXFAS, and computer simulation, are being applied. Solid state (high resolution) NMR studies are awaited with impatience. Results of such studies, in which resolution comparable with liquid state NMR is achieved by "magic angle" spinning, will be critical in resolving the controversies concerning chemical environments and mobile ion fractions. The second question lies in a grey area where experimental techniques are lacking - except perhaps for isotope replacement difference neutron scattering and anomalous x-ray and neutron scattering techniques - but in which computer simulation offers promise. For the third question, techniques such as small angle neutron or x-ray scattering

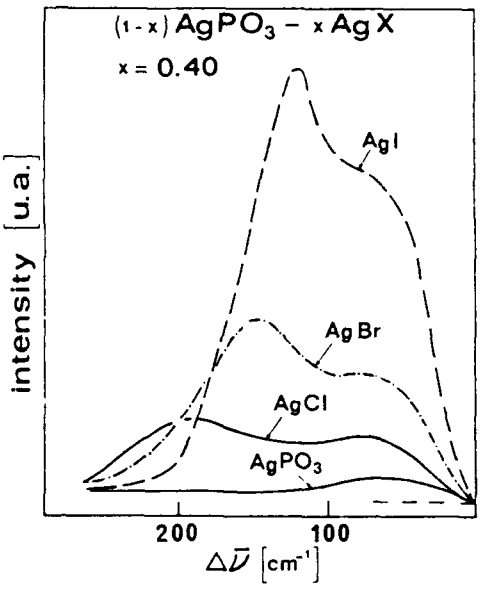

Figure 5.
Reduced Raman spectra of Ag halide - Ag metaphosphate glasses at (after Malugani and Mercier[40a]).

are useful.

Raman spectra of Ag halide - Ag oxysalt and thiosalt glasses have been reported by Malugani and Mercier[40a], and give evidence of distinct Ag halide, and Ag oxysalt- like environments (see Fig. 5). Low frequency Raman spectra have also been reported[40b]; application of Martin-Brenig theory leads to the conclusion that structual correlations increase with AgI content with correlation lengths of order 10A. Thin film mid-IR studies have been made of sodium borate, and AgI - $AgPO_3$ type glasses by Liu in this laboratory[41] and of AgI-$Ag_2O{\cdot}GeO_2$ and AgI-Ag_2MoO_4 by Minami[19]. In the first case, as in ref 40b, results show variable populations of three and four-coordinated boron, and composition-dependent cage "rattling" modes for the mobile cations, of which more is said below. Similar observations have been

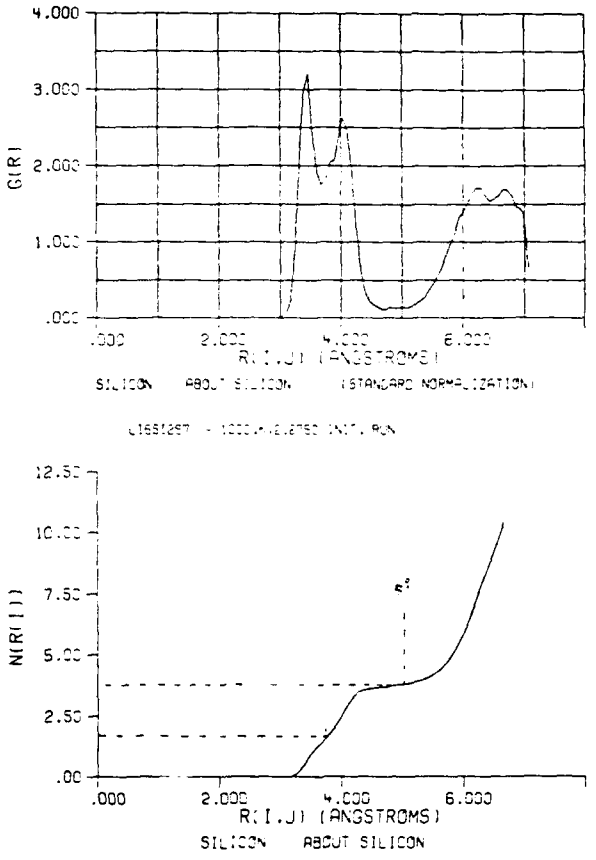

Figure 6.
Radial distribution functions and coordination numbers for Si about Si in $Li_2Si_2S_7$ glass from computer simulation study. Note evidence for both corner - sharing and edge - sharing tetrahedra.

reported by Button et al[42]. Short range structural information on AgI-Ag oxysalt glasses from EXAFS and inelastic neutron scattering studies are given in this volume[43,44].

NMR measurements, which give information primarily on the motion of mobile cations but which have been interpreted in terms of mobile and immobile cation fractions, have been reported by several groups[45-47] in the past two years, most recently by Martin et al[47]. The latter suggest that at high, but not at low, temperatures all Ag^+ ions are mobile on the NMR time scale.

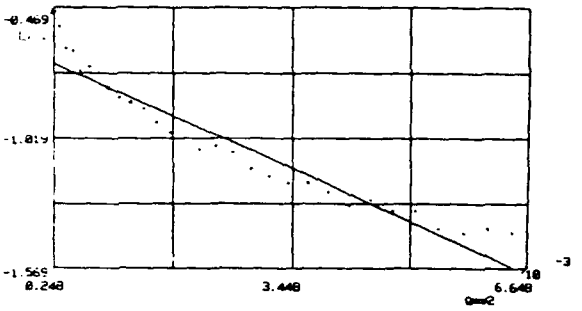

Figure 7.
Guinier plot of small angle neutron scattering intensity of AgI-$AgPO_3$ FIC glass. (after Tachez et al[44],)

Computer simulation studies of Li_2S-SiS_2[48], and Ag_2O - B_2O_3[49] glasses have been performed and it is reasonable to hope that some assistance in the identification of clustering tendencies in AgI - Ag oxysalts may be forthcoming from extensions of these latter studies. Fig. 6 shows the way in which these simulations can help identify different structural motifs in fast ion conducting glasses. The existence of two distinct Si distances with two of the four Si neighbors at each distance (Fig. 6b.),implies that both corner-linking and edge-linking of $[SiS_4]$ tetrahedra may be equally probable in these glasses.

The question of clustering has been addressed by small angle neutron scattering studies of which only preliminary reports are available[50]. Distinct excess scattering consistent with the presence of density inhomogeneities with correlation lengths of order 20 A have been observed (see Fig. 7).

2.5 Mobile ion transport mechanism

An understanding of the mechanism of conduction in fast ion conductors demands an understanding of both long- and short-time aspects of the ion motion within the vitreous quasi-lattice and the relationship between them, and an appreciation of how these are determined by the chemical characteristics of the glass as a whole. The extremes of the motion are illus-

trated in Fig. 8, which is the projection onto one side of the "computational box" of the lithium ion motions in a computer simulated vitreous lithium thiosilicate FIC[1,48]. The short-time motions are essentially the anharmonic rattling of an ion in a potential well from which it is at least temporarily unable to escape: the motion is manifested by the absorption of infra-red photons in the far IR region of the electromagnetic spectrum. An example due to Liu[41] for a sodium borate glass is given in Fig. 9. The long-time aspects of the particle motion are the diffusive drifts between potential wells following a local thermal fluctuation ("activation") and these are the motions which determine the d.c. conductivity, see Fig. 8.

The absorption coefficients for the alkali cation rattling motion, which are proportional to the infra-red electrical conductivities[1, 51] have been measured for sodium borate glass films of different thicknesses as a function of Na^+ content and found to vary linearly, see Fig. 9. This contrasts with the dependence of σ_{dc} on composition, which is usually exponential. The distinction is, of course, because the IR conductivity represents the limiting high value when all ion motions are conductive, and this σ_{max} is reduced by the Boltzmann probability $\exp(-E_a/RT)$ that any given cage transit will result in escape (diffusion).

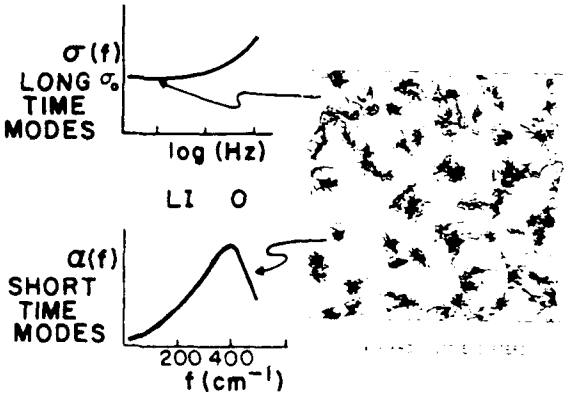

Figure 8.
Limiting modes of motion, and their experimental manifestation, based on projected trajectories of computer simulated $Li_2Si_2S_7$ glass.

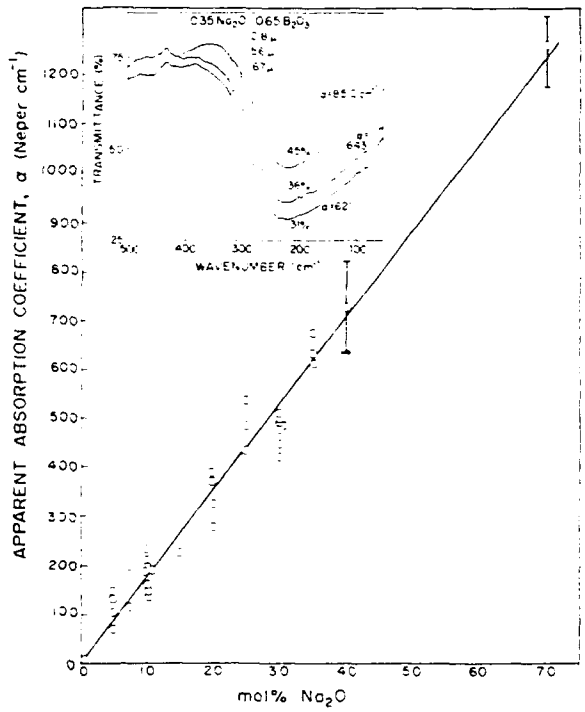

Figure 9.
Apparent absorption coefficients form variable-thickness thin film far IR absorption spectra of Na_2O-B_2O_3 glasses. Insert: raw far IR spectra.

The connection between the d.c. conductivity and the infra-red conductivity can be seen in a frequency plane plot of the a.c. conductivity shown in Fig. 10 for the sodium borate case using the new quantitative IR conductivity data. The correspondence of the IR conductivity with the fully activated limit represented by a Fulcher-type extrapolation to $1/T = 0$ in the case of liquid 35 Na_2O · 65 B_2O_3 (supported by data for liquid LiCl), is shown in the overlay Arrhenius plot in Fig. 10.

Attention must now be turned to the region between the d.c. limit and the IR limit. This is the domain of "relaxation spectroscopy" which has been given relatively little attention in the discussion of fast ion motion in solids to date. It is frequently

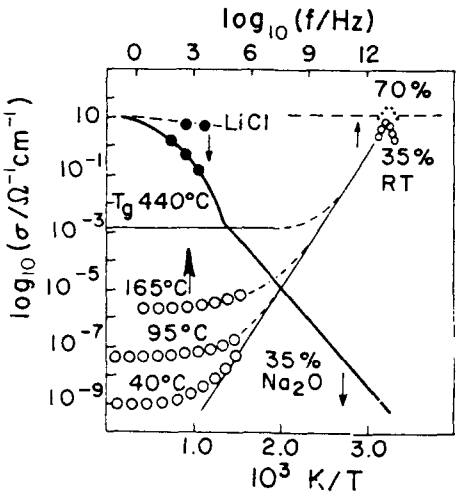

Figure 10.
Connection between dc conductivity and Far IR conductivity and the relation of Far IR conductivity to the high temperature limiting value (Na_2O - B_2O_3).

assumed that when the state of equilibrium of a condensed material is disturbed by some external force the system will return to equilibrium exponentially. In this case the departure from the d.c. conductivity regime, Fig. 10, would have a predictable form which, however, is not found in practice. Rather, the upward bend in σ_{ac} with increasing f seen in Fig. 10 is smeared out over a wider frequency range than is predicted by single relaxation time theory. Furthermore, where only a single relaxation process is involved, a sigmoid curve with a high-frequency plateau would be predicted in place of the continuously rising form seen in Fig. 10. There is thus much to be understood in the observed behavior.

Phenomenologically, one can interpret the observations by replacing the exponential response to perturbations by a non-exponential response, effectively introducing a "spectrum of relaxation times". Particular forms of this spectrum have been found to give a good description of the observations, at least in the region of initial increase (51,52). The most popular of these is the so-called KWW expression which, in the time domain, takes the form

$$\phi(t) = e^{-(t/\tau)^{\beta}}, \qquad (2)$$

Experimentally, the exponent β of Eq. 2 is found to be highest in those glasses which have the highest room temperature conductivity[24] Since all determinations of data are being carried out in roughly the same frequency regime (10 - 10^6 Hz) the latter observation can be recast in the form that β is smaller the lower the temperature at which the measurements from which it is determined are carried out. This would be consistent with the observations from mechanical spectroscopy (referred to below) that the spectrum of relaxation times narrows up dramatically as the frequency of the perturbing stress is increased to hypersonic values[53]. The latter measurements will be referred to below but first it is appropriate to note, by inspection of Fig. 10, that activation energies for conductivity measured at constant frequency will undergo a rapid decrease as the measuring frequency is taken from the low frequency d.c. regime to the **high** frequency a.c. regime, or if a transition between the two regimes is effected during temperature change. If the measurement is made at constant frequency, therefore, the high temperature results will yield a larger activation energy than the low temperature results. This is the same behavior seen in NMR studies of the spin lattice relaxation time measured in T scans at different fixed field frequencies.[45-47,50a] For ^{7}Li NMR, for instance, a f-independent regime at T $>$ T($T_{1,min}$) gives the same E_a as E_σ.[50a] Pre-exponents for the microscopic τs also concur. The whole T_1 curve can be modelled using EQ. 2[50b] or its nearest equivalent.[45] Opposite results ($E_a = E_\sigma$ at low Ts) were obtained[46] using the Hendrickson-Bray equation, which is therefore suspect. The motion of cations has also been studied by neutron quasi-elastic scattering and an E_a for diffusion compatible with that for σ has been obtained[50c].

It is important to compare findings from electrical response measurements with those from responses

to mechanical stresses. The latter can be examined at very low frequency using such techniques as the torsion pendulum or the dynamic modulus measurement [54,55], at MHz frequencies by the use of ultrasonic attenuation[56,57], and at GHz frequencies by the Brillouin scattering technique[53,59]. A preliminary comparison of mechanical and electrical relaxations in fast ion conducting glasses due to Liu was given in this review in 1983, since which time considerable work in this area has been performed. A number of ultrasonic studies are now available[57,60-64], particularly from the work of Carini and colleagues, but the direct comparison of mechanical and electrical spectral widths has still only been made for low frequency spectra. An example of recent findings[58] is shown in Fig. 6 of the paper by Liu et al in this volume. More complete comparisons are made in ref. 58. The mechanical response is strikingly broader in the 1/T plot of constant frequency, variable temperature scans, which implies that the width in a constant temperature, variable frequency scan would likewise be much greater. Evidently there are both fast and slow motions which are excited by mechanical stresses and which are not affected by electrical stresses. The nature of these electrically neutral modes has yet to be determined. Carini and colleagues[60-61] argue for a Gaussian distribution of activation energies as an explanation of the mechanical spectrum width. Surprisingly, the spectral width is greatest for the all-halide glasses described by Liu et al, this volume, in which equivalence of silver sites would seem more probable than in AgI-Ag oxysalts.

The most probable value of the response time for the two types of stresses, however, is closely similar, and the activation energy for this most probable time is the same within experimental uncertainty. For one case, 60 AgI - 40 $Ag_2O{\cdot}2B_2O_3$, mechanical relaxation data are also available in the ultrasonic range[60] and recently (this volume, Torell and co-workers) in the hypersonic range. The ultrasonic relaxation has only a slightly smaller width than the subaudio relaxation[59,63], but in the hypersonic range it is found that the loss can be fitted with a single relaxation time equation. Evidently a dramatic narrowing occurs in the frequency range 10^6-10^{10}Hz. As pointed out earlier, this can also be interpreted in terms of the change in temperature which is made when the centroid of the relaxation is to be observed at different frequencies. A proper explanation of this narrowing remains to be provided, since it seems to have different characteristics for mechanical and electrical responses, as do the spectral forms. Electrical responses seem to be of the KWW form, whereas the mechanical response seems to be more symmetrical, possibly log gaussian[59-64].

The activation energy for the mechanical and electrical responses can now be observed over a relaxation time range of some 10 decades. The values are shown in Fig. 11 (taken from ref.59 . and the pattern observed is a simple one. Included in Fig. 11 are data for other glasses in which the frequency range of mechanical studies is not as extensive as in the iodide - borate case. Fig. 11 includes an insert for the far IR spectrum of the iodide-borate glass, and it is noted that, while data for the different glasses appear to converge on this point, they require different degrees of departure from Arrhenius behaviour at high temperatures for the convergence.

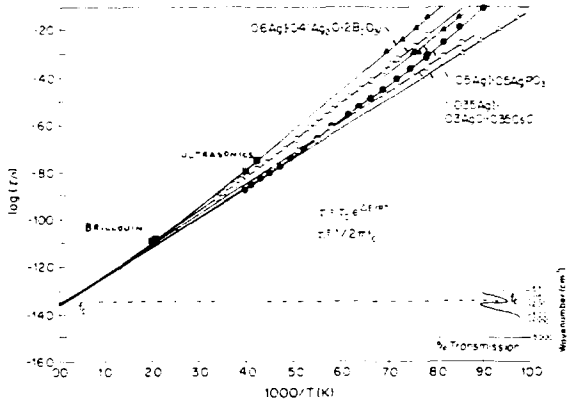

Figure 11.
Conductivity and mechanical relaxation times for various FIC glasses, showing extrapolation to Far IR quasi-lattice vibration time.

The matter of non-Arrhenius behavior in superionic glasses is of considerable interest but has only been subject to thorough study in one case, described by Ingram et al[65]. These workers observed that the non-Arrhenius character could be annealed out, and it remains to be seen if this is a general finding. It may be significant that the all-halide glasses ,which are self-annealing at room temperature, show the smallest degree of non-Arrhenius behavior in Fig. 11.

Another feature of mechanical relaxation spectroscopy of fast ion glasses is that, in contrast with the electrical response, the modulus remains finite on the low frequency side of the relaxation. In this respect, the response is like that of a polar liquid to an electric field. The relaxing part of the modulus is a thermodynamic quantity. If the mechanical stress is isotropic and of low frequency, it reflects (inversely) the change in isothermal compressibilty of the glass due to the displaceable cations. If the number of displaceable cations falls by orders of magnitude with decrease in (e.g.) AgI content at constant temperatures, or with decrease in temperature at fixed composition as weak electrolytes models suggest, then the magnitude of the relaxing modulus should change accordingly. In fact, the relaxation strength seems to be greatest at low temperatures and only weakly dependent on AgI contents, (see Borgesson et al, this volume and Liu and Angell[58]). The position is obscured by the fact that the pure compressive modulus is usually not obtained, though it is possible to obtain it from combination of shear and longitudinal wave data in ultrasonic measurements.

The change in compressibility can crudely be described by a two-state model in which there is an incremental volume change for each ion that is displaced. One way to rationalize an increasing $\Delta\kappa_T$ with decreasing temperature within the WE model would be to suppose that the "volume of excitation" increases exponentially with decreasing T. However, this seems improbable. The conclusion would seem to be that all ions contribute to the relaxation at all temperatures but that the response time is longer at low T (i.e. a strong electrolyte model would be more consistent with the observations.)

2.6 Models and theories.

Space restrictions have dictated that this review concentrate on phenomenology, and we give only very brief mention to the types of models and theories currently being discussed. These fall into different categories.

In the pictorial model category, representations of the local structure based on the spectroscopic evidence have been presented by Minami[19] et al and Schiraldi[66]. Less pictorial, and more directed at quantitative interpretation of mixed cation phenomenology, has been the special pair interstitialcy model of Ingram[67], and its refinements[68] (the most recent is in this volume). Ingram, Moynihan and coworkers[69,70] have in essence extended the original "weak electrolyte" model of Ravaine and Souquet[71] to make quantitative predictions of transport behavior in dilute solutions and provide a more microscopic basis for the model. An attempt to show the relation between the weak electrolyte and the Anderson - Stuart strong electrolyte models, and simultaneously to account qualitatively for the difference in conductivities of borate, silicate, and phosphate FICs, has been given by Martin and the author [24] ,and essential features can be seen in the article by Martin in this volume.

More formal theories for hopping and multiple trapping transport in disordered systems have been described by Movaghar et al[72] and Dyre[73]. Dyre gives an interesting argument to the effect that in amorphous materials the conductance process should assume a one-dimensional character due to the relative paucity of links in the "Scher-lax lattice". The preferred path idea goes back to Miller and Abrams[74]. This suggested the relevance of a suitable percolation theory for the frequency dependence of the conductivity, an example of which has been given by Bottger et al[75], who obtained a relationship consistent with

the behavior of σ (f) in Fig. 10.

2.7 Mixed ionic-electronic conductors

For electrode materials it is often desirable to have a material in which both electron and ions are mobile. Certain glasses have the ability to accept large changes in redox state by accepting charge compensating alkali ions into the structure. Such materials, whose potential has been described by Pagnier et al[76-78] are of much interest and deserve more detailed work. The relative transport numbers of electrons and ions, the mechanism of electron conduction (which usually does not conform to the extant theories) represent a challenge. Kim and the author[28] have observed that the mechanical relaxation strength in such glasses is a strong function of alkali content, (electron hopping is not expected to give rise to large volume or shear relaxations, buth that the mechanical relaxation time can predict the high temperature electrical relaxation time even at quite small alkali contents implying ion transport dominance of the conductivity at higher temperatures in most of the composition range.

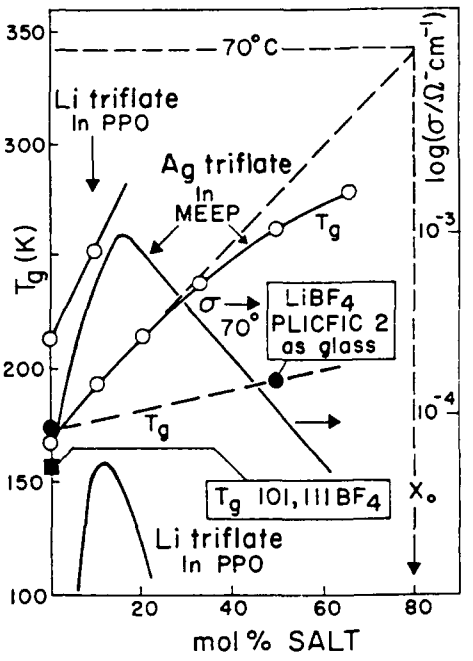

Figure 12.
Glass transition temperatures for polymer salt solutions and PLICFICs, and conductivity versus salt content relations. The origin and position of maxima are discussed in the text.

3. POLYMER ELECTROLYTE SOLUTIONS AND PLICFICS (Super- T_g Materials)

3.1 New systems: polymer-salts

Despite a great deal of activity in this promising class of "solid" electrolytes since the pioneering work of Wright and et al [80] and Armand and co-workers[82], there had been no dramatic improvements on the early findings until the very recent announcement by Shriver and coworkers[83] of a polyphosphazine backbone polymer to which ion-solvating groups had been grafted. The polyphosphazine backbone provides the low - stiffness requirement which was imperative for improved polymer electrolyte systems in order to increase the temperature interval [T(application) - Tg] which enters the transport equation as $\exp(T-T_o)^{-1}$, where $T_o \simeq 0.8T_g$.

The new system has a T_g for the salt-free polymer of 158K compared with 212K for polypropylene oxide, which has been, to date, the most favorable fully amorphous polymer case described in the open literature (PEO-salt complexes which give better conductivity, are largely crystalline). While very little imformation on the new systems is available, some pertinent observations and comparisons may be made. For these we refer to Fig. 12 which compares data for Ag CF_3SO_3 (Ag triflate) in MEEP (the solvating derivative of polydichlorophosphazene) with data for Li triflate in PPO[1,82] at 70°C. It appears that the Li triflate and MEEP solution would fall about a factor of 3 below the data for the Ag^+ case[83] i.e. still a great improvement on the PPO-based system. The

maximum in the conductivity is predicted by the configurational entropy theory for solution conductance[84] which leads to

$$\sigma = A\,N\exp(-B/Q(N_o-N) \qquad (3)$$

This equation was first derived[84] for the description of conductance in concentrated aqueous solutions[84,85] but should apply equally well to systems with polymeric solvents. In EQ. 3 N is the charge concentration, Q is the concentration dependence of T_g, and N_o is the concentration at which T_g extrapolates to the temperature of the isotherm. A and B are constants. Finding that T_g was more linear in mol % salt than in charge concentration, Angell and Bressel[85] modified EQ. 4 to the form

$$\sigma = AX\exp[-B/Q(X_o-X)] \qquad (4)$$

but the physics remains unchanged. Angell and Bressel used EQ. 4 (which is derived from the Adam Gibbs entropy theory for transport processes in glassforming liquids[90]) to correlate temperature and composition dependence of transport in electrolyte solutions and correctly to predict the position of the conductance maximum observed in these systems. The maximum originates in the competition between simple buildup of the charge carrier concentration (pre-exponential N, X) and the fact that increase in concentration **in general** raises the glass transistion temperature hence decreases the ion mobility. This physics applies equally well to polymer salt solutions, indeed the same line of thought was adopted by Papke et al[91] in their recent treatment of polymer-salt transport properties.

It can be seen that EQs 3 and 4 predict the maximum to lie at smaller salt contents the greater the dependence of T_g on salt content, and that relationship is borne out by the data in Fig. 12. To describe the behavior of lithium triflate-in-MEEP solution in the vicinity of the conductance maximum, a value of $X_o = 80$ in EQ. 4 would be needed according to Fig. 12. It is immaterial that the system with 80% salt could in practice not be formed. We will show elsewhere that the decoupling index for the polymer-salt systems is actually less than unity; in fact, $R_\tau \simeq 10^{-3}$, implying that in polymer-salt systems the ions are coupled not only to the solvent but also to themselves (i.e. associated). This problem will have to be dealt with before truly satisfactory conductivities can be obtained. In the meantime, efforts to keep T_g of the solution as low as possible must be continued.

It is interesting ,with respect to the last remark, to note the line marked $LiBF_4$ PLICFIC in Fig. 12. This represents the glass transition of the liquid (not plastic crystal) state of a system described elsewhere in this volume[92] for its potential as an alternative to polymer salt "solid" electrolytes. Frequently plastic crystals and their liquid states have similar T_gs and the point in Fig. 6 therefore emphasizes the potential of the PLICFIC (PLastIc Crystal Fast Ion Conductor) type system. We deal with this in the next section.

3.2 New Systems: PLICFICs.

In this volume, Cooper and the author[92] introduce some low temperature analogs of the orientationally amorphous crystal fast ion conductors, and point out that they have much in common with polymer salt systems in-so-far as most of the liquid-like degrees of freedom are excited, and as their domain of high conductivity is above the "glassy crystal" T_g. The organic salt which is companion to solvent for the active salt $LiBF_4$ can have a lower T_g than the best pure polymer solvent. Performance, however, depends on the existence of a favorable low temperature disordering transition in the double salt. Details are given elsewhere in this volume.

There is much room for further research in this area. One point of encouragement is the evidence, provided for the prototype PLICFIC Li_2SO_4 by Borgesson and Torell,[93] that the coupling characteristics in PLICFICS can be much more favorable than in polymer salt solutions. By Raman line broadening measurements, the latter authors showed that the anion reorientation time (which plays the role of the solvent reorganization time in polymer salt solutions) was of the order of 1.0 ps under conditions where the

conductivity was of the order of $1\Omega^{-1}$ cm^{-1}. This means $\tau_\sigma \simeq 1.0$ ps, implying that at least $R_\tau \simeq 1$ is possible for these systems which is a marked improvement over the polymer-salt solution case. We note that $R_\tau \simeq 1$ is consistent with the "paddlewheel" mechanism[93]. It is possible that there will be cases where the conduction is not determined (and limited) by this mechanism so that more favorable decouplings will be realisable. On the other hand, to the extent that the analogy between highly plastic crystals and highly excited liquids is valid, large decoupling ratios are presumably not to be expected[1] until the liquid-like motions are slowed down considerably - which would also diminish the conductivity. Optimised PLICFICS may prove to be the best compromise of all the fast ion conducting systems for applications purposes, but little is known of their characteristics and limitations at this time.

CONCLUDING REMARKS.

Despite the high level of research activity in the amorphous materials area of FIC phenomenology, some intriguing and promising lines of development are still waiting to be exploited. Much progress in the understanding and unification of the phenomena, and in their theoretical interpretation, can be expected before the next SSI Congress. We are conscious, in writing this review under pressure of time and space, of giving inadequate attention to certain research directions. In particular,the omission of investigations of the Soret effect and its interpretation by Schiraldi and coworkers,and of the relation of beta-Al_2O_3 behavior to glass behavior by Almond, West. and co-workers is regrettable. It is left to future reviews to remedy such defects.

ACKNOWLEDGEMENTS:

The author is indebted to the Office of Naval Research and the Department of Energy for support of this research under Grant Nos. N00014-84-K-0289 and DE-FG02-84ER45102 , respectively. He is grateful to his colleagues K. H. Kim, A. Kulkarni, Changle Liu, S. W. Martin and H. G. K. Sundar for permission to quote certain of their results in advance of publication, and for many stimulating discussions. He also thanks Hemlata Senapati for assistance with data analysis.

REFERENCES

1. C. A. Angell, Solid State Ionics. **9 & 10** (1983), 3.
2. M. A. DeBolt. A. J. Easteal, P.B. Macedo, and C. T. Moynihan. J. am Ceram, Soc. **59** (1976) 16.
3. Barkatt and C. A. Angell, J. Chem. Phys., **70** (1979) 901.
4. C. A. Angell, in "Relaxation in Complex Systems" Eds K. Ngai and G.B.Wright, U.S. Government Printing House, 1984 (in press), pp. 1-11.
5. S. W. Martin and C. A. Angell, J. Non-Cryst. Sol. **66** (1984) 429.
6. M.Tatsumisago. T.Minami and M.Tanaka, J. Amer. Ceram. Soc. **64** (1984) C97.
7. M.Tatsumisago, T.Minami and M.Tanaka, Glastechn. Ber. **56 K** (1983) 943.
8. M.Tatsumisago. T.Minami and M.Tanaka, J. Amer. Ceram. Soc. **66** (1983) 890.
9. M.Tatsumisago, A. Hamada, T. Minami and M. Tanaka, J.Non-Cryst.Sol. **56** (1983) 423.
10. Ravaine, J. Traore, L. C. Klein and I. Schwartz, Mat. Res. Soc. Symp. Proc. Vol. **32** (1984) 139.
11. A. M Glass, M. E. Lines, K. Nassau, and J. W. Shiever, Appl. Phys. Lett. **31** (1977) 249.
12. M. Yoshiygawa and M. Tomozawa, J. de Physique, **43** (1982) C9-41.
13. J. E. Kasper, S. A. Feller and G. L. Sumcad, J. Amer Ceram. Soc. **67 (1984) C-71.**
14. A. Levasseur, M. Kbala, P. Hagenmuller, A. Coutrier and Y. Danto, SolidState Ionics, **9/10** (1983) 1455.

15. Y. Ito, K. Miyauchi, and T. Oi, J. Non-Cryst. Sol. **57** (1983) 389.

16. S. Sahami, S. W. Shea, J. H. Kennedy, J. Electrochem. Soc. (1985) 985.

17. T. Minami and H. Kaneko, Sol. State Ionics **7** 1985 (in press).

18. Ravaine, A. Seminel, Y. Charbouillot and M. Vincens (to be published).

19a. Minami, J. Non-Cryst. Sol. **56** (1983) 15.

19b. T. Minami, J. Non-Cryst. Sol., **73** (1985) 293.

20. S. W. Martin and A. Schiraldi, J. Phys. Chem. **89** (1985) 2071.

21. W. Burckhardt, M. Makta, A. Levasseur and P. Hagenmuller, Mat. Res. Bull., **19** (1984) 1083.

22a. S. Sahami, S. W. Shea and J. H. Kennedy, J. Electrochem. Soc. (1985) 985.

22b. S. Susman, C. Delbecq, (private communication).

23. J. L. Souquet, Solid State Ionics, **5** (1981) 77.

24. S. W. Martin, C. A. Angell, J. Non-Cryst. Sol.(in press)

25. H. Senapati (to be published).

26. Changle Liu, H.G.K. Sundar and C. A. Angell, Mat. Res. Bull **20** (1985) 525.

27. Changle Liu, H.G.K. Sundar, C. A. Angell, All-halide glasses, this volume.

28. K.H.Kim and C. A. Angell, (to be published).

29. B. Dunn and G. C. Farrington, Mat. Res. Bull. **15** (1980) 1773.

30. A. Kvist, A. Bengtzelius, and U. Trolle, Z. Naturforsch., **23a** (1968) 2042.

31. P. M. Schleitweiler and W. B. Johnson, Pb^{2+} conduction in borate-iodide glasses, this volume.

32. H.G.K. Sundar, S. W. Martin, and C. A. Angell, High-conducting lead metaphosphate lead halide glasses, this volume.

33a. P. C. Schultz and M. S. Mizzoni, J. amer. Ceram. Soc. **56** (1972) 65.

33b. J. Shelby, J. Amer. Ceram. Soc. **68** (1985) C-177.

34. A. Kulkarni and C. A. Angell (to be published).

35. C. C. Hunter and M. D. Ingram, Solid State Ionics **14** (1984) 31.

36. M. D. Ingram, J. Non. Cryst. Sol. **73** (1985) 247.

37. M. Ryan and S. Smedley, J. Non-Cryst. Sol. **65** (1984) 29.

38. H. Senapati, G. Parthasarathy, K. J. Rao and E. S. R. Gopal, Pramana, **23** (1984) L269.

39. H. Senapati, G. Parthasarathy, S. T. Lakshmikumar and K. J. Rao, Phil. Mag. B, **47** (1983) 291.

40a. J. P. Malugani and R. Mercier, Sol. State Ionics **13** (1984) 293.

40b. A. Fontana, G. Mariotto, E. Cazzanelli, G. Carini, M. Cutroni, and M. Federico, Phys. Lett. **93A** (1983) 209.

41. Changle Liu and C. A. Angell, J. Non. Cryst. Sol. (submitted).

42 D. P. Button, L. S. Mason, H. L. Tuller and D. R. Uhlmann, Solid State Ionics, **9 & 10** (1983) 585.

43a. G. Dalba, A. Fontana, F. Fornassini and F. Rocca, EXAFS studies, this volume.

43b. S. Trachant. S. Peytavin, M. Ribes, A. M. Plank, H. Dexpert, and J. P. Lagarde, EXAFS studies, this volume.

44. M. Tachez, R. Mercier, J. P. Malugani, Quasi elastic and inelastic neutron scattering studies of $AgPO_3$-AgI, this volume.

45. J. Senegas and J. Olivier-Fourcade, J. Phys. Chem. Sol. **44** (1983) 1033.

46. S. J. Visco, P. Spellane, and J. H. Kennedy, J. Electrochem Soc, **132** (1985) 75; **132** (1985) 1770.

47. S. W. Martin, H. J. Bischot, M. Mali, J. Roos and D. Brinkman, ^{109}Ag NMR of $(AgI)_x$·$(Ag_2 \cdot 2B_2O_3)$, glasses, this volume.

48. C. A. Angell, S. Tamaddon, and P. A. Cheeseman (to be published).

49. M. C. Abramo, G. Pizzimenti and G. Carini (preprint).

50a. W. Muller-Warmuth, "From Simple to Complex Liquids," Presented at a Conference at the University of Bielefeld, W. Germany, Sept 1985: E. Gobel, W. Muller-Warmuth and H. Olyschlager, J. Mag. Resonance, **36** (1979) 371.

50b. K. L. Ngai and H. Jain, Conductivity and spin lattice relaxation in Li borates, this volume.

50c. M. Tachez, R. Mercier, J. P. Malugani, and A. J. Dianoux, Inst. Laje-Langevin Exp. Rep. **2** (1985) 278.

51. J. Wong and C. A. Angell, "Glass: Structure by Spectroscopy", Marcel Dekker, New York, 1976, Chap. 11, p.717

52. C. T. Moynihan, L. D. Boesch and N. L. Laberge, Phys. Chem. Glasses, **14** (1973) 122.

52. A. Miller and E. Abrahams, Phys. Rev. **120** (1960) 745.

53. L. Borgesson, S. W. Martin, L. M. Torell and C. A. Angell, this volume.

54. J. E. Shelby and D. E. Day, J. Amer. Ceram. Soc., **52** (1969) 169

55. T. Atake and C. A. Angell, J. Non-Cryst. Sol., **38&39** (1980) 439

56. J. Phalippou, S. Masson, A. Boyer, and J. Zarzycki,J. Non-Cryst. Sol. **14** (1974) 178

57. G. Carini, M. Cutroni, M. Federico and G. Galli, Solid State Comm. **44** (1982) 1427.

58. Changle Liu,and C. A. Angell,J. de Physique, (in press)

59 L. M. Torell, Phys. Rev. B. **31** (1985) 4103

60. G. Carini, M. Cutroni, M. Federico, G. Galli and G. Tripodo, J. Non.Cryst. Sol. **56** (1983) 393-398.

60. G. Carini, M. Cutroni, A. Fontana, G. Mariotto and F. Rocca, Phys. Review B. **29** (1984) 3567.

61. G. Carini, M. Cutroni, M. Federico, G. Galli, and G. Tripodo, Phys. Review B. **30** (1984) 7219.

62. G. Carini, M. Cutroni, M. Federico, G. Triopodo, Anelastic Relaxations in AgI-doped borophosphate glasses, this volume.

63. R. Bogue, R. J. Sladek, J. d. Physique Colloq. 1985 (in press).

64. D. P. Almond, G. K. Duncan and A.R. West, J. Non. Cryst. Sol. 1985, (in press).

65. M. D. Ingram, C. A. Vincent and A. R. Wandless, J. Non. Cryst. Sol. **53** (1982) 73.

66. A. Schiraldi, Electrochim. Acta, **23** (1978) 109.

67. M. D. Ingram, J. Amer. Ceram. Soc., **93** (1980) 248.

68. M. D. Ingram, J. Non-Cryst. Sol. (in press)

69. C. T. Moynihan and A. V. Lesikar, J. Non-Cryst. Sol. **38&39** (1980) 371.

70. M. D. Ingram, C. T. Moynihan and A. V. Lesikar, J. Non-Cryst. Sol. **38/39** (1980) 371.

71. D. Ravaine and J. L. Souquet, Phys. Chem.Glasses, **18** (1977) 27.

72. B. Movaghar, M. Grunewald, B. Bohlmann, B. Wurtz and W. Schirmacher, Symp.on Random Walks, Gaithersburg, Md.,June 1982.Plenum, (1983), p.315.

73a. J .C. Dyre, Phys. Lett. A. 1985 (in press).

73b. J. C. Dyre, 1985. (preprint).

74. A. Miller and E. Abrahams, Phys. Rev. **120** (1960) 745.

75. H. Bottger, V. V. Bryskin, and G. Y. Yashin, J. Phys. C **12** (1979) 3951.

79. P. R. Sorenson, T. Jacobsen, Solid State Ionics, **7** (1982) 75.

80. J. Fontanella, M. C. Wintersgill, J.P. Calame, F.P. Pursel, D.R. C. R. A. Catlow, A. V. Chadwick, G. N. Greaves, L.M. Moroney and M.R. Worboys, **9/10** (1983) 1107.

81. C.R.A. Catlow, A.V. Chadwick, G.N. Greaves, L.M. Moroney and M.R. Worboys, Sol. State Ionics **9/10** (1983) 1107.

82. R. Dupon, B.L. Papke, M.A. Ratner, and D.F. Shriver, J. Electrochem. Soc. **131** (1984) 586.

83. S. G. Greenbaum, Solid State Ionics **15** (1985) 259.

84. D. E. Fenton J. M. Parker, P.V. Wright, Polymer **14** (1973) 589.

85. M. Armand, Solid State Ionics, **9/10** (1983) 745, and references cited therein.

86. P.M. Blonsky, D.F. Shriver, P. Austin and H.R. Allcock, J. Amer. Chem. Soc. **106** (1984) 6854.

87 C. A. Angell, J. Phys. Chem., **70** (1966) 3988.

88 C. A. Angell, Aust. J. Chem., **23** (1970) 280.

89 C. A. Angell and R. D. Bressel, J. Phys. Chem., **76** (1972) 3244.

90. G. Adam and J. H. Gibbs, J. Chem. Phys. **43** (1965) 139.

91. B. L. Papke, M. A. Ratner, and D. F. Shriver, J. Electrochem. Soc., **49** (1982) 1694.

92. E. I. Cooper and C. A. Angell, Ambient temperature plastic crystal FICs, this volume.

93a. L. Borgesson and L. M. Torell, Phys. Rev. B **32** (1985) 2471.

93b. L. Borgesson and L. M. Torell, Reorientation time of SO_4^{2-} in Li_2SO_4, this volume.

Solid State Ionics 18 & 19 (1986) 570-576
North-Holland, Amsterdam

AMBIENT TEMPERATURE PLASTIC CRYSTAL FAST ION CONDUCTORS (PLICFICS)

E. I. COOPER * and C.A. ANGELL

Department of Chemistry, Purdue University, West Lafayette, IN 47907, USA

Polymer-salt type solid electrolytes are currently in favor because the electrolyte can change shape under mechanical stress without failure. A disadvantage, however, is that anion transport numbers are not zero. We think the former advantage can be had without the latter disadvantage by using an appropriate anion rotator phase in which the cation, or one of the cations, is mobile. Li_2SO_4 is the prototype material of this type but is limited to high temperature applications. We describe a low temperature material - a double salt of $LiBF_4$ and methoxyethyldimethyl ethyl ammonium - fluoroborate - which may conduct by the same mechanism as Li_2SO_4 since it exhibits a strong disordering transition at -90°C, and a relatively small entropy of fusion. At 75°C this substance conducts almost as well as the best polyethylene oxide + Li salt combination reported to date. Some variants on the structural theme and their properties and performance will also be described.

INTRODUCTION

A requirement of the electrolyte in a solid state battery, which is as important as its d.c. conductivity, is its ability to adhere to and maintain good ohmic contact with the electrode materials. It is primarily this property which has led to the choice of polymer solvent + salt solutions for developmental solid state battery systems,[1,2] despite their rather poor ambient temperature conductances.[3]

Polymeric materials can distort easily and recoverably because of the existence of many liquid-like degrees of freedom which allow their constituent particles to rearrange locally under deforming stresses. Larger scale plastic flow is inhibited by polymer chain entanglements. Another type of solid which is characterized by the existence of many liquid- like degrees of freedom is the plastic crystal. In these, the presence of relatively free rotation are of a fraction of the constituent particles, gives both a low elastic modulus and an ability to distort by local plastic flow involving molecular diffusion. It is therefore natural that effort be expended to find plastic crystalline materials in which ions of electrochemical interest such as Li^+ are rapidly diffusing. Such materials merit the acronym PLICFIC (Plastic Crystalline Fast Ionic Conductor).

One of the most impressive of the known PLICFICs is Li_2SO_4 in which the conductivity in the region immediately below the fusion point is of order 1 ohm^{-1} cm^{-1} and in which fusion is actually accompanied by a decrease in conductivity. This compound, extensively studied by the Chalmers group[4-6] and recently examined in molecular detail by molecular dynamics methods,[7] is thought to conduct via a coupled anion rotation-cation diffusion ("paddle wheel" or "revolving door") mechanism.[4-6] The material is remarkable for the number of liquid-like degrees of freedom which it

*Present address: IBM T.J. Watson Research Center, P.O. Box 218, Yorktown Heights, NY 10598

manifests, the center-of-mass order of the anion sublattice being the only crystalline structural characteristic which it retains.

The Li_2SO_4 FIC phase unfortunately becomes unstable below 500°C, and in any case, its conductivity extrapolated to the interesting temperature range 0-100°C is not of special interest ($\sim 10^{-6}$ ohm^{-1} cm^{-1}). Clearly what is desirable is a low temperature analogue of this type of material.

The appropriate route to such a material evidently will involve a reduction in the cohesive forces, hence a reduction in the anion charge. Indeed, considerable effort has been expended in the study of compounds such as $LiMCl_4$ [8,9] with this aim in mind. Phases with rotationally excited states of the tetrahedral anion appear to exist in $LiAlCl_4$ and $LiFeCl_4$ near the respective fusion points but are unstable at lower temperatures.

Further reductions in cohesive forces may be expected if large organic cations are introduced into the structure. An attractive possibility in such compounds is that plasticity may be enhanced by temperature-induced rotational disorder of quasi-ellipsoidal organic cations. We have described elsewhere [10] several tetraalkylammonium salts which exhibit the thermodynamic characteristics of plastic crystals. We have also found that Li salts frequently form 1:1 compounds with tetraalkylammonium salts. We were therefore quite prepared to find our first low-temperature "PLICFIC" among these compounds, although its discovery was somewhat accidental. While investigating the conductivity of a supercooled liquid in the system $LiBF_4$ + $CH_3OCH_2CH_2N^+Me_2EtBF_4^-$, the sample froze unnoticed and the conductivity measured was found surprisingly to be only slightly lower than that of the liquid. Our attention naturally turned to the 1:1 compound in this system, which was the main phase in the frozen mixture. In this paper we describe this compound (and a few others closely related to it) and express the hope that it may be the forerunner of a family of such materials, some of which may have useful applications in solid state electrochemical devices.

EXPERIMENTAL SECTION

Materials

$LiBF_4$ was obtained 98% pure from Alfa Inorganics. Since water was the main impurity it was dried in vacuo at 100°, under a BF_3 partial pressure slightly exceeding its own, which was supplied by a "sacrificial" portion of $LiBF_4$ (previously dried with slight decomposition) held at ca. 130°.

The various quaternary ammonium salts detailed below (Table 1) were prepared in 2 or 3 steps, following largely standard procedures:

a) Conversion of the commercially available chloroethyl methyl ether (or chloroalkane) into the iodide by refluxing with NaI in acetone.

(b) Reaction of the organic iodide (or of the original organic chloride) with a tertiary amine (NMe_3, NMe_2Et), in acetonitrile, in a pressure bottle (or, when the chloride was chloromethyl methyl ether - in dry ether with cooling), to form the quaternary ammonium halide. This was subsequently recrystallized from acetonitrile, ethanol or acetone by addition of anhydrous tetrahydrofuran or ether.

(c) Preparation of the quaternary ammonium tetrafluoroborate by addition of a stoichiometric amount of $AgBF_4$ (Ozark-Mahoning, 99%) as its 10% solution in acetone to a solution of the halide in acetonitrile or acetone. If solid at $T < 50$°C, the product was recrystallized from acetone or dichloromethane by addition of tetrahydrofuran or chloroform. Liquid salts were redissolved several times in dry tetrahydrofuran which was then evaporated in vacuo by rotary evaporator. Repeated extractions with chloroform were found helpful in the removal of most remaining halide from the liquid and lower-melting salts. A similar procedure, lead perchlorate in aqueous acetone replacing the silver salt, was followed to obtain the perchlorate (**3** in Table 1).

Purity of the products was checked by elemental analysis; in several cases the virtual absence of water

was ascertained by Karl-Fischer titration. (The elemental analysis of compounds **7** , **12** and **14** in Table 1 must be considered less than satisfactory, but DSC runs leave no doubt as to the distinct character of the compounds.) The tetrafluoroborate salts had the melting points included in Table 1.

To obtain the double salts with lithium tetrafluoroborate, perchlorate, or iodide, weighed quantities of the components were fused in a dry box at 120-150°C. The melting points of the double salts are included in Table 1. Attempts were also made to prepare tetrachloroaluminates and tetrachlorogallate double salts of the same type (see Discussion).

Thermal characterization.

The various phase transitions and melting points of the substances under study were determined using ~10 mg samples contained in sealed aluminum pans using the Perkin-Elmer DSC-4 differential scanning calorimeter. All runs were conducted at 20° min^{-1}

Table 1. Phase transitions of tetraalkylammonium salts and their lithium salt complexes.

No.	Compound	T_g [a,b]/°C	T_{tr}/°C(ΔH_{tr})[c]	T_m(ΔH_m)[c]
1	$MeOCH_2CH_2N^+EtMe_2\ BF_4^-$	-98	-	13(21.7)
2	$MeOCH_2CH_2N^+EtMe_2\ BF_4 \cdot LiBF_4$	-79	-79(3.9);62(1.7)	98(5.6)
3	$MeOCH_2CH_2N^+EtMe_2\ ClO_4$	-90	-	2 (14.7)
4	$MeOCH_2CH_2N^+EtMe_2\ ClO_4 \cdot LiClO_4$	-	26(0.8);40(1.2)[d]	124(6.6)
5	$MeOCH_2CH_2N^+EtMe_2I^-$	-52	-	47
6	$MeOCH_2CH_2N^+EtMe_2I^- \cdot LiI$	-6	-	104(4.4)
7	$MeOCH_2CH_2N^+Me_3\ BF_4^-$	-	-53(0.5)	64(20.9)
8	$MeOCH_2CH_2N^+Me_3\ BF_4 \cdot LiBF_4$	-61	-110(0.5);-78(2.1)	106(10.0)
9	Mixture 75% of 2 - 25% of 1	-74	-107(1)	83(7.0)
10	Mixture 50% of 2 - 50% of 8	-71	-133	83
11	Mixture 25% of 2 - 75% of 8	-65	-95(1)	89(8.4)
12[e]	$MeOCH_2N^+EtMe_2\ BF_4^-$	-115	-	-16(16.1)
13	$MeOCH_2N^+EtMe_2 \cdot LiBF_4$	-	-85(0.4);-22(0.7)	90(4.2)
-	-	-	10(0.9);27(0.8)	-
14	$MeOCH_2N^+Me_3\ BF_4^-$	-	-	46(12.6)
15	$MeOCH_2N^+Me_3 \cdot LiBF_4$	-68	-18; 12(1.2);40(1.1)	66(1.9)
16	$CH_3(CH_2)_3N^+EtMe_2BF_4^-$	-	-68(0.7);38(1.7)	158(3.6)
17	$CH_3(CH_2)_3N^+EtMe_2BF_4 \cdot LiBF_4$	-	-139(1.5);-45(0.2);	165(8.2)
-	-	-	34(0.8);79(.05)	

a - degrees °C; **b** - glass transition temperature (vitrification by liquid N_2 quench except for No. 6 which vitrifies in DSC at 320°/min); **c** - enthalpies of transition and of melting in cal/g; **d** - this compound also shows a complex pattern of low-temperature phase transitions, very history-dependent; **e** - the cation of this salt is apparently reported here for the first time.

heating rates. The heats of transformation were determined using the Perkin-Elmer software on the data station, using indium as a reference. Melting points are believed correct to $\pm 2^{\circ}C$, and transition enthalpies to $\pm 5\%$.

Electrical conductivity.

The electrical conductivities were determined on samples which were crystallized in a conductivity cell the design of which has been described elsewhere[11]. The cell constant was 0.327, the distance between the platinized electrodes (0.5 cm) prevented trapping of air bubbles between them. The state of the sample could be observed periodically since the cell is of Pyrex glass. The conductance was measured using a GENRAD Model 1689 Digibridge, operating in the frequency range 12 -10^5 Hz. Some problems were encountered with crystal-electrode contact which could be partly lost after quick cooling, especially during the initial crystallization from the melt. For compound **2** (see Table 1), cooling from 100° melt to R.T. at 15°/hr yielded results reproducible to within 5% at R.T. on second use. At lower temperatures, the annealing effects were more pronounced and the conductivities drifted upward; e.g., after cooling to $-24^{\circ}C$ the conductivity changed from 0.77×10^{-7} to 1.15×10^{-7} ohm^{-1} cm^{-1} over a period of 10 hrs. Frequency dependence of conductivity was negligible at and above room temperature. Although this study is preliminary in nature we believe the conductivities of this salt to be correct to within 5%, which is satisfactory given the number of steps involved in the total synthetic-purification-measurement series.

Reproducibility of conductivity results was poorer for the other salts (e.g., for **4** , σ drifted upward by 20% at R.T. over a month period) and the frequency dependence of conductivity was significant. Cole-Cole plots showed clearly the presence of extraneous effects (electrode contacts, grain boundaries).

RESULTS

The double salts prepared as described above in most cases appeared as translucent masses which, however, were not as soft to mechanical probing as might have been expected from the magnitude of the thermal transitions reported below. After passage through the phase transitions at low temperatures, the translucence was lost, but could be regenerated by refusion and crystallization. Microscopic examination of a sample of **2** inside the transparent conductivity cell revealed that the stress caused by the shrinkage on slow cooling from the melt did not result in separation between the sample and either the electrodes or the glass walls of the cell, but rather in formation of what seem to be thin, elongated bubbles. Since gas bubbles were practically absent from the melt, their rounded contours seem to testify to relatively rapid crack healing and partial sintering along grain boundaries formed during freezing. This is precisely the behavior expected from a mass of plastic crystals, and it is also consistent with the positive drift of conductivity with time. A sample of the analogous perchlorate complex (compound **4**) displayed a similar appearance. By contrast, a sample of **17** (in which the methoxyethyl group is replaced by the butyl group which is similar in size and shape but much more restricted in motion), shows a pattern of sharp, unhealed cracks and straight grain boundaries; it is also more hard and brittle and has a very low conductivity.

As seen in Table 1, there are significant differences in melting points between the tetrafluoroborates and iodides. Since the volume excluded by BF_4^- and I^- are only a little different, and since the packing in the salts must be determined primarily by the bulky cations, it would seem that the difference in melting points reflects differences in polarization energies rather than coulomb energies. The wealth of solid-solid phase transitions in the tetrafluoroborates and perchlorates, as opposed to the iodides, is probably related to the non-spherical symmetry of the BF_4^- and ClO_4^- anions.

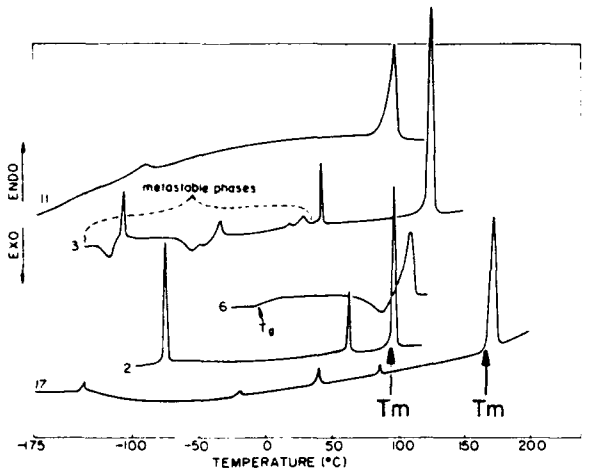

Fig. 1. DSC heating curves of some of the double salts listed in Table 1. All runs were performed after quenching from the melt at -320°/min. Note that only the double iodide **6** is glass-forming at this cooling rate, so only one glass transition is seen in Fig. 1. For the other compounds, except the perchlorate **3** , the heating curves of the quenched samples are similar to those of slow-cooled ones (not shown). Note that only the tetrafluoroborate **2** has a large net endothermic transition below room temperature.

The results of thermal characterization studies are shown in Figure 1. The important feature to be noted is the magnitude of the low temperature solid-solid transition enthalpies compared to the subsequent fusion enthalpies. Since the transitions are well separated in temperature, the **entropy** change in the low temperature transition is relatively more important than the enthalpy change, indeed ΔS for the low temperature transition in **2** is greater than the entropy of fusion.

Results of the conductivity studies are presented in Fig. 2 in the form of an Arrhenius plot which contains also various data points from earlier studies of materials of comparable technological interest.

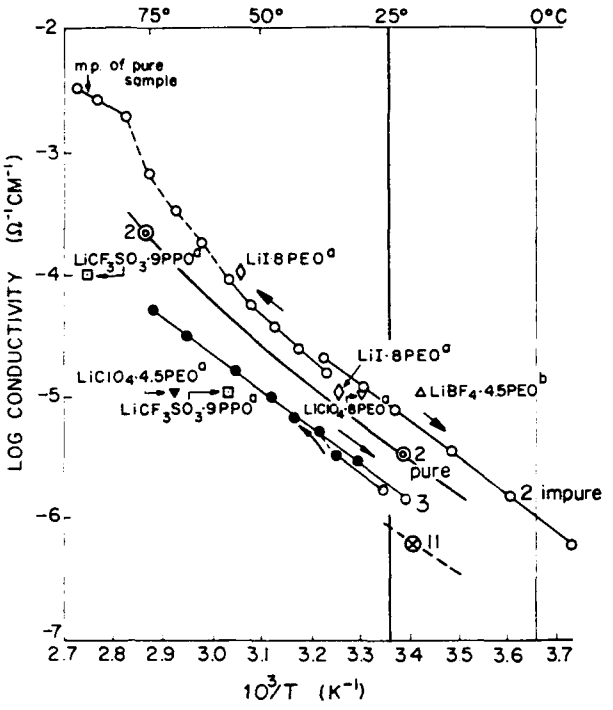

Fig. 2. Comparison of conductivities of some compounds described in this work with the best conductors published in the class of lithium salt-polymer complexes.

o - $MeOCH_2CH_2N^+EtMe_2BF_4$ $LiBF_4$ (compound 2), preliminary results

o - same, purified sample (< 0.05% H_2O)

2, 3, 11 - compound numbers from Table 1

a - ref 3.; b - ref 1.; the high conductivity of this sample was not reproduced and may have been due to partial decomposition (M. Armand, private communication).

"9PPO" 9 monomeric units of poly(propylene oxide)

"8PEO" 8 monomeric units of poly(ethylene oxide)

The arrows show the chronological order of measurements (heating from room temperature - left-hand segment - was done first).

DISCUSSION

Until the recent announcement of polyphosphazine-based polymer-salt "solid" electrolytes[3b], the present conductivities compared favorably with the best polymer-salt electrolytes available. Data published by Armand and co-workers on different occasions in the development of the polyether solvent based systems[1,3] are included in Figure 2.

We note that only one case, that of polyethylene oxide + lithium iodide, has a superior conductivity. The activation energies are comparable, as are the electrochemical stabilities, so that the relative merits of the two lithium-conducting systems must be decided on other issues. In this respect the following advantages of the PLICFIC-type of solid electrolyte should be emphasized.

Because the anions are located on the points of a crystal lattice[12], their diffusivity is necessarily small compared with that of the disordered Li^+ species, so the transport number of Li^+ should be close to unity. This compares favorably with the situation in the polymer electrolytes in which estimates of the transport numbers of the anions range between 0.1 and 0.6,[3b] but in no instance are zero. Finite transport numbers for the anions lead to a distinct decrease in electrochemical efficiency, and thus it is probable that the PLICFIC-type electrolyte is preferable in principle. We should, however, make the cautionary note that anion mobility has been observed in crystalline quaternary ammonium bromides[13], though the conductivities remain some three orders of magnitude below the present values at the comparable temperatures. Also it seems unlikely that an asymmetric ion like BF_4^- could diffuse with the ease of a bromide anion.

The principal advantage of polymer-based systems is their ability to deform under mechanical stress, and thus to adjust to changes in electrode volume. Although the plasticity of the solid electrolytes we describe here has not been quantitatively evaluated at this time, the expectation is that in optimized cases, the ability to deform under stress will approach or exceed that of lithium sulfate in its FIC phase which is almost waxy, in its behavior. The rheological properties of Li_2SO_4 have been studied using penetration viscometry techniques[14], and these methods will be applied to the present systems in future work.

The question now becomes one of improving on the properties of the methoxy-ethyl dimethyl ethylammonium tetrafluoroborate based double salt **2** which was the first prepared in this study. We have sought to increase the solid-solid transition enthalpy, with the possibility of both thermodynamical and kinetic improvements in mind. Thermodynamically, a higher ΔH_{tr} is likely to result in a increased entropic stabilization of the plastic phase, hence a higher melting point, thus widening the useful temperature range of the PLICFIC. Kinetically, one would expect the lower melting enthalpy to be accompanied by higher solid state plasticity and faster ion reorientation rates at ambient temperature, hence improved conductivity. To this end we have followed three lines of investigation, none of which have so far yielded the sought-after results.

(a) In the first place we have reduced the asymmetry of the head group by replacing the ethyl side chain by a third methyl in the hope of improving the rotational freedom of the cation, (to which it is reasonable to expect the rotational freedom of the anion to be related). This was done using two different tail groups, methoxy-methyl and the original methoxy-ethyl. The size-reduction of the organic ion by one or two CH_2 groups was expected to raise the melting point. In all these cases, however and also for some mixtures of the compounds, the low-temperature transitions were smaller in magnitude and no significant gain in melting point was obtained. Lower melting enthalpies were obtained in two cases, **13** and **15** , however, and these compounds merit further work. **15** in particular should be pursued since the entropy of fusion is characteristic of a true "plastic" crystal. The conductivity of a mixture of two compounds entry **11** in Table 1 was measured and found to be almost an order of magnitude lower than that of our best compound.

(b) As a second variation we retained the original head group but replaced the methyloxyethyl tail group by an equally long alkane group (**17** in Table 1). This also led to a decreased conductivity. It seems probable that the ether group plays a role in the easy migration of the Li^+, possibly by providing

a modified energy barrier between most favored Li^+ sites.

(c) A third approach was to try to improve plasticity, and possibly to decrease activation energy for conduction, by replacing the BF_4^- ion with larger complex ions. To this end we prepared some of the tetrachlorogallates of the quaternary cations listed in Table 1 (preparation of the tetrachloroaluminates failed because of the high reactivity of $AlCl_3$ towards the ether oxygen). We were encouraged to find some extremely soft plastic crystals in this group. Preparation of their complexes with $LiGaCl_4$ or $LiAlCl_4$ failed, however, because of incomplete dissolution of the lithium salts in the melt, and of considerable decomposition. Preliminary results seem to indicate that analogous silver-based compounds, with plastic characteristics, exist. This approach seems sound in principle and warrants further work.

Thus while the potential of the PLICFIC material is established by the data of Figure 2, it is not clear at this point how to proceed from the promising to the superior material. A possible synthetic improvement to this could be the replacement of the ether oxygen in the organic cation with sulfur, since thioethers are known to be much more resistant to Lewis acid attack than ethers[15] and are also more conformationally labile[16]. While sulfur would probably be less effective than oxygen in solubilizing Li^+, it may be very effective with softer cations (Ag^+, Cu^+). We should emphasize that it is not yet established that the conductance mechanism involves the coupling of cation motion to the anion rotations (paddle wheel mechanism) as suggested for Li_2SO_4.[4,6] One of the features of the latter material which indicates the paddle wheel mechanism is that not only the Li^+ but other cations, including divalent cations which are doped into the host structures, exhibit unusual mobilities. We have yet to test the present PLICFICs for such interesting and diagnostic behavior. Solid state ^6Li and ^{11}B NMR studies on compound **2** , which suggest that the anions are rotating rapidly above 60 - 70°C and that the Li^+ cations are mobile will be reported in a separate paper[17].

ACKNOWLEDGEMENTS.

We are grateful to the Office of Naval Research for support of the initial stages of this research under Agreement No. 84K0289, and to the Department of Energy with whose support the later work was performed, under Grant numbers DE-AGo2-83ER45044 and DE-FG02-84ER45102.

REFERENCES

1. M. B. Armand, J.M. Chabagno, M.J. Duclot, in "Fast Ion Transport in Solids" Ed. J. N. Mundy, G. K. Shenoy, Pergammon Press, N.Y. 1979, 131.
2. J. Jensen, A. Levasseur, and B.C.H. Steele, 7eme Symposium International du Vehicule Electrique Routier, Versailles, July 1984.
3a. M. B. Armand, Solid State Ionics **9 & 10** (1983) 745.
3b. P. M. Blonsky and D. F. Shriver, J. Amer. Chem. Soc. **106** (1984) 6854.
4. R. Aronsson, B. Jansson, H. E. G. Knape, A. Lunden, L. Nilsson, C. A. Sjoblom, and L. M. Torell, J. de Phys. Colloq. C6, **41** (1980) 6.
5. R. Aronson, H. E. G. Knape, and L. M. Torell, J. Chem. Phys. **77** (1982) 677.
6. L. Borgesson and L. M. Torell, Phys. Rev. B. **32** (1985) 2471.
7. R. W. Impey, M. L. Klein and I. R. McDonald, J. Phys. C. Solid State Phys. **17** (1984) 3941.
8. W. Weppner and R. A. Huggins, J. Electrochem Soc. **124** (1975) 35, Phys. Lett. **58A** (1976) 245, Solid State Ionics **1** (1980) 3.
9. M. Spiesser, P. Palvadean, C. Guillot, J. Cerisier, **9 & 10** (1983) 103.
10a. C. A. Angell, L. E. Busse, E. I. Cooper, R. K. Kadiyala, a. Dworkin, M. Ghelfenstein, H. Szwarc, and A. Vassal, J. Chim. Phys. **82** (1985) 268.
10b. E. I. Cooper, and C. A. Angell, (to be published).
11. E. I. Cooper and C. A. Angell, Solid State Ionics **9/10** (1983) 617.
12. The BF_4^- are not even rapidly rotating on the NMR time scale below≃ 60°C according to current solid state NMR studies by F. Taulelle (private communication).
13. J. Shimizu, T. Nogani and H. Miquawa, Solid State Comm. **54** (1985) 1009. Solid State Ionics **14** (1984) 153.
14. B. Jansson and C. A. Sjoblom, Rheol. Acta, **16** (1977) 628.
15. L. Braudsma and J. F. Arens, in "The Chemistry of the Ether Linkage", Interscience, 1967; Saul Patai, ed.; pp. 583-585.
16. See for example H. Matsuura, I. Harada, T. Shimanouchi, Proc. Int. Conf. Raman Spectrosc., 5th, 1976, 40-1, Chem. Abst. **88** 6197.
17. F. Taulelle, E. I. Cooper, and C. A. Angell (to be published).

MATERIALS FOR SOLID STATE BATTERIES, pp. 31-38
edited by B. V. R. Chowdari & S. Radhakrishna

Glassy Solids and dc Conductivity in the Liquid and Glassy States

C. A. Angell
Department of Chemistry
Purdue Univeristy
West Lafayette, IN 47907

INTRODUCTION

Three major classes of materials are currently under consideration as possible solutions to the problem of developing suitable ion conducting membranes for use in solid state electrochemical technology. They are (i) crystalline solids (ii) glassy solids and (iii) high-polymer + salt solutions. The following lectures are devoted to the discussion of the second of these classes. We give a review of the features which lead to high ionic conductivities in the glassy state and describe some characteristics of the conduction mechanism in such materials.

1. Glass Formation and the Glassy State

To have a suitable basis for the discussion of the phenomenon of fast ion conduction in disordered solids it is first necessary to have an understanding of the nature of the glassy state itself and how it is produced.

There are many ways of obtaining amorphous solids and only sometimes do the products deserve classification as "glasses". The most general of manner of producing glassy solids is by the cooling of the liquid state under conditions where crystallization does not occur.[1,2] When the interparticle forces are sufficiently large, the viscosity of such a liquid will increase to such large values before room temperature is reached that a material which is mechanically in the solid state is obtained. The transition from the liquid to the glassy state is generally considered to occur when the time for relaxation of a mechanical stress becomes of the order of minutes or greater. This condition corresponds to viscosities of 10^{11} poise or greater.

The transition from the liquid to the glassy state is not a sharp phenomenon, since the process is a relaxation controlled by the kinetics of diffusion. The "glass transition" is characterized by a decrease in thermodynamic intensive properties (such as the heat capacity or thermal expansivity) occurring over a temperature interval of some 20 -50 degrees depending on the particular structural characteristics of the liquid. The phenomenon is illustrated in Fig. 1 of which part (a) shows the glass transition for the popular fast ion conducting glass $60AgI.40Ag_2WO_4$. Part (b) compares the phenomenon for a variety of glasses of different structure type using a cal/K/g atom basis for the y-axis and the temperature of the glass transition as a scaling parameter for the temperature–axis.[3] Clearly the relative change of heat capacity can vary greatly from one substance to another.

The same phenomenon may be observed for many amorphous materials which have been deposited from the vapor state. Depending on the particular chemicals involved the glass transition observed for vapor deposits may be found at the same temperature as for the melt cooled glasses or at some lower temperature reflecting the more molecular nature of some deposits. In the latter cases the glass transition can usually be observed to return to its normal value on sufficient annealing.[4] Vapor deposition or sputtering offers a means of obtaining amorphous solids in composition regions where the kinetics of crystallization are too fast to permit glass formation by the normal melt cooling method.

2. Mobility Decoupling and Fast Ion Glasses

Fortunately for the field of solid electrolytes not all the particles in the material suffer this great decrease of mobility as temperature is decreased. In many cases a subset of the ions, which may be either cations or anions depending on the system under consideration, may show much smaller temperature coefficients of their mobility. When the glass transition temperature is reached, may still be diffusing only one or two orders of magnitude less rapidly than they were in the mobile liquid state. This behavior is at variance with the expectations from one of the best known equations for describing the diffusivity of one molecular species moving in the medium of itself or some solution containing it, viz. the Stokes-Einstein equation

$$D_i = kT/6\pi\eta r_i$$

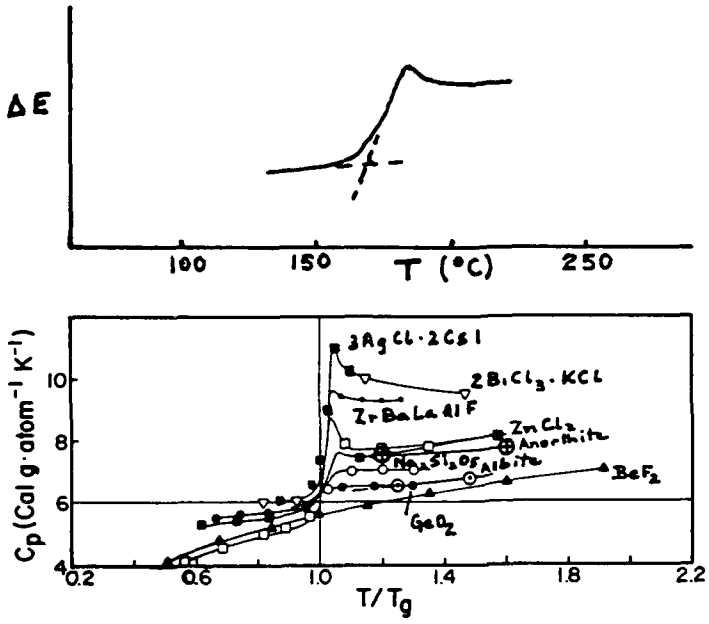

Figure 1. The glass transition phenomenon, according to specific heat measurements (a) for $60AgI{\cdot}40Ag_2WO_4$ (b) comparison of different systems.

where D_i is the diffusion coefficient of species i, r_i is its radius, and η is the liquid viscosity. The Stokes Einstein equation is based on the notion that the frictional force impeding the movement of a particle in the liquid state is a viscous force established by all of its neighbors. For a solid electrolyte to be interesting as a potential battery component, the Stokes-Einstein equation must fail by some 12 orders of magnitude between the high temperature region and the glass transition.

A way of demonstrating the progressive breakdown of the Stokes-Einstein equation is to compare the relaxation times for shear and electrical stresses on the medium over a wide range of temperature. The relaxation times may be defined, following Maxwell, as the ratio of the common transport parameters viscosity and dc conductivity, to the respective elastic properties of the immobile medium namely, the high frequency shear modulus G_∞, and the M_∞ the the inverse of the high frequency dielectric constant, Σ_∞a better known quantity. The latter two quantities are known from experimental studies of the glassy state at almost any frequency, and from high frequency studies in the liquid state. Without devoting further detail to these quantities we show in Fig. 2 the temperature dependence of the shear and conductivity relaxation times for two substances where sufficient data in the liquid, as well as glassy states are available. One of these is 35 $Na_2O{\cdot}65B_2O_3$, one of the classical oxide glasses, in which the sodium ion is relatively mobile in the glassy state. The other is a recently developed all-halide glass in which the silver ions are highly mobile. Fig. 2 shows how the relaxation time for electrical stresses retains its high temperature characteristics irrespective of the highly non-Arrhenius behavior of the viscosity which leads the system into the glassy state at 350°C and 20°C, respectively.

The ratio of the shear relaxation time to the conductivity relaxation time at the glass transition can be taken as a measure of the extent to which the fast ion diffusive modes are decoupled from the viscous modes at the temperature where the glass structure is arrested.[6] This ration or decoupling index can vary from unity for some glasses which are not of interest to this study, to values as high as 10^{14}.[7] Clearly a high decoupling index is a requirement of a good solid electrolyte glass. In Table 1 we summarize our relevant data for a variety of different glass compositions.sp

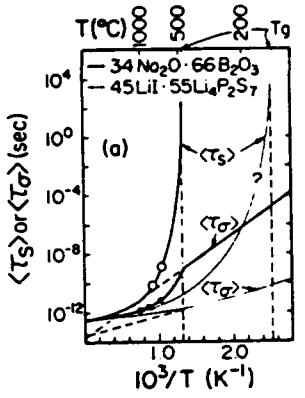

Figure 2. Demonstration of the decoupling of conducting from viscous modes by comparison of relaxation times for electrical and shear stresses.

Table 1. Decoupling indexes $R\tau = \tau_s/\tau_\sigma$ for various fast ion conducting glasses at their T_g.[7]

No.	System	σ_{25} Ω^{-1} cm^{-1}	T_g K	σ_{T_g} Ω^{-1} cm^{-1}	$\tau_{\sigma(T_g)}$ sec.	$R_{\tau(T_g)}$
1	75 AgI · 25 Ag_2MoO_4	$13{\cdot}6\times10^{-3}$	325	2.8×10^{-2}	3.8×10^{-11}	5.3×10^{12}
2	73 AgI·20 Ag_2MoO_4· 7 $Ag_2Mo_2O_7$	22.4×10^{-4}	344	9.08×10^{-2}	11.7×10^{-12}	1.7×10^{13}
3	20 AgI·80 (Ag_2O·B_2O_3)	1.5×10^{-5}	603	2.2×10^{-2}	4.73×10^{-11}	$4{\cdot}23\times10^{12}$
4	80 AgI·20(Ag_2O·B_2O_3)	3.1×10^{-2}	483	$38{\cdot}0\times10^{-2}$	$2{\cdot}8\times10^{-12}$	$7{\cdot}15\times10^{13}$
5	66.7 AgI 25 Ag_2O 8·3P_2O_5:(AgI-Ag orthophosphate)	1.5×10^{-2}	323	$2{\cdot}47\times10^{-2}$	$4{\cdot}30\times10^{-11}$	$4{\cdot}\times10^{12}$
6	65 AgI·23·3 Ag_2O 11.7 P_2O_5 (AgI-Ag pyrophosphate)	2.0×10^{-2}	321	$2{\cdot}96\times10^{-2}$	$3{\cdot}59\times10^{-11}$	$5{\cdot}57\times10^{12}$
7	50 AgI·25 Ag_2O·25 P_2O_5 (AgI-Ag metaphosphate)	5.0×10^{-3}	337	$1{\cdot}25\times10^{-2}$	8×10^{-11}	$2{\cdot}35\times10^{12}$
8	35 AgCl·45 AgI·20 CsCl	$4{\cdot}7\times10^{-2}$	259	$1{\cdot}26\times10^{-2}$	$8{\cdot}44\times10^{-11}$	$2{\cdot}37\times10^{12}$
9	36 GeS_2·24 Li_2S·40 LiI	1.0×10^{-4}	499	$18{\cdot}51\times10^{-2}$	$5{\cdot}74\times10^{-12}$	$3{\cdot}48\ 10^{13}$
10	($Na_{3.75}Zr_{1.1}Si_{2.75}P_{0.25}O_{10.2}$) NaSiglass	1.9×10^{-3}	1035	$5{\cdot}2\times10^{-1}$	$1{\cdot}53\times10^{-12}$	$1{\cdot}30\times10^{14}$

Solid Electrolyte Systems

An enormous number of different inorganic, and some organic, glassy systems have been found to exhibit high to very high electrical conductivity in the glassy state. We will not attempt to review them all here. Rather, some examples illustrating the chemical principles involved will be used.

The most extensive observations have been made on the classical alkali oxide + glassforming oxide (SiO_2, B_2O_3, P_2O_5, GeO_2) which have been under study for many decades. Except for peculiarities near the pure glass former composition (particularly in the cases of B_2O_3 and GeO_2) the general observation is that the ionic conductivity increases exponentially with mole fraction of alkali oxide. The highest conductivities are almost always encountered at the limit of glass formation on the alkali-rich side of the binary system.

Increases beyond the limits of binary oxides can be obtained in several ways. The most successful is to add an alkali halide to one of the stronger glassforming compositions in the binary system. A widely studied system of this type is $Li_2O{\cdot}2B_2O_3$ + Li halide. The second route to increasing the conductivity is to replace some or all of the oxide ions with sulfide ions.[8] The more polarizable sulfide ions apparently provide low energy pathways for the migration of alkali ions. The largest alkali ion conductivity so far reported has been made in the system combining both these principle viz. $Li_2P_2S_7$ + LiI studied by Malugani et al.[9] An important function of these latter chemical substitutions seems to be the lowering of the glass transition temperature to values closer to room temperature. For instance, the system with the largest cation matrix decoupling index on record, NaSiglass,[7,24] is actually only a moderately good conductor at room temperature because the glass transition temperature is so high. Thus high conductivity requires a combination of mobility decoupling at T_g, and low T_g. Some of these relationships are depicted in Fig. 3.

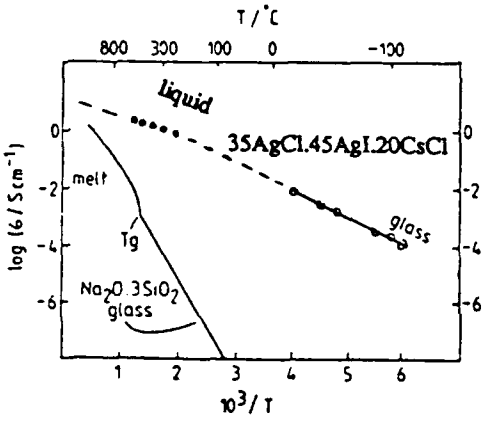

Figure 3. Comparison of Ag^+ fast ion conducting glass and liquid states with corresponding behavior of classic alkali oxide glass system.

Even higher conductivities may be found in glassy solids if alkali ions are replaced with the more polarizable group 1A atoms, Ag^+ and Cu^+.[10,11]

A new type of superionic glass in which there are no Lewis acid cations (highly charged species) such as Si(IV) P(V), has recently been described by Liu and Sundar[0] from the author's laboratory. In these, the framework supporting the motion of the fast cation is based on the large-ion combination $Cs^+ + I^-$. These systems are vitreous analogs of the well known crystalline conductor $RbAg_4I_5$ and would be very interesting materials except for the low glass transition temperatures they exhibit.

The relative merits of these different systems are summarized in Fig. 4 taken from a recent review paper based on data accumulated by Minami.[10] Greater detail on these systems and their properties may be found in references 7 and 12.

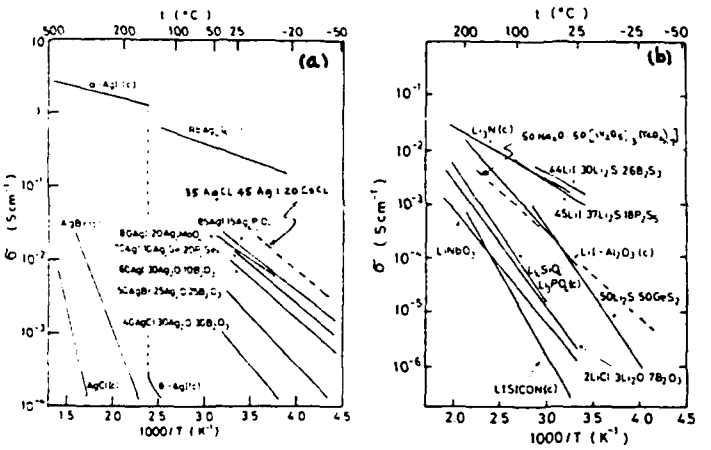

Figure 4.
Arrhenius plot of conductivities of various Ag^+ and Li^+ conducting systems (after Minami[15]) including two recent high conducting systems (one of them an Na^+ conductor.) See dashed lines.

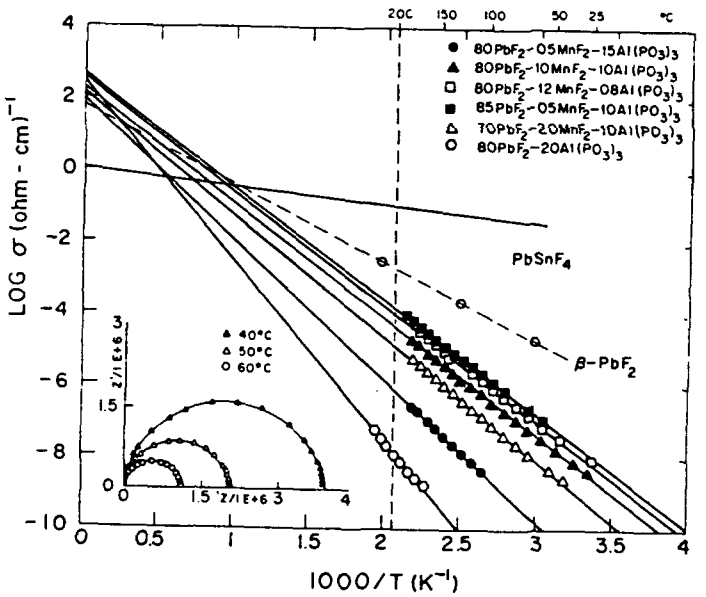

Figure 5. Arrhenius plot of d.c. conductivity of fluoride ion conducting glasses specified in legend. Insert shows typical complex impedance plots from which σ was obtained.

Some very recent studies have shown that conductivities rivalling the alkali conductivities described above can be obtained in fluoride-based systems. In these the conductivity is due to mobile fluoride ions. The best examples appear to be those containing high mole fractions of lead fluoride,[13,14] but the studies are too recent for all the promising possibilities to have been examined. Some results from the author's laboratory are

contained in Fig. 5. The consequent possibility of producing glass forming systems in which the main current carrier changes from anion to cation with composition changes has been demonstrated in studies by Sun etal,[15] and Kulkarni.[16]

4. Conductivity Mechanisms and Structure

The fact that the fast ion conducting glasses in a majority of cases exhibit Arrhenius temperature dependences with attempt frequencies on the vibrational timescale (discussed further in the next paper) suggests that the conductivity process can be interpreted in terms of a simple "rattle and jump" mechanism. The question of interest concerns the nature of the medium in which the jumps are occurring. On this matter there are different schools of thought. The most general belief, expressed for glasses containing large mole fractions of halide salts, is that the conduction pathways occur within microregions enriched in the halide[17,18]- a type of incipient liquid-liquid phase separation. Small angle scattering studies[19] have in fact indicated the presence of microheterogeneities of the order of 20Å in diameter. This seems reasonable since it is known that at sufficiently large halide contents the liquids become immiscible. At the metastable miscibility gap edge, presumably, the phenomenon of clustering must occur. This is a question which should be answerable by solid state NMR on ^{109}Ag.

Some insight into the behavior of simpler systems has been gained from studies using the techniques of computer simulation. Ion dynamics studies have been carried out on several compositions e.g. $Na_2O{\cdot}3SiO_2$[20] and Li_4SiS_4[21] and "$Ag_2O{\cdot}B_2O_3$".[22] These results show that in the alkali silicate case the conduction pathways are limited in number and occur along the lines of high concentrations of nonbridging oxygens.[20] Studies in which the mass of the vibrating particles has been artifically manipulated suggested that the barriers in migration are determined by the bridging rather than by the nonbridging oxygens. A model incorporating this observation and distinguishing between the energy barriers discriptive of strong electrolyte versus weak electrolyte conductivity behavior has recently been given by Martin and the author.[23] The main ideas are conveyed by Fig. 6 taken from the latter article.

In the case in which all the anions are nonbridging in character, the number of pathways is greatly increased and the conduction mechanism becomes more closely akin to that described to the system AgI by investigators of crystalline state conductors. Again the mechanism involves high frequency attempts resulting in strong absorption in the far IR region of the electromagnetic spectrum (see next paper) but in this case no specific channel structure is observed. Rather, conduction can occur at all points in the structure.

Computer simulation studies, unfortunately, can only describe the behavior at extremely high ion mobility conditions which are usually only encountered in the liquid state of these materials. However there is reason to believe the laboratory glass mechanisms are closely akin to those revealed by simulation studies.

For greater detail on the conduction mechanisms in the experimental substances it is necessary to extend the study of conduction process to include frequency dependent investigations. These and related studies are reviewed in the next paper. (abstract only - see refs 6. and 7.)

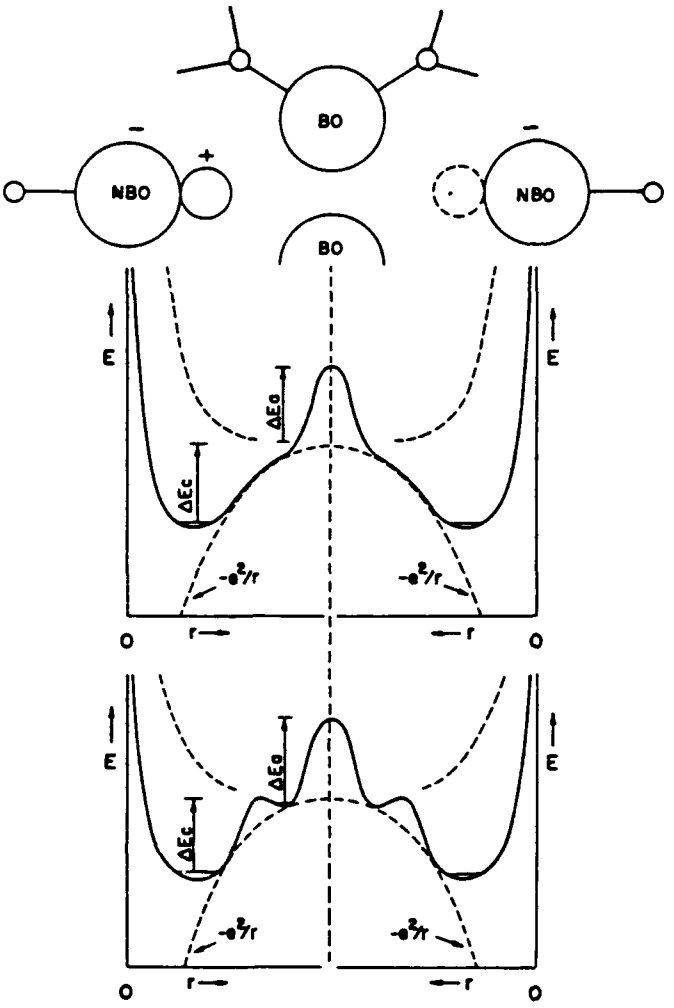

Figure 6. Representation of the energetics of cation conducting process, according to strong electrolyte (Anderson-Stuart model) and weak electrolyte (WE) concepts. To highlight the relationships the promotion energy in the latter case is assumed to have the same electrostatic origin as the Coulomb term in the A-S model. the structural origin of the subsidiary barriers in the weak electrolyte model is left undefined. The short-range repulsive contribution is assumed, following molecular dynamics experiments to be due to 'gate passing' between bridging oxides as sketched in the simplified microstructure model at the top.

ACKNOWLEDGEMENTS

This work has been supported by the Department of Energy under Grant No. 84ER45102 and by the Office of Naval Research under Grant No. N00014-84-K-0289. The author is grateful to his coworkers M. McLin, and H. Senapati for permission to incorporate some of their recent data on $Ag^{+}Cs^{+}I^{-}Cl^{-}$ glasses and liquids in advance of publication.

REFERENCES

1. "Chemistry of Glasses", A. Paul, Chapman and Hall (1982) Chapter 1. 293.
2. C. A. Angell, L. E. Busse, E. E. Cooper, R. K. Kadiyala, A. Dworkin, M. Ghelfenstein, H. Szwarc, and A. Vassal, J. de Chim. Phys. 82, 267 (1985).

3. (a) M. A. DeBolt, A. J. Easteal, P. B. Macedo, and C. T. Moynihan, J. Am. Ceram. Soc. 59, 16 (1976).
   (b) A.Barkatt and C. A. Angell, J. Chem. Phys., 70 (1979) 901.
4. C. A. Angell in "Relaxations in Complex Systems" ed. K. Ngai and G. B. Wright, National Technical Information Service, U. S. Department of Commerce, Springfield, VA 22161 (1985) p. 1.
5. (a) P. C. Taylor, Ann. N. Y. Acad. Sci. publication from Conf. on "Structure and Mobility in Atomic and Molecular Glasses", New York, 1981.
   (b) G. N. Papatheodorou, and S. A. Solin, Phys. Rev. B., 13, 1741 (1976).
6. C. A. Angell, Solid State Ionics, 9 & 10 (1983), 3.
7. C. A. Angell, Solid State Ionics, 18 & 19, 72 (1986).
8. J. L. Souquet, Solid State Ionics, 5 (1981) 77.
9. (a) J. P. Malugani, A. Wasniewski, M. Doreau, G. Robert and A. Al Rikabi, Mat. REs. Bull. 13, 427 (1978).
   (b)2 G. Robert, J. P. Malugani, A. Saida, Solid State Ioncs 3-4 91981) 311.
10. T. Minami, J. Non-Cryst. Sol. 56 (1983) 15.
11. (a) C. Liu and C. A. Angell, Solid State Ionics 13, 105 (1984).
   (b) Changle Liu, H. G. K. Sundar, and C. A. Angell, Mat Res. Bull.20 , 525 (1985)
12. T. Minami, J. Non-Cryst. Sol., 73 (1985) 293.
13. A. R. Kulkarni and C. A. Angell Mat. Res. Bull. (1986).
14. J. E. Shelby and A. E. Lewis, and A. Van DeBogart, (to be published).
15. Hong Wei Sun, B. Tanguy, J. M. Reau and J. Portier, (preprint).
16. A. R. Kulkarni, (unpublished work)
17. J. P. Malugani and R. Mercier, Sol. State Ionics 13 (1984) 293.
18. S. W. Martin and A. Schiraldi, J. Phys. Chem. 89 (1985) 2071.
19. M. Tachez, R. Mercier, J. P. Malugani, and A. J. Dianoux, Inst. Laje-Langevin Exp. Rep. 2 (1985) 278.
20. C. A. Angell, L. Boehm, P. A. Cheeseman and S. Tamaddon, Solid State Ionics, 5, 659 (1981).
21. C. A. Angell and Sina Tamaddon (unpublished work - see ref. 7).
22. M. C. Abramo, G. Pizzimenti and G. Carini (preprint).
23. S. W. Martin and C. A. Angell, J. Non-Cryst. Solids, 1986 (in press).
24. S. Susman, C. J. Delbecq, J. A. McMillan, and M. F. Roche, Solid State Ionics, 9&10, 667 (1983).

Materials Chemistry and Physics, *23* (1989) 143–169

CORRELATION OF MECHANICAL AND ELECTRICAL RELAXATION PHENOMENA IN SUPERIONIC CONDUCTING GLASSES

C.A. ANGELL

Department of Chemistry, Purdue University, West Lafayette, IN 47907 (U.S.A)

ABSTRACT

The phenomenon of mechanical and electrical relaxation due to fast diffusing ions in glasses is placed in the context of relaxing dipolar and ionic liquids, and observations made at constant temperature are compared with those made at constant frequency. With this background several questions provoked by the apparent relation between mechanical and electrical responses are posed and answered within the limitations of currently available experimental data. Comparisons of average relaxation times, and of widths and shapes of relaxation spectra, are made. Finally, we present unifying plots which relate relaxational to vibrational responses for both electrical and mechanical stresses, the latter, we believe, for the first time.

INTRODUCTION

Fast ion conduction in certain glassy materials is made possible by the decoupling, during vitrification, of the diffusive motions of a subset of ionic particles from those of the majority species which freeze out at T_g [1]. In the absence of decoupling, electrical and mechanical relaxation phenomena, which depend on diffusive motions, occur on almost the same timescale as seen in Figs. 1 and 2 which we discuss briefly by way of introduction.

In dipolar liquids such as glycerol (illustrated in Fig. 1) the quantities to be compared are the complex dielectric susceptibility ϵ^* and the complex isothermal compressibility κ_T^* ($\kappa_T^* = 1/K$, K is the bulk modulus) since both have finite values above and below the

0254-0584/89/$3.50

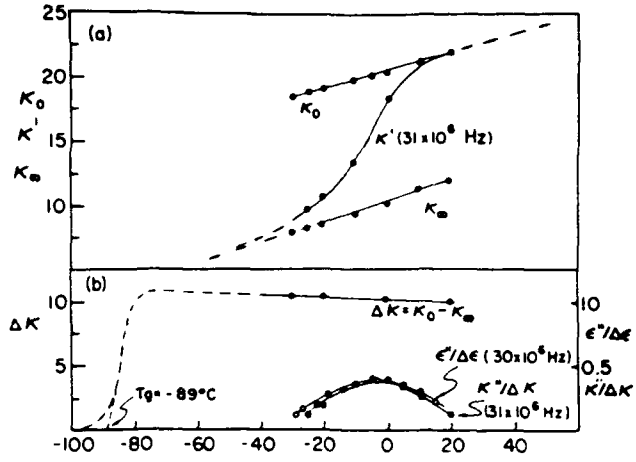

Fig. 1. (a) Illustration of the dispersion in temperature of the mechanical susceptibility (bulk compressibility κ') measured at constant frequency for the case of liquid glycerol. κ_0 is the static (or liquid-like) compressibility and κ_∞ the glass-like compressibility.
(b) Difference between static and high frequency compressibility for glycerol showing its disappearance at the glass transition temperature, and comparison of the imaginary part of the compressibility and dielectric susceptibility (reduced by the respective dispersions, $\Delta\kappa$ and $\Delta\varepsilon$).

relaxation [2]. Figure 1a shows [3] the dispersion in the compressibility κ_T' (the real part of κ^*) which *increases* as the system becomes mobile enough, with increasing temperature, to follow the cyclic compressional stress. This is the high frequency mechanical analog of the increase in (zero frequency) heat capacity (thermal response) observed on heating through the glass transition. Figure 1b shows the corresponding zero frequency behavior of the compressibility increment $\Delta\kappa_T$, and the imaginary (out of phase) part of the compressibility κ_T'' which shows a maximum corresponding with the rise in the real part. The corresponding *electrical* quantity, the dielectric loss ϵ'', shows a maximum at essentially the same temperature [3], (see Fig. 1). The relaxation time (most probable value) is given by

$$\tau = 1/2\pi f \qquad (1)$$

where f is the frequency of maximum loss in Hz. $\Delta\kappa$ (= κ_0–κ_∞) and $\Delta\varepsilon$ (= ε_0–ε_∞) measure the extent to which the liquid polarizes (displaces) in response to unit applied field.

In the case of a *conducting* liquid in which the ionic motions remain fully coupled to the viscous modes, the same correlation of electrical and mechanical relaxations may be observed, except that the data must now be cast in the electrical modulus formalism $M^* = 1/\epsilon^*$ in order to avoid dominance of ϵ'' by the DC conductivity at low frequencies [4]

(or at high temperatures for a constant frequency scan). The correct mechanical analog is now the complex shear modulus G^* the real part of which, like the real part of the electrical modulus, vanishes above the relaxation. An example is the case of lithium chloride in water illustrated in Fig. 2 [5, 6]. In such cases the moduli measured under *static* conditions during continuous cooling will *both* increase to glasslike values in the same temperature interval about T_g as the system becomes non-ergodic. The expectation for the static shear modulus (which has only been measured at a constant 88 MHz, see Fig. 2) during cooling at 10 deg/min is shown as a dashed line in Fig. 2. The imaginary part G″ is not available for comparison with the electrical loss in M″ at the same frequency (as in the case of glycerol, Fig. 1) but the temperature at which the maximum in G″ measured at 1 MHz would be reached can be estimated closely from the known shear relaxation time τ_s *vs.* temperature relation [6], and is shown as an arrow. ($f_{m(G'')} = 10^6$). It is clear that the two processes bear a close relationship as in the case of glycerol.

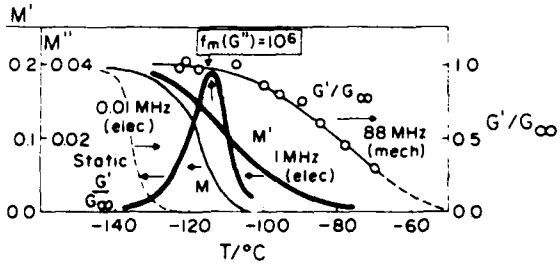

Fig. 2. Temperature dependence of the real and imaginary parts of the electrical modulus measured at 1 MHz (thick lines) [5] compared with the values of the normalized shear modulus measured at 88 MHz [6]. Also shown are the electrical modulus at 0.01 MHz, and an estimated plot for both shear and electrical moduli measured statically during continuous cooling at 10 deg/min. To show the close relation of mechanical and electrical moduli in this system, the point in temperature at which the maximum in G″ measured at 1 MHz would occur is shown by an arrow.

In contrast with the above, when one of the ionic species is relatively mobile, the real part of the electrical modulus M′ during cooling remains zero in the region of temperature in which the shear modulus G′ increases to a glass-like value. M′ instead exhibits its increase at a lower temperature which is determined by the condition that the electrical relaxation time becomes comparable with the cooling rate. At this temperature a further dispersion in the mechanical modulus is seen [7, 8], due to the fact that stress can be relaxed within the glassy matrix by a local relocation of the mobile ions, see Fig. 3. The loss of this relaxation leads to the additional ~ 10% increase in the shear modulus in the case of $Na_2O{\cdot}3SiO_2$ glass seen in Fig. 3. This is the first of a number of instances we will show

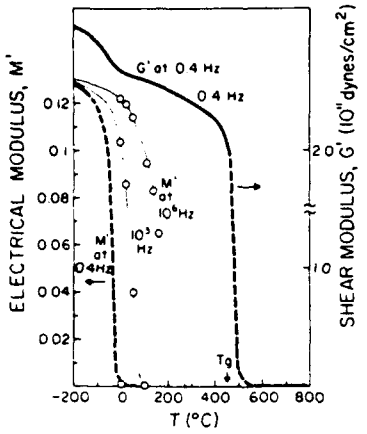

Fig. 3. Shear modulus and electrical modulus for sodium trisilicate glass from the liquid down through the region of the mobile ion (Na^+) relaxation, showing the second step in the mechanical modulus, and its coincidence with the primary electrical modulus increase. (Based on data from Day [8] for G' and Provenzano et. al. [28] for M', reproduced by permission).

of the correspondence in timescales of mechanical and electrical phenomena within the *glassy* state.

In glasses the type of mechanical modulus that is measured varies from experiment to experiment. The torsion pendulum measurement follows the shear modulus G^* directly, while the Rheovibron measures Young's modulus (the tensile modulus) E^* and ultrasonic and hypersonic (by Brillouin scattering) absorption and dispersion studies follow either G^* or the longitudinal modulus M_l^* depending on the cut of the exciting crystal. E^* and M_l^* are analyzable as different combinations of the fundamental moduli bulk and shear K^* and G^* according to the relations

$$E^* = G^* \left[\frac{3K^* - 4G^*}{K^* - G^*} \right] \tag{2}$$

$$M_l^* = K^* + 4/3\, G^* \tag{3}$$

It can be seen from eqns. (1) and (2) that in the liquid state where the shear modulus G' vanishes M'_l will remain finite but E' will also vanish.

The questions that are of interest in this phenomenology are:

(1) Is there *always* a mechanical relaxation to be observed in the temperature range where the electrical modulus becomes finite?

(2) Is the mechanical relaxation when observed always found at the same temperature as the electrical relaxation?

(3) Is the *width* of the mechanical relaxation, irrespective of the position of its center frequency with respect to that of the electrical relaxation, greater than, equal to, or less than the width of the electrical relaxation?

(4) If the widths *are* different, then are the *shapes* the same or not?

(5) What characteristics change when the phenomenon is followed over very wide ranges of temperature, and relaxation time, particularly towards the short time limit?

(6) Is there something which distinguishes fast ion conducting glasses from other glasses, and if so what can we learn about the nature of the electrical relaxation in superionic glasses from the study of the mechanical relaxation?

It should be noted at the outset that there is an intrinsic difference between the electrical and mechanical phenomena [9]. The electrical relaxation is a *primary* relaxation, insofar as it is the first phenomenon by which the system acquires a finite modulus, (i.e. ability to store rather than completely dissipate the energy of the perturbing field). The mechanical relaxation, on the other hand, is a *secondary* relaxation insofar as the system has already lost its ability to flow at the glass transition since this is where the shear modulus increases from zero to finite values, see Fig. 3. As expected for a secondary relaxation [2], its temperature dependence is much smaller than for the primary relaxation, and it is usually Arrhenius in character.

REAL AND IMAGINIARY PARTS OF THE MODULI IN CONSTANT FREQUENCY AND CONSTANT TEMPERATURE SCANS

In Fig. 3 we displayed the behavior of the real parts of the electrical and mechanical moduli as temperature is lowered from above the glass transition temperature. We now focus on the behavior of the system at temperatures well *below* T_g and consider the observations under conditions of constant temperature as is usually the situation for electrical measurements, and under constant frequency which is the usual condition of experimentation in the more restricted mechanical relaxation studies.

Figure 4(a) and (b) shows the real M′ and imaginary M″ parts of the complex electrical modulus for the well studied case of the superionic glass 0.6 AgI - 0.4 ($Ag_2B_4O_7$) [10–13] as frequency is scanned from 12 Hz to 10^5 Hz. We observe that the real part of the modulus, which is zero at low frequencies (where there is time for the mobile ions to completely dissipate the field acting on the system) increases to a value which is only slowing varying with frequency at high frequencies (where the system is acting as a slightly lossy insulator). In the ideal case where only a single relaxation process was being observed the modulus would become constant at high frequencies and M″ would be symmetrical (Lorentzian). (We will discuss later the connection between the continued high frequency losses and the global picture of ionic motions in a glassy solid.) In Fig. 4(c) we show the

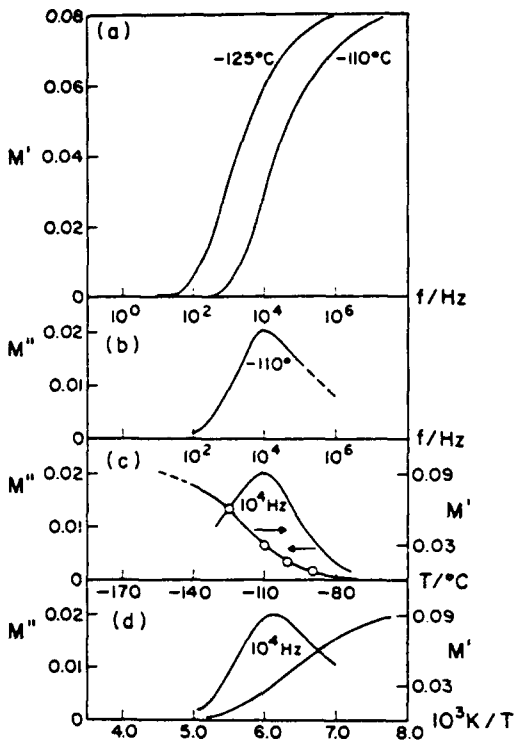

Fig. 4. (a) Real parts of the electrical modulus for the superionic glass 0.6AgI·0.4 ($Ag_2B_4O_7$) measured at -110 and -125°C.
(b) Imaginary part of the electrical modulus for the same system measured at 110°C. Note maximum loss at 10^4 Hz where T = 110°C. for Hz.
(c) Real and imaginary parts of the electrical modulus for the same system at constant frequency of 10^4 Hz measured as a function of temperature.
(d) Real and imaginary parts of the electrical modulus for the same system plotted vs. reciprocal temperature. Note identical shape of M″ in parts (b) and (d).

corresponding 'spectra' observed when the frequency is held constant at 10^3 Hz and the observations are recorded during a scan in temperature. We see that the situation of Fig. 4(a) is reversed, the quasi-insulating behavior now being seen at the left-hand (low temperature) end of the diagram. The shape of the spectrum seen in Fig. 4(b) can now be entirely recovered by plotting the moduli *vs.* *reciprocal* temperature as is shown in Fig. 4(d). The conditions which must be met for the spectral shape to be fully recovered are that (a) the temperature-dependence of the most probable relaxation time be Arrhenius in character and (b) the relaxation spectrum be independent of temperature, *i.e.* all elements of the spectrum have the same activation energy. These two conditions are frequently met in the study of glassy solids.

While there are a few instances reported of mechanical relaxation studies over a wide range of frequencies [14–16], the more common studies of mechanical relaxation involve the

use of a single frequency [8, 9] or a narrow range of frequencies [11, 17–19], and results are then reported in the form of Fig. 4(c). Examples are provided in Fig. 5 for the case of AgI-$AgPO_3$ glasses [19]. Where more detailed studies are available it has been found (see later) that, for mechanical relaxation due to mobile ions, the relaxation spectrum is also not very dependent on temperature [12] though it is not of identical shape to that of the conductivity relaxation spectrum. To the extent that this is the general case the shape of the relaxation spectrum, and consequently the parameters describing the departure from exponential relaxation, can be obtained by casting the data in the form of Fig. 4(d).

Although the case chosen for illustration in Fig. 4 is one in which the frequency ranges used in mechanical and electrical studies overlap [12], a frequent problem encountered in comparing electrical and mechanical responses is that the mechanical studies are made at a rather low frequency (e.g. by ~ 0.5 Hz torsion pendulum measurements) which is outside the range of commercial electrical admittance bridges (typically 12 - 100,000 Hz). So long as the two conditions of frequency independent spectral shapes and Arrhenius temperature-dependence are met, however, the failure of experimental time scales to overlap is not a big problem, and shifts of spectra along the frequency axis allow direct comparisons of the mechanical and electrical responses to be made. It is on this basis that many of the comparisons to be made below are possible.

MAGNITUDE OF MODULUS DISPERSIONS DUE TO MOBILE ION MOTION

In the remainder of this paper we will deal sequentially with the questions raised in the introduction. The first of these questions dealt with the extent to which mechanical counterparts of electrical relaxations (which can always be measured when the DC conductivity can be measured) exist. The answer to this question seems to be in the affirmative but is limited by the smaller sensitivity of experiments capable of detecting the mechanical response. As Day and Stevels [18] noted long ago, the magnitude of the mechanical loss, determined in many experiments as the internal friction Q seems to scale with the DC conductivity at some reference temperature, e.g. 298 K. This means that for insulating glasses the internal friction is so small that it cannot be detected by most existing techniques. For alkali silicate glasses the torsion pendulum, which can detect mechanical losses corresponding to phase angles, tan δ, as low as 0.001, is effective and, as Fig. 3 shows there is indeed a mechanical response complimentary to the electrical one. In fact it seems that the weaker the response the closer the relationship between electrical and mechanical phenomena (see, for instance, the subsequent discussion of Fig. 1).

The manner in which composition changes which increase the conductivity also increase the peak value of the imaginary part of the mechanical modulus (and how,

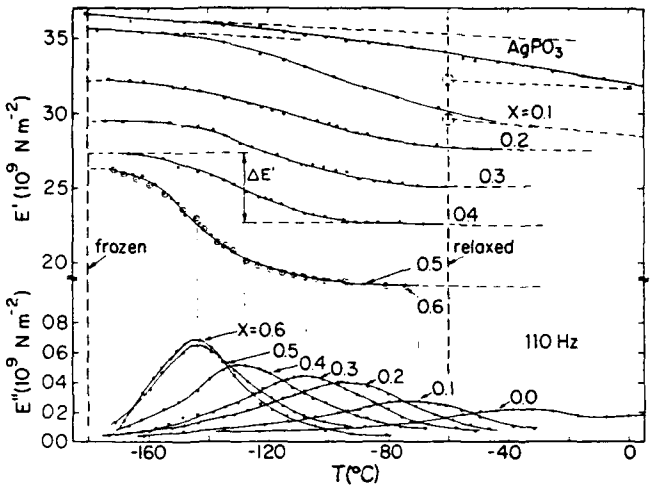

Fig. 5. Real and imaginary parts of the complex tensile modulus E^* for AgI–$AgPO_3$ glasses, showing increase of E''_{max} with increasing AgI content and increasing conductivity. The dispersion in the tensile modulus due to the mobile cation relaxation is shown at midpoint of the relaxation for the case $X_{AgI} = 0.4$ (from Ref. 19, by permission).

correspondingly, the temperature at which the dispersion in the real part E′ is observed increases) is shown in Fig. 5 using a series of AgI - $AgPO_3$ glasses [19]. These show much greater magnitudes of the dispersion than in the case of silicate glasses and are conveniently studied with simply operated mechanical spectrometers of the type used by polymer chemists, e.g. the Rheovibron, with which the data in Fig. 5 were recorded.

At the limit of *low* conductivity when conducting and viscous modes are fully coupled, the response to the electrical field comes into the same time range as the viscous response to a mechanical stress and the conductivity relaxation overlaps the *primary* mechanical relaxation. Correspondingly, the secondary mechanical relaxation due to the conducting ions merges with the primary relaxation which constitutes the glass transition, as in Fig. 2. To the best of the author's understanding there is no such thing as an electrical relaxation which is *slower* than the primary mechanical relaxation in inorganic glasses, though this is the common observation in polymer salt electrolytes [20]. In this latter case the conductivity response is slower because the ions are distributed in the solvent largely in the form of interacting ion pairs or multiplets and decoupling of these aggregates must occur before the 'free' ions can relax (on the same time scale as the solvent medium). In this case, no separate mechanical relaxation associated with the electrical relaxation can be observed since the viscous liquid dissipates a shear stress acting on the system before any response due to the conducting ions can be detected.

RELATION OF MECHANICAL TO ELECTRICAL RELAXATION TIMES

In the cases illustrated so far, which have been for cation conducting glasses, the relationship between the relaxation time for conductivity and that for mechanical relaxation is a close one, to judge by the similar temperatures at which the step changes in moduli (Fig. 3) or the maxima in loss (see Fig. 8 below for the AgI-$AgPO_3$ system) occur for temperature scans at constant frequency. This is also the case for a fluoride *anion* conducting glass of conductivity comparable to the sodium silicate glass of Fig. 3, according to data recently presented by Mai and co-workers [16] for the case of the fluoride ion conducting glass ZrF_4–BaF_2–LaF_3, which are reproduced in Fig. 6.

That a correspondence of electrical and mechanical relaxation times need not always occur is made very clear by the data for systems in which more than one type of alkali cation is present. Here the so-called mixed alkali effect results in the elimination of the low-temperature (at constant frequency) fast cation mechanical relaxation peak and its replacement with a much stronger 'mixed alkali' peak at higher temperatures (implying a much slower relaxation process) [8]. Although it is well-known that the conductivity of a mixed alkali glass is much lower than that of the corresponding single alkali glasses studied at the same temperature, the slowing down of the conducting modes is evidently much less pronounced than that of the modes dominating mechanical relaxation. This may be seen from Fig. 7 in which the results of mechanical and electrical relaxations are, for the same composition, displayed on the same diagram. In this *constant temperature* plot (in which the extended frequency range representation of the mechanical relaxation is obtained by a reduction of data of smaller frequency range from a number of different temperatures assuming constant shape), it appears that the conductivity relaxation is occurring by means

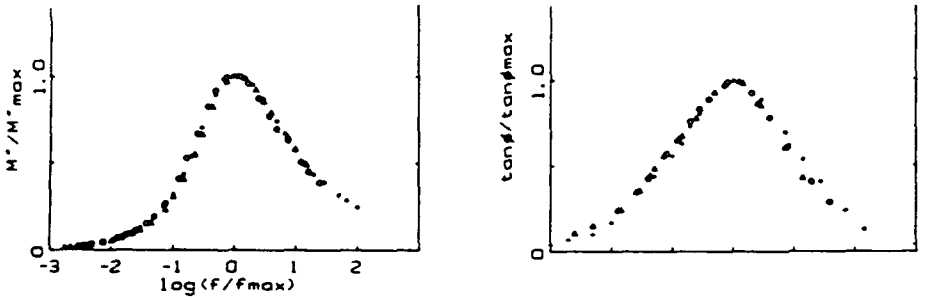

Fig. 6. Comparison of mechanical and electrical losses for heavy metal fluoride glass (an anion conductor) data were taken isothermally over at least three orders of magnitude and are presented normalized to the loss maximum at each temperature. Superposition of data points establishes constancy of spectral shapes. Note difference in spectral form at frequencies below f_{max}. For weak relaxations, the form of tan δ is indistinguishable from the form of G_{max}''. (from Ref. 17, by permission).

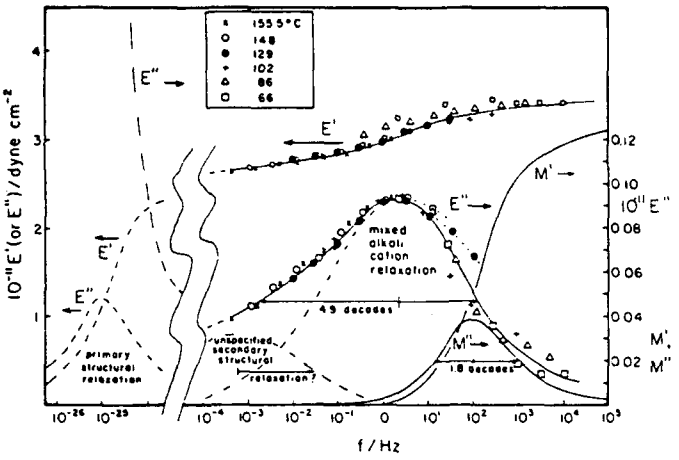

Fig. 7. Comparison of mechanical relaxation (master plot) with electrical relaxation for a mixed alkali glass $(Na_2O{\cdot}K_2O){\cdot}3SiO_2$, showing ~ two order of magnitude difference in peak frequencies. Left-hand side of diagram shows extrapolated behavior of the moduli at the primary structural relaxation which would be effective on extremely long timescales at the normalization temperature, 129°C. (from Ref. 15, by permission).

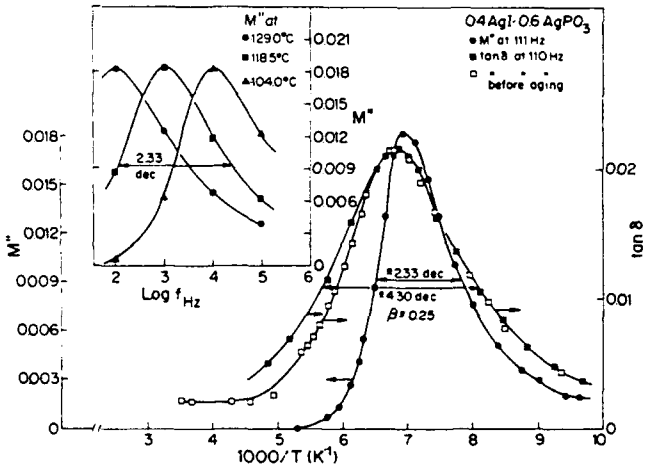

Fig. 8. Comparison of electrical and mechanical relaxations in the reciprocal temperature representation showing similarity of temperature of maximum loss, but major differences in "spectral" halfwidths. Inset shows the thermal behavior of electrical relaxation with which the equivalent halfwidths in the 1/T "spectra" were calibrated. (from Ref. 19, by permission).

of the highest frequency components of the very broad mechanical relaxation. The fact that the spectra are of temperature independent shape implies that the activation energy for conductivity and mechanical relaxation should be the same, as indeed is found to be the case [15].

Most of the systems characterized by superionic conductivity consist of a single mobile species so that major differences in conductivity and mechanical relaxation times such as those observed in Fig. 7 are not to be expected. On the other hand, many fast ion conducting systems in which the high conductivity is obtained by the addition of silver iodide to glassforming hosts such as silver metaphosphate [19, 21] or silver molybdate [22] are expected to have different environments for different fractions of the Ag^+ ions. Then it might be expected that electrical relaxation times, which would be determined by the fastest moving species, would be shorter than mechanical relaxation times which on average should be determined by the slowest moving species (since the system polarizes to mechanical stresses, and all modes should be active). Indeed, such a difference in the *most probable* time is observed [19] as shown in Fig. 8 by the larger 1/T value for the peak of M'' (elec) compared to that for tanδ (mech) for the composition $(AgI)_{0.4}$ $(AgPO_3)_{0.6}$ in Fig. 8. However, the reverse is the case for anion-conducting glasses in the system PbF_2–MnF_2–$Al(PO_3)_3$ [23]. What is surprising is that, in both cases, not only the longest relaxation times but also the *shortest* times (those elements still active at the lowest temperatures) are those associated with the mechanical relaxation process. The former feature is more pronounced than the latter. What we are actually observing and what in one sense explains the above statements, is that the frequency spectrum for mechanical relaxation is much *broader* than that for electrical relaxation. The generality of this observation and the associated discussion of differences in spectral shape, is addressed in the next section.

RELATIVE WIDTHS AND SHAPES OF MECHANICAL AND ELECTRICAL RELAXATIONS

It was observed in the last section that in at least two cases, the mixed alkali case and the Ag^+ conducting superionic glass case, the relaxation spectrum for mechanical stresses is much broader than that for electrical stresses. In the AgI–$AgPO_3$ case, this was inferred from the comparison of reciprocal temperature plots at constant frequency. Since we consider this matter in detail in the present section, it will be better if the comparisons, as far as possible, are put on a variable frequency scale. In the absence of broad frequency range spectra, this is best done by taking advantage of the evidence that spectral shapes are constant and relaxation times are in general of Arrhenius temperature dependence to utilize the possibility of converting temperature scan data to their frequency scan equivalent (as implied by the comparisons in Fig. 4(b) and (d)). This can formally be done by plotting the moduli as a function of $\omega\tau$ where ω is the fixed angular frequency and τ is the relaxation time (most probable value) obtained from an Arrhenius plot. The slope of the Arrhenius plot must be obtained either from data obtained at at least two different mechanical stress frequencies, or by assuming that the activation energy is the same as that meas-

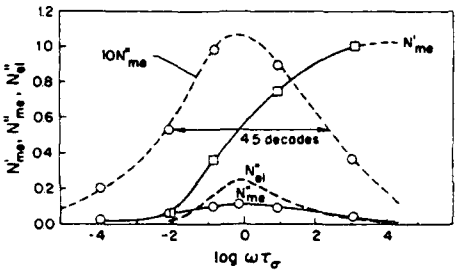

Fig. 9. Frequency dependence of the normalized moduli M''_{elec} and M''_{mech}, mechanical data for mechanical and electrical relaxations are obtained at fixed frequency and spectral form is obtained by plotting moduli *vs.* $\omega\tau_\sigma$, where τ_σ is the temperature-dependent electrical relaxation time. Blowup of N'' for mechanical relaxation shows clearly the very large halfwidth for mechanical relaxation. (Reproduced from Ref 19 by permission).

ured for the DC conductivity (or for the conductivity relaxation time). The results corresponding to the data in Fig. 8 are presented in Fig. 9 [17].

Figure 9 shows that, as observed for the mixed alkali glass, the mechanical relaxation spectrum is decades broader than that for electrical relaxation though, in the superionic glass case, the most probable relaxation times are in fairly close proximity. It also appears from Fig. 9 that the shape of the spectrum for mechanical relaxation is different from that for electrical relaxation in the sense of being more symmetrical despite its increased width. The same shape and width are found in independent studies made in the ultrasonic regime [24].

The electrical relaxation is found, particularly in poorly conducting glasses, to be well fitted to at least one decade above the frequency of maximum loss by an appropriate Fourier transform of the Kohlrausch-Williams-Watts (KWW) stretched exponential function,

$$\theta(t) = e^{-(t/\tau)^\beta} \quad , \quad 0 < \beta < 1 \qquad (4)$$

which seems to describe a great many time-dependent processes in amorphous materials [2, 25, 26]. This implies that the mechanical relaxation is not always well described by this otherwise seemingly ubiquitous relaxation form. This is not always the case, however. The system 0.6 AgI - 0.4 $Ag_2B_2O_7$ which has been studied at low frequencies by the Rheovibron [17] and in the MHz range by ultrasonics [11] shows a spectrum in the 1/T representation (Fig. 10) which is as well represented by the KWW function (with β values of 0.29 and 0.35 respectively (solid lines through points) as by the alternative function suggested by the original authors [11]. The mechanical relaxation, however, is much broader than the corresponding electrical relaxation, for which data at the same frequency, 110 Hz, are included in Fig. 10.

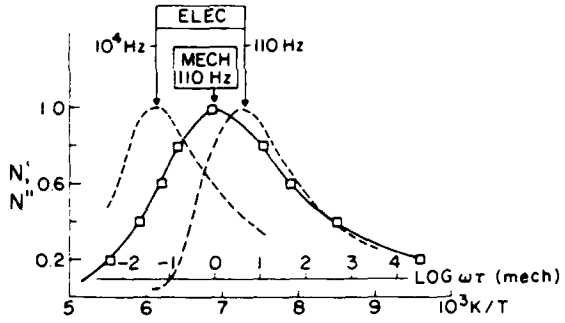

Fig. 10. Reciprocal temperature display of imaginary parts of the electrical and mechanical relaxation for the case of $0.6AgI{\cdot}0.4Ag_2B_4O_7$, showing displacement of the temperature of maximum loss for the two different stresses in the presence of similarity of spectral form. Solid curve through points for mechanical relaxation is the KWW function with $\beta = 0.29$. Electrical relaxations are well described by the same form with $\beta = 0.48$. An equivalent *frequency* scale is displayed for the mechanical relaxation centered at the peak frequency. The same scale size applies to the electrical relaxations since the activation energies for each process are essentially the same.

The contrasting findings of Figs. 9 and 10 leave the question of spectral shapes for mechanical relaxation unsettled. Since we have so far only examined *superionic* glass mechanical relaxations it is therefore of interest to examine the behavior of the mechanical relaxation relative to that for electrical relaxation under conditions where the relaxation is relatively weak.

Weak mechanical relaxations cannot be studied with the convenient Rheovibron instrument used to acquire much of the data given in the foregoing figures. Fortunately, there has been a recent study of mechanical and electrical relaxation in poorly conducting systems by Mai and colleagues [16]. They used a sensitive wide frequency range mechanical spectrometer [27] to study anion-conducting glasses in the system $ZrF_4-BaF_2-LaF_3$.

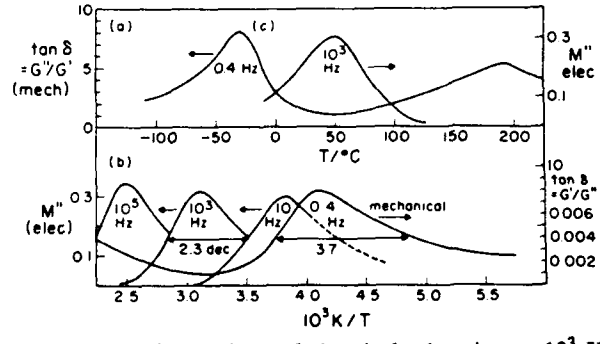

Fig. 11. (a) Comparison of electrical relaxation at 10^3 Hz and mechanical relaxation 0.4 Hz for $Na_2O{\cdot}3SiO_2$ glass during temperature scans.
(b) Reciprocal temperature representation of the data of part (a) to permit comparison of spectral shapes and halfwidths. Both electrical and mechanical spectra show KWW form though mechanical spectrum is considerably broader.

Their findings, which allow us to compare mechanical and electrical spectral shapes under rather stringent conditions, have already been displayed in Fig. 6. It would appear from Fig. 6 that when the relaxation is weak (implying either that the total number of ions able to relocate under mechanical stress is small or that the displacement per ion is small) the spectral widths for the two response functions are similar. The shapes, however, are clearly different in the same respect as seen already for AgI–$AgPO_3$ glasses in Figs. 8 and 9. An analysis, shown in Fig. 11, of temperature scans at 0.4 Hz for the single alkali silicate glasses $Na_2O{\cdot}3SiO_2$ given by Day [8], suggests that poorly conducting *alkali* conductors also have narrower mechanical relaxation spectra than the superionics, though they are not as narrow as for the fluorozirconate glass. This is consistent with their-order-of-magnitude higher conductivities and a factor of two higher mechanical loss maxima [8, 16]. In Fig. 11, we compare electrical [28] and mechanical [8] relaxations for $Na_2O{\cdot}3SiO_2$ glass in both T and 1/T representations and see that the shape in 1/T of the mechanical relaxation is quite similar to that for electrical relaxation while being broader, as in the case of the more highly conducting glass of Fig. 10.

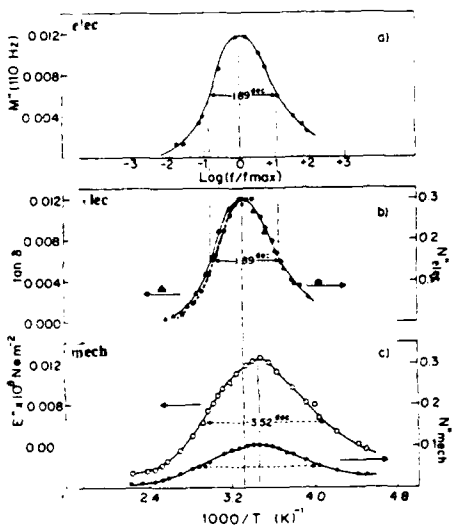

Fig. 11. Relaxation in F^- anion conducting glasses. Imaginary part of the electrical modulus, M'', *versus* reduced frequency for $75PbF_2{\cdot}10MnF_2{\cdot}15Al(PO_3)_3$ glass at 100°C. (b) $M''/M'_\sigma = \tan\delta$, (solid line, LH scale) and $M''/M'_\sigma = N''$ (dashed line, RH scale) as a function of 1/T at 110 Hz. Scales are chosen so that spectral halfwidth remains the same in each plot to facilitate comparisons with tensile modulus plots (part c). (c) Dissipative part of the complex tensile glass, E'' (LH scale) and normalized tensile modulus $N''_{mech} = E''/\Delta E'$, *versus* 1/T with same 1/T scale as for part b. Note the greatly increased half width and lower N'' relative to the conductivity relaxation, and the displacement of the peak of the mechanical spectrum to lower T (or higher frequency). (by permission).

Thus we have the interesting situation in which a poor conductor (the fluorozirconate glass) and a superionic conductor ($AgI–AgPO_3$) have mechanical relaxation spectra which are non-KWW while being of very different widths, and a poor conductor ($Na_2O{\cdot}3SiO_2$) and a superionic conductor ($AgI–Ag_2B_2O_7$) which are KWW in form, and have mechanical spectra of comparable widths (~ 3.5 decades). As mentioned above, all electrical relaxations so far studied are approximately KWW in form. As a final indication of the complexity of this situation we present, in Fig. 12, data for the recently developed fast fluoride ion conducting glass, 75 $PbF_2{\cdot}10MnF_2{\cdot}15Al(PO_3)_3$ [23]. This is the case mentioned earlier in which the electrical relaxation has the longer most probable relaxation time. We see in Fig. 12 that the electrical relaxation is quite narrow (actually narrower than for the more poorly conducting fluorozirconate glass) while the mechanical relaxation is again 3.5 decades in width and non-KWW.

All that can be said at this time is that *when* the mechanical relaxation differs from the KWW form it does so by adding extra strength at low frequencies.

Since some of the above comparisons are based on the 1/T representation of single frequency studies there is a possibility of confusion due to the presence of temperature dependent spectral shapes in some cases and experimental inconsistencies, even artifacts, in others. Detailed consideration of the variations in shapes should therefore probably be deferred until wider frequency range studies of mechanical relaxation become more generally available. Limits on shape variations can, however, be placed in one case where the mechanical relaxation has been studied over an exceptionally wide frequency range. We consider this in the next section.

EXTENDED RELAXATION TIME - FREQUENCY RANGE MECHANICAL STUDIES

In all of the above-mentioned work the frequency of the mechanical relaxation studies has not exceeded the 100 MHz range provided by ultrasonics. It is also possible to make mechanical relaxation studies at extremely high frequencies in the GHz range by inelastic light scattering techniques. A visible light beam, for instance, will interact with the natural density fluctuations in the material to produce or annihilate acoustic phonons and yield a scattered beam, the Brillouin line, which gives information on the frequency, velocity, and damping of these phonons. The damping is reflected by the halfwidth of the scattered light beam. Such scattering techniques have been very valuable in the study of viscous liquids [28] and may be applied to the study of mechanical relaxation in fast conducting solids if the strength of the associated relaxation is large enough. A couple of cases which satisfy this condition have recently been reported in the literature [12, 13, 29] and we briefly summarize the value of such studies here.

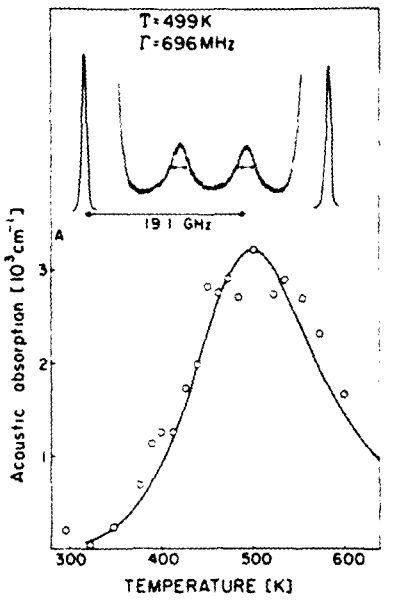

Fig. 13. Brillouin spectra for $0.6AgI{\cdot}0.4{\cdot}Ag_2B_4O_7$ glass at 499K, showing frequency shift from central exciting line and Brillouin halfwidth. Lower portion shows absorption coefficients at different temperatures obtained from the Brillouin linewidths of the upper portion. Solid line is fitted using a single exponential relaxation equation with activation energy obtained from ultrasonic data of Ref. 11.

The first case in question is the $AgI–Ag_2B_4O_7$ system in which there already existed extensive data at lower frequencies covering the range 1-110 Hz (by dynamic mechanical studies discussed earlier [19], see Fig. 10) and by ultrasonic studies [11]. The relaxation in this glass is one which satisfies the two conditions, high relaxation strength and exceptionally short relaxation time at T_g, which are necessary for the observation of GHz phonon damping at temperatures below the glass transition temperature.

Figure 13 shows, in the upper portion, the basic experimental observation, *viz.*, the scattered Brillouin peak in relation to the central exciting line, and (in the lower portion) the important relaxation data in the form of absorption coefficients obtained at each temperature from the width of the Brillouin line. We see in Fig. 13 how the absorption coefficient passes through a maximum at a temperature, 500°C, some 180°C below the glass transition temperature for this system. Similar results have since been observed for a range of glasses in the same $AgI–Ag_2BO_4O_7$ system and also in the alkali halide containing system $LiCl–LiB_2O_7$[30].

These data can be put in the reciprocal temperature form and displayed informatively with the results of the lower frequency experiments as shown in Fig. 14.

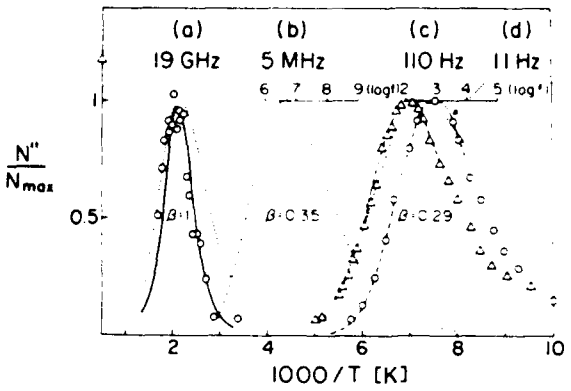

Fig. 14. Comparison of normalized moduli for mechanical relaxation over wide temperature and frequency regimes using 1/T representation of spectral form. Note that the spectrum at 5 MHz (from Ref. 11) and 11 Hz are approximately the same in shape while high temperature high frequency spectrum is narrow. Dotted lines show predicted shapes at GHz and low frequencies according to Gaussian activation energy distribution model of Ref. 11. The frequency scales attached to the 5 MHz and 110Hz plots are based on the equivalence of 1/T and log f discussed earlier under Fig. 4. Each scale has its origin fixed such that the peak of the modulus plot falls at the appropriate fixed frequency, 5MHz or 110Hz.

Since the evidence from both electrical conductivity and low frequency mechanical relaxation is that the activation energy for the mobile ion relaxation is independent of temperature, we can assume that the data displayed in Fig. 14 reflect the spectral form of the relaxation as discussed using Fig. 4. In this case, we may make the important observation from Fig. 14 that the departure from exponential relaxation which is so pronounced at low temperatures is greatly reduced in the high frequency short relaxation time range explored by the Brillouin scattering technique. Indeed the width of the relaxation in 1/T can be accounted for almost quantitatively under the assumption of a single relaxation time. This appears also to be the case for the lithium cation motion in the $LiCl-LiB_2O_7$ system [30], hence is probably of general validity.

With this extended frequency/relaxation time data now in mind, it is helpful to make a summary representation of the variations of relaxation time with temperature which have been observed in different systems. Figure 15 shows a relaxation time map for the system $AgI-AgPO_3$ and includes some short longitudinal relaxation time data obtained by Brillouin scattering in the *liquid* state [31], in addition to the various glassy state data discussed in earlier papers. Figure 15 shows three important features which we note again here.

In the first place it shows that for both electrical and mechanical relaxation the activation energy changes systematically with composition in such a way that the slope of the least rapidly relaxing compositions tends towards the (much greater) slope of the viscoelastic relaxation.

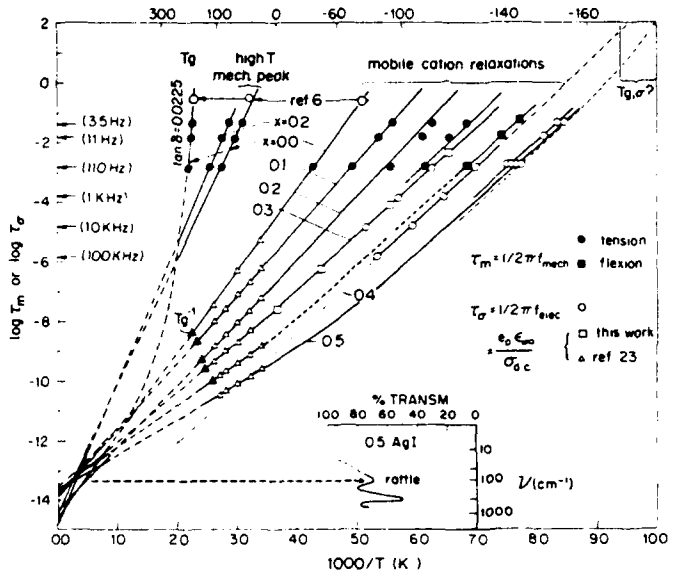

Fig. 15. Relaxation "map" for mechanical and electrical relaxation in $AgI–AgPO_3$ glasses. See text for details. High temperature conductivity data from Ref. (23) have been converted to electrical relaxation times (τ_σ), assuming a high frequency dielectric constant of 15 for all cases. Inset: Low frequency portion of thin film transmission IR spectra for 0.5 $AgI{\cdot}0.5AgPO_3$ glass. Note coincidence of far IR peaks (quasi-lattice vibration modes) with attempt frequency for relaxation modes. (From Ref. 19 by permission).

Secondly, we note that the most rapidly relaxing compositions showed distinct departures from Arrhenius behavior in both electrical and mechanical relaxation. Whether or not this can be associated, as for viscous liquids [32], with measurable contributions to the thermodynamic properties (heat capacity, compressibility, etc.) from configurational degrees of freedom which are localized so as to be dissociated from the main viscoelastic relaxation, is not known at this time.

Thirdly, all modes (including some secondary mechanical relaxation modes *not* associated with mobile cations which we have not discussed) appear to be extrapolating towards a high temperature limit which is broadly consistent with the 'quasi-lattice' vibrational times observable by far infrared spectroscopy on these systems [33].

Figure 16 shows the relaxation times for the mobile ion modes alone for three different fast ion conducting systems and establishes that the very fast relaxing systems are not necessarily associated with departures from Arrhenius behavior. Indeed the one detailed study of this curvature in the literature [34] suggests that it is a strong function of thermal treatment and indeed disappears after the glass has been properly annealed.

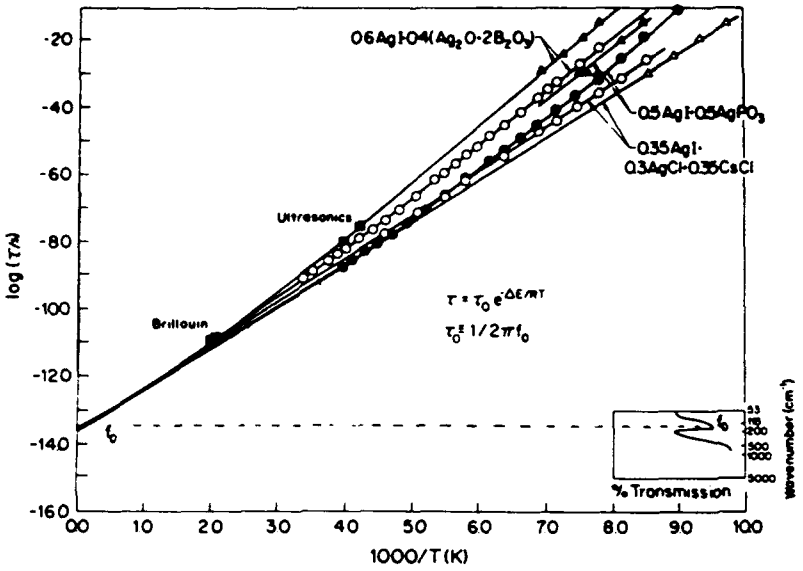

Fig. 16. Arrhenius plot of relaxation times for mechanical and electrical mobile ion controlled processes in three different fast ion conducting glass systems, one containing only halide ions. Note that the latter shows Arrhenius behavior over the whole temperature range with direct extrapolation to the quasi-lattice vibration time. Plot contains results of high frequency study of Figs. 13 and 14.[13]

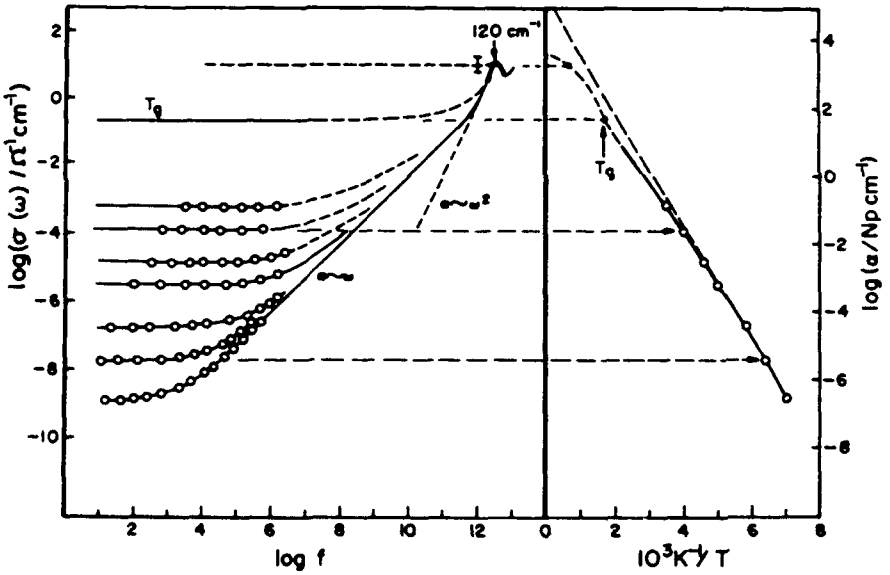

Fig. 17. Frequency dependence of electrical conductivity $\sigma(\omega)$ (left hand ordinate) and absorption coefficient α_ω (right hand ordinate) due to fast ion motion at different temperatures for the fast ion conducting system 0.6 AgI·0.4($(Ag_2O·2B_2O_3)$, (part (a)) and temperature dependence (Arrhenius plot) (part (b)), showing near equivalence of limiting high frequency conductivity, obtained from the far IR quasilattice absorption, and limiting high temperature conductivity of the liquid state. Note changeover from a first power frequency dependence of AC conductivity in most of the range to an ω^2 dependence near the quasilattice resonance absorption region.

Finally we show, in Figs. 17 and 18, connections between relaxational and vibrational modes associated with electrical and mechanical fast ion relaxation. Figure 17 shows how the temperature dependence and the frequency dependence of the conductivity can be related to the absorption of energy from the oscillating electrical field, an absorption which reaches its maximum at frequencies in the far infrared region of the electromagnetic spectrum *i.e.* for frequencies characteristic of the quasi-lattice vibrations. The (a.c.) conductivity at these frequencies is very high since every charged particle in the system is contributing in proportion to its charge as it vibrates at thermal velocities, creating an instantaneous fluctuating current. This conductivity can be measured by determining the loss of energy from a far infrared light beam as the electromagnetic wave couples to the oscillating atomic field and is absorbed [33].

The relation is given by

$$\alpha(\omega) = \sigma(\omega)/e_o\, c\, n(\omega) \qquad (5)$$

where e_o is the permittivity of free space, c is the velocity of light, and $n(\omega)$ is the frequency-dependent refractive index which, in a disordered transparent material, varies only weakly about the higher frequency value fixed by the electronic motions. Figure 17 has a conductivity scale on the left and the equivalent optical absorption coefficient scale on the right. Note how, as the temperature increases, the d.c. conductivity -- hence also the low frequency absorption coefficient -- rises towards a limit set by the absorption due to the vibrating ions in the quasilattice. The latter has been measured quite accurately for sodium borate glasses [33] but is less certain for the present case (see error bar in Fig. 17) because the film thickness of the blown silver ion glass film was only crudely measured [33]. It would appear, from Fig. 17, to be a measure of the limiting high d.c. conductivity obtainable in an ionic system. There is a need for more quantitative evaluation of far IR absorptivities in relation to temperature and composition in order that the physical picture given in Fig. 17 can be fully completed and confirmed.

Figure 17 gives the picture unifying vibrational and relaxational modes responding to *electrical* stresses and shows how they merge at the high temperature high frequency extreme. Since this article attempts to correlate mechanical and electrical phenomena it is reasonable to ask if there is an equivalent unifying relationship between short time and longer time mechanical modes. No such relationship has so far appeared in the literature to the best of the writer's knowledge.

Since the mechanical relaxation is one which leads to a thermodynamic state of polarization we cannot expect the equivalent of Fig. 17 for mechanical motions to have frequency-independent plateau as in Fig. 17 (though this would be the case for *shear* relaxation in *liquids*). Rather, the nearest equivalent would be the relaxation of a *polar* liquid. Data connecting dielectric relaxation and IR absorption were recently published for the

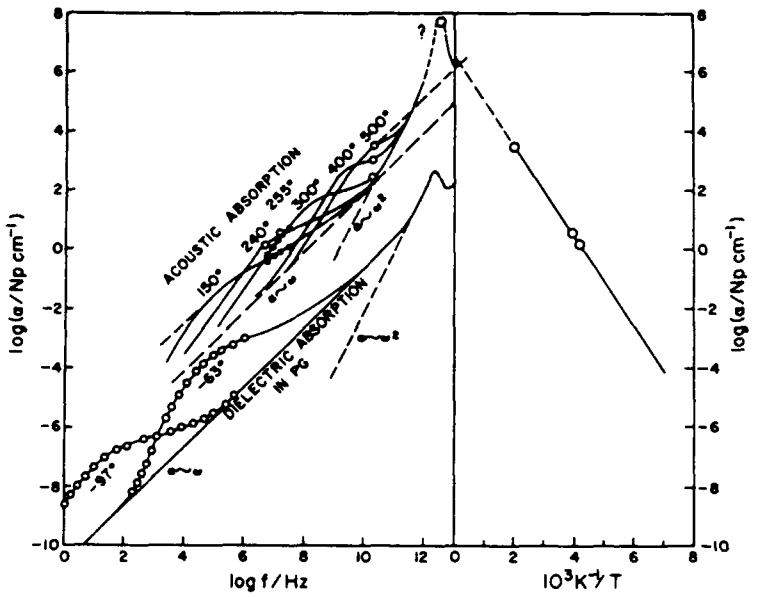

Fig. 18. Analog of Fig. 17 for absorption of *mechanical* energy in the same system, based on limited ultrasonic [11] and Brillouin scattering [31] data. For comparison, data for absorption of electromagnetic waves by a relaxing dipolar fluid, propane diol [47] over the same frequency range are included. Both seem to have similar $\alpha \sim f^{1.0}$ backgrounds over the major part of the frequency range. An Arrhenius temperature dependence for the acoustic absorption coefficient (at the frequency of the loss maximum) is a novel observation to the best of our knowledge.

case of propane diol [35] and are reproduced in Fig. 18, lower curves, to provide a basis for comparison with the mechanical analogue which we now discuss.

We choose for our example the case of one of the silver superionic glasses, 0.6AgI $0.4(Ag_2O{\cdot}2B_2O_3)$ for which some data are available. Figure 13, for example shows that the peak absorption in the GHz range 3.1×10^3 Np m^{-1} at 499 K [13]. Figure 14 includes data from the ultrasonic study of Carini et al. [11]. At the ultrasonic frequencies the peak values prove to be smaller in direct proportion to the lower frequency of the measurement, hence behave like their dielectric equivalent. These peak absorption data are entered in Fig. 18 as functions of frequency part (a) and of reciprocal temperature in part (b), as in Fig. 17. A few off peak absorptions at different ultrasonic frequencies allow us to estimate the form of the acoustic absorption 'waves' at different temperatures. We do not have the equivalent of a far infrared absorption coefficient for the mechanical modes but we *do* know that longitudinal acoustic excitations with the normal velocity of sound are observable in some glasses by neutron scattering in the equivalent of the second Brillouin zone at wave vectors for which the wave length is of order 10 Å [36]. Furthermore, these excitations [37] are not observable at large wave vectors in liquid or glassy states implying over-

damping. Therefore, we can write, for the smallest physically meaningful wave length λ_{min}, which is the interatomic spacing,

$$\alpha\lambda \overset{=}{>} 1 \tag{6}$$

which implies that the wave is completely damped in a simple wavelength. Furthermore this limiting high absorption coefficient will occur at a frequency given by

$$\lambda_{min} f_{max} = v \quad , \tag{7}$$

where a is the velocity of sound. Substituting $v = 2 \times 10^5$ cm sec^{-1} [11] and $\lambda_{min} = 2 \times 10^{-8}$ cm we find from eqns. (6) and (7) that $\alpha_{max} = 5x10^7$ cm^{-1} at $f = 1x10^{13}$ Hz. Entering this value in Fig. 18 and making the most natural connections to the variable temperature curves passing through lower frequency points [12] we recover a pattern quite similar to that for dielectric relaxation. The main difference is a more prominent peak absorption. This is due partly to the greater broadness of the mechanical relaxation which diminishes the maximum absorptivity of the lower frequency peaks, and partly we suppose to the different *physics* involved in the two highest frequency peaks. By different physics we mean that the wavelength of the excitation being damped at the mechanical absorption peak is quite different from that of the optical mode which is being excited at the center of the glassy state equivalent of the crystalline state Brillouin zone. The latter is strongly, but not completely, absorbed.

We find it of interest that, despite the different physics, there should be as much similarity as there is in the two cases. In particular it appears that there is a mechanical equivalent of the source of constant loss per unit wavelength at frequencies well above the relaxation peak. This is the contribution which is responsible for the failure of both simple Debye and non-exponential relaxation theories for dielectric relaxation, which both predict *steps* in the logα *vs.* logf plot rather than the $\omega = f^{\alpha}$ (with $\alpha \simeq 1$) relationship extending up to the infrared which is found experimentally [2]. (We should note, however, that Funke and coworkers have recently reported the observation of short steps in the AC conductivity just below the far IR resonance absorption region in the case of certain model molten salt and solid electrolyte systems, as anticipated by their jump relaxation model [38]. It will be necessary to resolve the origin of these experimental differences and, if steps are confirmed, examine why their mechanical equivalent is not seen in Fig. 18 in the same (microwave frequency) region).

DISCUSSION

In seeking physical origins for differences in the electrical and mechanical relaxation responses due to mobile ion motion in glasses, two possibilities come to mind.

The first and most obvious is the fact that the electrical relaxation in a conducting glass is a non-polarizing response [2]. By this we mean that when ions move in response to the electrical field they are capable of completely relaxing any perturbation due to an instantaneously created field e.g. a field produced by sudden application of a charge on one side of the conducting sample. This contrasts with the response of a dielectric fluid which polarizes to a well-defined time-independent terminal state. Likewise, the mechanical response, in the case of a substance which is already in the glassy state, is a *polarizing* response; the displaced ions can only move so far, and the stress be relaxed by a corresponding amount, before a resistance to further polarization is met. The implication is that in the latter case *all* the modes of motion which can relax the stress in this frequency range will be activated before the final state of polarization is achieved whereas in a non-polarizing response, certain modes of the same character, but characterized by longer relaxation times* will not be explored because of the easier route to stress relaxation offered by the lower barrier pathway. In this light, it would be reasonable to expect, for mechanical relaxation, a broader relaxation spectrum particularly at low frequencies.

It may well be that, if cluster models gain acceptance [38], the distinction between mechanical and electrical relaxations will become a valuable tool for characterizing the relation between 'tissue' and 'cluster' properties. Differences in the spectral shapes, for instance, could indicate the presence of clustering (which would not generally be related to whether the system is superionic or not) while a similarity of form (both relaxations being KWW in form but differing in width) could indicate a more homogeneous microtopology. Of particular importance in this respect would be a combination of these studies with more microscopic relaxation probes such as NMR [40] or probe ion electronic spectroscopy [42] so that the sort of sites associated with excess slow mechanical energy absorption can be characterized. A greater temperature dependence for the broader mechanical spectra may also be a characteristic of clustered systems. It should be mentioned here, however, that computer simulations of superionic systems [43], like the $LiCl-Li_2B_4O_7$ system [31, 43, 44], do not show any evidence of clustering, according to 3D images of the structure. Furthermore, the calculations show that these solutions evidently form with a significant decrease in energy and with negative deviations from ideal mixing volume laws, *i.e.* they tend to order rather than to cluster. Neutron scattering patterns on AgI-containing glasses show a remarkable pre-peaks [45] implying some sort of longer range ordering occurs but it is not clear at this time whether that is due to ordering or to clustering, and the lithium chloroborate glasses do not show a similar peak [45].

* (e.g., relaxation within the clusters of various glass theories, in particular the 'cluster bypass' model of Ingram [39] described in this volume (which has elements in common with the 'diffusion pathway' model of Minami [40].

The second possibility for interpreting the difference in electrical and mechanical relaxation characteristics is that the difference is related to the different nature of the stress fields and the manner in which they couple to mobile elements of the structure. The mechanical stress couples through the repulsive potential which mostly determines the steric arrangements of particles in the glass, while the electrical stress couples through a longer range coulomb interaction. It is perhaps surprising that there is as much similarity in the response functions as there is. Indeed the similarity may reflect the degree of restriction on the manner in which *any* stress irrespective of coupling mechanism, can be relieved in a glassy material.

CONCLUSIONS

In this review we have concentrated on presenting a systematic account of phenomenology of mechanical and electrical relaxation processes due to mobile ions in glassy structures, at the expense of theoretical interpretation. We believe that, with the recent acquisition of short time mechanical relaxation data on the systems $LiCl-Li_2B_4O_7$ [31], a system which can be computer simulated with adequate pairwise additive rigid ion potentials in the same time scale range [43], some rapid progress in understanding of structures and relaxation mechanisms in superionic glasses will be possible. We therefore defer evaluation of theoretical models [46–51] until the new information allows the mechanistic basis of fast ion motion in glasses to be better established. Clearly this is a research area with challenging problems in an era of rapid development.

ACKNOWLEDGEMENTS

The author is grateful to his coworkers who have performed many of the measurements reported here, to Dr. L.M. Torell whose group at Chalmers University of Technology with whom we have collaborated under NSF Grant No. INT 8412292, has performed some of the more demanding measurements discussed herein, and to the Department of Energy (DE-FG02-84ER45) and the Office of Naval Research (Agreement No. NOOO14-84-K0289) for financial support.

REFERENCES

1 (a) C.A. Angell, *Solid State Ionics, 9 & 10* (1983) 3.
(b) C.A. Angell, *Solid State Ionics, 18 & 19* (1986) 72.

2 J. Wong and C. A. Angell, Glass: Structure by Spectroscopy, Marcel Dekker, New York, chap. 11, 1976.

3 T.A. Litovitz and D. Sette, *J. Chem. Phys., 21* (1953) 17.

4 P.B. Macedo, C.T. Moynihan and R. Bose, *Phys. Chem. Glasses, 13* (1972) 171.

5 C.T. Moynihan, R.D. Bressel and C.A. Angell, *J. Chem. Phys., 55* (1971) 4414.

6 C.T. Moynihan, N. Balitactac, L. Boone and T.A. Litovitz, *J. Chem. Phys., 55* (1971) 3013.

7 C.A. Angell, *J. Non-Cryst. Sol., 102* (1988) 205.

8 D. E. Day, in R. W. Douglas and B. Ellis (eds.), *Amorphous Materials,* Wiley-Interscience, NY, 1972, p. 35.

9 W.E. Steinkamp, J.E. Shelby, and D.E. Day, *J. Am. Ceram. Soc., 53*, (1970) 182.

10 (a) A. Chiodelli and A. Magistris, *Mat. Res. Bull., 17* (1982) 1.
(b) A. Chiodelli. A. Magistris, M.Villa and J.L. Bjorkstram, *J. Non-Cryst. Sol., 51* (1983) 143.

11 G. Carini, M. Cutroni, M. Federico, G. Galli and G. Tripodo, *Phys. Rev. B 30* (1984) 7219; *32* (1985) 8264.

12 L. Borjesson, L.M. Torell, S.W. Martin, Changle Liu, and C.A. Angell, *Physics Letters, 125* (1987) 330.

13 L. Borjesson, *Phys. Rev., B 36* (1987) 4600.

14 (a) J. Phallipou, S. Masson, A. Boyer and J. Zarzicki, *J. Non-Cryst. Solids, 14* (1974) 178; (b) J. Phallipou, S. Masson, A. Boyer and J. Zarzycki, *Rev. Phys. Appl., 10* (1975) 437.

15 T. Atake and C.A. Angell, Proc. of the Int. Congress on Glass XII, Albuquerque, New Mexico, *J. Non-Cryst. Solids, 38 & 39* (1980) 439.

16 C. Mai, A. Assiero, G.P. Johari, S. Etienne and K. Abbes, *J. Non-Cryst. Sol., 93* (1987) 35.

17 Changle Liu and C.A. Angell, *J. de Physique Colloque C10, Suppl. No. 12, 46* (1985) 493.

18 D.E. Day and J.M. Stevels, *J. Non-Cryst. Sol., 13* (1973) 304.

19 Changle Liu and C.A. Angell, *J. Non-Cryst. Sol., 83* (1986) 162.

20 L.M. Torell and C.A. Angell, *Polymer J.* (Proc. 1st International Conference on Polymer Electrolytes) *20*, (1988).

21 J.P. Malugani, A. Wasniewski, M. Doreau, G. Robert and A. Al Rikabi, *Mat. Res. Bull., 13* (1978) 427.

22 T. Minami, *J. Non-Cryst. Sol., 73* (1985) 273.

23 A.R. Kulkarni and C.A. Angell, *Mat. Res. Bull., 21* (1986) 1115.

24 R. Bogue and R.J. Sladek, *Journal De Physique, 46* (1985) C10-489. Almond, et. al. (D.P. Almond, G.K. Duncan and A.R. West, *J. Non-Cryst. Sol., 74* (1985) 285) have claimed that both isothermal variable frequency studies of conductivity relaxation (R.J. Grant, M.D. Ingram, L.D.S. Turner and C.A. Vincent, J. Phys. Chem., *82* (1978) 2838) and isofrequency variable temperature studies of longitudinal modulus relaxation by ultrasonics can be fit by the same value of β (0.3), implying the same spectral shape, but our own assessment of the conductivity data is that $\beta = 0.4$ is more appropriate (the spectral halfwidth of 2.7 decades is one of the largest ever observed).

25 K.L. Ngai and G.B. Wright, (eds.), *Relaxations in Complex Systems*, National Technical Information Service, US Department of Commerce, Springfield, VA 1985.

26 See 'Dynamics of Structural Change near the Glass Transition,' Ann. N.Y. *Acad. Sci., 484* (1986) 241.

27 S. Etienne, J.Y. Cavaille, J. Perez, R. Point, and M. Salvia, *Rev. Sci. Instr., 53* (1982) 126.

28 V. Provezano, L.P. Boesch, V. Volterra, C.T. Moynihan and P.B. Macedo, *J. Am. Ceramic Soc., 55* (1972) 492.

29 L.M. Torell (a) *J. Chem. Phys., 76* (1982) 3467.
(b) G. Mamantov and R. Marassi (eds.), *Molten Salt Chemistry*, NATO ASI Series, Plenum Press, vol. 202, 1987, p. 123.

30 L. Borjesson and L.M. Torell, *Solid State Ionics, 25* (1987) 85.

31 (a) L.M. Torell, *Phys. Rev. B, 31* (1985) 4103.
(b) L. Borjesson, S.W. Martin, L.M. Torell and C.A. Angell, *Solid State Ionics, 18 & 19* (1986) 141.

32 See Ref. 2, Chapter 1.

33 C. Liu and C.A. Angell (to be published)

34 M.D. Ingram, C.A. Vincent and A.R. Wandless, *J. Non-Cryst. Sol., 53* (1982) 73.

35 L. Boehm, D.L. Smith and C.A. Angell, *J. Mol. Liquids, 36*, (1987) 153

36 A. J. Leadbetter, A. C. Wright and A. J. Apling, in R. W. Douglas and B. Ellis (eds.), *Amorphous Materials*, Wiley Interscience, London, 1972.

37 G.S. Grest, S.R. Nagel, and A. Rahman, *Phys. Rev. B, 29* (1984) 5968.

38 (a) K. Funke, (private communication) (b) K.Funke, *Solid State Ionics, 18/19*, 183, (1986); *28/29*, in press.

39 (a) K.J. Rao and C.N.R. Rao, *Mat. Res. Bull., 17* (1982) 1337. (b) M.D. Ingram, *Mater. Chem. Phys., 23* (1989) 51.

40 T. Minami, *J. Non-Cryst. Sol., 73* (1985) 273.

41 S.W. Martin, H.J. Bischof, M. Mali, J. Roos, and D. Brinkman, *Solid State Ionics, 18 & 19* (1986) 421.

42 A. Barkatt and C.A. Angell, *J. Chem. Phys., 70* (1979) 901.

43 R. Syed, J. Kieffer and C.A. Angell (to be published).

44 H.L. Tuller, D.P. Button, and D.R. Uhlmann, *J. Non-Cryst. Sol., 40* (1980) 93.

45 L. Borjesson, W.S. Howells and L.M. Torell, Phys. Rev. B *39*, (1989) 3404.,

46 J.C. Dyre, *J. Non-Cryst. Sol., 88* (1986) 271.

47 J. Kawamura and M. Shimoji, *J. Non-Cryst. Sol., 79* (1986) 367.

48 J. Kawamura and M. Shimoji, *J. Non-Cryst. Sol., 88* (1986) 295.

49 K. Funke, *Zeitschrift fur Physikalische Chemie Neue Folge, Bd. 154* (1987) S. 251.

50 K.L. Ngai and R.W. Rendell and H. Jain, *Phys. Rev. B, 30*(4) (1984) 2133.

51 J.C. Dyre, *J. Appl. Phys., 64*(5) (1988) 2456.

Solid State Ionics 34 (1989) 243–245
North-Holland, Amsterdam

EFFECT OF PRESSURE ON CONDUCTIVITY IN LIQUID AND GLASSY STATES OF A SUPERIONIC CONDUCTING GLASS

C.A. ANGELL and Jinfeng ZHOU
Department of Chemistry, Purdue University, West Lafayette, IN 47907, USA

Received 23 November 1988; accepted for publication 15 March 1989

To observe whether pressure acting on the liquid state of a fast ion conducting vitreous solid electrolyte has a very different effect from pressure acting on the fixed structure vitreous state, measurements have been performed on $(AgI)_{40}(AgPO_3)_{60}$ over a range of pressures and temperatures. Below T_g, conductivity decreases according to classic transition state theory expressions with volume of activation close to the mobile ion volume. Pressure applied near and above T_g has only a slightly different effect than the same pressure applied well below T_g below, in contrast to the strong pressure effect on viscosity above T_g. An explanation links weak pressure effects to previously known weak quenching (fictive temperature) effects, through the high decoupling index.

1. Introduction

While there have been a great many studies of electrical conductivity in glassy phases containing silver and other mobile cations [1–3] very few have dealt with the effects of pressure. Those that have [4–7], have in all cases considered only the effect of pressure on the *glassy* state of the substance under investigation, leaving uninvestigated the effects of pressure on a fast ion structure which can *rearrange* in response to the pressure. In such studies both decreases of conductivity [4,5,7] and also rather large increases [6] in conductivity have been observed, depending on the temperature of study and the type of cell construction employed. We felt that if in fact conductivity increases with pressure are obtainable then the possibility of freezing in the structures which are responsible (by vitrifying the liquid while under pressure) should be explored. We have therefore chosen the much studied system $AgI+AgPO_3$ [1–3,8,9] for a trial investigation of this phenomenology. The $AgPO_3$-based glass has the advantage that at high AgI contents the glass transition temperature is sufficiently low that oil in contact with the sample can be used as the pressure-transmitting medium.

2. Experimental aspects

Samples of $AgI–AgPO_3$ glass nominally of composition 40 mol% AgI were prepared by fusion of weighed quantities of analytical grade AgI and $AgNO_3$ and $(NH_4)_3PO_4$. The second sample appears, from the lower conductivity data, to have lost some iodide by air oxidation during melting (which is not of importance to the main points of this study). The melt was poured into the twin electrode cell of design shown in fig. 1, so as to cover the electrodes to a depth of at least 2 mm. The depth was chosen so as to avoid interference of the miniscus with the conductance path while maintaining the sample small enough to minimize the danger of sample cracking. This cell plus sample was immersed in oil in the interior of a steel pressure bomb described elsewhere [10], and subjected to pressure and temperature variations as described below.

The cell constant was determined with N/10 KCl solution, and was found to be 0.50 cm^{-1}.

The conductivity was measured using a GenRad Digibridge Model No. 1689 with frequency varying between 5 and 10^5 Hz, in two sequences, as follows. In the first series data were taken during increasing and decreasing pressure at room temperature to a limit of 1600 bar with the first sample, and up to 1400 bar with the second. In the second series, and using

the second sample, a cyclic path was followed with the object of separating liquid-like from glass-like effects of pressure on the conductivity. Starting at room temperature the temperature was raised until the value 57.5°C (somewhat below T_g so that thermal annealing and crystallisation would be avoided) was reached, at which point the pressure of 1500 bar was applied. After waiting for a sufficient period for complete structural equilibrium to be reached, the conductivity was measured during steadily decreasing temperature back to room temperature. At this point pressure was released resulting in a solid-like decompression and an increase of conductivity. The conductivity was then measured while the temperature again raised until T_g was passed and the frozen-in compression from run 2 was released resulting in a further conductivity increase. The temperature was then lowered to verify that the starting conductivity at 1 atmosphere pressure and room temperature could be re-established.

3. Results

The results of the two series of measurements are shown in figs. 1a and b. The solid circle in fig. 1a is from the earlier ambient pressure study of Malugani et al. [8].

There is a substantial difference between the conductivities of the two samples, which is probably due to air oxidation of iodide in the melt in the second case. However, the interest of the present study lies in variations of the conductivity with pressure at different temperatures, and the absolute accuracy of the measurements is not of great importance. It can be seen that the pressure dependence of the conductivity is very similar in the two cases.

4. Discussion

The effect of pressure on the glass at temperatures far below the glass transition is as might be expected from previous studies [4,5]. The slope of the fig. 1a plot can be converted to a volume of activation ΔV using the standard transition state expression

$$\mathrm{d}\log\sigma/\mathrm{d}P = -\Delta V/RT. \qquad (1)$$

The values of ΔV obtained from the slopes of the fig. 1a plots are 2.6 and 3.8 cm^3/mole respectively which compare reasonably well with the volume of a mole of silver ions of radius 0.95 Å. $V_m = 2.6$ cm^3/mole. Hamann [4] found $\Delta V = 3.5 \pm 0.3$ cm^3/mol for Na^+ conducting in sodium silicate glass ($r_{Na^+} = 0.95$ Å). In each case the activation volume is a little greater than the ionic volume, though this would be reversed if we used the Goldschmidt radius for Ag^+. If we assign $r_{Ag^+} = 1.26$ Å, for instance, the ionic volume becomes 5.0 cc/mole. The smaller activation volume would in this case need to be explained in terms of the higher polarisability of the Ag^+ ion. The larger Van der Waals attraction for I^- anions makes possible a closer approach in the transition state.

The results of principal interest for this study, however, are contained in fig. 1b, where we compare the effects of pressure on solid and liquid states of

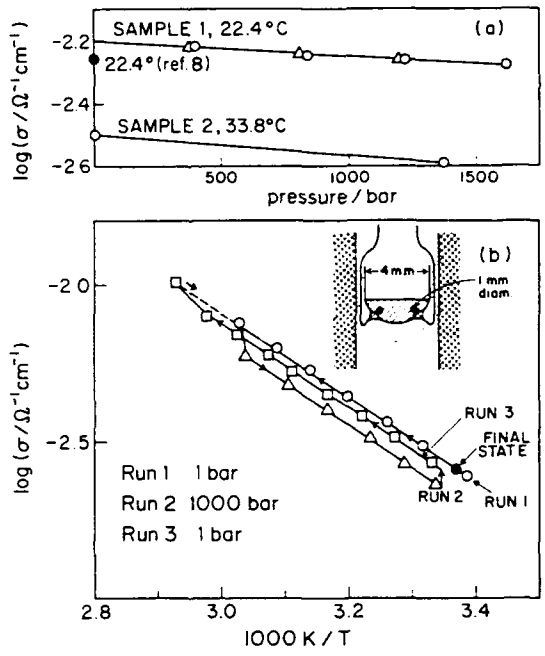

Fig. 1. (a) Effect of pressure on two $4AgI{\cdot}6AgPO_3$ glasses, far below T_g. (○) increasing pressure, (△) decreasing pressure, (●) datum from ref. [8]; (b) temperature dependence of conductivity of sample 2 of part (a) under ambient pressure (run 1) after compression to 1000 bar at 55°C close to T_g (run 2) and after decompression at room temperature, (run 3). Note restoration of original conductivity on relaxation above 55°C. Insert: The 4 mm cell, and twin electrode suspension leads are shown inside a section of the pressure bomb.

the sample. For instance, the compression at 57.5°C, at the limit of run 1 shows the combined effect of elastic (solid-like) and relaxational (liquid-like) compression on the conductivity.

Decompression at room temperature at the end of run 2, on the other hand, shows only the contribution of elastic compression to the conductivity since no configurational change can occur at 60° below T_g on a short time scale. The effect of temperature on the conductivity of a glass with frozen-in configurational compression is seen in fig. 1 run 3. The depression of conductivity due to the frozen-in compressed state $\Delta\sigma$ (conf) is released at the end of path 3 as the temperature approaches the glass transition temperature: the restoration of the original 1 atmosphere pressure conductivity at high temperature is observed satisfactorily. This is confirmed by the conductivity of the same sample on return to ambient temperature, as shown by the filled symbol at the end. Evidently the configurational contribution to the conductivity is relatively small.

It is striking that the elastic effect is much larger than the relaxation (or configurational) effect. Indeed, in some preliminary experiments conducted at constant temperature above T_g, it appeared that (in disaccord with the fig. 1b result) the effect of pressure on the liquid was actually smaller than that on the glass. In neither case, however, was there any confirmation of the initial *increases* of conductivity with increasing pressure seen in the $AgI-Ag_2MoO_4$ system [6].

The reason for the small influence of liquid-like compression on the conductivity of $AgI-AgPO_3$ is, we believe, the same as the reason that the rate of cooling through the glass transition has only weak effects on the conductivity of fast ion conducting glasses [11–13]. In each case the effect is diminished over the effect of the same variable on other structure-related properties, such as viscosity, because of the high degree of decoupling of the conducting modes from the viscous modes and from structural relaxation in general.

As recent studies of the liquid states of fast ion conductors have shown [14], the decoupling process commences in the high fluidity regime far above the glass transition temperature, and is directly responsible for the motional freedom of certain ionic species in the glassy state. As Kawamura and Shimoji [13] have emphasized, the conductivity at T_g can be related to the difference in the B parameters of the Vogel–Tammann–Fulcher equation for transport properties

$$\sigma, \eta^{-1}, D/T = A_i \exp -(B_i/(T-T_0)), \qquad (1)$$

where A_i, B_i and T_0 are constants, since this difference will determine the decoupling index τ_η/τ_σ at T_g [2]. It might therefore be anticipated that the magnitude of the configurational (liquid-like) compression effects on the conductivity will reflect the magnitude of decoupling of conductivity from structure, hence that $\Delta\sigma_{conf}/\Delta\sigma_{total}$ for a given pressure, will be proportional to the ratio B_σ/B_η. We note that Kawamura and Shimoji have suggested this ratio as a quality index for superionic conductors. For the liquid states of superionic conductors B_σ is much smaller than B_η [13,14]. Unfortunately, there is currently a lack of information on the viscosity of the liquid state of fast ion conducting glasses, so the correctness of the anticipated relationship cannot be checked at this time.

This work was supported by the Office of Naval Research under Agreement No. N00014-84-K-2089.

References

[1] T. Minami, J. Non-Cryst. Solids 56 (1983) 15; 73 (1985) 293.
[2] C.A. Angell, Solid State Ionics 9/10 (1983) 3; 18/19 (1986) 72.
[3] M.D. Ingram, Phys. Chem. Glasses 28 (1987) 215.
[4] S.D. Hamann, Aust. J. Chem. 18 (1965) 1.
[5] M. Ryan and S. Smedley, J. Non-Cryst. Solids 65 (1984) 29.
[6] H. Senapati, G. Parthasarathy, S.T. Lakshmikumar and K.J. Rao, Phil. Mag. 47 (1983) 29.
[7] H. Senapati, G. Parthasarathy, K.J. Rao and E. Gopal, Pramana 23 (1984) L269.
[8] J.P. Malugani, A. Wasniewski, M. Dorean, G. Robert and A. Al Rikabi, Mat. Res. Bull. 13 (1978) 427.
[9] T. Minami, V. Takumo and M. Tanaka, J. Am. Ceram. Soc. 60 (1977) 283.
[10] R. Xue and C.A. Angell, to be published.
[11] L. Boehm and C.A. Angell, J. Non-Cryst. Solids 40 (1980) 83.
[12] M. Yoshigawa and M. Tomazawa, J. Phys. (Paris) 43 (1982) C9-41.
[13] J. Kawamura and J. Shimoji, J. Non-Cryst. Solids 88 (1986) 286, 295.
[14] M. McLin and C.A. Angell, J. Phys. Chem. 92 (1988) 2083.

(9)

Reviews of Solid State Science, Vol. 3, Nos. 3 & 4 (1989) 465 – 480

FAST ION CONDUCTION IN GLASSES: THE NEW SOLID ELECTROLYTES

C.A. Angell
Department of Chemistry
Arizona State University
Tempe, AZ 85287

ABSTRACT

In this contribution we discuss the potential of glassy solids to solve the problem of solid electrolyte requirements for electrical power systems. We commence with a comparison of the rival amorphous systems, the fast ion glasses and the ion conducting polymer electrolyte solutions. Both can be related to the familiar aqueous electrolyte systems by concentration on the one hand and by solvent polymerization on the other. Essential difference between the physics of electrical conduction in the two cases will be discussed.

We will then concentrate on the *vitreous* electrolytes, considering how they are formed from the liquid state and the origin of the decoupling of conducting from viscous modes which must occur during the cooling process in order for fast ion conduction to be possible. With this phenomenology established, we will consider the different chemical factors which lead a given type of vitreous system to have superionic conducting properties. We consider cases of cation, proton, and anion conduction and give examples of the current best performing systems in each class.

Finally, we consider wider aspects of the problem by discussing other physical manifestations of the presence of mobile ions in the glassy structure and will speculate on the existence and character of a subsidiary mobile ion "glass transition" which must occur at lower temperatures. Finally, we consider models for conducting glasses and for the conduction mechanism and discuss some controversial issues associated with each of these areas. The application of computer simulation techniques to this problem will be discussed.

INTRODUCTION

Increasing demands are being placed on glasses with energy device potential as applications extend to remote power and communications in hostile cold and high vacuum conditions in polar and space applications. These have generated the need for electrochemical devices which contain no crystallizing or vaporizing materials to replace the usual liquid electrolyte devices. The high conductivity of aqueous electrolyte solutions has been the primary reason that so many battery systems have used them as the electrolytic part of the circuit. The reason that aqueous solutions are so satisfactory in this respect is that they combine the conditions of high dielectric constant (necessary to ensure separation of ionic species as

individual ions) with a low solvent viscosity which ensures that the drag exerted on the moving ions is minimized.

Any attempt to produce solid electrolytes must deal with the problem of maintaining, to the maximum extent, these latter two conditions. There are a few quite different approaches to accomplishing this aim.[1–4] One is to substitute for the aqueous environment a polymeric solvent. When the solvating groups are joined together into a macromolecule the vapor pressure of the solvent falls to zero. Further, if the polymer is of the appropriate structure, it is unable to undergo a crystallization process, thereby guaranteeing that the modes of motion necessary for migration of ions are maintained down to the much lower glass transition temperature T_g. When the polymer chains are sufficiently long another objective is simultaneously met; the chain entanglement phenomenon leads to the acquisition of a shear rigidity for the electrolyte solution so that the ability to flow disappears.[5] (at a temperature well above T_g). In this respect, a "solid" is produced, although microscopically the motion of the polymer chain segments continues to resemble that of a liquid, thus making possible the continued migration of the ions down to T_g.

The interaction between the ions and the solvating groups remains strong (as in water) so that the ion migration is coupled to the solvent relaxation.[6] If the temperature is lowered enough for the polymer to undergo the so-called glass transition where the chain segment rearrangement motion ceases, the electrical conductivity simultaneously vanishes. This is not the case in the alternative route to solid state electrolytes on which we will concentrate in this article. The alternative route we consider is that by which we obtain a vitreous phase as a result of systematic removal of the solvent species,e.g., by evaporation.

Under certain circumstances, the less highly charged ions in aqueous solution of certain salt mixtures can retain their mobility in the liquid while the solution is being concentrated indeed they can remain mobile in the absence of any solvent at all. This happens if a structuring of the complex ionic mixture occurs which leaves certain ions occupying channels in the structure along which migration can occur with relatively little resistance from the remainder. In *practice* such structures are produced by fusing the appropriate mixture of salts and cooling into the glassy state.[7] In the liquid state of such systems, all ions migrate at roughly comparable rates. As the liquid is cooled down, however, the rate at which the majority of the species slow down greatly exceeds the rate at which a minority of mobile, or decoupled, ions slow down. The result is that the glassy state may be entered while a fraction of the ions remains almost as free to move as in the hot liquid. Such distinctions may be revealed by comparing the "activation energies" for conductivity with those for viscosity in the same melts.[9]

The above points are illustrated by the set of activation energies displayed in Fig. 1 for aqueous electrolyte solutions, polymer electrolyte solutions and a molten salt which vitrifies to a fast ion conducting glass. All of the systems show comparable viscosity activation energy/temperature relations which are typical of ionic

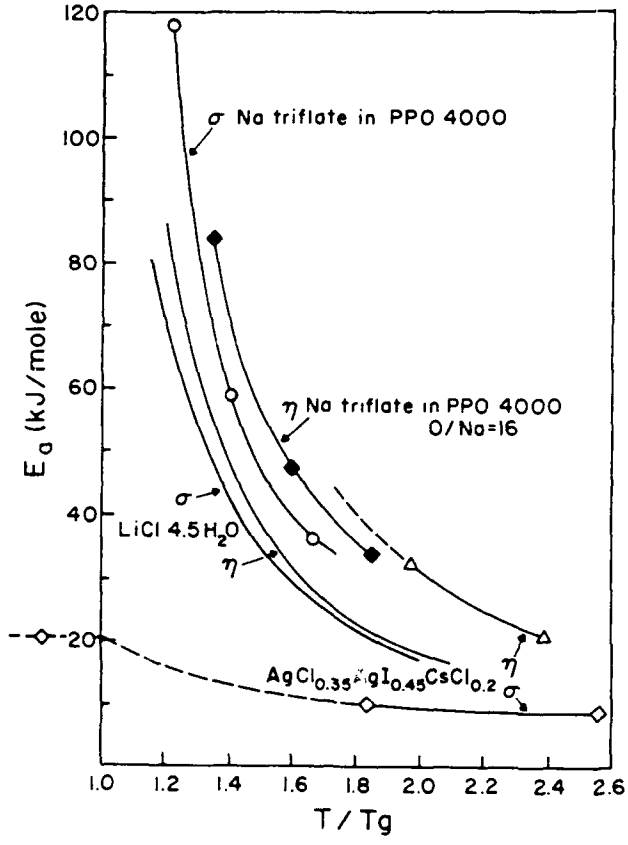

Figure 1. Comparison of the T_g-scaled temperature dependences of activation energies for conductivity and viscosity in three liquids: a salt-in-polymer solution, a salt-in-water solution, and molten salt mixture. The viscosities for *all* systems, and the conductivities of the *solutions*, behave the same strongly temperature dependent way. The low, and weakly temperature dependent, barrier for the *molten salt* conductivity results in a superionic conducting glassy state.

glassforming materials[7] and show an activation energy which diverges as the glass transition is approached. In the aqueous solution and polymer solution cases, the electrical conductivity activation energy shows the same behavior but in the glassy electrolyte the latter remains small at all temperatures. The ratio of viscosity to electrical conductivity activation energy can serve as an index of the quality of the system as a solid electrolyte[8] which is in some ways superior to the "decoupling index" used frequently for this purpose in the past[2]. The advantage of the activation energy ratio is that it remains constant over considerable ranges of temperature (e.g. in the high temperature Vogel-Fulcher region of the liquid, and in the low temperature Arrhenius region) while the "decoupling index", which is a ratio of relaxation times for shear and electrical stresses, varies continuously.

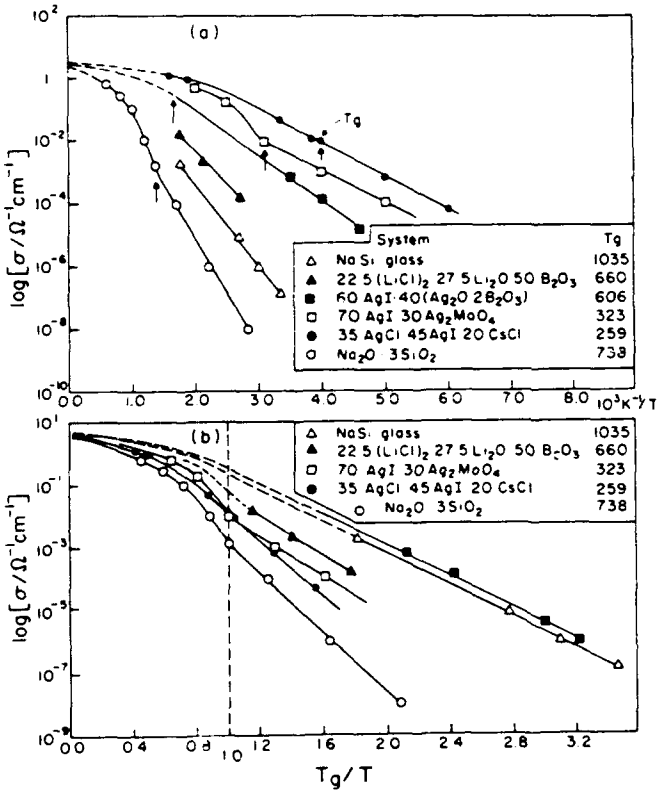

Figure 2. Arrhenius plots of conductivity data for glasses of different T_g and different decoupling indices showing how both factors play a role in determining the ambient temperature conductivity (part a). Part (b) shows how the relative decoupling in different cases can be displayed by a T_g-scaled Arrhenius plot.'

The latter, on the other hand, gives a direct indication of the extent to which the conductivity can proceed independent of the viscous processes in the medium. As will be seen, the decoupling index can reach values as high as 10^{14}. Another useful way of comparing the effectiveness of the mobile ion decoupling from the majority motions in a glassforming system is to put the conductivity data in a reduced form using the ratio T_g/T in place of the reciprocal temperature of the normal Arrhenius plot. A set of data for different fast ion glass systems is shown in Fig. 2. In the best cases it can be seen that passage through the glass transition at $T_g/T = 1.0$ has almost no effect on the conductivity of the material.

It is clearly of interest to examine the chemical factors which lead to behavior of this type. We do this in the following section.

SYSTEMS YIELDING FAST CATION AND FAST ANION CONDUCTING GLASSES

Cationic Conductors

The most studied of the cationic fast conducting glasses have been those in which the component AgI is dissolved in an oxide glass consisting of Ag_2O and one of the common Lewis acid glassformers.[9] The two most widely studied cases are those in which the Lewis acid is P_2O_5 or B_2O_3, the latter system being particularly interesting not only because of the apparently high decoupling indexes but also because of the high glass transition temperatures which it exhibits even at a mole fraction of silver iodide as high as 0.7[10]. Not only have the glassforming regions and the conductivities in these regions been determined for this system, but a range of mechanical relaxation studies extending over 10 orders of magnitude in frequency have been conducted. Some of these we will discuss in more detail later on.

Glasses with high conductivities can also be formed with the Lewis acids GeO_2[11] and no doubt Bi_2O_3, TeO_2, etc., but these have been less studied. The thio-analogs of such systems have also been broadly investigated and, although more difficult to work with because of their tendency to oxidize and to absorb water, they bestow the advantage of lower glass transition temperatures and thus higher conductivities, see Fig. 3. The highest ambient temperature conductivity yet reported is found in the system $AgI–Ag_2S–B_2S_3$.[12,13]

Slightly less complex in character are the related glasses in which silver iodide is mixed with an oxysalt of silver, such as Ag_2MoO_4 or Ag_2CrO_4. These are special cases of the first group in which the Lewis acid base reaction has been taken to the last stage when all $L^{n+}–O–L^{n+}$ bridges (L^{n+} is the Lewis acid cation e.g. B^{3+}, P^{5+}, Cr^{6+}) have been broken. They provide outstanding examples of the

breakdown of the Zachariasen rules for glassforming systems. Presumably, their glassforming ability is a consequence of the low lattice energies of their crystalline forms which causes them to melt at temperatures where the interionic interactions are still strong relative to kT. The result is a high viscosity at the liquidus temperature hence slow crystallisation kinetics. An interesting exception to the latter generalisation is the system AgI–Ag_2SO_4 which, despite exceptionally low liquidus temperatures, can only be vitrified by extremely fast quenching. There appear to be anomalously high nucleation rates in this system, perhaps associated with the nucleation of superionic anion-disordered crystals of entropy almost as high as those of the liquid from which they form.[14] Some interesting behavior is found in ternary systems in which the oxyanion shape is maintained constant, but the size is varied by changing the atom at the tetrahedron center from a small Se(VI) to the larger W(VI).[14] The (AgI-$Ag_2M[VI]O_4$) systems are characterized by low glass transition temperatures which, according to Fig. 2a, favors high ambient temperature conductivity, even when the decoupling indices are not exceptionally high.

The thio-analogs of these systems have so far not been studied to the best of the writer's knowledge. It seems reasonable, in view of the favorable effects of sulfide incorporation in oxide systems studied to date, to expect favorable consequences though it is also possible that the glass transition temperatures will become too low to be practical.

More recent and interesting amongst the cation-conducting superionic glass discoveries are those in which the maximum conductivity is *not* conditioned by the maximum content of α-AgI or its analog. There are two cases, each based on Ag^+ conductivity, in which the best conducting composition is a glass close in composition, and probably therefore similar in microstructure, to a superionic crystal of structure related to AgI. The crystal structures in question are $RbAg_4I_5$ and Ag_3SI. A vitreous phase analogous to the first of these was reported by Liu, et. al.[15] in the ternary system AgI-AgCl-CsCl, and presumably owes its existence to the disorder associated with the mixing of anions. The glass related to Ag_3SI is a composition almost identical to the crystal compound itself, but one which is stabilized in the glassy state (i.e., the crystallization kinetics slowed down in the liquid) by addition of a relatively small amount of a third component.[16] Sun et. al.[16] found that As_2S_3 and Sb_2S_3 were satisfactory but a number of others will probably also serve. Using twin roller quenching, the glassforming region can be pushed almost to the AgI-Ag_2S boundary. The possibility that mixing halide ions at the AgX–Ag_2S stoichiometry might as in the first case, promote glass formation, has not yet been investigated. The glass transition temperatures in each of these cases are very low and the ambient temperature conductivity of $0.9Ag_3SI{\cdot}0.1As_2S_3$ is among the highest yet recorded[16].

Most of the efforts to interpret the high conductivity of glasses in the AgI-Ag oxysalt systems have involved the assumption that some form of clustering of AgI is occurring with intercluster connections allowing for fast Ag^+ diffusion throughout the sample. Indeed, many of the properties in the pseudo-binary systems with AgI as one component tend to the behavior of α-AgI (the high temperature superionic phase of the pure compound) with increasing AgI content,[17] see Fig. 3. On the other hand, such a postulate flies in the face of one of the very few thermodynamic studies of solutions in this type of system[18] which showed clearly that the mixing of AgI with the second component (in this case $AgPO_3$) proceeded with the *release* of energy. Exothermic mixing implies a tendency to chemically *order* rather than to cluster, hence the AgI cluster hypothesis is not supported. We will discuss this important question in considerable detail in a later section with particular reference to the corresponding *alkali* halide + oxyanion systems.

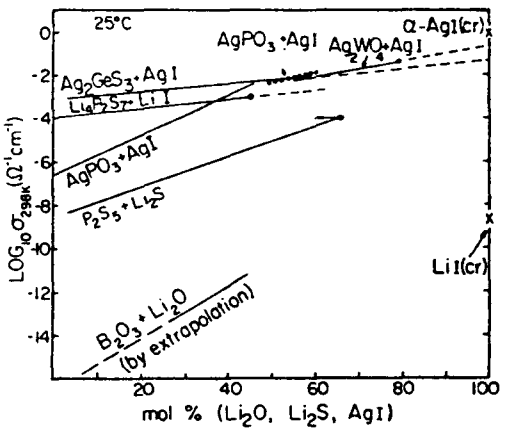

Figure 3. Variation of log conductivity of AgI-containing glasses indicating extrapolation to values for the fast conducting phase of crystalline silver iodide.

The superionic glasses with compositions essentially those of known superionic crystals are clearly disordered systems imitating the structures of the ordered phase. This implies that the decoupling which occurs during cooling is a reflection of the way in which increasingly well-formed amorphous phase versions of the open channel crystal structure can be generated as the configurational degeneracy of the hot liquid is reduced on cooling. In general, it must then be expected that the conductivity of glasses of these compositions will fall below those of the parent crystals, (a relation which is by no means general among ion conducting systems: vitrification may produce a conducting phase from an insulating crystalline material, as in the case of the lithium niobate glasses obtained by roller quenching).

All of the above Ag^+-conducting systems presumably have analogs in which the fast ion is Cu^+, or in some cases Tl^+. We will not discuss these here except to note that an attempt to obtain glasses with properties approaching the exceptional conductivity of the crystal $RbCu_4I_5$, was not successful.[19]

More important for high energy solid state batteries are the glasses in which the mobile cation is an alkali metal. Academically, these are also interesting because of the greater fidelity with which their behavior can be simulated by the methods of molecular dynamics due to the simpler forms of the pair interaction potentials which are appropriate for the inert gas structure cations.

Most of the principles governing the formation of silver ion-conducting glasses apply to the alkali containing systems. Thus the best ambient temperature *alkali* conducting glass is a low T_g system containing an alkali iodide, LiI, in large mole fraction in a thio analog of an oxysalt viz. $Li_4P_2S_7$[20a] or $Li_2S{\cdot}B_2S_3$.[20b] On the other hand, the equivalent of the AgI-Ag oxysalt and the AgI-CsCl type glasses are not yet known.

The most studied of these systems are the cases $LiI–LiPO_3$ and $LiI- LiP_2S_7$. The glasses, however, are hygroscopic and relatively difficult to work with, and for many purposes the less hygroscopic chloroborate systems have been preferred. A system on which a great deal of work has recently been performed is the system $LiCl–Li_2O–B_2O_3$ described initially by Button, et. al.[21]. Again, the highest conductivities are found at the edge of the glassforming range at the maximum LiCl content. The LiCl solubility in $Li_2O{\cdot}nB_2O_3$ (n=1,2,3) is significantly higher than that of LiBr or LiI so the LiCl-based system has the highest conductivity. We will discuss this system, with respect to structural insights from computer simulation studies, later on. For the moment we only note the existence of the naturally occurring compound boracite, the composition of which is $2LiCl{\cdot}2Li_2O{\cdot}3B_2O_3$, and the implication that a chemical ordering of LiCl in the glass may be involved in its favorable conductivity.

Again, as in the case of the silver containing systems, there are similar systems based on other Lewis acid oxides, GeO_2, P_2O_5, TeO_2, etc., and also there are higher conducting thio-analogs. A notable feature of the latter systems is that the glassforming range always extends to higher alkali in the case of thio rather than oxy compounds, e.g. where the orthosilicate glasses can only be obtained under extreme quenching conditions,[22] it is easy to obtain thio-based analog glasses at compositions even exceeding the ortho-thio-silicate composition.[23] Oddly enough it does not appear that the conductivity is as strongly favored by high basicity in these systems as in the oxides.

Among the more practical alkali conducting glasses, although certainly not the highest conducting at ambient temperatures, are the "Nasiglass" type compositions

described by Susman, et. al.[24] These are glassy analogs of the complex zirconium phosphosilicate "Nasicon" type fast ion conducting crystals, and owe their properties to the open network structure characteristic of the latter compound. These are systems with *high* glass transition temperatures and almost complete decoupling, see Fig. 2b. The decoupling index for Nasiglass at its T_g, for instance, is 10^{14}.

Anion-Conducting Glasses

Although fluoride anion conducting glasses such as the lead fluorosilicates[25] have been known for a long time, it is only recently that concerted efforts to obtain really high fluoride ion-conducting glasses have been made. The best cases so far reported have been those with high PbF_2 contents. These glasses are not obtained in the system which first comes to mind (PbF_2 + $Pb(PO_3)_2$) which only vitrifies at high $Pb(PO_3)_2$ contents[26]. However, it turns out that either a replacement of $Pb(PO_3)_2$ by $Al(PO_3)_3$[27] or addition of a third component such as MnF_2 to the all-lead cation system,[28] gives easy vitrification at lead fluoride contents as high as 80 mole percent. While by no means rivalling the silver or alkali cation conducting glasses, these latter anion-conducting systems and some B_2O_3-based analogs[29] reach conductivities of 10^{-4} $\Omega^{-1}cm^{-1}$ at 200°C, comparable with $Na_2O{\cdot}2B_2O_3$. Some data are shown in Fig. 4.

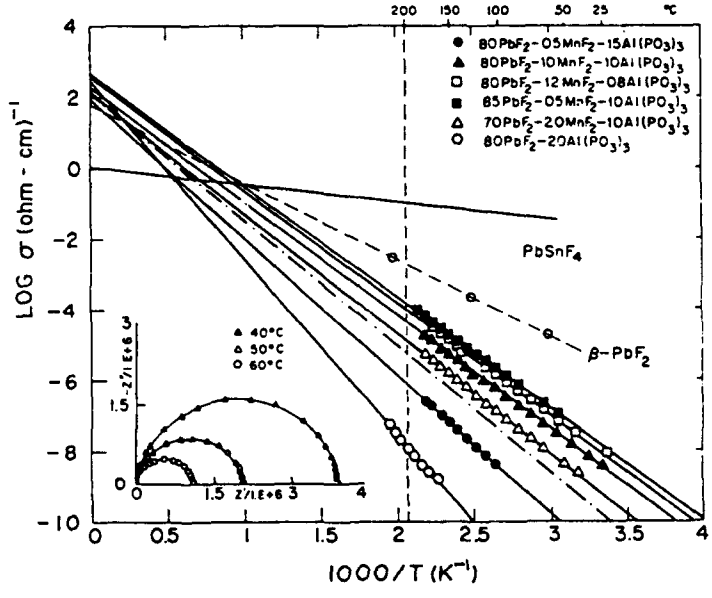

Figure 4. Arrhenius plots of data for high fluoride ion conductivity glasses. Comparisons are made with crystalline β–PbF_2 and $PbSnF_4$, the best fluoride ion solid electrolytes known. (from ref. 27, reproduced by permission).

The best *crystalline* fluoride ion conductor is the compound $PbSnF_4$ which shows a remarkable $10^{-1}\Omega^{-1}cm^{-1}$ at ambient temperature (see Fig. 4). Attempts to imitate this structure within the glassy state by addition of SnF_2 to the PbF_2+$Pb(PO_3)_2$ system, however, failed due to unsatisfactory glassforming ability. It now appears that extremely high fluoride ion conductivity may be obtained in a stannous fluoride-rich composition based on the binary SnF_2+$Sn(PO_3)_2$ described by Tick, et. al.[30] Details have yet to be published. *Mixed Anion-Cation Conducting Glasses*

Since the system PbF_2–$Al(PO_3)_3$ when rich in PbF_2 is a good fluoride ion conducting system and since one of the more startling early discoveries of high alkali conducting glasses was the LiF–$Al(PO_3)_3$ glass rich in LiF, it is reasonable to inquire about the possibility of pseudo-binary glasses cutting across the PbF_2–LiF–$Al(PO_3)_3$ system in which there is a transition from anion conduction to cation conduction. A hint that interesting phenomenology in such systems would be found was given by the study of Reau, et. al.[31] on the effect of LiF additions to a fluorozirconate anion-conducting glass. These authors showed that a sharp minimum in the ionic conductivity occurred at 20% added LiF where they supposed the transition from anion to cation conduction occurred.

A detailed study of the more straight-forward ternary system, LiF–PbF_2–$Al(PO_3)_3$ at constant 20 mole % $Al(PO_3)_3$ has allowed some clarification of this interesting situation. In brief, Kulkarni and the author[28b] concluded that the conductivity minimum is *not* due to a mobility crossover but is instead just a reflection of a minimum in the glass transition temperature and, more important, in the decoupling index. Their best estimate was that the changeover from anionic to cationic conductivity occurred at a higher LiF content of about 50 mol % and was indicated by a maximum in the dispersion of the electrical modulus. A resolution of this problem should be available through suitable pulsed-gradient diffusion coefficient measurements since both Li and F are very favorable nuclei for NMR studies.

COMPUTER SIMULATION STUDIES OF FAST ION CONDUCTING GLASSES

The power of computer simulation to give detailed molecular level information on particle dynamics and structure in condensed phases has so far been little applied to the problem of fast ion motion in glassy solids. Some introductory results, which were limited by the short simulation runs feasible at the time, were reported for a classical alkali silicate system[32] and also a fluoride anion conductor[33] in this laboratory in 1981-2. Cheeseman[34] has since produced and circulated pseudo-3D movies of sodium silicate and lithium chloroborate glasses. However, no detailed studies have yet appeared. A new study by Syed et. al.[35] goes some way towards

filling this gap.

Although the most interesting and structurally most controversial fast ion conducting systems are those involving silver iodide dissolved in various oxyanion matrices, these are the most difficult to simulate realistically because of the complexity of the potentials needed to properly represent the highly polarizable Ag^+ and I^- species. More feasible to simulate among the candidate materials for solid electrolyte applications are the mixed alkali chloride-alkali borate glasses since pair potentials of the Born-Mayer-Huggins type have long been known to permit realistic simulations of the properties of alkali halides.[36,37] Furthermore good agreement has been obtained[38,39] with the observed properties of B_2O_3 and alkali borosilicate systems using potentials of the same type. We have simulated several compositions, including the end members LiCl and $Li_2O{\cdot}2B_2O_3$, in both liquid and glassy states. Details are reported elsewhere[35] and we give here only some key findings.

In all compositions studied B^{3+} and O^{2-} are slow-moving species with very similar diffusivities while Li^+ and Cl^- are more mobile. Thus, during cooling, the system becomes non-ergodic (fails to properly sample its configuration space, hence enters the "glassy" state[40]) first with respect to the structure of the strongly bonded boron-oxygen network (perhaps better described as a trellis in this case) which weaves through all the binary melts in this system. Plots of the mean squared displacement of oxygen (which is the majority species in the composition $0.419(LiCl)_2{\cdot}0.581(Li_2O{\cdot}2B_2O_3)$ at the edge of the experimental glass-forming range) show that below 2000K diffusion of oxygen has effectively ceased on the time scale accessible to our simulation, hence the system has "vitrified." As expected this occurs at a much higher temperature than T_g of the laboratory glass (~ 770K). At the same temperature the Li^+ species is still freely moving, though the effective rigidification of the boron-oxygen network causes a pronounced change in the temperature dependence of the Li^+ diffusivity. This is seen in Fig. 5 which shows the behavior of all diffusing species in the above composition (except boron which is omitted for clarity.) What is surprising and unexpected in Fig. 5 is that the diffusivity of the chloride ion in the glassy state remains the same proportion of the lithium ion diffusivity that it was in the liquid state. It is possible that this high mobility of a large species, which would suggest "micro-pools" of liquid LiCl in the vitreous structure, is a consequence of the higher fictive temperature for the present system and would not be found in the laboratory glass, but it certainly stimulates an interest in determining experimentally whether Cl^- is in fact mobile in the chloroborate glasses. In computing the electrical conductivity in the glassy states of our system it is clearly necessary to take into account the chloride ion contribution.

Nernst-Einstein equation to convert individual Li and Cl diffusion coefficients D_i into partial conductivities, σ_i according to

$$\sigma_i = n_i z_i^2 e^2 D_i / k_B T$$

where n_i is the number density of species i, $z_i e$ is its charge (in coulombs), and the results are shown in Fig. 6.

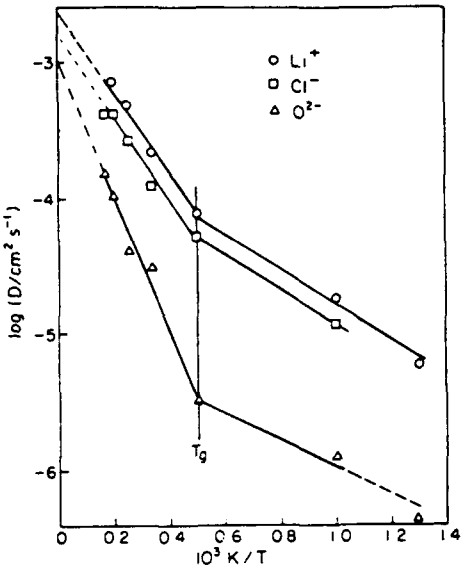

Figure 5. Temperature-dependence of computed diffusivities as Arrhenius plots for all species in the system $Li_2O{\cdot}2B_2O_3$ + 41.9%$(LiCl)_2$. Note how both Li^+ and Cl^- remain mobile in the glass.

The agreement of the computed conductivity of lithium chloride with the classic results of van Artsdalen and Jaffe[41] is extremely good although this must be partly fortuitous because we have neglected coulomb drag or ion pair migration effects which cause the ~ 25% deviations from the Nernst-Einstein equation found in laboratory studies.[42] The high temperature extensions of the experimental data made possible by this calculation give an improved indication of the limiting high conductivity for ionic systems and compare well with the values calculated from the far infrared absorptivities of alkali glasses.[43] The much lower value of the high temperature liquid conductivity for the chloroborate is misleading since the conductivity was calculated only from the lithium and chloride diffusivities. This is valid for the glassy state but clearly underestimates the liquid state conductivity to which contributions must be made from the (now rapidly rearranging) boroxy ZZ component.

The computed glassy conductivities for $41.9(LiCl)_2 \cdot 58.1(Li_2O \cdot 2B_2O_3)$ are compared with the experimental values in Fig. 6, open and filledcircles, respectively. The simulated values are higher, and have a smaller activation energy. However, this is expected since the very high fictive temperature of the computer glass leaves the mobile species unusually free to move in comparison with the experimental system. The fact that the difference is as *small* as it is at the experimental T_g in our opinion enhances the possibility that chloride mobility will be found in the experimental system. (The simulations suggest that the chloride diffusivity at the experimental T_g would be just within range of pulsed gradient NMR diffusion measurements. Since these can now be studied at high temperatures, there is a reasonable prospect that the simulation prediction can be checked in the near future.)

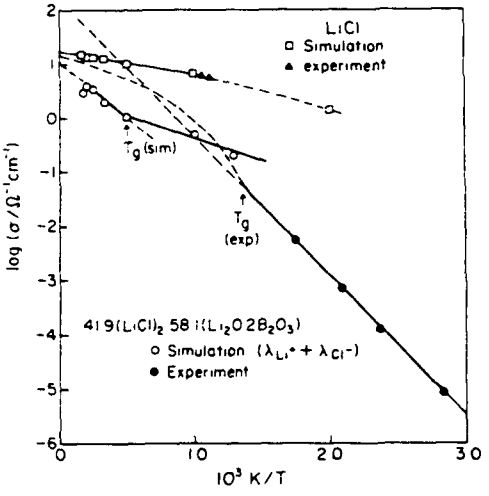

Figure 6. Arrhenius plots of calculated conductivity in liquid and glass states of $Li_2O \cdot 2B_2O_3$ + 41.9% $(LiCl)_2$, and liquid state of LiCl, compared with experimental data for each case. Note the excellent agreement in the case of liquid LiCl for which the simulated system is in full equilibrium. The deviation from experiment for the glass is in the direction expected from the high fictive temperature of the simulated glass.

A further comparison with experiment can be made using the light scattering based observations by Borjesson and Torell[44] that a maximum damping of ~ 28 GHz phonons in the glass 41.9 $(LiCl)_2 \cdot 59.1(Li_2O \cdot 2B_2O_3)$ occurs at 250°C. This was attributed to damping of the sound waves by Li diffusion on a time scale of $[2\pi(28 \times 10^9)]^{-1}$s, or 5.6×10^{-12}s. We may make a crude estimate of the expected relaxation time from the Einstein equation $D = l^2/6t$. If we assume the Li^+ ions relax the stress by jumping an ionic radius (0.66 Å) from their initial sites then we can identify τ_{Li^+} with the t of the Einstein equation. Then, with D_{Li^+} at 523 K of ~

$1x10^{-6}$ cm^2 sec^{-1}, we obtain $\tau_{Li^+} = 7.3x10^{-12}s$. The agreement is closer than should be expected, probably due to compensating fictive temperature and assumed jump distance errors.

The structure of the glass responsible for this behavior is, of course, of interest but space does not permit its discussion here. The reader is referred to a more detailed description given elsewhere.[45]

CONCLUDING REMARKS

The combination of laboratory and computer simulation studies of the same systems is a frutiful one and deserves further development of particular interest in the case of Nasiglas[24] in which extremely decoupled[2] Na^+ motion is obtained without resort to the addition of chloride or other low field anions. We will hope to report on such studies at a future workshop.

ACKNOWLEDGEMENTS

The author has benefited from the support of the Department of Energy under grant number DE-FG02-84ER45 and the Office of Naval Research under agreement No. N00014-84-K0289 in carrying out much of the research summarised in this article. The contributions of his many co-workers in this work is clear from the published works from this laboratory to which we have made frequent reference.

REFERENCES

1. J.L. Souquet, Solid State Ionics, *5*, 77 (1981).
2. (a) C.A. Angell, Solid State Ionics, *9 & 10*, 3 (1983).
   (b) C.A. Angell, Solid State Ionics, *18 & 19*, 72 (1986).
3. (a) M.B. Armand, J.M. Chabagno and M.J. Duclot in "Fast Ion Transport in Solids," Eds. P. Vashista, J.N. Mundy, and G.K. Shenoy, North-Holland 1979.
   (b) M.B. Armand, Solid State Ionics, *9/10*, 745 (1983).
4. E.I. Cooper and C.A. Angell, Solid State Ionics, *18 & 19*, 570 (1986).
5. J. D. Ferry, "Viscoelastic Properties of Polymers," Wiley, N.Y., 1980.
6. L.M. Torell and C.A. Angell, British Polymer Journal, *20*, 173 (1988).
7. M.D. Ingram and C.A. Vincent, Ann. Rep. Chem. Soc., 23 (1977).
8. M. McLin and C.A. Angell, J. Phys. Chem. (Letters Section), *92*, 2083 (1988).
9. (a) J. Kawamura and J. Shimoji, J. Non-Cryst. Sol., *88*, 295, 286 (1986).
   (b) C.A. Angell in *Solid Electrolytes*, Ed. T. Takahashi (in press).
10. A. Chiodelli and A. Magistris, Mat. Res. Bull., *17*, 1 (1982).

11. Souquet, J.L., Solid State Ionics, *5*, 77 (1981).
12. Carette, B., Robinel, E. and Ribes, M., Glass Tech. Ber: *24*, 157 (1983).
13. Burckhardt, W., Makta, M., Levasseur, A. and Hagenmuller, P., Mat. Res. Bull., *19*, 1083 (1984).
14. Senapati, H. and Angell, C.A. (to be published).
15. Liu, C., Sundar, H.G.K. and Angell, C.A., Mat. Res. Bull., *20*, 525 (1985).
16. Sun, H.W., Tanguy, B., Reau, J.M., Videau, J.J., Portier, J., and Hagenmuller, P., J. Solid. St. Chem. *70*, 141, (1987).
17. Martin, S.W. and Schiraldi, A., J. Phys. Chem., *89*, 2070 (1985).
18. Reggiani, J.C., Malugani, J.P. and Bernard, J., J. Chim. Phys., *75*, 846 (1978).
19. Liu, C. and Angell, C.A., Solid State Ionics, *13*, 105 (1984).
20. (a) Malugani, J.-P., Wasniewski, A., Dorean, M., Robert, G., and Al Rikabi, A., Mat. Res. Bull., *13*, 427 (1978).
    (b) Burckhardt, W., Makta, M., Levasseur, A. and Hagenmuller, P., Mat. Res. Bull., *19*, 1083 (1984).
21. Button, D.P., Tandon, P.P., Tuller, H.L. and Uhlmann, D.R., Solid State Ionics, *5*, 655 (1981).
22. Tatsumisago, M., Minami, T. and Tanaka, M., J. Amer. Ceram. Soc., *64*, C97 (1984); *66*, 890 (1983).
23. Susman, S., Boehm, L., Volin, H.J. and Delbecq, C.T., Solid State Ionics, *5*, 667 (1981).
24. Susman, S., Delbecq, C.J., McMillan, J.A. and Roche, M.F., Solid State Ionics, *9 & 10*, 667 (1983).
25. Shultz, P.C. and Mizzoni, M.S., J. Amer. Ceram. Soc., *56*, 65 (1972).
26. Sundar, H.G.K., Martin, S.W. and Angell, C.A., Solid State Ionics, *18 & 19*, 437 (1986).
27. Kulkarni, A.R. and Angell, C.A., Mat. Res. Bull., *21*, 1115, (1986).
28. (a) Kulkarni, A.R. and Angell, C.A., Mat. Res. Bull., *21*, 1115 (1986).
    (b) Kulkarni, A.R., Sundar, H.G.K. and Angell, C.A., Solid State Ionics, *24*, 253 (1987).
    (c) Kulkarni, A.R. and Angell, C.A., J. Non-Cryst. Sol., *99*, 195 (1988).
29. J.E. Shelby, J. Am. Ceram. Soc., *68*, C177 and 551 (1985).
30. P. Tick (unpublished work).
31. J.M. Reau, J. Senegas, H. Aomi, P. Hagenmuller and M. Poulain, J. Sol. St. Chem., *60*, 159 (1985).

32. C.A. Angell, L. Boehm, P.A. Cheeseman and S. Tamaddon, Solid State Ionics, *5*, 669 (1981).

33. C.A. Angell, P.A. Cheeseman and S. Tamaddon, J. De Physique Colloque, *43*, C9-381 (1982).

34. P.A. Cheeseman, Purdue University Computing Center Production -- video tape available.

35. R. Syed, J. Kieffer and C.A. Angell, Symp. Mat. Res. Soc., Dec. 1988.

36. L.V. Woodcock in Advances in Molten Salt Chemistry, 3, ed. J. Braunstein, G. Mamantov, and G.P. Smith, Plenum, 1973, p. 1.

37. E.M. Adams, I.R. McDonald and K. Singer, Proc. R. Soc. Lond. A., *357*, 37 (1977).

38. T.H. Soules, J. Chem. Phys, *73*, 4032 (1980).

39. T.H. Soules and A.K. Varshneya, J. Am. Ceram. Soc., *64*, 145 (1981).

40. C.A. Angell, J.H.R. Clarke and L.V. Woodcock, Adv. Chem. Phys., *48*, 397 (1981).

41. E.R. van Artsdalen and Jaffe, J. Phys. Chem., *59*, 118 (1955).

42. C.A. Angell, J. Phys. Chem., *69*, 399 (1965).

43. Changle Liu and C.A. Angell (to be published in J. Chem. Phys.); C.A. Angell, Solid State Ionics, *18&19*, 72 (1986).

44. L. Borjesson and L.M. Torell, Solid State Ionics, *25*, 85 (1987).

45. R. Syed, J. Kieffer and C.A. Angell (to be submitted to J. Chem. Phys.).

(10)

Dynamic Processes in Ionic Glasses

C. A. ANGELL

Department of Chemistry, Arizona State University, Tempe, Arizona 85287-1604

Received November 6, 1989 (Revised Manuscript Received February 14, 1990)

Contents

I. Introduction

The field of dynamic processes occurring within the glassy state of matter is too broad to be dealt with in a single article. There is, for instance, an enormous literature on the subject of tunneling modes (two-level systems) which leads glassy solids systematically to violate the Debye T^3 law for the low-temperature heat capacity of solids. To this must be added a relevant and rapidly growing literature on the "hole-burning" phenomenon. There is an even larger literature on secondary, tertiary, and quaternary relaxations in polymeric glasses, the understanding of which is of great importance for many technological applications of polymeric materials. Both of these research fields lie outside this reviewer's area of interest and competence. We will, accordingly, restrict out attention to a subsection of the broader subject and focus most of our attention on the phenomenology of dynamic processes in ionic glasses at temperatures well above 0 K. However, we will give an initial minireview section (section II) to locating the problem area that we will review within the broader subject.

While the author knows of no previous review that attempts to cover the same range of subject matter from the same approach, there are a number of important articles, which review in greater depth than we can here, various individual aspects of the subject. We assemble these references, several of which appear in a current thematic issue of *Materials Chemistry and Physics* (Vol. 23, nos. 1/2), in ref 1a. We will, however, refer to the most relevant articles individually in the text.

C. A. Angell was born in Canberra, Australia, in 1933, and studied to the M.Sc. level at the University of Melbourne. After working on molten salts in the electrochemistry group of J. O'M. Bockris at the University of Pennsylvania for 2 years, he became the Stanley Elmore Fellow at the Imperial College of Science, London. While there, he obtained a Ph.D. as a student of J. W. Tomlinson, winning the Armstrong medal for graduate research at Imperial College for 1959–1961. He then returned to Melbourne, but after 2 years as a lecturer in chemical metallurgy he came back to the United States as a Research Associate with D. M. Gruen at Argonne National Laboratory. In 1966 he joined Purdue University as an Assistant Professor, becoming full Professor in 1971. He has profited from one-semester sabbatical leaves in Holland (University of Amsterdam) in 1970, Australia (The National University) in 1975, and France (Inst. Laue Langevin in 1979 and Ecole de Physique et Chemie, Paris, in 1983). His research interests spread from water through aqueous and polymeric solutions to molten salts, glassy solid electrolytes, and glassy solids in general, with particular emphasis on the motion of particles and the time scales on which stresses imposed on liquid and glassy systems are relaxed. Recently he has become involved in geochemistry via his computer simulation and laboratory studies of liquid silicates and in the properties of liquids at negative pressures. In 1989 he accepted a position in the Department of Chemistry, Arizona State University, where he is pursuing several new lines of research in collaboration with ASU scientists specialized in high-pressure and microscience techniques.

Almost all liquids, when cooled either fast enough or in small enough sample sizes, will fail to find the channel in phase space leading to the crystalline state.[2] Then as the particle kinetic energies become too small to permit diffusion, the viscosity diverges and the system becomes locked into the amorphous state as a glass. Liquids as simple and familiar as toluene are easily vitrified in bulk, and even benzene may be vitrified on normal time scales when in the form of 2–300-Å droplets in microemulsions.[3,4]

To many workers, the process of slowing down of the viscous modes, which is currently the subject of a great deal of experimental and theoretical activity,[5] is one aspect of *glassy* dynamics, and the absence of a detailed discussion of the subject in this article may seem to be a serious if not glaring omission. However, while slow-

0009-2665/90/0790-0523$09.50/0

ing down in liquids is an area of great interest to this author, it is his view that the behavior of an amorphous phase in *metastable equilibrium* (i.e., when the sample under study is in internal equilibrium both before and after it is probed by the experimentalist) belongs to the field of *liquid* state, not *glassy* state, studies. Thus the many studies on dielectric relaxation, ultrasonic and hypersonic relaxation, NMR, and ac heat capacity in viscous liquids[5] will be excluded from the review. Rather, the review will focus on those modes of motion that remain active in the temperature (or pressure) regime that lies below (or above) the glass transition temperature (or pressure), i.e., in the state in which the majority of the particles in the system are "frozen" into a fixed configuration. The actual configuration is, of course, not unique, and much of the behavior that we will review will in fact be determined by the manner in which the system passes initially into the glassy (i.e., nonergodic) state. Let us thus first examine the process of vitrification.

II. Vitrification, Primary and Secondary Relaxation Processes in Amorphous Systems, and Scope of the Review

Vitrification occurs because of the crossing of the intrinsic liquid relaxation time scale and the external, experimentalist-controlled, observation time scale. Let us consider cooling as a series of stepwise decreases in temperature followed by short (isothermal) equilibration periods. Initially, when the liquid relaxation time is very short, the equilibration time Δt is quite sufficient for the system to explore its full configuration space before the next drop in temperature ΔT occurs. However, because the relaxation time τ is increasing with decreasing temperature (at a rate that depends on the liquid "fragility"; see below) at some point during the cooling, a temperature must be reached at which the liquid will not be fully equilibrated (ergodic) before the next ΔT decrease in temperature occurs. Since, after this next ΔT, the mismatch of τ and Δt will be worse, so the degree of equilibration achieved in the next (and in each subsequent) ΔT, will rapidly diminish—and will soon become undetectable (see Figure 5 of ref 6). At this point the liquid configuration (its "structure") has become fixed except for minor adjustments due to decreasing vibrational anharmonicity and to more or less localized, low energy barrier, configurational adjustments—the so-called secondary relaxations on which this review will be focused. The substance is said to be "vitreous" and textbooks describe it as a "frozen liquid". As we shall see, it is in fact alive with irreversible motions of different types. These motions can be so free as to lead, in some cases, to glassy materials that exhibit ambient temperature electrical conductivities not much below that of battery acid and, in others, to glasses with the ability to absorb large amounts of mechanical energy on very short time scales—e.g., in high impact strength polymers.

The temperature range over which the liquid passes from the fully ergodic metastable state into the glassy state (called the "glass transformation range") is effectively the temperature change needed to change the relaxation time by about 2 orders of magnitude across the experimental cooling time scale.[6-8] This temperature range is different for different systems and also for

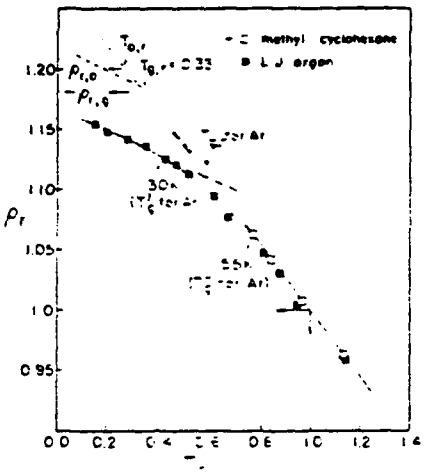

Figure 1. Dependence of glass density on quenching rate q using reduced variables. For methylcyclohexane $q = -10$ K/min, while for LJ argon $q = -10^{12}$ K/min (by computer simulation). Corresponding states are states of equal diffusivities, $D = 10^{-5}$ cm^2 s^{-1}. Reprinted from ref 10; copyright 1981 New York Academy of Sciences.

different cooling or compression rates. It is smallest for systems that have very large temperature dependences of their relaxation times in the region where equilibrium is being lost and that also have only narrow distributions of relaxation times. Since distributions tend to be narrowed under conditions where the temperature dependence is smaller (e.g., (i) "strong", as opposed to "fragile",[9] liquids being vitrified on normal time scales or (ii) fragile liquids being vitrified on short, as opposed to long, time scales), these effects are somewhat related. However, it is not of great importance for the purpose of this review that the relationships be analyzed. It *is* important, however, to emphasize the differences in density of the vitrified material that may result from differences in the rate of cooling through the glass transformation range, since the packing in the glass may be expected to play an important role in the dynamics of processes occurring in the glassy structure.

Figure 1 shows, in reduced units, an extreme case[10] where we compare the densities of two van der Waals glasses, one (methylcyclohexane) produced by ordinary laboratory time scale cooling and the other (Lennard-Jones argon) produced by the very fast quenching procedure employed (faute de mieux) in molecular dynamics computer simulation "experiments". The corresponding states used in the reduction (which are explained in the original publication[6,10]) were chosen as the states exhibiting liquid diffusion coefficients of 10^{-5} cm^2 s^{-1}. Figure 1 (from ref 10) shows that the slower cooled system achieves a density approximately 5% greater than that of the hyperquenched system. It can readily be imagined that the residual dynamics in the glassy state can be generally affected by such a difference in packing densities.

The presence of residual looseness in glassy phases implies that the system should exhibit an anelastic response to mechanical stresses. This is because the local displacement of particles at loose spots in the overall jammed structure can serve to relax the applied stress, in a reversible manner. Certainly, such elastic responses (which were predicted to be a universal feature of the glassy state in a classic paper by Goldstein[11]) are very generally (though not universally) observed.[12] If the

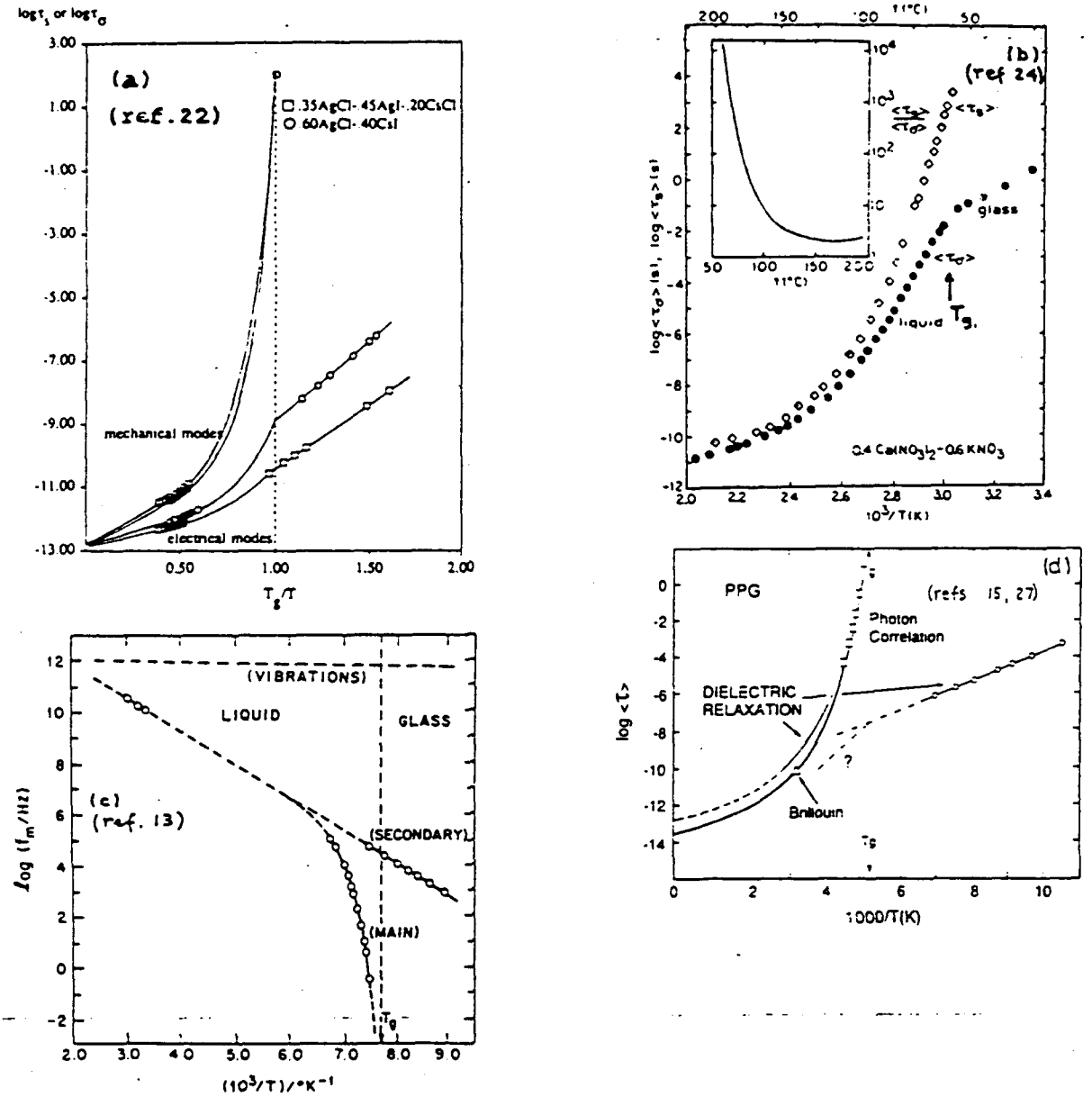

Figure 2. (a) Comparison of average shear and electical relaxation times, reflecting slow and fast processes for liquid and glassy states of ionic 3AgCl·2CsI solution (reprinted from ref 22; copyright 1988 American Chemical Society). (b) Comparison of average shear and electrical relaxation times, reflecting slow and fast processes for liquid and glassy $3KNO_3$-$2Ca(NO_3)_2$ solution (reprinted from ref 24a; copyright 1974 American Chemical Society). (c) Comparison of most probable dielectric relaxation times for slow (primary) and fast (secondary) relaxation processes in *cis*-decalin + 17.2% chlorobenzene solution.[15] Dashed line shows approximate behavior of the average relaxation time for the secondary process. (d) Comparison of most probable dielectric relaxation times for slow (primary) dielectric and mechanical relaxation times[27] and fast (secondary) dielectric relaxation times for poly(propylene oxide).[14] (Secondary relaxation data taken from ref 15).

local displacement involves a change of dipole moment, such relaxations can also be detected by electrical field relaxation or dielectric relaxation methods. In fact, the majority of studies of such localized relaxation processes in simple molecular glasses have been made by using dielectric relaxation techniques.[12,14-16]

The existence of anelastic processes detectable by frequency-dependent or time-dependent techniques implies the presence of at least one additional time scale in the dynamics of amorphous systems—a time scale that is short with respect to that of the viscoelastic process that leads to the glass transition. It is important in introducing this subject that the relation of these time scales be established. This is particularly so since the existence of a shorter time scale is a clear prediction of one of the most activity researched theoretical approaches to the slowing-down problem in liquids, viz., the mode coupling theory[17-20] (which is developed in elegant detail by Goetze in a recent lecture series[20]).

It seems that there are at least two distinct classes of dynamic processes residual in glasses to be considered: (i) short-time relaxation processes due to decoupled delocalized motion of a minority species in ionic glasses, and (ii) short-time processes due to strictly *localized* motions that are predominant in organic and polymer glasses but are also present in inorganic glasses, including the ionic cases. Metallic glasses may be close in nature to the ionic case insofar as a fraction of the particles may retain considerable long-range mobility in the frozen vitreous state.[21]

We depict the relationship of long- and short-time processes for four cases in Figure 2. In Figure 2a, which

shows relaxation time data for the system 3AgCl·2CsI (and a related composition) in both liquid and vitreous states,[22] the Ag^+ ion motions are highly decoupled from the remainder. Because Ag^+ is a charge carrier, the fast relaxation process is easily monitored via the electrical relaxation time $\langle\tau_\sigma\rangle$. $\langle\tau_\sigma\rangle$ here is a Maxwell-like relaxation time defined by the relation[23,24]

$$(\sigma_{dc})^{-1} = M_\infty\langle\tau_\sigma\rangle/e_0 \qquad (1)$$

where the electrical modulus, M_∞,[23] is the inverse of the dielectric constant measured at frequencies much higher than $(2\pi\langle\tau_\sigma\rangle)^{-1}$, e_0 is the permittivity of free space ($=8.85 \times 10^{-14}$ F cm^{-1}), and σ_{dc} is the dc electrical conductivity. τ_σ is written as an average value because, when studied as a function of frequency, the electrical relaxation process is found to be nonexponential in nature; i.e., it cannot be characterized by a single time constant (see below). The important observations in Figure 2a are (a) that the short-time process is always distinguishable in time scale ($\langle\tau_\sigma\rangle$) from the longer, viscoelastic (or structural relaxation) process ($\langle\tau_s\rangle$) and (b) the time scale ratio $\langle\tau_s\rangle/\langle\tau_\sigma\rangle$, which was first examined by Moynihan and colleagues[24] and is now known as the *decoupling index*, R_τ,[25] increases continuously with decreasing temperature. In this case R_τ reaches very large values, $\sim 10^{12}$, at the glass transition temperature T_g, though the system is exceptional (it is characteristic of the so-called "superionic" glasses which have liquid-like conductivities ($\sigma \approx 10^{-2}\ \Omega^{-1}$ cm^{-1}) at their glass transition temperature[25,26]). More generally, as shown for the much-studied molten nitrate system in Figure 2b, the electrical relaxation process in ionic systems is similar in time scale to the viscoelastic process when the temperature is high relative to T_g but progressively decouples from it as T falls below $\sim 1.3T_g$.[24] Both show non-Arrhenius behavior initially but the faster process frequently returns to Arrhenius behavior well before T_g is reached. At T_g the plot abruptly changes slope as the glassy state is entered and the overall structure freezes. The temperature dependence of the dc conductivity usually remains strictly Arrhenius in the glassy state though exceptions exist (see below). At lower temperatures, where the relaxation process occurs on time scales accessible to regular admittance bridges, more detailed studies of the process may be made via variable-frequency studies. These will be discussed in the body of the review to follow.

To contrast with the ionic glass formers, Figure 2c shows the behavior observed in simple *molecular* liquids, while Figure 2d shows data for a chain polymer system.[14,27] In the case of molecular glasses, most information on the faster process (usually called the *secondary* relaxation) has been acquired by dielectric relaxation studies.[12-15] While the overall appearance—Arrhenius behavior of the faster process below T_g with a tendency for it to join the primary relaxation in the liquid state—is similar to that seen in Figure 2a,b, there are distinct differences. The main difference, if we accept the data and extrapolations of the reporting authors, is that the secondary relaxations in the molecular systems are insensitive to the structural arrest occurring at the glass transition. An insensitivity to structural arrest implies that the frequency of maximum loss would not change on annealing (as the liquid relaxes to lower volumes), and Johari and

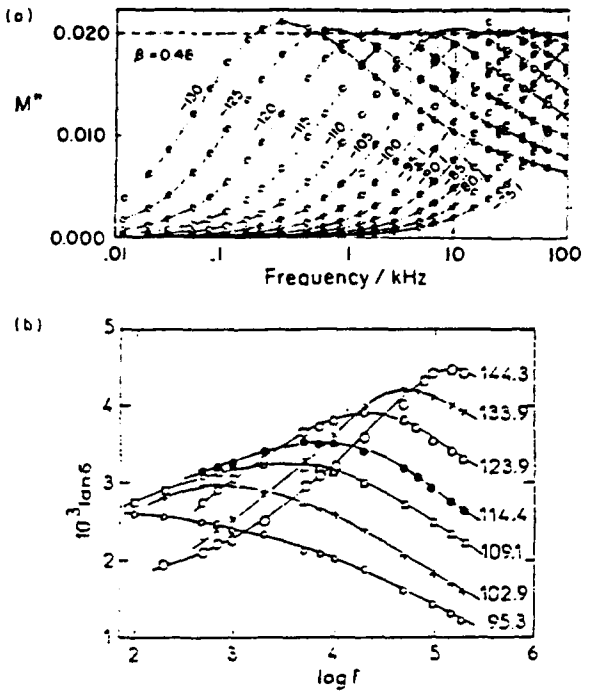

Figure 3. Contrast between secondary electrical relaxation spectra in (a) ionic $3AgI{\cdot}2Ag_2B_4O_7$[38] and (b) molecular poly(propylene oxide)[15] systems. In the ionic case all relaxation spectra have identical shapes, well described by a KWW function (eq 1) with $\delta = 0.55$. In the molecular cases the best description is open to debate (see text).

co-workers have provided evidence that this is the case for some molecular,[13] polymeric,[13] and covalent glasses.[28]

The contrast between the two secondary relaxations in Figure 2c,d illustrates a point of some dispute among workers in this area. The issue in dispute is whether the secondary process should be viewed as colliding with or merging with the primary process. A difficulty in the path of resolving this issue is raised by another major difference between ionic and nonionic cases—a difference that is not evident in Figure 2. This difference concerns the width and temperature dependence of the secondary relaxations in the two cases. In the ionic cases the width of the electrical relaxation (whether or not considered as a single process[24] or as a combination of conductivity and ion-pair dipolar relaxation processes,[29]) is as narrow as the primary viscoelastic relaxation. In the nonionic cases, however, the relaxation not only is much broader but is usually also strongly temperature dependent. This important distinction, which involves one of the fundamental issues of disordered-phase dynamics (viz., the origin of nonexponential relaxation kinetics), is illustrated in Figure 3.

Figure 3a shows that the "loss spectra", i.e., the out-of-phase, or imaginary, part of the complex electrical modulus discussed below, for the fast ion conducting glass $3AgI{\cdot}2Ag_2B_4O_7$ have a temperature-independent shape, in marked contrast with the case of the polymer poly(propylene oxide) (PPO). The rapidly changing shape of the spectra for PPO is typical of the observations for molecular and polymer glasses.[12-14] The rapidly changing shape in these cases means that the average relaxation time will have a different (larger) temperature dependence than the most probable value plotted in Figure 2d and so will show less tendency to intersect the primary relaxation. The broad spectra, the difficulty of separating out the contributions of the

primary process and background losses from those due to the secondary process, and the fact that the total polarization associated with the secondary relaxation decreases with decreasing temperature,[12-14] introduce an ambiguity into the relation between primary and secondary relaxations in the nonionic cases that is not present in the ionic cases. This ambiguity presents a challenge for future workers since it has been forcefully argued[30] that the secondary relaxations in molecular glasses are actually the source and necessary precursor of the primary relaxation which receives most of the theoretical as well as experimental attention.

In any event, Figure 2 now allows us to define the scope of this review in relation to the broader scheme of relaxation dynamics in amorphous systems. Rather than examining in detail all of the phenomena plotted in Figure 2 (not to mention the additional widely researched area of relaxation phenomena found at cryogenic temperatures (the so-called two-level systems)), we will concentrate on the behavior of the subset of processes that may be detected below T_g in ionic systems like those of Figure 2a,b, i.e., secondary relaxations due to mobile ions in ionic glasses. Many of the systematic aspects of the observations we will discuss will probably be found applicable to the organic systems when the detailed studies necessary to discuss the issues are performed. Many detailed studies of the type we will discuss for ionic systems have in fact *already* been performed on *polymeric* systems. These, however, constitute an entire research field of their own which is complicated by the presence of tertiary and quaternary (γ, δ) relaxations and which we make no attempt to enter. The interested reader may consult a rather exhaustive review of "relaxation maps" for polymer systems given by Tõrmälä.[31]

While the scope of our review may seem rather limited, we will, in fact, be examining results of a wide range of experiments covering 18 orders of magnitude in time scale and 1000 K in temperature. From the overview provided, a number of useful unifying patterns, and suggestions for future experimental and theoretical studies, will emerge.

There are three major problem areas to be addressed. They are as follows:

(1) What is the response function for the fast process, and how is it related to perturbing stress on the one hand and to the glass stucture on the other?

(2) What determines the value of the average relaxation time for the fast process at some reference temperature, e.g., the glass transition temperature at which slow processes have a common relaxation time ($\sim 10^2$ s). In other words, what determines the extent of decoupling of fast from slow processes.

(3) How are the fast processes related to the even faster degrees of freedom involved in the vibrational modes of the amorphous phase?

We will deal with these questions in this order but must first provide background material concerning the most appropriate manner of acquiring and presenting the desired information.

III. Relaxation Functions, Complex Moduli, and Constant T vs Constant f Experiments

Before examining in detail the observations on relaxation processes in ionic glasses, it is necessary to consider the sort of experiments that are commonly carried out and the manner in which the results are presented.

What is common to all the measurements we will discuss is that a system in an initial state is perturbed by some external force and the response is monitored. What is different is the nature of the perturbing stress and the way the stress is applied and the response observed. While it is conceptually simpler to produce an instantaneous perturbation of the system and monitor its decay in time, this is not the way most experiments in this field are performed. Rather, experiments are conducted in the frequency domain because details of the relaxation kinetics are in most cases more accurately acquired by frequency-domain techniques. Thus we will be considering mostly *electrical* perturbations that are applied sinusoidally at variable frequencies in a constant-temperature experiment and *mechanical* or *magnetic* perturbations that are applied sinusoidally at fixed frequency at varying temperatures. The differences are due to the exigencies of the experiment: it is much simpler to produce a wide range of frequencies in electrical experiments than in mechanical or magnetic (NMR) experiments.

Responses of the system are measured as real and imaginary parts of complex electrical or mechanical moduli

$$M^* = M' + iM'' = \frac{\epsilon'}{\epsilon'^2 + \epsilon''^2} - \frac{i\epsilon''}{\epsilon'^2 + \epsilon''^2} \qquad (2)$$

or the corresponding susceptibilities ϵ^*, depending on the formalism employed in the analysis. Opinions vary on which formalism is the more appropriate to use for a given set of measurements.[23,29,32,33] It must be remembered, however, that the characteristic relaxation time of a process extracted from a given set of data depends somewhat on the formalism employed in the analysis. The relationship is[1a(i)]

$$\frac{\tau(\text{susceptibility formalism})}{\tau(\text{modulus formalism})} = \frac{\epsilon_0}{\epsilon_\infty} = \frac{M_\infty}{M_0} \qquad (3)$$

Comparisons of response times for different processes should therefore always be made for data analyzed by the same formalism. Because the zero-frequency electrical modulus is always zero for electrically conducting systems such as the ionic glasses of this review, we will analyze all data in the modulus formalism. In ordinary circumstances, i.e., when the system reaches a thermodynamic state of polarization as a long-time response to the perturbation, it is preferable to compare different responses in the susceptibility formalism. This avoids the possibility of differences in response times to different perturbations, which result from analysis formalism rather than to real differences at the molecular level.

A typical set of data for an electrical relaxation experiment on ionic glasses is that shown in Figure 4 for $Na_2O{\cdot}3SiO_2$.[34] The upper portion shows how the real part of the electrical modulus rises from its low-frequency value of zero toward a high-frequency limit, the dispersion region moving to high frequencies as the temperature of the experiment is increased. The lower portion shows the imaginary part of the modulus, which is related to the energy dissipation taking place in the irreversible conduction process. The relaxation process

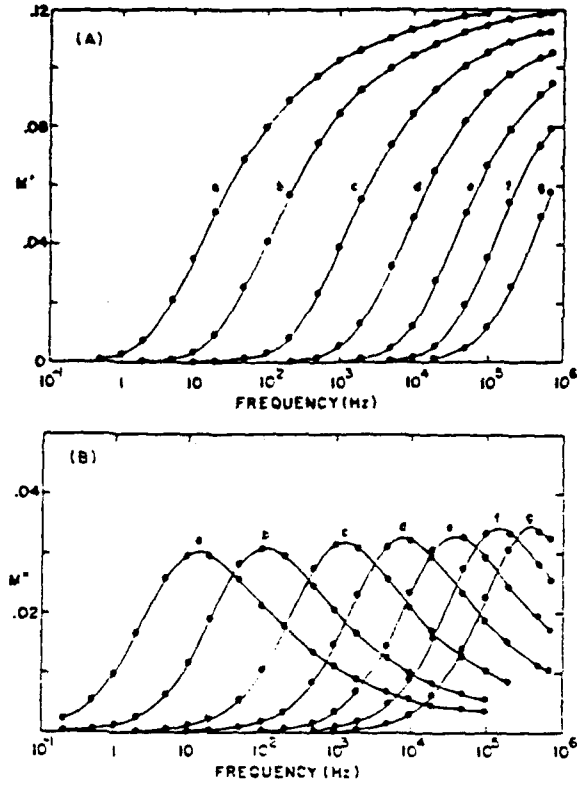

Figure 4. Electrical relaxation in a typical ionic glass. (A) Real, M', and (B) imaginary, M'', parts of the complex electrical modulus for $Na_2O{\cdot}3SiO_2$ glass over a range of temperatures below T_g: (a) −1, (b) 20.8, (c) 52.3, (d) 81.4, (e) 110.2, (f) 137.3, and (g) 163.4 °C. The spectra are well fitted by a Williams–Watts function (eq 1) with $\beta \approx 0.7$. *Reprinted from ref 34; copyright* 1972 American Ceramic Society.

is not exponential, $e^{-(t/\tau)}$, since the spectrum is not a Lorentzian. Its skewed shape is well represented, for poorly conducting glasses at least, by the appropriate Laplace transform of the Kohlrausch decay function

$$\phi(t) = e^{-[(t/\tau)^{\beta}]}, \quad 0 < \beta < 1 \qquad (4)$$

(where $\phi(t)$ is normalized by its value at $t = 0$) as was first recognized for ionic glasses by Moynihan et al.[35] and which has been abundantly documented for these and other systems by Ngai and co-workers[16] (see in particular ref 16b, which gives an exceptionally detailed account of this phenomenology and its relation to primary relaxations). The most probable relaxation time τ_e is obtained from the frequency at maximum loss by $\tau_e = (2\pi f_{max})^{-1}$. It is found to vary with temperature according to the Arrhenius law.

Before going any further, we should discuss the recent suggestion of Johari and Pathmanathan[29] that the M'' spectra for ionic glasses are actually a combination of an exponential conductivity relaxation spectrum (a Lorentzian) and an ion-pair dipole relaxation and that the former should be subtracted out before the latter is analyzed. As the authors point out, this is a new application of the idea common to the earlier studies of glasses[32] in which the more common susceptibility formalism[32] was used for data analysis and a dc contribution to the observed dielectric loss was subtracted out before the residual loss was analyzed (as has always been the practice in dielectric relaxation studies). Johari and Pathmanathan show that the M'' spectra can be quantitatively fitted under this assumption using a Kohlrausch–Williams–Watts (KWW) function for the dielectric component. By contrast, the single KWW function used by earlier authors leaves a high-frequency component of the observed modulus spectrum unaccounted for. The improved fit is, of course, obtained at the expense of introducing additional adjustable parameters, and the procedure should therefore be shown to have predictive value to warrant the loss of simplicity involved in adopting it.

One prediction pointed out in ref 29 was that, at low temperatures, the single spectrum normally seen would be resolved into two if the dipolar and conductivity relaxation processes were distinguished by different activation energies, as would seem reasonable. Conductivity relaxation measurements on insulating glasses are not easy to perform, so this possibility has yet to be fully checked out. At the limit of lightly doped silica, Simmons and Simmons[36] have observed a single-exponential relaxation and, so far, the broadest M'' peak seems to be correlated with the largest conductivities and largest decoupling indexes (see below). The fact that most M'' spectra, for both normal and superionic glasses, have shapes that are almost temperature independent[35,37,38] means that if separate conductivity and dipolar processes do exist, then they mostly involve the same energy barriers (unless variations in $d\Delta\epsilon/dT$ and $d\tau/dT$ happen to compensate so as to maintain constant shape). Therefore, until some unambiguous means of demonstrating their separate existence can be found, we will adopt the convenience of treating them as a single coupled process and will seek correlations between the parameters describing the electrical modulus dispersion and loss spectrum and other responses of the same systems to distinguishable stresses, e.g., mechanical and magnetic. We must, however, keep open the possibility that these modulus parameters may, in the future, need to be modified if the case for separating dielectric and conductivity responses becomes compelling.

In the latter respect, particular attention should be drawn to the recent work of Hyde and Tomazawa.[45] These authors use the conventional approach to extract a static dielectric constant, which they interpret as due to alkali diffusion-induced composition changes (as opposed to dipole relaxation) and, using an electrical analogue of Zener's anelasticity theory, relate to the (frozen-in) composition fluctuations associated with nonideal mixing. Indeed, they show rather persuasive correlations of the derived dielectric dispersion parameters with the known tendencies to phase separation in the three (Li, Na, K) alkali silicates and support the correlations with observations on the nonideality-suppressing effects of Al_2O_3 additions. This treatment leaves open the question of dielectric (or modulus) dispersion in ideally mixing or single-component conducting glasses. No information on the form of the loss spectrum and its dependence on composition was given.

Returning to the use of electrical modulus spectra and their comparison with corresponding responses to other perturbations, we note the special convenience of the finding (typified by Figures 3a and 4) that the spectra have a constant shape and that the f_{max} value is Arrhenius in temperature. It means that the shape of the isothermal relaxation spectra (on which theoretical models are tested) can be reproduced from a *constant-frequency*, variable-temperature experiment by

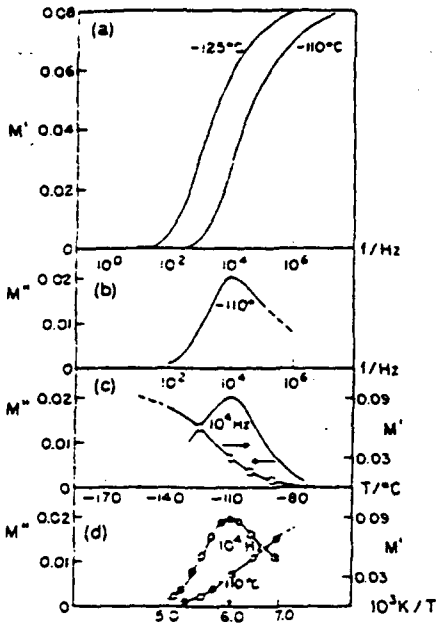

Figure 5. (a) Real parts of the electrical modulus for the superionic glass $0.6AgI\text{-}0.4Ag_2B_4O_7$ measured at −110 and −125 °C. (b) Imaginary part of the electrical modulus for the same system measured at −110 °C. Note maximum loss at 10^4 Hz for $T = -110$ °C. (c) Real and imaginary parts of the electrical modulus for the same system at a constant frequency of 10^4 Hz measured as a function of temperature. (d) Real and imaginary parts of the electrical modulus for the same system plotted vs reciprocal temperature. Note identical shape of M'' in parts b and d. The scale factor converting $1/T$ units to log f units is $E_a/2.30R$, where E_a is the activation energy for the relaxation process.

plotting M'' vs $1/T$. This is because such a plot is effectively a plot of M'' vs log $(\omega\tau)$ with ω constant and $\tau = \tau_0 \exp(E_a/RT)$: the scaling coefficient between log f and $1/T$ scales is therefore E_a/R. Its utility is demonstrated directly by the alternative plots of data for the superionic glass $3AgI\text{-}2Ag_2B_4O_7$[36] shown in Figure 5. The equivalence of constant-T and constant-frequency data representations shown by Figure 5 means that mechanical relaxation processes, which can only be studied in narrow frequency ranges in most laboratories, can be compared with electrical relaxation processes in the same system using $1/T$ data representations[16a] and the differences then related to probable differences in *isothermal* relaxational functions.

Before testing the usefulness of this observation (see section IV), it is necessary to comment on the different types of mechanical relaxation measurements commonly made, since the modulus whose relaxation is being monitored varies from experiment to experiment. The *torsion pendulum* measurement follows the shear modulus G^* directly, the *Rheovibron* measures Young's modulus (the tensile modulus) E^*, and *ultrasonic* and *hypersonic* (by Brillouin scattering) *absorption and dispersion* studies follow either G^* or the longitudinal modulus M_1^*, depending on the cut of the exciting crystal (ultrasonic) or the particular phonon studied (Brillouin scattering). E^* and M_1^* are analyzable as different combinations of the fundamental moduli, bulk and shear, K^* and G^*, according to the relations

$$E^* = G^*\left[\frac{3K^* - 4G^*}{K^* - G^*}\right] \tag{5}$$

$$M_1^* = K^* + \tfrac{4}{3}G^* \tag{6}$$

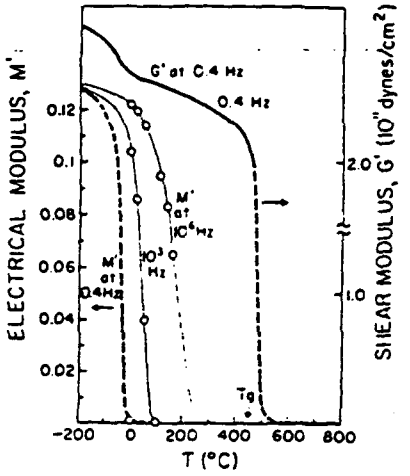

Figure 6. Variation of mechanical shear modulus (measured at 0.4 Hz) through fast and slow relaxation domains compared with that of the electrical modulus (measured at the same frequency). Note how the electrical modulus vanishes above the fast relaxation. (Data from refs 35 and 47 (solid lines) and from their extrapolations (dashed lines)).

It can be seen from eqs 5 and 6 that in the liquid state, where the shear modulus G^* vanishes, M_1' will remain finite but E' will also vanish. The electrical modulus M'_{el} vanishes at a temperature *well below* T_g in all except insulating glasses. These relationships are illustrated for the case of $Na_2O\text{-}3SiO_2$ in Figure 6 for electrical and mechanical measurements made at a common constant frequency of 0.4 Hz. Figure 6 also shows why it is acceptable, in comparing the results of mechanical with electrical relaxation data, to use the quantity tan δ (tan $\delta = E''/E'$ or G''/G') which is given directly by the experiment (rather than to make the extra measurements needed to obtain E', in order to obtain E'' separately). The reason is that G' and E' only change by 10% or less through the dispersion region, so the distortion of the spectrum introduced by use of tan δ instead of E'' etc. is not serious.

IV. Dependence of Glassy Dynamics on Thermal History

In Figure 1 we illustrated the effect that thermal history can have on the state of a molecular glass as indicated by its density. It is easy to imagine that such a density difference in an ionic glass could have a profound effect on the ability of small loosely bound particles to migrate through the structure: hence, the *average relaxation time* for a glassy-state relaxation should depend on the thermal history. We have already seen in Figure 4 that in a glass, i.e., an amorphous phase of fixed structure, the relaxation *function* for electical stresses is independent of temperature. But is this function dependent on the *particular* structure frozen in, and hence on the thermal history? Such a question is surely one of the first that should be answered concerning glassy dynamics.

It is interesting, in this respect, to examine how the relaxation function for a fast process, the electrical relaxation, varies with changing structure in the metastable *liquid* (ergodic) state as opposed to the nonergodic glassy state. Since a glass is frequently characterized by its fictive temperature (i.e., by the temperature at which some property, e.g., the enthalpy, is

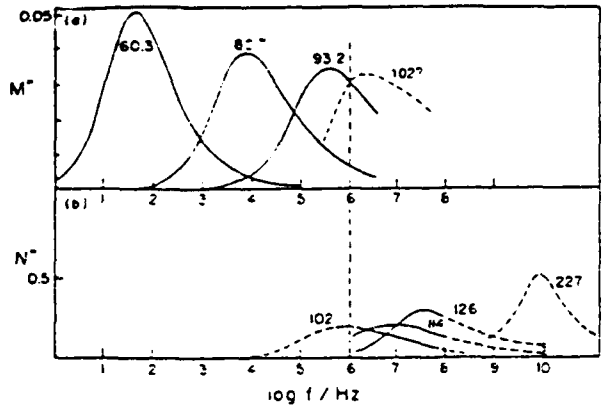

Figure 7. Comparison of loss spectra and their temperature dependences for electrical and mechanical relaxations in liquid $3KNO_3$·$2Ca(NO_3)_2$. Note that (i) at the same temperature, 102 °C, electrical relaxation is shorter (peak frequency higher) than the mechanical relaxation and (ii) the electrical relaxation spectrum narrows with decreasing temperature while the mechanical relaxation broadens.

the value for the ergodic state), it seems likely that the variations to be observed in the liquid will be those applying to the different frozen-in structures. Unfortunately, there are relatively few studies of electrical and/or mechanical relaxation in the ionic liquid state to serve as guidance. However, those that exist[26,35-42] are provocative and prove to have predictive value.

The usual behavior observed for the primary mechanical (*structural*) relaxation in the liquid state is one of increasingly non-Arrhenius average relaxation time, and increasingly nonexponential relaxation (i.e., decreasing β in eq 1), as temperature decreases. Typical is the behavior of the normalized longitudinal modulus for $3KNO_3$·$2Ca(NO_3)_2$ depicted in Figure 7b based on ultrasonic,[39] Brillouin scattering,[40] and recent digital correlation spectroscopy data.[41] Since the electrical relaxation time shows a comparable temperature dependence, similar spectral width behavior might have been expected for the electrical modulus. However, at least in the vicinity of T_g the opposite is found, according to the study of Howell et al.,[24a] whose results are shown in Figure 7a. The generality of this result, which has been correlated with aspects of the conductivity temperature dependence,[16a] is suggested by a similar narrowing seen with decreasing temperature for three mineral acid glass-forming systems by Hodge and Angell.[42] In each case the spectral width became fixed for T less than T_g, but the results clearly suggests that annealing the glass to a lower fictive temperature (enthalpy state) should result in a spectral narrowing.

A short extrapolation of the variation of β with temperature in the liquid state of $3KNO_3$·$2Ca(NO_3)_2$ (see Figure 8) suggests a value of unity (exponential relaxation) would be achieved at a temperature of 28 °C, 301 K, at which $T_g/T = 1.12$. In this case, $T_{\beta=1}$ corresponds to the Kauzmann temperature (if we may judge by T_g/T_K for the compound-forming liquid $BiCl_3$·2KCl of the same fragility as $2Ca(NO_3)_2$·$3KNO_3$[43]). This is particularly intriguing since several recent studies on the nonexponentiality of the *primary* relaxation in fragile liquids have suggested that $\beta \rightarrow 0$ at the Kauzmann temperature.[44] The conductivity behavior reflects the decreasing concentration of mobile cations in the increasingly dense structure, and hence the decrease in

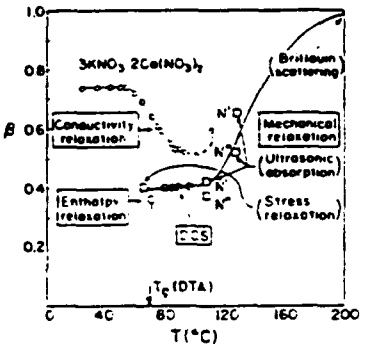

Figure 8. Contrasting temperature dependences of the KWW β parameter for (fast) electrical relaxation and (slow) mechanical relaxation processes for the system $3KNO_3$·$2Ca(NO_3)_2$ from various data sources.[8,24,39,41,88b]

the charge–charge interactions which may be the source of the nonexponentiality of the conductivity relaxation.[45]

The dependence of conductivity relaxation on fictive temperature in the ionic glasses may be compared with the effect of aging on secondary relaxation in molecular glasses.[13] In the latter, the reduction in the number of mobile units participating in the relaxation causes a decrease in $\Delta\epsilon$ rather than in the relaxation time or nonexponentiality.

Although no annealing studies (or for that matter quenching studies) have been carried out on $3KNO_3$·$2Ca(NO_3)_2$ to confirm or deny the suggested state dependence of the spectral width of the fast process in the *glass*, some data are available for a sodium silicate glass studied by Boesch and Moynihan.[46] These authors showed that on annealing, the width of the electrical loss peak M'' did indeed decrease in the manner expected from the above observations. Although the change in β for a 6% change in reduced fictive temperature, $\Delta T_f/T_b$, is much smaller in this system than in $Ca/K/NO_3$, so is the change in σ itself. However, if we normalize by the change in σ produced by the change in fictive temperature, the effects are comparable. This is consistent with a charge–charge interaction origin for the nonexponentiality of the conductivity relaxation.

Effects in the same direction have been seen recently by Mangion and Johari[37] for the case of $AgPO_3$ glass. In this case, however, some structure developed in the M'' spectra during the annealing. This subject merits more attention.

The unusual behavior of the conductivity relaxation with fictive temperature naturally raises the question of whether or not the *mechanical* loss, which must be associated with the mobile ion relaxation shows spectral width variations similar to those of the electrical relaxation (fast process) rather than to those of the structural relaxation (slow process). We compare electrical with structural relaxations in the same glass in the next section.

V. Comparison of Electrical and Mechanical Relaxation Spectra

In section III, it was pointed out that the combination of temperature-independent spectral width and Arrhenius temperature dependence of the peak frequencies found in electrical relaxation of glasses meant that

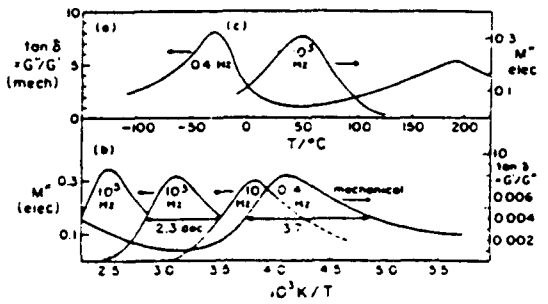

Figure 9. (a) Mechanical loss for $Na_2O{\cdot}3SiO_2$ glass at fixed frequency and varying temperature. Low-temperature component is due to Na^+ ion motion. (b) Comparison of "spectrum" for mechanical relaxation of $Na_2O{\cdot}3SiO_2$ using $1/T$ representation with equivalent electrical relaxation spectra showing small differences in peak loss position and large difference in half-width.

the shape of the isothermal relaxation spectrum could be obtained from constant-frequency measurements by plotting the moduli vs $1/T$. This implied that comparisons with the frequency-limited mechanical relaxation functions could be made by using the $1/T$ representations of the data. This is done for the case of $Na_2O{\cdot}3SiO_2$ glass in Figure 9, where mechanical (shear modulus) data taken at 0.4 Hz over a range of temperatures[47] (Figure 9a) are compared in the $1/T$ representation with isothermal *electrical* relaxation spectra of Figure 4. It is seen immediately that the mechanical relaxation spectrum is considerably broader than the electrical relaxation spectrum, which is itself constant in half-width. We will see that this increased spectral width for mechanical relaxation is a recurring feature of processes associated with mobile ion motion in ionic glasses. Before giving more detailed consideration to the description of these shapes, we need to present evidence for the suggestion that the mechanical, like the electrical, relaxation has a temperature-independent spectrum.

Allusion was made above to exceptions to the restricted frequency range of mechanical measurements. The development of a sensitive mechanical spectrometer at the Institut National des Sciences Appliquées in Lyon[48] has made possible the measurement of isothermal mechanical relaxation spectra over 3–4 orders of magnitude in frequency. Such measurements permit a check of the validity of attributing differences in $1/T$ "spectra" (as in Figure 5) to differences in the isothermal relaxation function, by showing that the shapes of isothermal mechanical relaxation spectra are also independent of temperature. This is done in Figure 10 for the case of a five-component heavy-metal fluoride glass (based on ZrF_4–BaF_2, the "ZBLAN" modification), in which the mobile particles are the fluoride ions (or at least a fraction of them), using the data of Mai et al.[49] The figure presents both electrical and mechanical data for several different temperatures. The individual isotherms have been superimposed by shifting along the frequency axis so that the peaks coincide. The finding that a single master plot can be obtained argues that the spectral shape is temperature independent for mechanical as well as for electrical relaxation processes in this system. Since this was approximately the case in an earlier wide frequency range study of mechanical relaxation in a mixed-alkali silicate glass,[50a] it seems likely that this finding will be general, as for electrical relaxation. In this case the analysis of constant-frequency data using the $1/T$ representation will be of general utility.

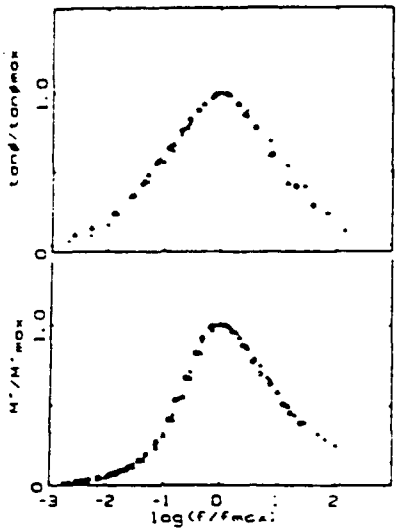

Figure 10. Master plots for electrical and mechanical relaxation in an anion-conducting (F^-) heavy-metal fluoride glass. Reprinted from ref 28; copyright 1985 Taylor & Francis Ltd.

The heavy-metal fluoride glass is an interesting case because the half-width of the mechanical relaxation is not much greater than that of the electrical relaxation (although the shape is clearly different). This is possibly to be correlated with the fact that the fluoride glass is a rather poor ionic conductor: its decoupling index is only of the order of 10^5 at T_g compared with 10^{11} for $Na_2O{\cdot}3SiO_2$. As for the case of $Na_2O{\cdot}3SiO_2$, the shape of the electrical relaxation spectrum is very well fitted by the Williams–Watts function. The KWW β value is 0.61, somewhat larger than the value of 0.55 fitting the $Na_2O{\cdot}3SiO_2$ data of Figure 9 and smaller than the value 0.74 fitting the glass state data for $3KNO_3{\cdot}2Ca(NO_3)_2$ (see Figure 8). The order of β values is the inverse of the order of decoupling indexes. This is a very significant correlation, which we will discuss more quantitatively below.

It is clear from Figure 10 that the mechanical relaxation in this fluoride glass, despite the similar half-width to the electrical case, is not well described by the KWW function. In fact, its asymmetry with respect to the ideal Lorentzian form is the opposite of that for the conductivity relaxation. A similar distortion was observed by Liu and Angell for the case of AgI–$AgPO_3$ glasses,[50b] though in this case the mechanical spectrum was much broader than the electrical. On the other hand, Ngai, in an exhaustive review of the older oxide glass literature,[16b] found that the mechanical spectrum could always be satisfactorily fitted with a KWW function and that in at least one case[51] the β value decreased markedly on annealing. This is the opposite of the behavior observed for the conductivity relaxation and is more akin to the behavior of the slow relaxation in molecular glasses.[52] The mechanical spectrum for these poorly conducting glasses was always much broader than that observed for the conductivity relaxation of the same glass (and is, in fact, always broader than the broadest electrical relaxation observed in *any* ionic glass at all).

As a final example we present data for a superionic conducting system, $3AgI{\cdot}2iAg_4B_2O_7$,[53] which has a decoupling index of $\sim 10^{14}$. Data for mechanical and

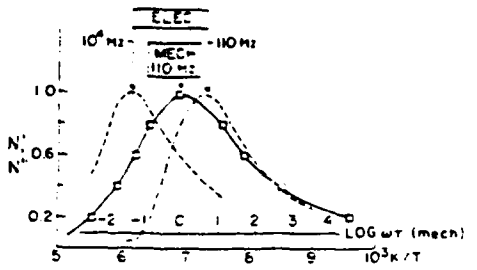

Figure 11. Comparison of electrical and mechanical relaxation spectra using $1/T$ representations of constant-frequency data. The spectrum is well described by a KWW function (eq 3) with $\beta = 0.29$. The electrical relaxations, which have almost the same peak temperature for the same frequency, are also of KWS form but are much narrower ($\beta = 0.48$).

electrical relaxation[35] are shown in the $1/T$ representation in Figure 11. It is clear from Figure 11 that the mechanical relaxation is again much broader than the electrical relaxation, though they can each be well described by KWW functions in contrast with the case of Figure 10. Since other examples are known in which the superionic glass mechanical relaxation is both broader and more symmetrical (non-KWW) than the electrical relaxation, it seems that at this time there are no general rules for the relationship except that the most probable times are similar and that the mechanical process is nearly always broader. We defer possible explanations until a later section.

For future studies, more cases are needed in which the (fast) mechanical relaxation function is well separated from the primary (slow) structural relaxation function so that the difficulty of deciding the appropriate background subtraction can be reduced. It is desirable also that the behavior with changing fictive temperature, preferably within the liquid state as pioneered by Torell,[54] can be determined and compared with the behavior seen in Figure 6. Favorable cases would seem to be the superionic systems 3AgI·2-$(Ag_2O·2B_2O_3)$[53] and "NaSi glass" ($Na_{3.75}Zr_{1.1}Si_{2.75}P_{0.25}O_{10.2}$),[55] which have decoupling indexes at T_g of $10^{13.5}$ and $10^{14.1}$, respectively.[24] Some sulfide glasses studied by Ribes and colleagues[56-58] and by Kennedy and coworkers[59,60] which have exceptionally high room temperature conductivity and relatively high T_gs may also be suitable. In addition, we must note the recently reported case of exceptional conductivity in the system $CuI–Cu_2O–MoO_3$. Minami and Machida[61] report σ_{298} values 10–20 times greater than their AgI equivalent, though a restricted glass-forming range limits the final maximum conductivity observable.

To complete this section, we must refer to the dynamic peculiarities of the *mixed* mobile ion glasses, i.e., glasses in which special features develop because more than one ionic species is free to move. The most celebrated case is the so-called "mixed-alkali" effect in which the mixing of two alkali oxide glasses (silicate, borate, phosphate, etc.) *of comparable conductivity* results in a glass of conductivity orders of magnitude lower than either.[62] The width of the electrical relaxation in the mixed glass does not seem much affected, though its peak frequency decreases greatly.[63] The mechanical spectrum, on the other hand, is greatly affected. From torsion pendulum studies,[64] a new intense loss peak ($\tan \delta$) appears at lower frequency on small additions of the second alkali and, partly because of its strength, completely overwhelms (if not annihilates) the single-alkali peak.[64] This peak falls at a frequency some 1.5 orders of magnitude below the frequency of the conductivity loss peak, whereas for single-alkali glasss the two loss peaks have essentially the same peak frequency. The mixed-alkali effect has been much discussed in the glass science literature, and the reader is referred to the paper by Ingram and Moynihan[65] for a current, if not yet generally accepted, explanation.

Several other "mixed-ion" effects have been noted, but their spectroscopic characterization is not yet very advanced. A mixed-anion effect that enhances rather than depresses conductivity has been observed in cation-conducting glasses such as $GeS_2–LiBr–LiI$[56] and $CuI–CuBr–Cu_2MoO_4$.[61] In anion conductors, on the other hand, mixing of anions produces depressed conductivities as in the mixed-alkali case.[61,66] Finally, in a mixed cation–anion conducting system, $LiF–PbF_2–Al(PO_3)_3$, the conductivity is depressed on mixing at a constant 20% $Al(PO_3)_3$. In this latter case, some spectroscopic data are available.[67] By contrast with the mixed-alkali glass, the conductivity relaxation spectrum broadens anomalously at mid range where the changeover from cation to anion dominance is expected, while the mechanical loss *decreases* from the pure alkali glass value on mixing. This is a research area where additional studies are needed and from which important and diagnostic correlations may emerge.

VI. Comparison of Electrical and Nuclear Magnetic Relaxation Data

In view of the differences observed in mobile ion glass responses to electrical and mechanical perturbations, it is of interest to observe what information may be obtainable on the relaxation function from nuclear magnetic relaxation measurements. In these studies the nuclear spin system, which is only very weakly coupled to the nuclear coordinate system, i.e., to the glass or liquid structure, is perturbed by a magnetic field, and the reestablishment of the spin equilibrium is monitored by a radiofrequency detection technique tied to the precession of the active nuclei in the magnetic field. The typical measurement, analogous to the typical mechanical spectrometry measurement, uses a fixed probe frequency determined by the intensity of the magnetic field in which the sample is placed and scans in temperature. The response of the system, for the case on which we focus attention, is measured as the spin–lattice relaxation time T_1. This has a minimum value when the atomic system to which the spectrometer is tuned has a decay time for structural fluctuations τ_c approximately equal to the inverse spectrometer frequency, i.e., $\omega\tau_c \approx 1$.

The method is applicable for any system containing nuclear species with a magnetic moment but is particularly suitable for systems with favorable (spin $^1/_2$) nuclei such as ^{23}Na, ^7Li, ^{19}F, and ^1H, which happen to be species of special interest in ionic glass dynamics phenomenology.

Until recently, most analyses of the T_1 temperature dependence in glasses[68-71] had been used on the Bloembergen, Purcell, and Pound (BPP) theory,[68] which assumes an exponential decay for the structural fluctuations involved in helping the spin system recover its

equilibrium state. It was recognized that the shape of the log T_1 vs $1/T$ plot deviated from that expected from BPP theory. Although it was not obviously connected to the weakness of the theory, it was also found[69] that the activation energy for the plot of log T_1 vs $1/T$ was not the same as for the dc conductivity;[70] it had been expected that the nuclear motions involved in relaxing the spin system would be the same as those involved in determining the dc conductivity. Furthermore, the prefactor found for the fluctuation correlation time, τ_c, Arrhenius law was unphysically low.

The origin of all these discrepancies has now been shown to lie in the inappropriateness of the BPP exponential relaxation assumption. Göbel et al.[71] showed that for various alkali silicate and borate glasses the asymmetric shape of the log $1/T_1$ vs $1/T$ plot could be well accounted for if the fluctuation frequency spectrum were assumed to follow the Cole–Davidson distribution. A more recent example, using data that extend further above the T minimum, is given by Pradel and Ribes.[72] Ngai[73] demonstrated that an equally good fit followed from use of the KWW function, so that NMR data showed yet another example of the near-universal occurrence of KWW (or, as aptly named,[74] "fractal time") character of fluctuation decay in disordered systems. A new example of the KWW fit, using T_1 data for Li_2S–SiS_2 glass, is given by Martin[75] in an excellent account of current developments in the subject. The relation between constant-frequency ac conductance and constant-frequency NMR studies, the study of which clarifies the origin of the depressed activation energy and unphysical prefactor found in the NMR studies, is considered in articles by Ngai,[16b,73b] Angell,[25b,76] Angell and Martin,[77] and Martin.[75]

The question immediately arises, is the departure from exponential relaxation seen in NMR closer to that for conductivity or that for mechanical relaxation? In both the lithium borate glass examined by Ngai[73] and the superionic lithium thiosilicate glass fitted by Martin,[75] it seems that the β value coincides with that for ac conductivity. The conductivity values, which seem to be much more reproducible and systematic in character than their mechanical equivalent, would thus seem to be the values that we should first seek to correlate with other structural and relaxational features of the system. This will be the subject of the next section. Before passing to this section, however, we should give brief attention to the origin and meaning of the low value of activation energy for NMR relaxation obtained from the log T_1 (or log T_1^{-1} as commonly plotted) vs $1/T$ plot below the temperature of the T_1 minimum, since this is currently subject to different interpretations.

Angell[25b,76] and Angell and Martin[77] have argued, by analogy to the much-studied case of frequency-dependent (ac) electrical conductivity, that the low activation energy relative to that for dc conductivity is a straightforward consequence of the fact that measurements have been made in a temperature range where $\omega\tau > 1$ in the presence of nonexponential relaxation. In ac conductance measurements, the activation energy agrees with the value obtained from dc measurements only so long as the period of the ac field is long compared with the ion jump time (or, more correctly, the conductivity relaxation time). Since low-frequency measurements are easily accessible with admittance

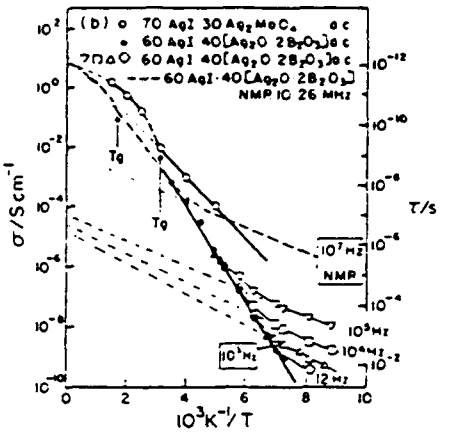

Figure 12. Arrhenius plot of ac conductivity (and relaxation times determined from it by a Maxwell relation valid only for conductivity measured where $\omega\tau \ll 1$) compared with NMR correlation times determined from data where $\omega\tau < 1$. Note that in both cases, NMR and low-temperature conductivity, the activation energy is well below the dc conductivity value, and the prefactor not only is unphysical but is frequency dependent. Both results are due to invalid data treatments that assume exponential relaxation.

bridges, it is easy to satisfy this requirement (hence most studies of dc conductivity are made by using ac techniques). When the jump time becomes longer than the inverse bridge frequency, a departure from the dc conductivity Arrhenius plot occurs, as shown for the case of the $60AgI{\cdot}40(Ag_2B_4O_7)$ superionic conductor[38] in Figure 12. The temperature of the break depends, of course, on the bridge frequency held constant. If we plot the data as *apparent* relaxation times using the relationship applicable to the *dc* conductivity (see eq 1)

$$\tau_\sigma = e_0/M_\infty\sigma \tag{7}$$

we obtain plots (see Figure 12) that extrapolate to $1/T = 0$ at τ_0 values (the Arrhenius law prefactor) that are even lower (hence more unphysical) than those found in the NMR studies. However in the ac conductivity case the reason is well understood, following Macedo et al.,[23] as a consequence of the fact that the conductivity (or coupled conductivity/dielectric[29]) relaxation is nonexponential. In this interpretation the (lower) ac "activation energy" has no meaning except as an indicator of the extent of departure from Debye relaxation. As a way of demonstrating that the low activation energies for the BPP correlation time, τ_c, and the low prefactors obtained from the NMR studies have the same explanation, we include in Figure 12, as a dashed line marked "10^7 Hz NMR", a plot for NMR τ_c data interpolated from results presented for $AgI{\cdot}Ag_2B_4O_7$ glasses of compositions 50 and 70% AgI by Martin et al.[78] The activation energy is seen to be similar to that for the ac conductivity. The main difference is that, due to the high spectrometer frequency, the onset of frequency-dependent behavior occurs at a higher temperature, so the prefactor found is higher than for the ac conductivity.

In this interpretation, the plot of log $1/T_1$ vs $1/T$ (e.g., Figure 4, in ref 72, for the case of Li_2S–SiS_2) should be regarded as the NMR equivalent of the modulus, M'', plots of Figures 5d and 11. (Accordingly, a plot of log M'' vs $1/T$ for T above the T_1 minimum yields an activation energy close to, but still somewhat smaller

than, the dc conductivity value. Agreement will only be quantitative when $\beta = 1$.) The equivalent of the persistent high-frequency loss causing deviations from the form predicted by KWW for the modulus at high frequencies (see section VIII) is the residual T_1^{-1} commonly seen in the low-temperature NMR data.[71,79]

An alternative interpretation of the low-temperature NMR data has been given by Ngai and co-workers.[80] They argue that the activation energy from T_1 data obtained well below the T_1 minimum is a microscopic activation energy of fundamental importance to understanding glassy-state dynamics. It represents, in their view, the activation energy for a "primitive" process initiated by perturbing stress, i.e., the relaxation at very short times before a coupling to the complex environment acts to slow down the relaxation rate and thus to lead, in the coupling model,[16,81] to the KWW behavior of the complete relaxation. In support of this argument they show a good agreement between the T_1 activation energy and the quantity βE_σ, where β is the KWW exponent from electrical relaxation studies and E_σ is the dc conductivity activation energy. This product is the value for the "primitive" process activation energy according to the coupling model, i.e., the value before "the slowing down of one primitive relaxing rate ω_0 to $\omega_0(\omega_c t)^{1-\beta}$ by cooperative interactions with other ions", which seems to be ubiquitous in glasses, takes over. (This work also emphasizes the sublinear frequency dependence observed at $\omega\tau \gg 1$ and gives an interpretation that is relevant to our discussion of connection betwen relaxation and vibrational modes given in section VIII.)

Clearly, this research area is in a state of active development and, with variable-frequency NMR being actively pursued,[75] much additional insight into the dynamics of ionic processes in glasses will soon be forthcoming.

The silver iodoborate case used in the above discussion has also been the subject of some very wide frequency range mechanical studies that make it of special value for analyses aimed at providing a unifying picture of the energy-dissipating processes in glassy ionic solids. We consider these in a final section after a brief but especially important section in which spectroscopic observations are tied into the broader phenomenology of slowing down in glass-forming liquids.

VII. Correlation of Relaxation Spectra with Decoupling Index and Structure

Having reviewed the main spectroscopic characteristics of dynamic processes in ionic glasses, we now turn to the important matter of correlating the findings with the broader phenomenology of viscous liquids and the vitrification process.

We noted at the beginning of this review that the glassy-state processes we have been characterizing are actually spawned in the high-temperature *liquid* state. It has been known for a very long time that, in molten salts, the electrical conductivity has a characteristically different temperature dependence from the shear viscosity. Both processes, P_i, have been found[82,83] to obey the famous Vogel–Tammann–Fulcher equation

$$P_i = P_{0,i} \exp[\pm B_i/(T - T_0)] \qquad (8)$$

where, subject to some privisos, the constant T_0 is identified with the Kauzmann vanishing excess entropy temperature, T_K,[83-85] which stands as the low-temperature limit on the liquid state. According to the experiments, both processes respect the same limit, T_0, initially, but the conductivity has a smaller B parameter. Representing the processes by their average relaxation times,[22] τ_σ and τ_s, we see that the processes must separate increasingly in time as temperature decreases (as in Figure 2a,b), the rates of separation depending on the difference in their B parameters. Kawamura and Shimoji[86] have therefore suggested that the ratio B_s/B_σ may serve as a temperature-independent index of the decoupling of conductivity from structural (viscosity) modes in a given system. This has an obvious advantage over the "decoupling index", $R_\tau = \tau_s/\tau_\sigma$, used by Angell,[25] which, in most cases of interest, has a different value at each temperature. However, this advantage is partly offset by the finding[87] that eq 8 usually breaks down before the glassy state is reached, such that the two processes return to an Arrhenius temperature dependence while still in the liquid state. Furthermore, the return to Arrhenius behavior occurs at a higher temperature for conductivity than for viscosity and is system dependent. In view of these complications we will continue to use the decoupling index determined at the glass transition temperature in discussing the origin of the different β values observed for conductivity relaxation in earlier sections. However, in future work efforts should be made to develop the Kawamura–Shimoji suggestion since the B_i ratio can be given a theoretical interpretation. If a free volume approach[86] is adopted, B_s/B_σ is a measure of the difference in free volume requirements for conductive vs viscous motion or, if we invoke our current preference[88] for an Adam–Gibbs[85] entropy-based interpretation of the transport phenomena, it is a measure of the difference in energy barriers for rearrangement of the minimum-size rearrangeable group involved in relaxing an electrical stress as opposed to a mechanical stress.

In light of the above discussion it seems reasonable to expect the kinetic processes in the glassy state to reflect in some measure the extent of decoupling from the viscous modes achieved in the liquid before vitrification. The differences among different glasses in this respect may be presented, as in refs 25 and 86, by a tabulation of decoupling indices at T_g. These may be easily estimated by combining eq 1, in which we insert a typical value of $M_\infty = 0.05$

$$\tau_\sigma = \epsilon_0/M_\infty\sigma_{dc} \approx 9 \times 10^{-13}/\sigma_{dc}\ \text{s} \qquad (9)$$

with the observation that, in general

$$\tau_s\ (\text{at } T_g) \approx 2 \times 10^2\ \text{s} \qquad (10)$$

so that

$$R_\tau \text{ at } T_g = \tau_s(T_g)/\tau_\sigma(T_g) \approx 2 \times 10^{14}\sigma_{T_g} \qquad (11)$$

However, a better feeling is obtained for the extreme differences that exist between different systems by a graphical presentation of the conductivities over a wide temperature range using a reduced Arrhenius plot such that all glasses have the same structural relaxation time at the scaling temperature. The natural choice for scaling temperature is T_g. The plot is presented in Figure 13, which includes a dashed line to represent a system in which the conductivity and viscosity modes

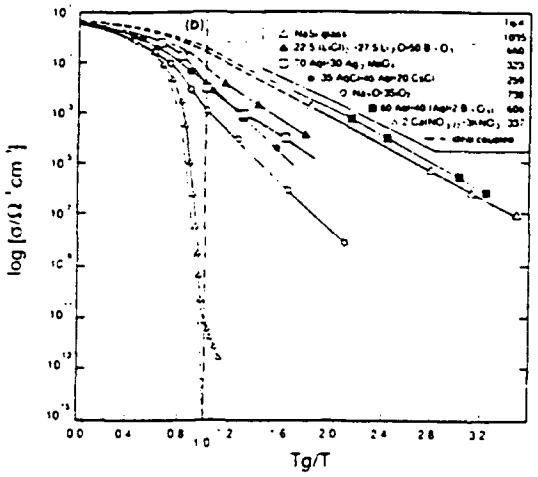

Figure 13. T_g-scaled Arrhenius plot of conductance of systems with widely differing degrees of decoupling of conductivity from structural modes. Dashed line shows behavior for fully coupled system.

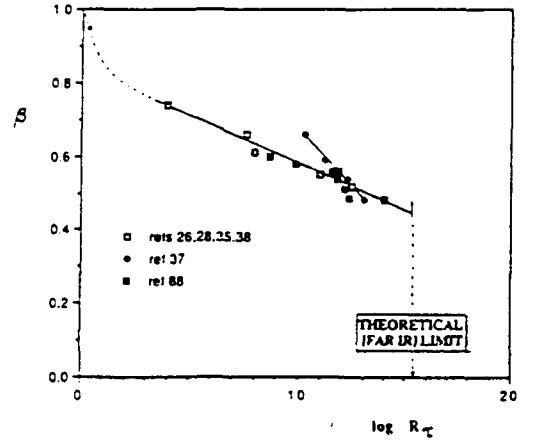

Figure 14. Correlation of nonexponentiality parameter β of Kohlrausch function with decoupling index R_τ for a variety of ionic glasses.

remain fully coupled over the entire temperature range.

Figure 13 is very similar to the theoretical plot of Kawamura and Shimoji[86] for a system of fixed B_σ (eq 8) being vitrified at a fixed rate, with variations in the value of B_σ. To this writer, the figure is quite evocative. It would seem surprising indeed if the extremely different time scales for electrical relaxation relative to a constant time scale for relaxation of mechanical stress were not reflected in some way in the spectroscopic characteristics of the conductivity relaxation in the glass. Thus we check in Figure 14 what seems the obvious correlation to investigate (but one not presented previously), viz., correlation of the nonexponentiality parameter β (in the glassy state) with the decoupling index R_τ at T_g (since T_g is where the bulk structure becomes arrested).

Despite the presence of some system-specific irregularities, Figure 14 shows a rather definite relationship: the more fully decoupled the conductivity at T_g, the more nonexponential the relaxation. There would seem to be a well-defined limit for β in ionic conducting systems since the theoretical limit for σ_{T_g} is given by the far-infrared conductivity, ~ 10 S cm^{-1}.[24,90] Thus the limiting value of $R_\tau(T_g)$ should be $\sim 10^{15.4}$, and hence the limit on β should be 0.44. Broader spectra may be obtainable by overlapping independent processes, as seems to happen near the mobile ion crossover in mixed mobile ion systems,[67] or in the presence of incipient phase separation, but such cases would always have a special explanation. The rapid decrease in β at the left-hand side of the diagram (based on data in dilute alkali silicates and germanates) has been interpreted by Martin[75] in terms of the rapid change in cation–cation separation.

A correlation of β with another system parameter that is as impressive as Figure 14 (though, to the present author, a little less provocative) is that described by Ngai and Martin.[80b] These authors modify an earlier correlation[89] of β with dc conductivity activation energy E_σ^* by converting E_σ^* to a "primitive" activation energy βE_σ^* and plotting this against β (actually against $n = 1 - \beta$) and are able to superpose data from many different systems. While the presence of β on both axes aids the correlation somewhat, it is theoretically justified.

To interpret these observations further, one should ask what Figure 14 implies about the structure within which the mobile ion displacements are occurring and consider this in relation to current models for nonexponential relaxation.

It is tempting to answer this question in terms of microheterogeneity models.[90–92] In such models it is supposed that the viscosity and structural relaxation are controlled by the approach to percolation of growing clusters of dense-packed material, while the intercluster matter, in which conductivity occurs, remains relatively loose and liquid-like. This picture is essentially that invoked in the "cluster bypass" model for high ionic conductivity advanced recently by Ingram.[93] It is orthogonal to the widely espoused "α-AgI cluster overlap" model[94] which explains the tendency of most AgI-containing glasses to approach the properties of α-AgI crystals as AgI content increases in terms of overlap of growing clusters of mobile material (but which seems inconsistent with the similar behavior of Ag_2S–$AgPO_3$ glasses[95]). This general picture emphasizing loose intercluster material is also consistent with recent evidence that, in many, though certainly not all, "fragile" liquids, the time scales for shear relaxation and structural or enthalpy relaxation begin to separate as T_g is closely approached.

The connection to Figure 14 by models for nonexponential relaxation could then be made in at least two ways. Both depend on the idea that in the highly decoupled, i.e., large R_τ systems, the matrix material of the cluster bypass model must be particularly liquid-like and/or perhaps involve a particularly large proportion of the mobile, low-charged, ions in the structure.

(1) In the "coupling" model of Ngai and colleagues,[16,97] the departure from exponentiality (quantified by $n = 1 - \beta$ in their model) is a function of the level of disorder in the environment of the "primitive species", which should be greater in a highly decoupled system matrix. We note the success of this model in explaining the isotope effect in alkali borate glasses[98,99] and suggest such experiments be repeated for the systems representing the accessible extremes of the decoupling phenomenon.

(2) In the Tomazawa model,[45a] which is specific to the behavior of ionic systems, the explanation of the greater departure from exponentiality in highly decoupled

glasses would follow directly from the larger concentration of mobile species in matrix material. This is also the view of Martin.[75b] The source of their nonexponential relaxation is the well-known Debye–Falkenhagen effect, which, however, can only account quantitatively for the first 5% increase in spectral width (hence the initial drop in β, Figure 14) according to Lesikar and Moynihan.[96] A more recent analysis by McGahay and Tomazawa[45c] goes some way toward removing this limitation.

It should be very interesting, in this respect, to study the spectroscopic characteristics of conductivity in the ultrafast quenched glasses of Tatsumisago et al.[100] in which the fraction of mobile material in the structure should be maximized.[86] Also lacking in the present data base are oxide glasses designed to be insulating glasses—e.g., alkali-free lead or barium silicates.

VIII. Connections between Relaxational and Vibrational Responses

In the foregoing sections we have reviewed the detailed kinetics of various processes that occur within the "frozen" glass structure and have attempted to connect their characteristics to the process by which they form. While they are spawned in the high-temperature liquid where all relaxation times are short, they have their own short- and long-time characteristics. Most of the studies reviewed to date have been concerned with the medium to long time regime. It is of considerable interest to investigate the behavior of the glassy-state processes, both mechanical and electrical, as the frequency range of the measurement approaches the microscopic short-time (vibrational) limit. Thanks to the existence of some glasses in which the conductivity mode decoupling is exceptional, it is possible to extend the glassy-state studies to within three decades of the typical vibrational frequency. Because of the value we place on the conceptual unification that can be achieved by considering vibrational and relaxational processes in the same scheme, we devote a final section to this subject. Here we follow closely the development used in a recent review article.[1a(iii)]

In all the work reviewed so far, the frequency of the mechanical relaxation studies has not exceeded the 100-MHz range provided by ultrasonics. It is possible, though not easy, to make mechanical relaxation studies of glassy relaxations at extremely high frequencies in the gigahertz range by inelastic light scattering techniques. A visible light beam, for instance, will interact with the natural density (refractive index) fluctuations in the material to produce or annihilate acoustic phonons and yield a scattered beam, the Brillouin line, which gives information on the frequency, velocity, and damping of these phonons. The damping is reflected in the half-width of the Brillouin line. Such scattering techniques have been very valuable in the study of viscous liquids[8,54,101-103] and may be applied to the study of mechanical relaxation in fast-conducting solids if the strength of the associated relaxation is large enough. A couple of cases that satisfy this condition have recently been reported in the literature,[38,104,105] and we briefly summarize the value of such studies here.

The first case in question is the $AgI-Ag_2B_4O_7$ system in which there already existed extensive data at lower frequencies covering the range 1–110 Hz (by dynamic mechanical studies discussed earlier;[38] see Figure 11) and by ultrasonic studies.[106] The relaxation in this glass is one that satisfies the two conditions, high relaxation strength and exceptionally short relaxation time at T_g, which are necessary for the observation of gigahertz phonon damping at temperatures below the glass transition temperature.

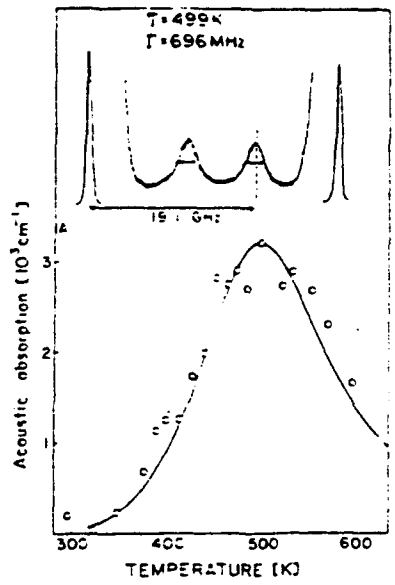

Figure 15. Brillouin spectra for $0.6AgI-0.4Ag_2B_4O_7$ glass at 499 K, showing 19.1-GHz frequency shift from central exciting line and Brillouin half-width. Lower portion shows absorption coefficients at different temperatures obtained from Brillouin line widths of the upper portion.

Figure 15 shows, in the upper portion, the basic experimental observation viz., the scattered Brillouin peak in relation to the central exciting line, and (in the lower portion) the important relaxation data in the form of absorption coefficients obtained at each temperature from the width of the Brillouin line. We see in Figure 11 how the absorption coefficient passes through a maximum at a temperature. 499 K, some 180 °C below the glass transition temperature for this system. Similar results have since been observed for a range of compositions in the same $AgI-Ag_2B_4O_7$ system[104] and also in the alkali halide containing system $LiCl-LiB_2O_7$.[105]

These data can be put in the reciprocal temperature form and displayed informatively with the results of the lower frequency experiments as shown in Figure 16.

Since the evidence from both electrical conductivity and low-frequency mechanical relaxation is that the activation energy for the mobile ion relaxation is mostly independent of temperature, we can assume (remembering the evidence in section V that, where studied, the spectral shape was constant with temperature) that the data displayed in Figure 16 reflect the spectral form of the relaxation as discussed using Figure 5. In this case, we may make the important observation from Figure 12 that the departure from exponential relaxation which is so pronounced at low temperatures is greatly reduced in the high-frequency short relaxation time range explored by the Brillouin scattering technique. Indeed the width of the relaxation in $1/T$ can be accounted for almost quantitatively under the assumption of a single relaxation time. This appears also to be the case for the lithium cation motion in the $LiCl-LiB_2O_7$ system[105] and hence is probably of general

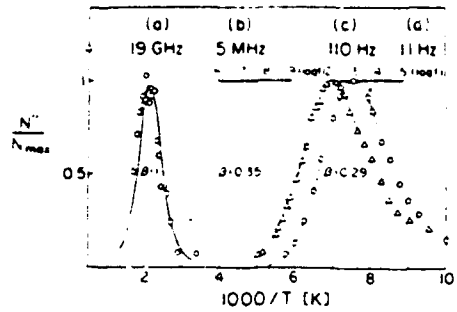

Figure 16. Comparison of normalized moduli for mechanical relaxation over wide temperature and frequency regimes using $1/T$ representation of spectra form. Note that the spectra at 5 MHz (from ref 106) and 11 Hz are approximately the same in shape, while the high-temperature high-frequency spectrum is narrow. Dotted lines show predicted shapes at gigahertz and low frequencies according to the Gaussian activation energy distribution model of ref 106. The frequency scales attached to the 5-MHz and 110-Hz plots are based on the equivalence of $1/T$ and log f discussed earlier under Figure 4. Each scale has its origin fixed such that the peak of the modulus plot falls at the appropriate fixed frequency, 5 MHz or 110 Hz.

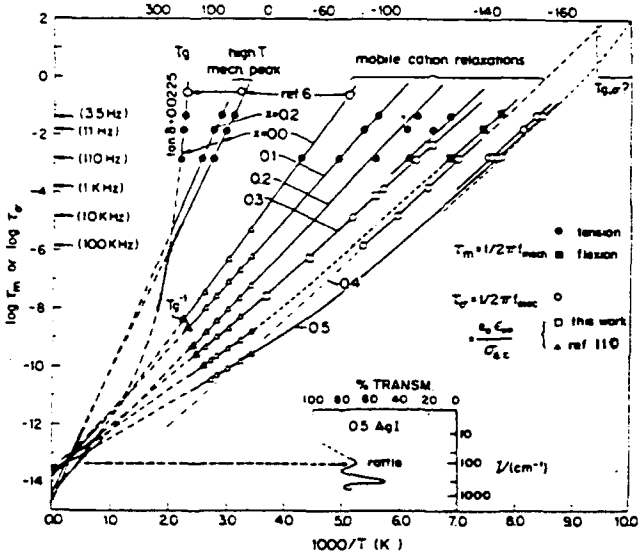

Figure 17. Relaxation "map" for mechanical and electrical relaxation in AgI–$AgPO_3$ glasses. High-temperature conductivity data from ref 110 have been converted to electrical relaxation times (τ_e), assuming a high-frequency dielectric constant of 15 for all cases. Conductivity and mechanical relaxation data are now available for the *liquid* states of this sytem but are omitted for clarity. Inset: Low-frequency portion of thin-film transmission IR spectra for 0.5 AgI-0.5$AgPO_3$ glass. Note coincidence of far-IR peaks (quasi-lattice vibration modes) with attempt frequency for relaxation modes. Reprinted from ref 50; copyright 1980 Elsevier Science Publishers B.V.

validity. An account of how the results of these studies can be accounted for within the coupling model has been given Ngai and Rendell.[107]

With this extended frequency/relaxation time data now in mind, it is helpful to make a summary representation of the variations of relaxation time with temperature that have been observed in different systems. Figure 17 shows a relaxation time map for the system AgI–$AgPO_3$[50] and includes some short longitudinal relaxation time data obtained by Brillouin scattering in the liquid state,[54] in addition to the various glassy-state data discussed in earlier papers. Figure 17 shows three important features, which we note again here.

First, it shows that for both electrical and mechanical relaxation the activation energy changes systematically

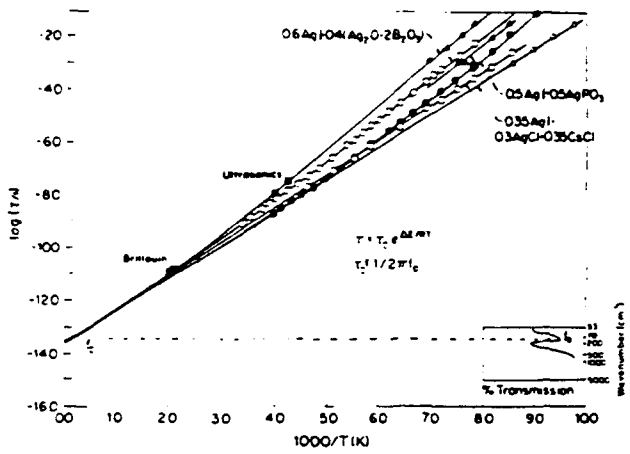

Figure 18. Arrhenius plot of relaxation times for mechanical and electrical mobile ion controlled processes in three different fast ion conducting glass systems, one containing only halide ions. Note that the latter, which has fully annealed, shows Arrhenius behavior over the whole temperature range with direct extrapolation to the quasi-lattice vibration time. Plot contains results of high-frequency study of Figures 15 and 16.[104,105]

with composition in such a way that the slope of the least rapidly relaxing compositions tends toward the (much greater) slope of the viscoelastic relaxation.

Second, we note that (in contrast with other cases mentioned above, and included in Figures 13 and 14) the most rapidly relaxing compositions showed distinct departures from Arrhenius behavior in both electrical and mechanical relaxation. Whether or not this can be associated, as for viscous liquids, with measurable contributions to the thermodynamic properties (heat capacity, compressibility, etc.) from configurational degrees of freedom that are localized so as to be dissociated from the main viscoelastic relaxation, is not known at this time.

Third, all modes (including some secondary mechanical relaxation modes which are not associated with mobile cations and which we have not discussed) appear to be extrapolating toward a high-temperatue limit which is broadly consistent with the "quasi-lattice" vibrational times observable by far-infrared spectroscopy on these systems.[50,108]

Figure 18 shows the relaxation times for the mobile ion modes alone for three different fast ion conducting systems and establishes that the very fast relaxing systems are not necessarily associated with departures from Arrhenius behavior. Indeed the one detailed study of this curvature in the literature, performed on the system AgI–Ag_2MoO_4[109] suggests that it is a strong function of thermal treatment and indeed disappears after the glass has been properly annealed. We note here that a new study on AgI–$AgPO_3$ glasses by Malugani and Johari,[110] who used carefully annealed samples, has also found Arrhenius behavior at all compositions. This question deserves more detailed study.

Finally, we show in Figures 19 and 20 connections between relaxational and vibrational modes associated with electrical and mechanical fast ion relaxation. Figure 19 shows how the temperature dependence and the frequency dependence of the conductivity can be related to the absorption of energy from the oscillating electrical field, an absorption that reaches its maximum at frequencies in the far-infrared region of the electromagnetic spectrum, i.e., at frequencies characteristic of

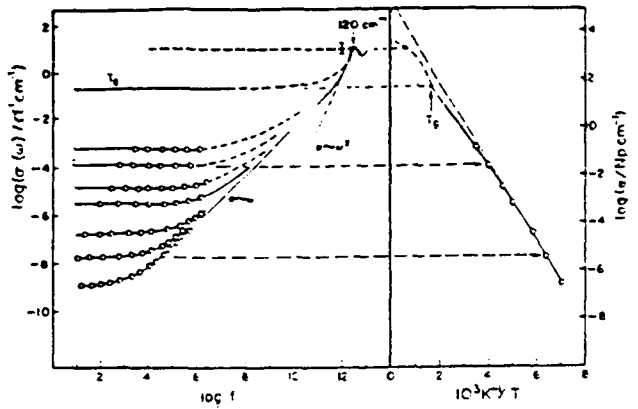

Figure 19. Frequency dependence of electrical conductivity $\sigma(\omega)$ (left-hand ordinate) and absorption coefficient α_ω (right-hand ordinate) due to fast ion motion at different temperatures for the fast ion conducting system $0.6AgI\text{-}0.4(Ag_2O\text{-}2B_2O_3)$ (part a) and temperature dependence (Arrhenius plot) (part b), showing near equivalence of limiting high-frequency conductivity of the liquid state. Note changeover from a first-power frequency dependence of ac conductivity in most of the range to an ω^2 dependence near the quasi-lattice resonance absorption region.

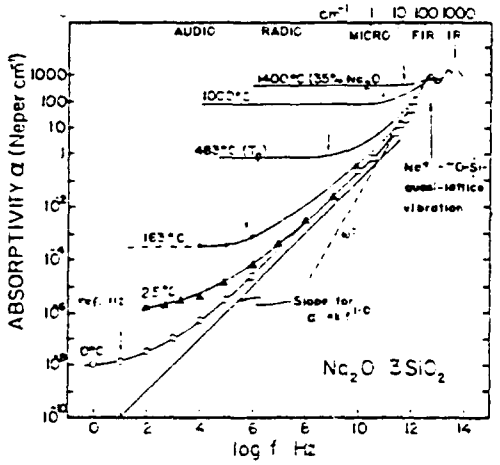

Figure 20. Dependence of ac conductivity $\sigma(f)$ and the related optical absorptivity α on frequency for the case of $Na_2O\text{-}3SiO_2$, for which the most extensive data are available. Diagram shows connection of low-frequency dispersion region to infrared resonance absorption region via linear and quadratic dependence regimes for which fractal and anharmonic dynamics, respectively, are believed responsible.

the quasi-lattice vibrations. The (ac) conductivity at these frequencies is very high since every charged particle in the system is contributing in proportion to its charge as it vibrates at thermal velocities, creating an instantaneous fluctuating current. This conductivity can be measured by determining the loss of energy from a far-infrared light beam as the electromagnetic wave couples to the oscillating electric field and is absorbed.[108]

The relation is given by

$$\alpha(\omega) = \sigma(\omega)/\epsilon_0 c n(\omega) \qquad (12)$$

where ϵ_0 is the permittivity of free space, c is the velocity of light, and $n(\omega)$ is the frequency-dependent refractive index, which, in a disordered transparent material, varies only weakly about the higher frequency value fixed by the electronic motions. Figure 19 has a conductivity scale on the right and the equivalent optical absorption coefficient scale on the left. Note how, as the temperature increases, the dc conductivity—hence also the low-frequency absorption coefficient—rises toward a limit set by the absorption due to the vibrating ions in the quasi-lattice. The latter has been measured quite accurately for sodium borate glasses[106] but is less certain for the present case (see error bar in Figure 19) because the film thickness of the blown silver ion glass film was only crudely measured.[111] It would appear from Figure 19 to be a measure of the limiting high dc conductivity obtainable in an ionic system. There is need for more quantitative evaluation of far-IR absorptivities in relation to temperature and composition in order that the physical picture given in Figure 19 can be fully completed and confirmed.

Figure 19 gives the picture unifying vibrational and relaxational modes responding to electrical stresses. It shows how the absorption (per cm^{-1}) by relaxational modes increases continuously with decreasing relaxation time, until they merge at the high-temperature, high-frequency extreme. The extrapolation between admittance bridge and far-IR absorption data in Figure 19 may seem unacceptably speculative. However, it may be justified by reference to systems for which the data are much more complete, thanks to recent gigahertz bridge measurements by Sridhar on $AgI\text{–}AgPO_3$ glass[112] and time-domain reflectivity measurements by Burns, Cole, and Risen.[113] In Figure 20 we add data of the latter authors on $Na_2O\text{·}3SiO_2$ to the original diagram from ref 1a(iii) to support the simple $\sigma(\omega) \propto \omega^{1.0}$ connection we have suggested as the link between the low-temperature dc and high-frequency (infrared) ac conductivity regimes.

The origin of the implied constant loss, irrespective of wavelength (the existence of which has been suggested at various times in the past),[35,100,114] must be a matter of concern. Length scale independence is, of course, the hallmark of fractal systems and, although glasses are unquestionably Euclidean geometrical objects, there are strong theoretical indications,[115] supported by molecular dynamics simulations[116] and, to an extent, experiment,[117] to suggest that their *dynamics* may be fractal at least over some range. Kieffer and Angell, for instance, recently showed by simulations on stretch-ruptured vitreous SiO_2[116] that the SiO_2 structure remains Euclidean until the point of spinodal rupture at ~70% of normal density and then develops a self-similar porosity with a Hausdorff dimension that changes systematically with density. The same structure exhibited the features of fractal dynamics with a fracton dimension falling a constant interval below the Hausdorff dimension except in the prerupture regime. In the latter regime, where the Hausdorff dimension was 3.0, the fracton dimension continued to change. However, it *remained less than 3.0 at normal density*, in accord with the Alexander–Orbach theory.[114]

If fractal dynamics are involved in the frequency-independent loss in glassy systems, then it should not be only electrical absorptivities that reveal them. We therefore turn to the results of ultrasonic and hypersonic studies to see whether similar behavior is manifested. Certainly it is known that the absorptivity in ultrasonic studies increases very rapidly with increasing frequency, and this usually sets the high-frequency limit on ultrasonic measurements.

For our example we choose the superionic glass $3AgI\text{-}2Ag_2B_4O_7$ on which both high-quality ultrasonic

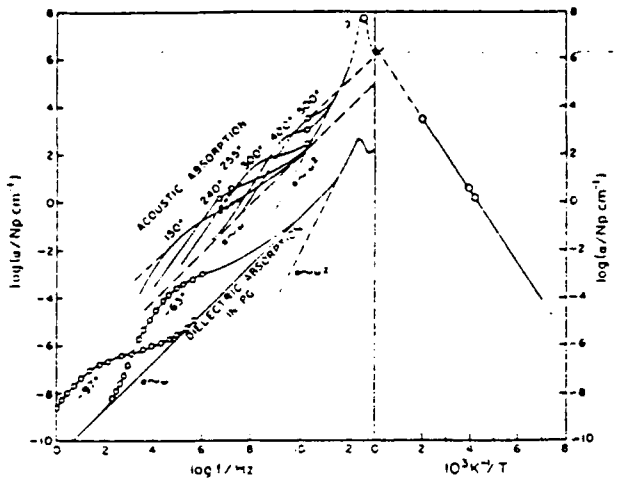

Figure 21. Analogue of Figure 19 for absorption of *mechanical* energy in the same system, based on limited ultrasonic[11] and Brillouin scattering[31] data. For comparison, data for absorption of electromagnetic waves by a relaxing dipolar fluid, propanediol,[47] over the same frequency range are included. Both seem to have similar $\alpha \sim f^{1.0}$ backgrounds over the major part of the frequency range. An Arrhenius temperature dependence for the acoustic absorption coefficient (at the frequency of the loss maximum) is a novel observation to the best of our knowledge.

data[106] and hypersonic data[36,104] exist. Figure 15, for example, shows that peak absorption in the gigahertz range is 3.1×10^3 Np m^{-1} at 499 K. The data are plotted in Figure 21 along with additional data discussed below.

Since the mechanical relaxation is one which leads to a thermodynamic state of polarization, we cannot expect the equivalent of Figure 19 for mechanical motions to have the frequency-independent plateaus of Figure 19 (though this would be the case for shear relaxation in liquids). Rather, the nearest equivalent would be the relaxation of a polar liquid. Data connecting dielectric relaxation and IR absorption were recently published for the case of propanediol[118] and are reproduced in Figure 21 (part a lower curves) to provide a basis for comparison with the mechanical analogue which we now discuss.

The peak absorption data from ultrasonic studies are entered in Figure 21 as functions of frequency in part a and of reciprocal temperature in part b, as in Figure 19. A few off-peak absorptivities at different ultrasonic frequencies allow us to estimate the form of the acoustic absorption shoulders at different temperatures. We do not have the equivalent of a far-infrared absorption coefficient for the mechanical modes, but we do know that longitudinal acoustic excitations with the normal velocity of sound are observable in some glasses by neutron scattering in the equivalent of the second Brillouin zone at wave vectors for which the wavelength is of the order of 10 Å.[119] Furthermore, these excitations[120] are not observable at lower wave vectors in liquid or glassy states, which implies overdamping. Therefore, we can write, for the smallest physically meaningful wavelength λ_{min}, which is the interatomic spacing

$$\alpha\lambda_{min} \geq 1 \tag{13}$$

which implies that the wave is completely damped in a single wavelength. Furthermore, this limiting high absorption coefficient will occur at a frequency given by

$$\lambda_{min} f_{max} = V \tag{14}$$

where v is the velocity of sound. Substituting $v = 2 \times 10^5$ cm s^{-1}[106] and $\lambda_{min} = 2 \times 10^{-8}$ cm we find from eqs 13 and 14 that $\alpha_{max} = 5 \times 10^7$ cm^{-1} at $f = 1 \times 10^{13}$ Hz. This, however, must be an underestimate because the sound velocity at such short wavelengths must be much smaller than the normal value. Entering this value in Figure 21 and making the most natural connections to the isothermal curves passing through lower frequency points, we recover a pattern quite similar to that for dielectric relaxation. The main difference is a more prominent peak absorption. This is due partly to the greater broadness of the mechanical relaxation, which diminishes the maximum absorptivity of the lower frequency peaks. Some difference might also be expected from the different physics involved in the respective highest frequency peaks. By different physics we mean that the wavelength of the excitation being damped at the mechanical absorption peak is quite different from that of the optical mode that is being excited at the center of the glassy-state equivalent of the crystalline-state Brillouin zone. The latter is strongly, but not completely, absorbed.

We find it of interest that, despite the different physics, there should be as much similarity as there is in the two cases. In particular, the apparent presence of a mechanical equivalent of the source of constant loss per unit wavelength at frequencies well above the relaxation peak is encouraging. This implies a common origin and would be consistent with our speculation that fracton modes may be involved as a common explanation. Indeed, a crossover from phonon to fracton dynamics in lithium borate glasses has recently been suggested by Borjesson[121] to explain particular light-scattering observations. We note again the evidence for a constant $1/T_1$, which is equivalent to a constant loss in modulus spectroscopy, in the studies of low-temperature Li NMR spectroscopy,[71,79] so the phenomenon is common to all of the dynamic probes we have considered in this article.

From study of a variety of systems, it would appear that the magnitude of the constant background loss can vary greatly from system to system and may be sensitive to thermal annealing. We have observed[121] more than two-decade variations from system to system with no particular pattern or correlation with glass composition or liquid class so far emerging. It would seem to present a substantial challenge to future experimental and theoretical endeavor.

IX. Omissions

I am well aware of, and concerned about, the fact that this review is incomplete. Most obvious by its absence is any analysis of the many current theoretical interpretations of different aspects of the phenomenology we have described. However, even some significant aspects of the phenomenology—e.g., the effect of the pressure variable—have not been dealt with, and the studies by computer simulation largely from laboratory have been omitted completely. These must await future reviews.

For the moment, we compromise by only noting the existence of new or alternative theoretical accounts (in addition to those mentioned in the earlier text) of the

origin of nonexponential relaxation in conducting solids by Funke,[123] Shlesinger,[74] Schirmacher,[124] and Dyre[125] and a new treatment of the motion of ions over or through a fluctuating energy barrier by Stein et al.[126] Recent simulation results can be seen in refs 127–129.

I extend an apology to all authors whose significant contributions to this interesting subject area have been inadequately dealt with and exhort future reviewers of this area to excel where I have faltered.

X. Conclusions

Decoupled ion motions in glassy solids lead to a rich variety of relaxation phenomena. Comparison of electrically, mechanically, and magnetically stimulated relaxation phenomena reveals considerable common character, particularly with respect to the relaxation function. This is mostly, though not universally, of stretched exponential (fractal time, or KWW) form, though the departure from exponentiality varies from probe to probe; mechanical relaxation tends to be less exponential, while NMR and conductivity relaxations have very similar functions.

On the basis of the more widely available electrical relaxation data, we establish a linear correlation between the nonexponentiality parameter, β of the KWW function, and the decoupling index R_τ which quantifies the independence of fast-ion modes from viscosity modes: the more decoupled the conductivity, the more nonexponential the relaxation.

Finally, we observe, in all relaxations, evidence for a constant frequency-independent loss between resonance and relaxation frequency domains which we speculate may be connected to fracton dynamics endemic to the glassy state.

XI. Acknowledgments

I acknowledge very helpful discussions with R. W. Rendell and G. P. Johari. This work has benefited from the financial support of the Department of Energy under Grant No. DE-F602-89ER45398 and the Office of Naval Research under Agreement No. N00014-84-K-0289.

XII. References

(1) (a) Relaxation and relaxation spectroscopy in glasses and viscous liquids: (i) Lamb, J. *Rheol. Acta* 1973, *12*, 438; (ii) Brawer, S. A. *Relaxation in Viscous Liquids*; American Ceramic Society: Columbus, OH, 1985; (iii) Wong, J.; Angell, C. A. *Glass: Structure by Spectroscopy*; Marcel Dekker: New York, 1976; Chapter 13; (iv) Angell, C. A. *Mater. Chem. Phys.* 1989, *23*, 143. (b) Nonexponential relaxation in condensed matter: (i) Ngai, K. In *Non-Debye Relaxation in Condensed Matter*; Ramakrishnan, T. V., Raj Lakshmi, M., Eds.; World Scientific: Singapore, 1987; p 23; (ii) Stein, D. L.; Palmer, R. G. Glasses I: Phenomenology (includes a brief review of theoretical models). In *Lectures in the Sciences of Complexity*; Stein, D. C., Ed.; Addison-Wesley: New York, 1989; (iii) Shlesinger, M. F. *Annu. Rev. Phys. Chem.* 1988, *39*, 269. (c) Fast ion motion in glasses: (i) Souquet, J.-L. *Solid State Ionics* 1981, *5*; *Annu. Rev. Mater. Sci.* 1981, *11*, 211; (ii) Tuller, H. L.; Button, D. P.; Uhlmann, D. R. *J. Non-Cryst. Solids* 1983, *40*, 93; (iii) Minami, T. *J. Non-Cryst. Solids* 1985, *73*, 273; (iv) Angell, C. A. *Solid State Ionics* 1983, *9 & 10*, 3; 1986, *18 & 19*, 72. (v) Ingram, M. D. *J. Non-Cryst. Solids* 1985, *73*, 247. (d) Nuclear magnetic resonance studies of ionic motion in glasses: (i) Bray, P. J.; Geissburger, A. E.; Buchaltz, F.; Harris, I. A. *J. Non-Cryst. Solids* 1982, *52*, 45; (ii) Müller-Warmuth, W.; Eckert, H. *Phys. Rep.* 1982, *88*, 91; (iii) Martin, S. W. *Mater. Chem. Phys.* 1989, *23*, 225. (e) Mechanical and dielectric relaxation in polymeric solids: (i) McCrum, M. G.; Reid, B. E.; Williams, G. *Anelastic and Dielectric Effects in Polymeric Solids*; Wiley: London, New York, 1967. (f) Low-temperature phenomena: hole-burning relaxation studies: (i) Hayes, J. M.; Jankowiak, R.; Small, G. J. In *Topics in Current Physics. Persistent Spectral Hole Burning: Science and Applications*. Moerner, W. E., Ed.; Springer-Verlag: New York, 1988.

(2) (a) Turnbull, D. *Contemp. Phys.* 1969, *10*, 473. (b) Turnbull, D.; Cohen, M. H. *J. Chem. Phys.* 1970, *52*, 3038.

(3) Dubochet, J.; Adrian, M.; Teixeira, J.; Alba, C. M.; Kadivala, R. D.; MacFarlane, D. R.; Angell, C. A. *J. Phys. Chem.* 1984, *88*, 6727.

(4) Hilderbrand, E. A.; McKinnon, I. R.; MacFarlane, D. R. *J. Chem. Phys.* 1986, *90*, 2784.

(5) See, for instance: *Dynamic Aspects of Structural Change in Liquids and Glasses*; Angell, C. A., Goldstein, M., Eds.; Ann. N.Y. Acad. Sci. 484; New York Academy of Sciences: New York, 1986. Also see reviews by: (a) Wolynes, P. G. In *Proceedings of the International Symposium on Frontiers in Science*; Chan, S. S., Debrunner, P. G., Eds.; AIP Conf. Proc. 180, 1988. (b) Jackle, J. *Rep. Prog. Phys.* 1986, *49*, 171.

(6) Angell, C. A.; Clarke, J. H. R.; Woodcock, L. V. *Adv. Chem. Phys.* 1981, *48*, 397.

(7) Brawer, S. A. *Relaxation in Viscous Liquids*; American Ceramic Society: Columbus, OH, 1985.

(8) Torell, L. M.; Angell, C. A. *J. Chem. Phys.* 1983, *78*, 937.

(9) Angell, C. A. In *Relaxations in Complex Systems*; Ngai, K., Wright, G. B., Eds.; National Technical Information Service, U.S. Department of Commerce: Springfield, VA, 1985; p 1. The descriptions "strong" and "fragile" for liquids, while now frequently seen in the literature, are a recent arrival and may not be familiar to the reader. In essence they refer to behavior associated with the degree of departure of liquid viscosity from the Arrhenius law. Large departures over wide temperature ranges, implying very large activation energies near T_g, signal "fragile" behavior (examples: toluene, o-terphenyl, KNO_3–$Ca(NO_3)_2$ melts). Strong liquids conform to the Arrhenius law over the whole liquid range down to T_g (example: SiO_2).

(10) Angell, C. A. *Ann. N.Y. Acad. Sci.* 1981, *371*, 136.

(11) Goldstein, M. *J. Chem. Phys.* 1969, *51*, 3728.

(12) Johari, G. P.; Goldstein, M. *J. Chem. Phys.* 1970, *53*, 2372; 1971, *55*, 4245.

(13) Johari, G. P. (a) *J. Phys. Colloq.* 1985, *46* (C8), 567. (b) In *Relaxation in Complex Systems*; Ngai, K., Wright, G. B., Eds.; National Technical Information Service, U.S. Department of Commerce: Springfield VA, 1984; p 17.

(14) Fischer, E. W.; Hellman, G. P.; Spiess, H. W.; Horth, F. J.; Ecarius, U.; Wehrle, M. *Macromol. Chem. Phys.* 1985, *Suppl. No. 12*, 189.

(15) Johari, G. P. *J. Chem. Phys.* 1973, *58*, 1755; *Polymer* 1986, *27*, 566.

(16) Many examples for polymer glasses have been described and analyzed: (a) McCrum, M. G.; Reid, B. E.; Williams, G. *Anelastic and Dielectric Effects in Polymeric Solids*; Wiley: London, New York, 1967. (b) Ngai, K. In *Non-Debye Relaxation in Condensed Matter*; Ramakrishnan, T. V., Raj Lakshmi, M., Eds.; World Scientific: Singapore, 1987; p 23. (c) Ngai, K. L.; Rendell, R. W.; Rajagopal, A. K.; Teitler, S. *Ann. N.Y. Acad. Sci.* 1986, *484*, 150. (d) Ngai, K. *Solid State Ionics* 1987, *5*, 27.

(17) Geszti, T. *J. Phys. C: Solid State Phys.* 1980, *101A*, 477.

(18) (a) Leutheusser, E. *Phys. Rev.* 1984, *A29*, 2765. (b) Bengtzelius, V.; Goeze, W.; Sjölander, A. *J. Phys. C.: Solid State Phys.* 1984, *17*, 5915.

(19) (a) Das, S. P.; Mazenko, G. F. *Phys. Rev.* 1986, *A34*, 2265. Das, S. P. *Phys. Rev.* 1987, *A36*, 211. (b) Götze, W.; Sjögren, L. *Z. Phys.* 1987, *B65*, 415.

(20) Goetze, W. In *Liquids, Freezing, and the Glass Transition*; Hansen, J.-P., Levesque, D., Eds.; NATO-ASI Series; Plenum: New York, in press.

(21) Spaepen, F. *Ann. N.Y. Acad. Sci.* 1981, *371*, 218.

(22) McLin, M.; Angell, C. A. *J. Phys. Chem.* 1988, *92*, 2083.

(23) Macedo, P. B.; Moynihan, C. T.; Bose, R. *Phys. Chem. Glasses* 1972, *13*, 171.

(24) (a) Howell, F. S.; Bose, R. A.; Macedo, P. B.; Moynihan, C. T. *J. Phys. Chem.* 1974, *78*, 639. (b) Moynihan, C. T.; Balitactac, N.; Boone, L.; Litovitz, T. A. *J. Chem. Phys.* 1971, *55*, 3013.

(25) Angell, C. A. (a) *Solid State Ionics* 1983, *9/10*, 3; (b) 1986, *18/19*, 72.

(26) Souquet, J. L. *Annu. Rev. Mater. Sci.* 1981, *11*, 211.

(27) Borjesson, L.; Stevens, J. R.; Torell, L. M. *Polymer* 1987, *28*, 1803.

(28) Etienne, S.; Cavaille, Y.; Perez, J.; Johari, G. P. *Philos. Mag.* 1985, *51*, L35.

(29) Johari, G. P.; Pathmanathan, K. *Phys. Chem. Glasses* 1988, *29*, 219.

(30) Cavaille, J. Y.; Perez, J.; Johari, G. P. *Phys. Rev. B* 1989, *39*, 2411.

(31) Tormala, P. *J. Macromol. Sci., Rev. Macromol. Chem. 17*, 297; *28*, 2567.
(32) Hakim, R. M.; Uhlmann, D. R. *Phys. Chem. Glasses* 1971, *12*, 132.
(33) Wong, J.; Angell, C. A. *Glass: Structure by Spectroscopy*; Marcel Dekker: New York, 1976; Chapter 11.
(34) Provenzano, V.; Boesch, L. P.; Volterra, V.; Moynihan, C. T.; Macedo, P. B. *J. Am. Ceram. Soc.* 1972, *55*, 494.
(35) Moynihan, C. T.; Boesch, L. P.; Laberge, N. L. *Phys. Chem. Glasses* 1973, *14*, 122.
(36) Simmons, K.; Simmons, J. *J. Am. Ceram. Soc.* 1979, *62*, 479.
(37) Mangion, M. B. M.; Johari, G. P. *Phys. Chem. Glasses* 1988, *29*, 225; 1989, *30*, 180.
(38) Borjesson, L.; Torell, L. M.; Martin, S. W.; Changle Liu; Angell, C. A. *Phys. Lett.* 1987, *125*, 330.
(39) Weiler, R.; Bose, R.; Maceco, P. B. *J. Chem. Phys.* 1970, *53*, 1258.
(40) (a) Torell, L. M. *J. Chem. Phys.* 1982, *76*, 3467. (b) Torell, L. M.; Angell, C. A. *J. Chem. Phys.* 1983, *78*, 937.
(41) Sidebottom, D.; Sorenson, C. *Phys. Rev. B* 1990, in press. We note that the recent impulsive light scattering study by Cheng et al. (Cheng, L.-T.; Yan, Y.-Z.; Nelson, K. A. *J. Chem. Phys.* 1989, *91*, 6052) yields data in qualitative agreement, but significant quantitative disagreement, with the data of Figure 8.
(42) Hodge, I. M.; Angell, C. A. *J. Chem. Phys.* 1977, *67*, 4.
(43) Torell, L. M.; Ziegler, D. C.; Angell, C. A. *J. Chem. Phys.* 1984, *81*, 5053.
(44) Dixon, P.; Nagel, S. *Phys. Rev. Lett.* 1988, *61*, 341 and private communication.
(45) (a) Tomazawa, M. In *Treatise on Materials Science*; Tomazawa, M., Doremus, R. H., Eds.; Academic: New York, 1977; Vol. XII, p 335. (b) Hyde, J. M.; Tomazawa, M. *J. Non-Cryst. Solids* 1989, *109*, 18. (c) McGahay, V.; Tomazawa, M. *J. Non-Cryst. Solids* 1989, *109*, 27.
(46) Boesch, L. P.; Moynihan, C. T. *J. Non-Cryst. Solids* 1975, *17*, 144.
(47) Day, D. E.; Stevels, J. M. *J. Non-Cryst. Solids* 1973, *13*, 304.
(48) Etienne, S.; Cavaille, J. Y.; Perez, J.; Point, R.; Salvia, M. *Rev. Sci. Instrum.* 1982, *53*, 126.
(49) Mai, C.; Assiero, A.; Johari, G. P.; Etienne, S.; Abbes, K. *J. Non-Cryst. Solids* 1987, *93*, 35.
(50) (a) Atake, T.; Angell, C. A. *J. Non-Cryst. Solids* 1980, *39/39*, 439. (b) Liu, C.; Angell, C. A. *J. Non-Cryst. Solids* 1986, *83*, 162.
(51) Copley, G. J.; Oakley, D. R. *Phys. Chem. Glasses* 1968, *9*, 141.
(52) Dixon, P. K.; Nagel, S. R. *Phys. Rev. Lett.* 1988, *61*, 341, communication.
(53) (a) Chiodelli, A.; Magistris, A. *Mater. Res. Bull.* 1982, *17*, 1.
(54) (a) Torell, L. M. *Phys. Rev.* 1985, *B31*, 4103. (b) Borjesson, L.; Martin, S. W.; Torell, L. M.; Angell, C. A. *Solid State Ionics* 1986, *18/19*, 141.
(55) Susman, S.; Boehm, L.; Volin, H. J.; Delbecq, C. T. *Solid State Ionics* 1981, *5*, 667.
(56) Carette, B.; Ribes, M.; Souquet, J. L. *Solid State Ionics* 1985, *9/10*, 735.
(57) Pradel, A.; Ribes, M.; Maurin, M., to be published in *Solid State Ionics*.
(58) Robinel, E.; Carette, B.; Ribes, M. *J. Non-Cryst. Solids*, 1983, *57*, 49.
(59) Kennedy, J. H.; Yang, Y. *J. Solid State Chem.* 19878, *69*, 252.
(60) Kennedy, J. H.; Zhang, Z. *Solid State Ionics* 1988, *28/30*, 726.
(61) Minami, T.; Machida, N. *Mater. Chem. Phys.* 1989, *23*, 63.
(62) Doremus, R. H. *Glass Science*; Wiley: New York, 1973.
(63) Day, D. E. In *Amorphous Solids*; Douglas, R. W., Ellis, B., Eds.; Wiley: London, 1972; p 39.
(64) Moore, D. W.; Day, D. E. *Phys. Chem. Glasses*, 1971, *12*, 75.
(65) Ingram, M. D.; Moynihan, C. T. *Phys. Chem. Glasses* 1985, *26*, 132.
(66) Kulkarni, A. R., unpublished work.
(67) Kulkarni, A. R.; Angell, C. A. *J. Non-Cryst. Solids* 1988, *99*, 195.
(68) Bloembergen, N.; Purcell, E. M.; Pound, R. V. *Phys. Rev.* 1978, *73*, 679.
(69) Bray, P. J.; Geissburger, A. E.; Buchaltz, F.; Harris, I. A. *J. Non-Cryst. Solids* 1982, *52*, 45.
(70) Müller-Warmuth, H.; Eckert, H. *Phys. Rep.* 1982, *88*, 91.
(71) Göbel, E.; Müller-Warmuth, W.; Olyschläger, H. *J. Magn. Reson.* 1979, *36*, 371.
(72) Pradel, A.; Ribes, M. *Mater. Chem. Phys.* 1989, *23*, 121.
(73) (a) Ngai, K., In *Fast Ion Transport in Solids*; Vashishta, P., Mundy, J. N., Shenoy, G. K. Eds.; North-Holland: New York, 1979; p 203. (b) *Solid State Ionics* 1981, *5*, 27. (These references actually addressed similar phenomena in nonvitreous disordered materials.)
(74) Shlesinger, M. F. *Annu. Rev. Phys. Chem.* 1988, *39*, 269.
(75) (a) Martin, S. W. *Mater. Chem. Phys.* 1989, *23*, 225. (b) *Appl. Phys. A* (Special edition), in press.
(76) Angell, C. A. In Phenomenology of fast ion conducting glasses: Facts and confusions. *Solid Electrolytes*; Takahashi, T., Ed.; World Scientific Press: Singapore, 1989; p 89.
(77) Angell, C. A.; Martin, S. W. *Symp. Mater. Res. Soc.* 1989, *135*, 63.
(78) Martin, S. W.; Bischof, H. J.; Mali, M.; Roos, J.; Brinkman, D. *Solid State Ionics* 1986, *18/19*, 421.
(79) (a) Reinecke, T. L.; Ngai, K. L. *Phys. Rev.* 1975, *B12*, 3476. (b) Seftel, J.; Alloul, H. *J. Non-Cryst. Solids* 1978, *29*, 253. (c) Greenbaum, S. G.; Strom, U.; Rubinstein, M. *Phys. Rev.* 1982, *B26*, 5226. (d) Sisco, S. J.; Spellane, P.; Kennedy, J. H. *J. Electrochem. Soc.* 1985, *132*, 1766. (e) Balzer-Jollenbeck, G.; Kanert, O.; Steinert, J.; Jain, H. *Solid State Commun.* 1988, *65*, 3.
(80) (a) Balzer-Jöllenbeck, G.; Kanert, O.; Jain, H.; Ngai, K. L. *Phys. Rev. B* 1989, *39*, 6071. (b) Ngai, K. L.; Martin, S. W. *Phys. Rev. B* 1989, *40*, 10550.
(81) Rendell, R. W.; Ngai, K. L.; Fong, G. R.; Aklonis, J. J. *Macromolecules* 1987, *20*, 1070.
(82) Angell, C. A. *J. Chem. Phys.* 1967, *46*, 4673.
(83) Angell, C. A.; Moynihan, C. T. In *Molten Salts: Characterization and Analysis*; Mamantov, G., Ed.; Marcel Dekker: New York, 1969; p 315.
(84) Kauzmann, W. *Chem. Rev.* 1948, *46*, 219.
(85) Adam, G.; Gibbs, J. H. *J. Chem. Phys.* 1965, *43*, 139.
(86) (a) Kawamura, J.; Shimoji, M. *J. Non-Cryst. Solids* 1986, *88*, 295. Kawamura, J.; Shimoji, M. *Mater. Chem. Phys.* 1989, *23*, 99.
(87) (a) Bose, B.; Weiler, R.; Macedo, P. B. *Phys. Chem. Glasses* 1970, *11*, 117. (b) Tweer, H.; Laberge, N.; Macedo, P. B. *J. Am. Ceram. Soc.* 1971, *54*, 122.
(88) (a) Angell, C. A. *J. Phys. Chem. Solids* 1988, *49*(8), 863. (b) *J. Non-Cryst. Solids* 1988, *102*, 205.
(89) Martin, S. W.; Angell, C. A. *J. Non-Cryst. Solids* 1986, *83*, 185.
(90) Liu, C.; Angell, C. A. *J. Chem. Phys.*, in press.
(91) Rao, K. J.; Rao, C. N. R. *Mater. Res. Bull.* 1982, *17*, 1337.
(92) Goodman, C. H. L. *Phys. Chem. Glasses* 1985, *26*, 1.
(93) (a) Ingram, M. D. *Mater. Chem. Phys.* 1989, *23*, 51; *Philos. Mag.* 1989, *60*, 0000. (b) Ingram, M. D.; MacKenzie, M. A.; Müller, W.; Torge, M. *Solid State Ionics*, in press.
(94) See, for instance: Mercier R.; Tachez, M.; Malugani, J. P.; Rousselet, C. *Mater. Chem. Phys.* 1989, *23*, 13. Maugion, M.; Johari, G. P. *Phys. Rev. B* 1987, *36*, 8845.
(95) Jun, L.; Portier, J.; Tanguy, B.; Videau, J.-J.; Angell, C. A. *Solid State Ionics*, in press.
(96) Lesikar, A. V.; Simmons, C. J.; Moynihan, C. T. *J. Non-Cryst. Solids* 1980, *40*, 9171.
(97) Rendell, R. W.; Ngai, K. L.; Fong, G. R.; Aklonis, J. J. *Macromolecules* 1987, *20*, 1070.
(98) (a) Downing, H. L.; Peterson, N. L.; Jain, H. *J. Non-Cryst. Solids* 1982, *50*, 203. (b) Jain, H.; Peterser. N. L. *Philos. Mag.* 1982, *A46*, 351.
(99) Ngai, K. L.; Rendell, R. W.; Jain, H. *Phys. Rev. B* 1984, *30*, 2133.
(100) Tatsumisago, M.; Hamada, A.; Minami, T.; Tanaka, M. *J. Non-Cryst. Solids* 1983, *56*, 423; *J. Am. Ceram. Soc.* 1983, *66*, 890.
(101) Pinnow, D. A.; Candace, S. J.; LaMacchia, J. T.; Litovitz, T. A. *J. Account. Soc. Am.* 1968, *43*, 131.
(102) Higashigaki, Y.; Wang, C. H. *J. Chem. Phys.* 1981, *74*, 3175.
(103) Patterson, G. *Annu. Rev. Phys. Chem.* 1987, *38*, 191.
(104) Borjesson, L. *Phys. Rev.* 1987, *B36*, 4600.
(105) Borjesson, L.; Torell, L. M. *Solid State Ionics* 1987, *25*, 85.
(106) Carini, G.; Cutroni, M.; Federico, M.; Galli, G.; Tripodo, G. *Phys. Rev.* 1984, *B30*, 7219; 1985, *B32*, 8264.
(107) Ngai, K. L.; Rendell, R. W. *Phys. Rev. B* 1988, *B38*, 9987.
(108) Liu, C.; Angell, C. A. *J. Chem. Phys.*, in press.
(109) Ingram, M. D.; Vincent, C. A.; Wandless, A. R. *J. Non-Cryst. Solids* 1982, *53*, 73.
(110) Malugani, J. P.; Wasniesnski, A.; Dorean, M.; Robert, G.; Al Rikabi, A. *Mater. Res. Bull.* 1978, *13*, 427.
(111) Liu, Changle, unpublished work.
(112) Sridhar, S., to be published.
(113) Burns, A. V.; Cole, R. H.; Chrysachoas, G.; Risen, W. *Phys. Chem. Glasses* 1989, *30*, 264.
(114) Ngai, K. L.; Strom, V. *Phys. Rev. B* 1983, *B27*, 603.
(115) Alexander, S.; Orbach, R. *J. Phys. Lett.* 1982, *43*, L-625.
(116) Kieffer, J. A.; Angell, C. A. *J. Non-Cryst. Solids* 1988, *106*, 336.
(117) Xhonneux, P.; Courtens, E.; Pelous, J.; Vacher, R. *Europhys. Lett.* 1989, *10*, 733.
(118) Boehm, L.; Smith, D. L.; Angell, C. A. *J. Mol. Liquids* 1987, *36*, 153.
(119) Leadbetter, A. J.; Wright, A. C.; Apling, A. J. In *Amorphous Materials*; Douglas, R. W., Ellis, B., Eds.; Wiley-Interscience: London, 1972.
(120) Grest, G. S.; Nagel, S. R.; Rahman, A. *Phys. Rev. B* 1984, *B29*, 5968.
(121) Borjesson, L. In *Dynamics of Disordered Materials*; Richter, D., Dianoux, A. J., Petry, W., Teixeira, J., Eds.; Springer-Verlag: Berlin, 1989; Vol. 37, p 126.

(122) Angell, C. A. Unpublished work.
(123) Funke, K.; Hoppe, R. *Solid State Ionics* 1986, *18–19*, 183; 1988, *28–30*, 100; 1990, in press.
(124) Movaghar, B.; Schirmacher, W. *J. Phys.* 1981, *C14*, 859.
(125) Dyre, J. C. *J. Appl. Phys.* 1988, *64*, 2456 and earlier references therein.
(126) Stein, D. L.; Palmer, R. G.; Van Hemmen, J. L.; Doering, C. R. *Phys. Lett.* 1989, *136*, 353.
(127) Angell, C. A.; Boehm, L.; Cheeseman, P. A.; Tamaddon, S. *Solid State Ionics* 1981, *5*, 659.
(128) Angell, C. A.; Cheeseman, P. A.; Tamaddon, S. *J. Phys. Colloq.* 1982, *43*, C9–381.
(129) Syed, R.; Kieffer, J. A.; Angell, C. A. *Symp. Mater. Res. Soc.* 1989, *135*, 73.

British Polymer Journal **20** (1988) 173–179

Ion–Matrix Coupling in Polymer Electrolytes from Relaxation Time Studies

L. M. Torell

Department of Physics, Chalmers University of Technology, Goteborg, S-41296, Sweden

and

C. A. Angell

Department of Chemistry, Purdue University, West Lafayette, IN 47906, USA

(Received 10 August 1987; accepted 26 September 1987)

Abstract: We review the effects of temperature on conductance and viscosity in the liquid state of vitreous ionic conductors and show how differences may be best understood by comparison of *relaxation times* for electrical and mechanical stresses acting on liquid or glassy states of the material. This leads to the definition of a conductivity viscosity mode *decoupling index*, useful as a figure of merit for the solid electrolyte. In applying the same approach to polymer electrolyte systems a problem is encountered due to the molecular weight dependence of the viscosity. This is resolved by deriving a 'monomer' shear relaxation time for the polymer electrolyte solution and showing that this quantity corresponds closely with the 'local' mechanical relaxation time obtained from light scattering studies (which is a molecular weight independent quantity for pure polypropylene oxide and other polymers of low T_g). Comparison of the electrical relaxation times of the polymer solution with the 'local' (or 'matrix') relaxation times then shows that the relationship found for superionic glass-forming systems is inverted in the case of polymer electrolytes. The latter have fractional decoupling indexes which may be interpreted in terms of serial coupling phenomena; i.e. ions must first decouple from their partner ions (in ion pairs), or from their intramolecular solvation states, before they can contribute to conductivity relaxation which is itself coupled to the local polymer matrix relaxation. An extreme case is illustrated using the weak electrolyte, lithium acetate, for which the decoupling index is $\sim 6 \times 10^{-5}$.

Key words: Polymer electrolytes, relaxation, decoupling index, light scattering, conductivity.

1 INTRODUCTION

In this paper we show how the combination of light scattering[1] and conductivity[2] data can provide a phenomenological scheme for the discussion of conductivity in relation to polymer chain segmental motion in polymer electrolytes. This scheme permits the relationship between different polymer–salt systems and (the alternative) solid electrolyte systems based on inorganic glasses to be clearly seen. The basis that we propose for organizing observations on polymer systems should make it simpler to define the limiting factors on polymer electrolyte performance and lead to improvements in that performance.

It is generally recognized that the mechanism for conductance in polymer–salt systems is intrinsically different from that in fast-ion conducting glasses. In

British Polymer Journal 0007-1641/88/$03.50

the former a highly flexible polymer backbone structure is essential. This has the concomitant requirement that the glass transition phenomenon, which signals the 'bottom' of the liquid-like regime of behaviour, lies at temperatures far below that of the application. The polymer 'solid' electrolyte then owes its mechanical stability to the chain entanglement phenomenon, or to crosslinking in the case of shorter chains. On the other hand, it is obvious that in the case of fast-ion conducting glasses (which are no more than deeply supercooled ionic liquids), the glass transition temperature must lie above the temperature of intended application if the electrolyte is to have a fixed shape. Since a 'good' performance in each type of system is defined by having d.c. conductivities no less than 10^{-3} S cm^{-1} at the intended service temperature, it is clear that in the superionic glass case the mobile ion motions must be essentially independent of the modes of motion which determine the glass transition. In the polymer electrolyte case, by contrast, the two types of motion must be closely related. Indeed, it is now the general view that ions in polymer–salt systems move cooperatively in some manner with the segmental motions of the polymer. It is with the definition and interpretation of the time scales for these processes that this contribution is concerned. It will be seen that light scattering techniques applied to polymer solvents[3–6] and recently to polymer solutions[1] provide the most direct relevant probes of the polymer (or 'matrix') time scales.

2 FAST-ION CONDUCTING GLASSES

For our investigation of polymer–salt solution behaviour, it will be helpful to review briefly the related scheme that has been used to discuss fast-ion conduction in liquid and glassy solids.[7] This scheme takes the equilibrium liquid state as its starting point.

In the ionic liquid state, in contrast to polymer electrolytes above T_g, the electrical conductivity is extremely high. For instance, at 150° above its T_g the conductivity of the most simply constituted 'superionic' glass, $CsAg_4(ICl)_5$ is 0·4 S cm^{-1} [2,8] (cf. $\sim 10^{-3}$ for the best polymer electrolyte[7]). Between (T_g + 150) and T_g (at −21 C), the conductivity of this material decreases by only some three orders of magnitude. The viscosity, however, increases by more than 15 orders of magnitude in the same T-range. Evidently, unlike the classical Walden electrolytes, the conductivity process is not closely coupled to the viscosity in these systems, except at very high temperatures. This behaviour is similar in character to that known for diffusion of gases or small molecule solutes in polymer solutions.[9]

Such differences in the effect of temperature change on transport processes can be presented in a useful manner by comparing the time scales on which the system responds with the stresses which drive the processes. These response times, or *relaxation times* τ, may be obtained directly from frequency-dependent studies of the conductance process (by a.c. admittance bridge techniques)[10] and of the viscous flow process (by ultrasonic absorption[11] and Brillouin scattering[12] techniques) or indirectly by the use of Maxwell relations[13]

$$\langle \tau_\sigma \rangle = e_0 \rho_{dc} / M_\infty \tag{1}$$

and

$$\langle \tau_s \rangle = \eta_\infty / G_\infty \tag{2}$$

which connect liquid-like properties, d.c. resistivity ρ_{dc}, and shear viscosity η_∞, to solid-like properties, electrical modulus M_∞ ($M_\infty = 1/\varepsilon_\infty$; ε the dielectric constant) and shear modulus G_∞, and e_0 is the permittivity of free space. Equations (1) and (2) yield average relaxation times $\langle \tau \rangle$, while the frequency-dependent studies give directly the most probable value and also information on the 'distribution of relaxation times' if the relaxation process is non-exponential.

When the data are presented in this manner one observes that at high temperatures the electrical and mechanical response times, τ_σ and τ_s, are rather close, suggesting comparable relaxation mechanisms or a coupling of mechanisms. However, with

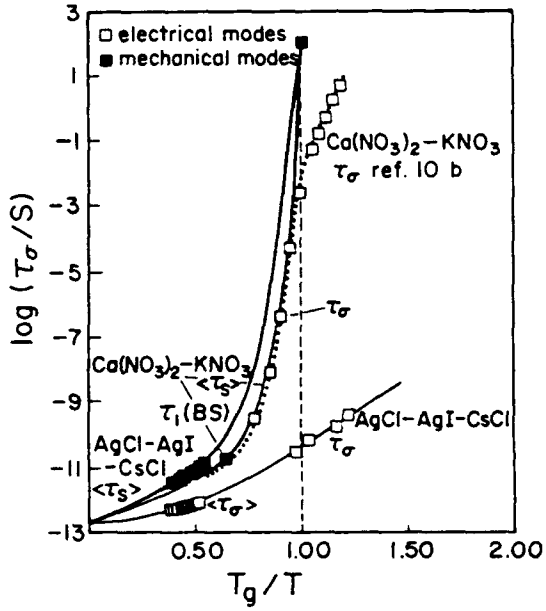

Fig. 1. Average mechanical (shear) and electrical relaxation times. $\langle \tau_s \rangle$ and $\langle \tau_\sigma \rangle$, for liquid and glassy states of the fast-ion conductor AgCl–AgI–CsCl and the poor conductor $2Ca(NO_3)_2 . 3KNO_3$. In the latter case, the shear relaxation times coincide with the longitudinal relaxation time determined by Brillouin scattering τ_1(BS). Also note the close correspondence between $\langle \tau_s \rangle$ and $\langle \tau_\sigma \rangle$ for $T > T_g$ in this case.

decreasing temperature (and increasingly well-defined short and intermediate range order of the liquid) the two response times separate increasingly (see Fig. 1), implying a progressive *decoupling* of the mechanisms. The ratio of the relaxation times τ_s/τ_σ reflects the decoupling and has been called the *decoupling index*, R_τ.[7] Its value at the glass transition temperature T_g where the intermediate range order becomes frozen for all lower temperatures, has been suggested as a figure of merit for fast-ion conducting glasses.

We will use the same index in this paper as a figure of merit for polymer–salt electrolytes, though the values of maximum merit will be seen to differ by some 14 orders of magnitude from those of high performance fast-ion conducting glasses. To provide an example with which to compare polymer electrolyte behaviour, we show in Fig. 1 the relation between viscosity and conductivity relaxation times obtained from ultrasonic,[11] Brillouin scattering,[12] shear viscosity,[8] and conductivity[8,10] data for liquid and glassy states of two vitreous systems, using a reduced Arrhenius plot presentation with T_g scaling. One of the systems, AgI–AgCl–CsCl, yields a superionic glass,[14] while the other, $2Ca(NO_3)_2.3KNO_3$ yields a low-conducting glass.[10b]

3 POLYMER–SALT SOLUTIONS

3.1 Mechanical responses

To examine the coupling relations for polymer–salt solutions we must first clarify the relation between viscosity-based and other relaxation times. To this end we examine basic data for a fully amorphous polymer–salt system, poly(propylene oxide) PPO–sodium triflate ($NaCF_3SO_3$), using solvents of molecular weight 425 and 4000. We choose a salt concentration such that the ratio R of monomer unit [$CH(CH_3)CH_2O$] to salt units, $NaCF_3SO_3$, (written [—O—]/[Na^+]) is 16:1 in each case. This concentration is on the high concentration side of the conductivity maximum for this system if, as expected, it behaves like $LiClO_4$ in PPO.[15] Details on the measurements are to be found in a report of more extended studies being published elsewhere.[1,2]

Figure 2 shows an Arrhenius plot of rotating spindle viscosity data for the solutions. The data extend over two orders of magnitude. We include viscosity data for the pure solvents taken from the literature.[16,17] Figure 3 shows the results of a Brillouin scattering study of the solution of polymer having MW 4000. Absorption coefficients α/n (n = refractive index) for ~5·3 GHz sound waves, obtained in the manner recently described for the pure PPO solvents,[5,6] are plotted as a function of

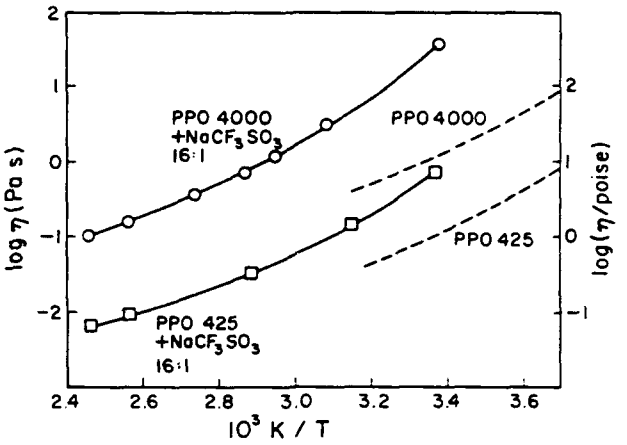

Fig. 2. Viscosity data for PPO solutions of sodium triflate 16:1. Dashed lines are data for pure solvents from Refs 3*b* and 16.

temperature. At the absorption maximum the condition $\omega_B\tau_1 = 1$ is satisfied so, at 107°C, we find that the relaxation time τ_1 for longitudinal stresses is 3×10^{-11} s. Based on the results for non-polymeric liquids[12,18] (see Fig. 1), this will also be the microscopic relaxation time for shear stress at hypersonic frequencies.

To compare this longitudinal value, which we refer to hereafter as τ_1 (BS) with the relaxation times characterizing the macroscopic viscosities of Fig. 2 we must use the Maxwell relation (eqn 2). Lacking G_∞ data for the solution at this time, we use the values found for the pure solvents of comparable molecular weight by Lamb and Erginsav using an ultrasonic technique.[17] Since the glass transition temperatures differ by only ~20 K (see below) and since G_∞ usually scales with T_g, this substitution will not lead to errors in excess of 10%. As will be seen, the effects of interest to us are orders of magnitude in τ, so the G_∞ choice is not an important source of uncertainty.

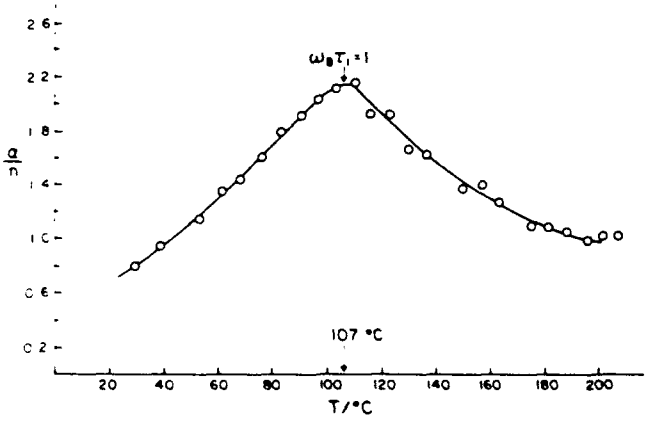

Fig. 3. Absorption coefficient α divided by refractive index n as a function of temperature for 16:1 sodium triflate in PPO 4000. The peak falls at 107 C, cf. 56 C for pure PPO 4000.

Using the expression

$$G_\infty^{-1} = 1 \times 10^{-10} + 1{\cdot}85 \times 10^{-11}(T - 180{\cdot}1) \quad (3)$$

for the polymer of MW 4000,[17] and the viscosity data of Fig. 2, we obtain the average shear relaxation times $\langle\tau_s\rangle$ shown as open circles in Fig. 4. As expected these times are much longer than for the value obtained from Brillouin scattering (open square). The latter is independent of molecular weight for pure PPOs and appears to reflect some local process,[3-6] while viscosities in polymers increase as the first power of the molecular weight up to the chain entanglement point.[19]

We now test the proposal[3-6] that the Brillouin relaxation time τ_1 (BS) is a truly microscopic relaxation time by comparing its value with that of a derived local relaxation time $\langle\tau_{s,1}\rangle$ obtained by extrapolating the molecular weight dependent shear relaxation time back to the single repeat unit limit. Since, as noted above, $\eta \propto MW$,[19] we obtain $\langle\tau_{s,1}\rangle$ from the obvious relation

$$\langle\tau_{s,1}\rangle = \langle\tau_{s,n}\rangle/n \quad (4)$$

where n is the number of repeat units $[CH(CH_3)CH_2O]$ in the average chain, viz. 69 for the 4000 PPO and 7 (including end oxygens) for 425 PPO. The values of $\langle\tau_{s,1}\rangle$ from the PPO 4000 solution are plotted as filled circles in Fig. 4 where it is seen that they fall very close to (at slightly shorter times than) the Brillouin value. We use a reduced temperature scale in Fig. 4 in order to incorporate $\langle\tau_s\rangle$ values for other Na triflate solutions and τ_1 (BS) data for *pure* PPO. To avoid confusion in Fig. 4, we do not include $\langle\tau_{s,1}\rangle$ values from the 425 MW solutions, but note here that they fall systematically 0·3 log units to shorter times than those from the 4000 MW solution. Although such a difference would be expected in an ordinary Arrhenius plot simply because, as Fig. 2 shows, η at constant concentration is larger when the solvent molecular weight is larger, this effect should have been scaled out by the T_g-reduced temperature scale of Fig. 4. Since the difference may simply be a result of using the pure solvent G_∞ data in calculating $\langle\tau_{s,1}\rangle$, we will not concern ourselves wth possible differences until we have obtained G_∞ data for the actual salt solutions.

To further support the correlation of Brillouin and 'monomer' shear relaxation times, we may add data from the literature for the *pure* PPO solvents. The dashed line in Fig. 4 is the light-scattering-based longitudinal relaxation time τ_1 (BS) for pure PPO 4000 and other molecular weights taken from a recent paper[5] in which short-time Brillouin scattering data were combined with the longer-time (10^{-1}–10^{-4} s) digital correlation spectroscopy results of Wang *et al.*[3] Here τ_1 is plotted using

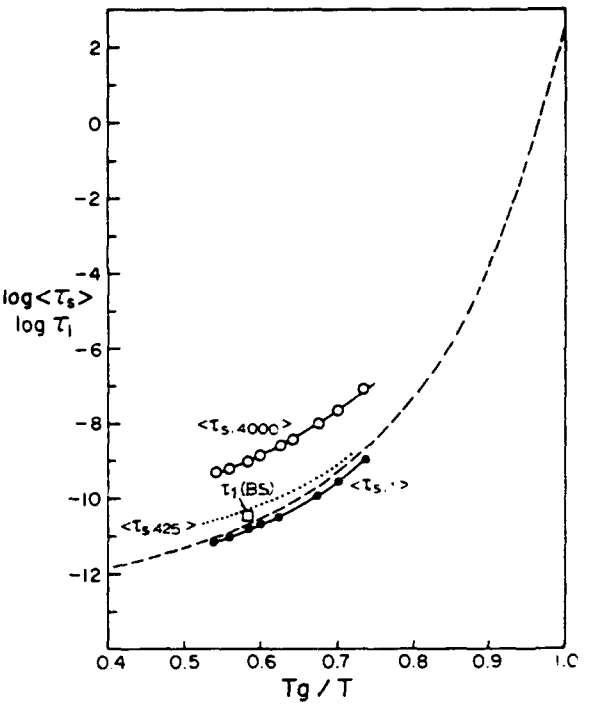

Fig. 4. Average shear relaxation times $\langle\tau_s\rangle$ for sodium triflate solutions, 16:1 in PPO 4000 (open circles) and PPO 425 (dotted line) and derived 'monomer' relaxation time ($\langle\tau_{s,1}\rangle$) (filled circles) for PPO 4000 salt solution shown in relation to the longitudinal relaxation times of the solution from Brillouin scattering τ_1 (BS) (open square). Longitudinal relaxation times from light scattering for the *pure* PPO solvent of various molecular weights are shown as dashed line.

$T_g = 201$ K as scaling parameter. Since both the Brillouin study[6] and the digital correlation spectroscopy study[3] of PPOs in the MW range 400–5600 find only a very weak molecular weight dependence, and since T_g is likewise independent of MW, the dashed curve in Fig. 4 is also molecular weight independent, at least for pure solvents. The small displacement of the salt solution τ_1(BS) point (square) from the pure solvent value (dashed line) may be partly due to the choice of T_g value 218 K (rather than 223 K—see Fig. 6) used in the temperature scaling (see below) but could also reflect real changes in the temperature dependence of the relaxation time as the salt cations transiently crosslink the polymer chains.

On the basis of the findings in Fig. 4 we conclude that light scattering measurements, or chain number-reduced viscosity measurements, may provide data on local *structural relaxation times in polymer electrolytes which are equivalent to the* $\langle\tau_s\rangle$ *values with which the electrical relaxation time was compared in the case of the liquid and glassy inorganic electrolytes of Fig. 1.*

It is of interest to know how large is the locally relaxing group of segments detected by the light scattering experiment. The relative placement of the

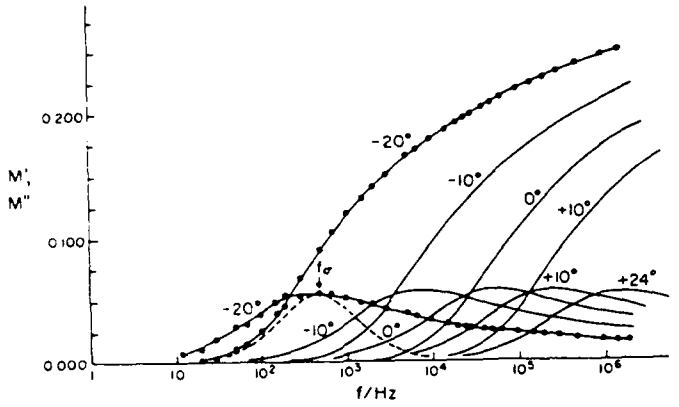

Fig. 5. Real M' (rising curves) and imaginary M'' (curves with maxima) parts of the electrical modulus as a function of frequency for sodium triflate solution (16:1) in PPO 4000. Dashed line under −20 C curve shows shape of loss spectrum for exponential relaxation (single relaxation time).

points for $\langle\tau_{s,-}\rangle$ (MW 425), τ_1(BS), and $\langle\tau_{s,1}\rangle$ in Fig. 4 suggests that it is larger than one PPO repeat unit, but perhaps smaller than seven.† The relaxing group size may also depend a little on salt concentration (which should have some influence on the refractive index fluctuations detected by light scattering) since comparison of $\langle\tau_{s,1}\rangle$ values for *pure* PPO 4000 solvent (not shown in Fig. 4) with light scattering values shows a difference which is twice that seen between τ_1 (BS) and $\langle\tau_{s,1}\rangle$ seen in Fig. 4 for the solution data.

3.2 Electrical relaxation times and coupling relations

With a plausible measure of the relevant 'matrix' relaxation time available, we now seek electrical relaxation times for the polymer—salt electrolytes in order to compare the polymers with the Fig. 1 phenomenology. In Fig. 5 we show real M' and imaginary M'' parts of the electrical modulus M^* ($M^* = 1/\varepsilon^*$)[13] obtained from automated admittance bridge measurements on the $R = 16$ sodium triflate solution in PPO 4000 in the temperature range −20 to +24°C. The solution was contained in an all-metal cell to avoid spurious secondary dielectric effects which may arise when glass containers are used with low conducting solutions. Details are available elsewhere.[2]

Figure 5 contains, for comparison, the M'' vs frequency plot for a system relaxing with a single relaxation time with the same value as the most probable relaxation time for the present triflate solution at −20°C, see dashed curve. The comparison makes clear that the triflate solution, at this concentration at least, is complex and is characterized by a very broad 'spectrum of relaxation times'. This is also indicated by the unusually smeared-out glass transition for this composition shown, along with data for the PPO 425 triflate solution and the pure solvents, in Fig. 6. The complexity seems peculiar to a narrow range of compositions around $R = 16$ and its origin will be dealt with elsewhere.[2] It is sufficient to note here that the broad loss curves of Fig. 5 cannot be well fitted with the usual Williams–Watts function which describes well the narrower spectra found at higher concentrations.

We now take the most probable conductivity relaxation times from the M'' peak frequencies of Fig. 5, $\tau_\sigma = 1/2\pi f_{\sigma,\max}$, and plot them in Fig. 7 together with the 'monomer' shear relaxation times, and the Brillouin relaxation time from Fig. 4. The conductivity relaxation time plot may be extended to higher temperatures by including *average* conductivity relaxation times $\langle\tau_\sigma\rangle$ obtained from the d.c. conductivities and eqn (1), with M_∞ taken as the value of M' in Fig. 6 at three decades above the M'' maximum.

Comparison of Fig. 7 and Fig. 1 shows that in polymer electrolytes the coupling relations are the opposite of those found in the fast-ion conducting glass case; the electrical field is now relaxed more slowly by ionic migration than is local mechanical stress. Quantitatively, the decoupling index R_τ, which we suggest as a figure of merit, for 16:1 sodium triflate in PPO 4000 is $\sim 2 \times 10^{-2}$, independent of temperature. This implies that the solvent or matrix structural rearrangements determining $\tau_{s,1}$ and τ_1

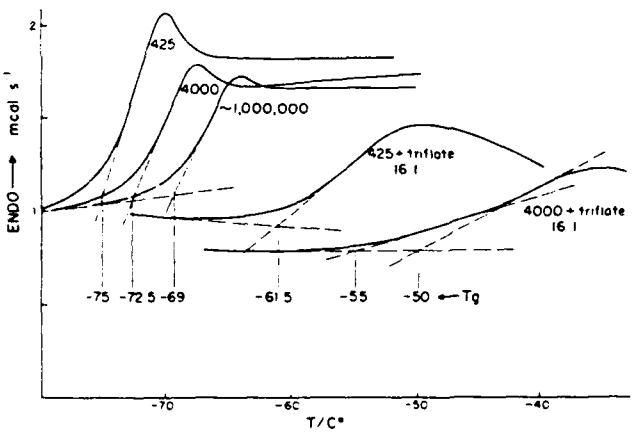

Fig. 6. D.s.c. scans of the glass transition phenomenon in pure PPO solvents of MW 425, 4000, and ~ 10^6 compared with those for 16:1 solutions of sodium triflate in PPO 425 and PPO 4000. In the latter case the definition of the glass transition is ambiguous.

† It is interesting to note that the $\omega\tau = 1$ condition in ultrasonic relaxation of the pure PPOs, although also much less dependent on molecular weight than viscosity, occurs at much longer times than in Brillouin scattering and indeed at even longer times than the shear relaxation time for the 4000 MW.[14] The ultrasonic relaxation is also more nearly exponential than in the hypersonic case, and presumably proves a quite different process.

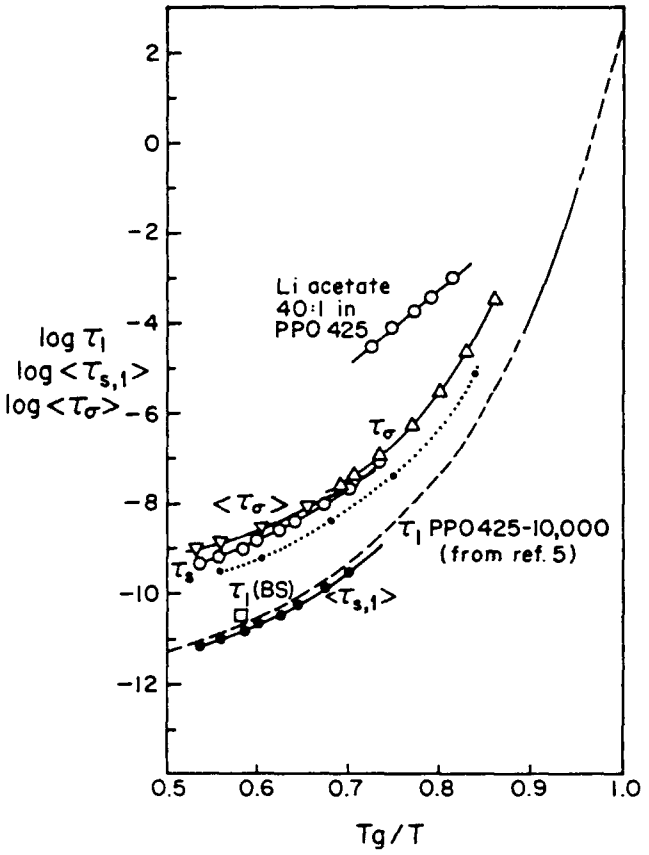

Fig. 7. Comparison of most probable and average conductivity relaxation times, τ_σ and $\langle\tau_\sigma\rangle$, respectively, with average shear relaxation time $\langle\tau_s\rangle$ and local structure relaxation times derived from light scattering τ_l(BS) and 'monomer' shear relaxation time $\langle\tau_{s,1}\rangle$, for sodium triflate solutions (16:1) in PPO 4000. Dashed line is light-scattering-based longitudinal relaxation time for pure PPO from Ref. 5. Also shown are conductivity relaxation times for the weak electrolyte lithium acetate 40:1 in PPO 425 (T_g = 198 K). For comparison, the dotted line shows τ_σ of sodium triflate 16:1 in PPO 425.

(BS), while obviously necessary for charge migration to occur, are not always accompanied by charge migration.

This latter conclusion may be interpreted in different ways. The most obvious one would be that the migrating ions 'see' a less microscopic viscosity than that seen by the locally rearranging chain segments probed by Brillouin scattering (τ^1 (BS) $\simeq \tau_{s,1}$). A molecular level explanation could be that polarization clusters of chain segments form around dissolved ions and cause the rearranging group involved in conductivity relaxation to be larger than the $n = 1$–7 group suggested above for Brillouin scattering. In the absence of other factors, the $\langle\tau_{s,1}\rangle$–τ_σ gap could then serve to estimate the size of the rearranging cluster. The close correspondence of τ_σ and $\langle\tau_s\rangle$ for PPO 4000 ($n = 69$) seen in Fig. 7 might suggest a group size of 69 repeat units, which seems too large.

The other obvious interpretation would be in terms of the ion-pairing phenomenon which is anticipated in low dielectric constant media, and which has been observed spectroscopically[20,21] and quantitatively evaluated in one case.[21] Conductivity relaxation does not occur if a structural relaxation is accompanied by the displacement of a bound ion pair because no net charge displacement occurs (provided we restrict considerations to solutions of the 1:1 electrolytes which are of principal interest to solid electrolyte studies). The presence of ion pairs would, therefore, lengthen τ_σ relative to $\tau_{s,1}$ in the observed manner.

To show this effect unambiguously we include in Fig. 7 some conductivity relaxation time data[22] from a 40:1 solution of lithium acetate in PPO 425 (higher concentrations not being easily obtained). Due to the high charge density on the CH_3COO^- oxygens, lithium acetate dissociates only weakly in polymer solutions; the free ion population must be $\sim$1000 fold smaller than in the corresponding strong electrolyte solutions (e.g. $LiClO_4$) since the conductivities of the respective solutions differ by almost three orders of magnitude.[15,23,24] The small free ion population is then reflected in Fig. 7 by the much larger, and also temperature-dependent, gap betwen the $\tau_{s,1}$ and τ_σ curves of Fig. 7. The decoupling index in this case is $\sim 6 \times 10^{-5}$. It is appropriate to think of such a value as a reflection of a serial decoupling phenomenon; in order to migrate via a solvent-coupled mechanism, the ion must first decouple from its ion-paired partner.

Some assistance in resolving these issues may come from current spectroscopic studies of the temperature dependence of the free ion population. A simple coupling of ionic mobility to local viscosity implies equal temperature dependences of τ_σ and $\tau_{s,1}$ (as in the typical aqueous solutions[25]). Therefore changes in free ion population with temperature should become evident in changes in the separation of $\tau_{s,1}$ and τ_σ curves of Fig. 7. It is obvious that the curves are not parallel, and the $\sim$0·3 log units change in separation between 36 and 139°C could imply a factor of 2 decreases in free ion population between 36 and 139 K. A decrease of $\sim$40% has been observed in a current Raman spectral study of this solution.[1] Whether or not intra- vs intermolecular solution phenomena[26] have a role to play remains to be seen.

These considerations are in a preliminary stage of development, and clearer correlations and interpretations will be possible when additional experimental data are at hand.

ACKNOWLEDGEMENTS

The authors are indebted to the US National Science Foundation, Office of International Programs for

support of this collaborative project under Grant No. INT 8619785, and to the Swedish National Board for Technical Development and the US Office of Naval Research Agreement No. N00014-84K-0289 for support of the experimental studies on which our analysis has been based. We are grateful to a number of our coworkers, S. Schantz, J. Sandahl, L. Borjesson, J. Stevens, M. McLin, Rongjian Xue, and A. Kulkarni for their willingness to let us use some of their unpublished results in support of the ideas presented in this manuscript.

REFERENCES

1 Schantz, S., Sandhal, J., Borjesson, L., Torell, L. M. & Stevens, J., *Solid State Ionics*, 1988, in press.
2 McLin, M. & Angell, C. A., *J. Phys. Chem. (Letters Section)*, 1988, **92**, in press.
3*a* Wang, C. H. & Huang, Y. Y., *J. Chem. Phys.*, 1976, **64**, 4847; *b* Wang, C. H., Fytas, G., Lilge, D. & Dorfmuller, Th., *Macromolecules*, 1981, **14**, 1363.
4 Patterson, G. D., Douglass, D. C. & Latham, J. P., *Macromolecules*, 1978, **11**, 263.
5 Borjesson, L., Stevens, J. R. & Torell, L. M., *Polymer*, 1987, **28**, 1803.
6 Borjesson, L., Stevens, J. R. & Torell, L. M., *Physica Scripta*, 1987, **35**, 692.
7 Angell, C. A., *Solid State Ionics*, 1983, **9 & 10**, 3; 1986, **18 & 19**, 72.
8 McLin, M. & Angell, C. A., to be published; Angell, C. A., *Materials for Solid State Batteries*, Eds Chowdari, B. V. R. and Radhakrishna, S., 1986, pp. 31–40, Singapore: World Scientific Publ. Co.
9 Sillescu, H., priv. comm.
10*a* Moynihan, C. T., Bressel, R. D. & Angell, C. A., *J. Chem. Phys.*, 1971, **55**, 4414; *b* Howell, F. S., Bose, R. A., Macedo, P. B. & Moynihan, C. T., *J. Phys. Chem.*, 1974, **78**, 639.
11 Weiler, R., Bose, R. & Macedo, P. B., *J. Chem. Phys.*, 1970, **53**, 1258.
12 Torell, L. M., *J. Chem. Phys.*, 1982, **76**, 3467.
13*a* Macedo, P. B., Moynihan, C. T. & Bose, R. A., *Phys. Chem. Glasses*, 1972, **11**, 171; *b* Wong, J. & Angell, C. A., *Glass Structure by Spectroscopy*, 1976, Chapter 11, New York: Marcel Dekker.
14 Changle Liu, Sundar, H. G. K. & Angell, C. A., *Mat. Res. Bull.*, 1985, **20**, 525.
15 Watanabe, M., Ikeda, J. & Shinohara, I., *Polymer J.*, 1983, **15**, 65, 175.
16 Baur, M. E. & Stockmayer, W. H., *J. Chem. Phys.*, 1965, **43**, 4319.
17 Lamb, A. J. & Erginsav, A., *Polymer*, 1975, **16**, 110.
18 Angell, C. A. & Torell, L. M., *J. Chem. Phys.*, 1983, **78**, 937.
19 Berry, G. C. & Fox, T. G., *Adv. Polymer Sci.*, 1968, **5**, 261.
20 Teeters, D. & Frech, R., *Solid State Ionics*, 1986, **18 & 19**, 271.
21 Schantz, S., Sandahl, J., Borjesson, L., Torell, L. M. & Stevens, J. M., *Solid State Ionics*, 1988, to be published.
22 Wintersgill, M. C., Fontanella, J. T., Greenbaum, S. G. & Adamič, K. J., *British Polymer J.*, 1988, **20**, 195.
23 Watanabe, M., Sanui, K., Ogata, N., Kobayashi, T. & Ohtaki, Z., *J. Appl. Phys.*, 1985, **57**, 13.
24 Rongjian Xue & Angell, C. A., to be published.
25 Moynihan, C. T., Balitactac, N., Boone, L. & Litovitz, T. A., *J. Chem. Phys.*, 1971, **55**, 3013.
26 Cameron, G. G., Harvie, J. L., Ingram, M. D. & Sorrie, G. A., *British Polymer J.*, 1988, **20**, 199; Ingram, M. D., priv. comm.

Reprinted from The Journal of Physical Chemistry, 1988, 92, 2083.

(12)

Contrasting Conductance/Viscosity Relations in Liquid States of Vitreous and Polymer "Solid" Electrolytes

M. McLin and C. A. Angell*

Department of Chemistry, Purdue University, West Lafayette, Indiana 47907 *(Received: November 30, 1987; In Final Form: February 22, 1988)*

In order to contrast conductivity mechanisms in fast ion glassy and rubbery polymer electrolytes, the *liquid* states of two prototypical cases have been studied. Viscosity and conductivity measurements have been performed on molten (as opposed to glassy) $(AgCl)_{0.35}$–$(AgI)_{0.45}$–$(CsCl)_{0.20}$ and on solutions of sodium triflate in low molecular weight poly(propylene oxide), PPO (as opposed to high molecular weight, 10^6, rubbery solid PPO). Both types of system show non-Arrhenius viscosity with divergent behavior near T_g. The energetics of the conductivity processes, however, are very different. This is emphasized by reduced temperature scale (T/T_g) plotting of (temperature-dependent) activation energies. For the polymer salt systems, as for normal molten salt systems and aqueous solutions, conductance and viscosity energetics are comparable at all temperatures; hence the processes are coupled. For the liquid salt the conductivity process becomes decoupled as the glassy solid state is approached. Using reduced temperature plots of polymer solutions and glass-forming aqueous solution data we show the relative importance of T_g and ion association factors in limiting polymer electrolyte performance.

Introduction

Amorphous solid conductors offer the best practical solutions to the ambient temperature solid-state electrochemical device electrolyte problem because of their combination of high ionic conductivity and ease of fabrication into thin films. Within the amorphous solid family there are two contrasting subgroups, the vitreous conductors and the elastomeric polymer + salt conductors. It is generally recognized that the mechanism of conductance in these subgroups is different.[1,2] In the polymer electrolyte case good performance depends on the service temperature being far above the glass–rubber transition temperature T_g, whereas, for vitreous electrolytes, the requirements of dimensional stability and stability against devitrification demand the reverse service temperature/T_g relationship. This implies that the mobile ion–vitreous matrix interactions must be weak in superionic glasses, whereas it would appear that the reverse must be true in polymer electrolytes in view of the solvation interaction on which the solubility of salt in polymer depends.

While these distinctions seem entirely reasonable, there is a lack of quantitative physical data on which to base them. We thought some comparative study of the two types of systems in common regions *above* T_g could make a useful contribution to understanding the respective mechanisms. So far there has only been one study of conductivity in the *liquid* state of a superionic conducting glass system—the recent work of Kawamura and Shimoji on AgI–Ag_2MoO_4 mixtures.[3] However, the comparison we wish to make is between viscosity and conductance in the two types of system, and no viscosity data are available for the liquid state of AgI–Ag_2MoO_4. Since most of the superionic conducting systems studied to date contain oxyanions and therefore are rather high-melting and also corrosive in the liquid state there has been some reluctance to develop the techniques necessary to measure their liquid-state properties.

The resolution of this problem is found in the all-halide superionic glass systems recently described in papers from this and other laboratories.[4-6] The liquid states of these low melting materials can be studied by conventional molten salt techniques[7] using Pyrex glass capillary cells of high cell constant to measure the (very low) liquid resistivities, and Ubbelohde capillary viscometers to determine the (very low) viscosities.

We have carried out a series of measurements on two compositions in the system AgI–AgCl–CsCl, one of which has a very high ambient temperature conductivity, and also a subambient T_g, −11.5 °C, which is not far above that of T_g in the much studied rubbery polymer electrolyte system $(PPO)_{12}NaCF_3SO_3$[7] ($T_g \simeq$ −40 °C).

The high molecular weight polymer (MW $\simeq 10^6$) is rubbery rather than liquid because of the large molecular weight dependence of the viscosity in polymer electrolytes, and the chain entanglement phenomenon.[8] Since we wish to compare the energetics of viscous flow and electrical migration processes and since the molecular weight dependence of viscosity in pure PPO polymers appears to reside mainly in the preexponent of the appropriate expression for the viscosity,[8] our objectives can be met by investigating solutions in low molecular weight solvents. Thus, to compare with the liquid Ag^+ superionic conductor system, we choose solutions of $NaCF_3SO_3$ in PPO solvents of molecular weights differing by one order of magnitude, viz., 425 and 4000, keeping the monomer/salt ratio (O/Na) constant at 16:1.

Experimental Section

The AgI–AgCl–CsCl melts were prepared by weighing of analytical grade reagents from Merck and Mallinkrodt which were used without further purification. The weighted mixtures were fused and filtered into a 1.5 cm diameter test tube which was just wide enough to accept a standard Pyrex capillary conductivity cell, of cell constant 574.8 (determined with 0.1 *m* KCl). The test tube with contents was mounted in an aluminum block furnace, the temperature of which was controlled to ±0.1 °C by means of a Eurotherm proportional temperature controller. The temperature was uniform to 0.1 °C over the length of the capillary cell. Measurements of the conductance and capacitance were made using an automated Hewlett-Packard Model 4192A admittance bridge, and the dc conductivity was determined from a complex admittance plot. For the same liquid, the kinetic viscosity was determined by using small-sample Ubbelohde viscometers, of viscometer constants 0.014 44 and 0.003 978 cS/s. The viscometer was mounted in a tall aluminum block[9] which guaranteed that the variation of temperature across the capillary section of the viscometer was no more than 0.1 °C. The same

(1) Armand, M. *Solid State Ionics* **1983**, *9*, *10*, 745.
(2) Angell, C. A. *Solid State Ionics* **1983**, *9*, *10*, 3; **1986**, *18*, *19*, 72.
(3) Kawamura, J.; Shimoji, M. *J. Non-Cryst. Solids* **1986**, *79*, 281.
(4) Liu, C.; Sundar, H. G. K.; Angell, C. A. *Mater. Res. Bull.*, **1985**, *20*, 525.
(5) Liu, C.; Sundar, H. G. K.; Angell, C. A. *Solid State Ionics* **1986**, *18*, *19*, 442.
(6) Nishii, J.; Kaite, Y.; Yamagishi, T. *J. Non. Cryst. Solids* **1985**, *74*, 411.
(7) Armand, M. B.; Chabagno, J. M.; Duclot, M. J. *Fast Ion Transport in Solids*; North Holland: Amsterdam, 1979; p 131.
(8) (a) Wang, C. H.; Fytas, G.; Lilge, D.; Dorfmuller, Th. *Macromolecules* **1981**, *14*, 1363. (b) Berry, G. C.; Fox, T. G. *Adv. Polym. Sci.* **1968**, *5*, 261.
(9) (a) Ziegler, D. C. Ph.D. Thesis, Purdue University, 1984. (b) Torell, L. M.; Ziegler, D. C.; Angell, C. A. *J. Chem. Phys.* **1984**, *81*, 5053.

0022-3654/88/2092-2083$01.50/0

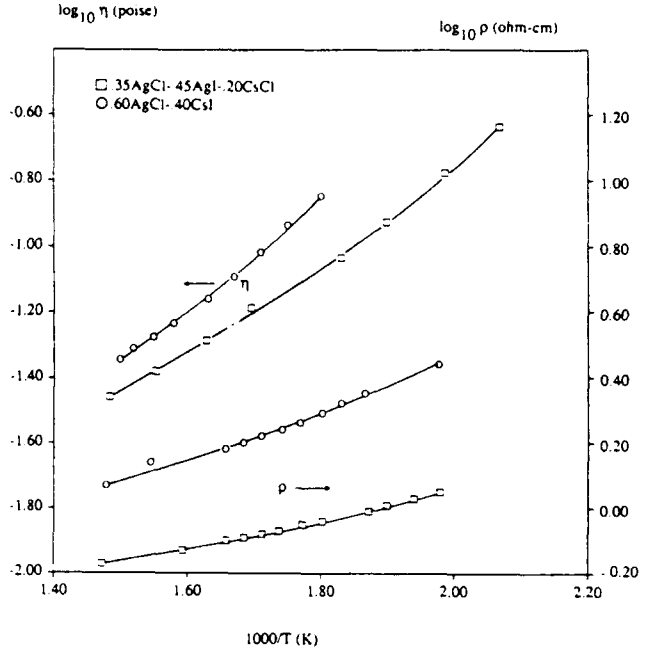

Figure 1. Arrhenius plot of the specific resistivity, ρ, and viscosity, η, for the molten salt mixtures 0.6AgCl·0.4 CsCl, and 0.35AgCl·0.45AgI·0.20CsCl. Note difference in resistivity and viscosity plot slopes.

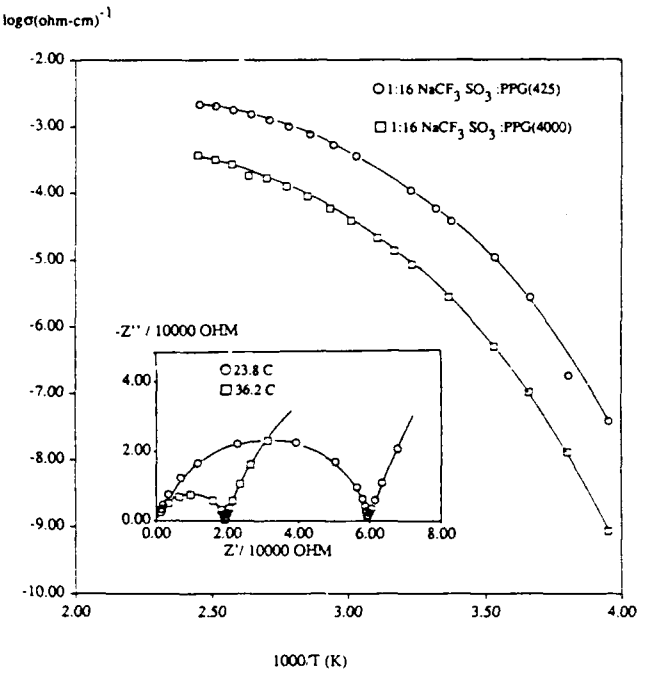

Figure 2. Specific conductivity of sodium triflate solutions O/Na = 16, in PPO solutions with respective molecular weights 425 and 4000. Insert: complex impedance plots of the 1:16 $NaCF_3SO_3$–PPO 4000 sodium triflate solution at two different temperatures showing definition of the dc resistivity.

melt which had been used in the conductivity experiment was then transferred into the viscometer and readings were made at approximately 10 K intervals in the temperature range from 300 °C down to a low limit of ~190 °C determined by the freezing of the supercooled liquid.

The polymer electrolytes were prepared by vacuum drying of pure 425 and 4000 MW polymers obtained from Polyscience Corp. at 65 °C for 5 h and then adding measured amounts of sodium trifilate dissolved in methanol. The methanol was then quantitatively removed by vacuum oven drying at 65 °C. The conductivities of these solutions were much lower than those of the molten salts so a low cell constant all-metal conductivity cell was used. This had the advantage that the low temperature, low conductivity range could be explored and the frequency-dependent characteristics of the bulk electrolyte solutions determined. Measurements were conducted in an automated system using the HP 4192 bridge in the temperature range −20 to +135 °C.

Viscosities of the (higher viscosity) polymer–salt solutions were determined with a digital Brookfield rotating cylinder viscometer. The commerical Brookfield thermo cell containing the sample was controlled to ±0.1 °C by a Eurotherm on/off controller.

Glass transition temperatures were determined by differential scanning calorimetry (Perkin-Elmer DSC-4) at 10 deg/min scans.

Results

Results of the conductivity measurements on the compositions 0.6AgCl·0.4CsCl and 0.35AgCl·0.45AgI·0.20CsCl are displayed as specific resistivities in Figure 1 in the form of an Arrhenius plot. The corresponding viscosity data are included in Figure 1, using a log scale of the same division size, so that the plot slopes are proportional to the respective activation energies. The higher temperature dependence of the viscosity in each case is obvious.

In Figure 2 the conductivity data for the $R = 16$ sodium triflate solutions in 425 and 4000 MW PPO are displayed. The data in this case cover some 5 orders of magnitude in σ. The values plotted are obtained in each case from the complex impedance plots, examples of which are shown as an insert to Figure 2. In Figure 3 the viscosity data determined over a smaller temperature range for the same two solutions are shown. The difference in viscosity between the two solutions is in part due to the molecular weight dependence of the viscosity which is general for polymers and in part to a molecular weight dependence of the glass transition temperature for equal concentration electrolyte solutions which is not found for the pure polymers. The glass transition temperatures were determined by differential calorimetry using a Perkin Elmer DSC-4 instrument and the 10 deg/min scans are shown in the insert to Figure 3.

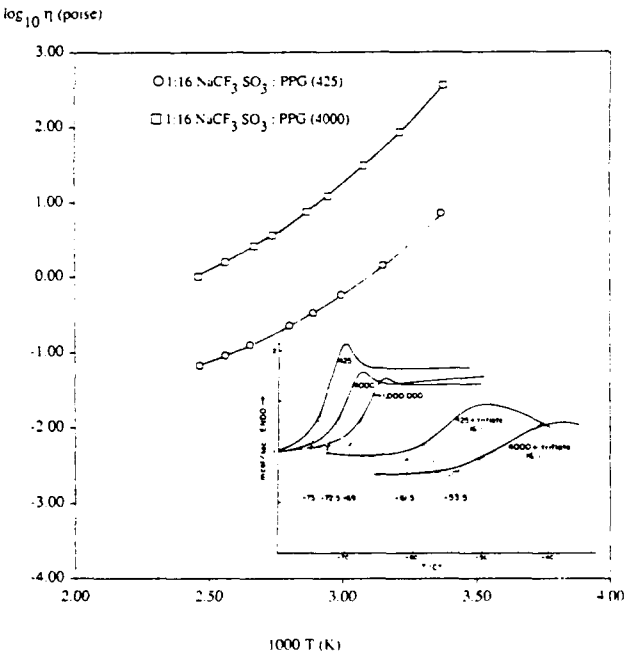

Figure 3. Viscosities of the two sodium triflate solutions of Figure 2 in Arrhenius plot form. Insert: DSC scans through the glass transition region for different molecular weight pure polymers and the two sodium triflate solutions of this study.

Discussion

In recent articles one of us has discussed the phenomenon of fast ion conduction in glasses in terms of the decoupling of electrical modes from viscoelastic modes during cooling from the high-temperature liquid state.[2] In the absence of suitable data on liquid fast ion conductors, these speculations have taken their experimental support from the literature on liquid states of the classic alkali metal oxide glasses.[10] The decoupling is demon-

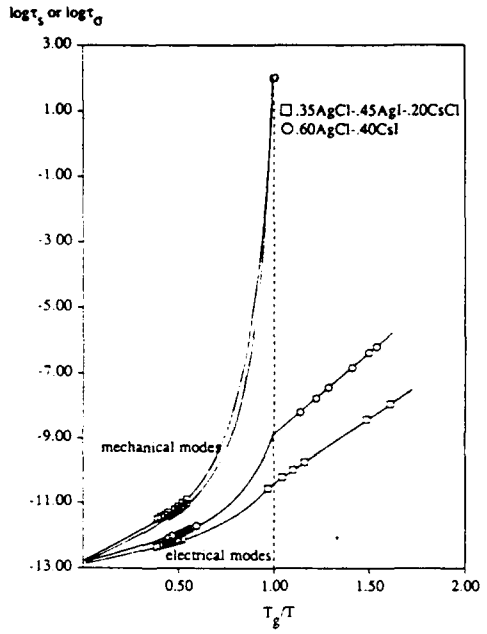

Figure 4. T_g-reduced Arrhenius plot of shear and conductivity relaxation times for the two melts of the study, including conductivity times measured in the glassy state. The T_g values are 261.5 K (□) and 298.5 K (○).

strated by converting the viscosity and conductivity data into appropriate relaxation times for shear and electrical stresses and then comparing the effect of temperature on the system in terms of the relative behavior of these relaxation times. Average relaxation times may be obtained from the viscosity and conductivity data by using Maxwell relations which connect the liquidlike properties shear viscosity η_s and dc resistivity ρ to the solidlike properties shear modulus G_∞ and electrical modulus M_∞. The relations are

$$\tau_s = \eta_s/G_\infty \quad (1)$$

$$\tau_\sigma = \rho e_0/M_\infty \quad (2)$$

where e_0 is the permittivity of free space.

The electrical modulus can be obtained, to good approximation, from the glassy state measurements of Liu et al.[4] on the superionic glass states of the AgI–AgCl–CsCl system. There are, unfortunately, no frequency-dependent viscosity/shear modulus data for this system, but a reasonable value for G_∞ may be taken from the results of a light-scattering study[11] of the glass-forming salt system $2Ca(NO_3)_2{\cdot}3KNO_3$, which has a glass transition temperature 68 °C, not too different from that of the more viscous composition of the present study, 20 °C. (G_∞ usually scales with T_g, so the error involved is probably no greater than 15%.)

The conductivity and shear relaxation times for AgI–AgCl–CsCl melts are compared in Figure 4 where they are combined with conductivity relaxation times in the glassy state obtained from the work of Liu et. al.,[4] and with an approximate shear relaxation time at the glass transition temperature based on the known results for comparable systems.[12] By using a reduced temperature scale based on T_g as scaling parameter, we collapse the viscosity data almost to a single curve while the electrical relaxation data show two distinct plots which reflect the different extents to which the conducting modes in these two compositions become decoupled from the viscoelastic modes during cooling. Most of the decoupling evidently occurs at low thermal excitations approaching T_g where unfortunately measurements were precluded by crystallization. A good idea of the conductivity behavior in this regime may be obtained from the unbroken σ/T plots seen in ref 3. We note that,

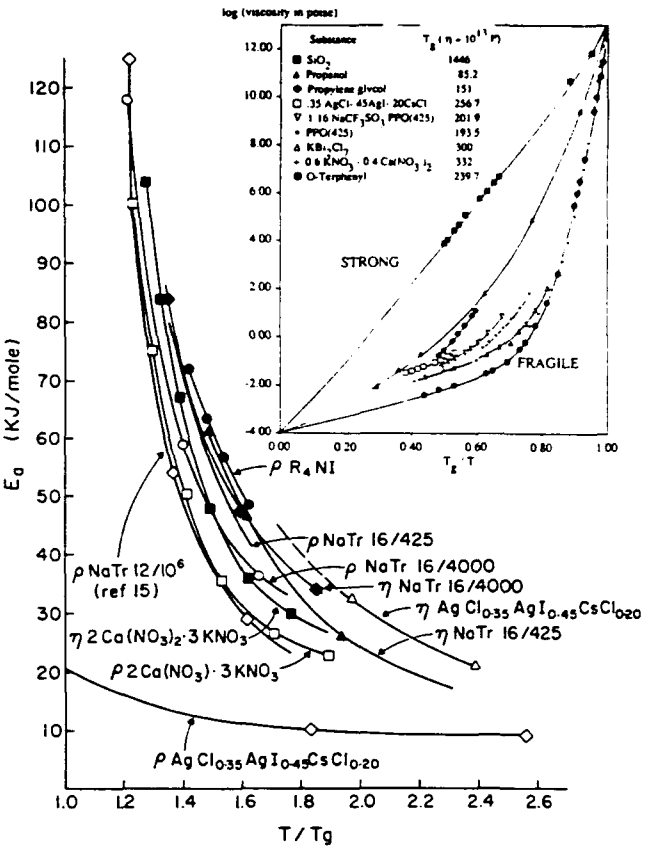

Figure 5. Reduced temperature plot of activation energies for resistivity and viscosity of the polymer solutions of this study (notation: NaTr 16/425 ≡ sodium triflate at concentration O/Na = 16 in PPO of mol wt 425) compared with corresponding plots for the liquid fast ion conducting salt mixture. Figure includes data for a model molten salt system $2Ca(NO_3)_2{\cdot}3KNO_3$ which is a poor conductor in the glassy state (coupled system) and a simple tetrasubstituted ammonium iodide in which both ions are large (coupled system). Note diverging activation energies as T_g is approached in all cases except the conductivity of the fast ion salt melt. Insert: Reduced Arrhenius plot of viscosities of liquids of this study, excluding the PPO 4000 solution, and selected others to indicate their position within the strong-fragile pattern for glass-forming liquids.[21] T_g here is chosen as the temperature of the calorimetric glass transition from 10 deg/min scanning.

in the most favorable case, the conductivity relaxation time decreases by only 2 orders of magnitude between the high-temperature liquid-state regime of the present study and the onset of the glassy state, implying that the decoupling is almost complete. The decoupling can be quantified through the relaxation time ratio τ_s/τ_σ which has been called the "decoupling index" R_τ[2], and in the more conducting solution in the present system reaches 10^{13} at T_g. It is notable that, even in the highly fluid state of this system R_τ explored in our measurements, the conductivity time is still almost an order of magnitude shorter than the shear relaxation time, though extrapolation to $T_g/T = 0$ implies that the preexponent for each process is essentially the same (and corresponds well with quasi-lattice vibration time found for similar systems from far infrared spectroscopic studies).[14]

The fact that the rubbery polymer electrolytes[15] can conduct electricity almost as well as the *liquid* polymer electrolytes of this study (particularly if the comparison is made at equal T/T_g) (see below) might at first suggest that, in polymer electrolytes, the conducting modes are also highly decoupled from the matrix modes as in the glassy FIC case. However, the distinction between the two cases is made obvious if we plot the (temperature-dependent)

(10) Shartsis, L.; Capps, W.; Spinner, S. *J. Am. Ceramic Soc.* **1953**, *36*, 319.
(11) Torell, L. M.; Aronsson, R. *J. Chem. Phys.* **1983**, *78*, 1121.
(12) Moynihan, C. T.; Sasabe, H.; Tucker, J. C. *Molten Salts*; Pensler, Ed.; Electrochemical Society: Pennington, NJ, 1976; p 182.
(13) Torell, L. M.; Angell, C. A. *J. Chem. Phys.*, **1983**, *78*, 937.
(14) Angell, C. A.; Liu, C.; Sundar, H. G. K. *Mater. Sci. Forum* **1985**, *6*, 449.
(15) Armand, M. B.; Chabagne, J. M.; Duclot, M. J. *Fast Ion Transport in Solids*, Vashista, P., Mundy, J. N., Shenoy, G. K. Eds.; Elsevier; Amsterdam, 1979; p 131.

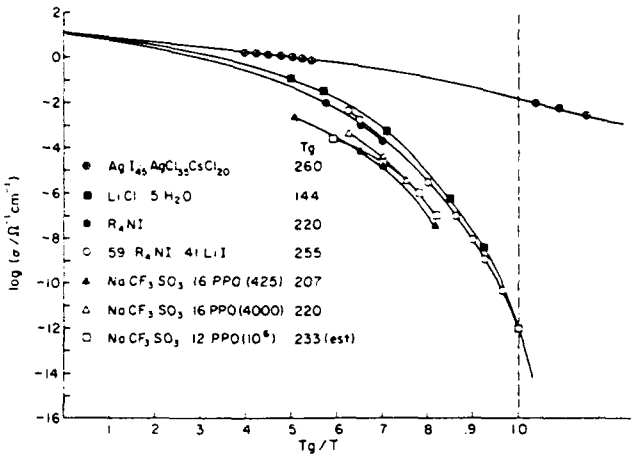

Figure 6. Reduced Arrhenius plot of specific conductivity for the melts and solutions of this study compared with behavior of fully coupled fully dissociated $LiCl \cdot 5H_2O$ system and large ion molten salt (R_4NI). Data from rubbery polymer PPO (106) (ref 15) are included for comparison.

activation energies for both conductivity and viscosity on the same diagram. This is done for both molten salt and polymer systems in Figure 5, using a reduced temperature scale to remove those differences at given temperatures which are due only to the different temperature intervals above T_g. Included in the figure are (i) data for another molten salt system in which there are no "fast" ions, viz., the tetra-substituted ammonium iodide (methoxyethyltrimethylammonium iodide) prepared by Cooper as a glass-forming solvent for LiI,[16] and (ii) data for the much studied model molten salt system $2Ca(NO_3)_2 \cdot 3KNO_3$.[17-19]

The important point of Figure 5 is the manner in which both viscosity and conductivity activity energies increase rapidly to very large values as T_g is approached in all cases except the ("decoupled") conductivity of the superionic glass-former. The spread of curves is of secondary importance and reflects differences in "fragility" amongst the different systems.[21]

Figure 5 suggests that, when the *energetics* of transport processes are compared at equal T_g, polymer electrolytes and ordinary molten salts have much in common. The activation energies of both the conductance process and viscous flow process are in each case comparable. Thus, with respect to the fundamental mass transporting energy fluctuation, the polymer–salt conductivity is *not* decoupled from the matrix motions.

Recalling that the resistivity activation energy data for sodium triflate O/Na = 12 in high molecular weight (10^6) PPO (designated ρ NaTr12/10^6 in Figure 5) are for a *rubbery solid* material, we conclude that both high molecular weight polymer electrolytes and superionic glasses are very distinct from ordinary salts and solutions, but that the origins of their distinction are quite different. In superionic glasses the distinction arises because the basic energetics of transport are very different; the energy required for a fast-ion diffusive step to occur is small at all temperatures due to energy decoupling from structural and viscous modes as $T \rightarrow T_g$. In rubbery "solid" polymers on the other hand, it is because the *nonenergetic* component of the viscosity, viz., the preexponential factor, is so large that quite moderate decreases in temperature are sufficient to cause the macroscopic fluidity to vanish, i.e., to impose a finite shear modulus on the system at ambient temperature. This occurs while the *energetic* events which control local rearrangements of chain segments, hence ion transporting motions, remain quite probable, indeed just as probable as in a molten salt of comparable T_g (according to Figure 5).

With the energetics of conductivity in polymer electrolytes thereby established as unexceptional in character, it remains to discuss the origin of their relatively poor performance as electrolytes compared with aqueous solutions.

One factor which must be of major importance is the difference in the temperature at which the probability of a local ion-transporting rearrangement becomes vanishingly small, which we can associate with the glass transition, T_g. T_g is considerably higher for polymer solutions than for all but the most concentrated aqueous solutions. We may scale out the effect of the effect of the T_g factor on electrolyte performance by plotting data using a T_g-reduced temperature scale, and thereby reveal other factors which affect the relative performance. Thus we compare, in Figure 6, the conductivity performance for the polymer electrolyte solutions of this study, and of Armand's rubbery polymer electrolyte, with that of an aqueous solution, $LiCl \cdot 5H_2O$, for which data over an exceptionally wide range of temperature and conductivity exist.[22-24]

We include, in Figure 6, data for the tetra-substituted ammonium iodide (seen in Figure 5) and its glass-forming mixture with LiI, to show the broad view similarity of the aqueous solution and the anhydrous molten ammonium salt. These are two systems which we believe approach the condition described by the term "completely dissociated". Ionic dissociation, which is a well-defined concept for dilute solutions, requires an operational definition for systems as highly concentrated in ions as those under consideration in this paper. Noting that the relaxation times for shear and electrical stresses are essentially the same in the $LiCl \cdot 5H_2O$ system,[21] we assume that the behavior of the concentrated LiCl + H_2O solution seen in Figure 6 is that of a "fully dissociated system". The order of magnitude lower conductivity of the polymer triflate solutions is therefore to be attributed to some form of "ion association". We take this to mean that, relative to the aqueous solution, ions in the polymer solutions spend as much as 90% of their time in sufficiently intimate association with ions of the opposite charge that, when an energy fluctuation sufficient for local structure rearrangement occurs, the oppositely charged ions move in unison, i.e., no net current flows.

The spectroscopic signatures, though not the lifetimes, of contact and solvent-separated ion pairs and clusters in the present solutions have recently been reported by Torell and co-workers,[25] and lend semiquantitative support to the latter conclusion. In particular, the increasing separation of aqueous and polymer curves at high T accords with the spectroscopic evidence for increasing association at the higher temperatures.[25] A study in which systematic variations in composition to fill the gap between aqueous and polymer solvent environments are made is evidently needed to clarify this phenomenology.

Acknowledgment. We are indebted to the National Science Foundation, Solid State Chemistry Grant, for support of the molten salt component of this work and to the Office of Naval Research for support of the polymer electrolyte solutions under Agreement No. N00014-84K0289. We acknowledge helpful discussions of this general problem area with Dr. L. M. Torell of Chalmers University of Technology, Goteborg, Sweden, under the auspices of NSF Grant No. INT 8619785.

(16) Cooper, E. I. *Solid State Ionics* **1983**, *9*, *10*, 617.
(17) Tweer, H.; Laberge, N.; Macedo, P. B. *J. Am. Ceram. Soc.* **1971**, *54*, 121.
(18) Weiler, R.; Blaser, S.; Macedo, P. B. *J. Phys. Chem.* **1969**, *73*, 4147.
(19) Rhodes, E.; Smith, W. E.; Ubbelohde, A. R. *Proc. R. Soc. A2* **1965**, *85*, 263.
(20) Angell, C. A. *J. Phys. Chem.* **1964**, *68*, 218.
(21) Angell, C. A. In *Relaxation in Complex Systems*"; Ngai, K., Wright, G. B., National Technical Information Service, U.S. Department of Commerce: Springfield, VA, 1985, p 1; *J. Non-Cryst. Solids, Kreidl Symp.* **1985**, *73*, 1. (The "fragility" of a glass-forming liquid is a description of the departure from the Arrhenius behavior as the liquid viscosity changes from a defined value at T_g (10^{13} P by classical definition or $\sim 10^{11}$ P at the calorimetric T_g) to a high-temperature limit of $\sim 10^{-3}$–10^{-4} P.)
(22) Moynihan, C. T.; Balitatac, N.; Boone, L.; Litovitz, T. A. *J. Chem. Phys.* **1971**, *55*, 3013.
(23) Angell, C. A.; Bressel R. D.; Gammel, P. M. *J. Non-Crystalline Solids* **1972**, *7*, 295.
(24) Bressel, R. D. Ph.D. Thesis, Purdue University, 1971.
(25) Schantz, S.; Sandahl, J.; Borjesson, L.; Torell, L. M.; Stevens, J. R. *Solid State Ionics*, in press.

Reprinted from The Journal of Physical Chemistry, 1991, 95.

Ion-Pairing Effects on Viscosity/Conductance Relations in Raman-Characterized Polymer Electrolytes: $LiClO_4$ and $NaCF_3SO_3$ in PPG(4000)

M. G. McLin† and C. A. Angell*

Department of Chemistry, Arizona State University, Tempe, Arizona 85287-1604, and Department of Chemistry, Purdue University, West Lafayette, Indiana 47907 *(Received: February 19, 1991)*

Precise measurements of viscosity and conductivity have been made of the solutions of sodium triflate and lithium perchlorate in poly(propylene oxide) of MW 4000 (PPG(4000)) studied spectroscopically by Torell and co-workers for the extent of ion association. Viscosity, but not conductivity, data conform very well to the VTF equation and yield ideal glass transition temperatures that track the measured glass transition temperatures as closely as in the case of glass-forming aqueous solutions. The differences in temperature dependences of the two processes are demonstrated by using Walden rule plots. Using the data of Torell et al. at ambient temperature as a calibration point, we show that the deviations of conductivity from viscosity-dictated behavior predict almost quantitatively the strong temperature dependence of the free ion concentration found by Torell et al. up to the high temperature limit of their measurements.

Introduction

Interest in polymer electrolytes is primarily due to their potential application as electrolytes for secondary batteries. These have now been under intensive study since the pioneering work of Wright[1] and Armand.[2] However, although much progress has been made in improving electrolyte performance, a detailed microscopic mechanism for ionic conduction in these materials remains elusive. The recognition that ionic conduction occurs in the amorphous phase of PEO electrolytes and that mobility was controlled primarily by the temperature interval above the glass transition temperature, T_g, by Armand[2,3] marked significant progress toward this goal. Armand showed that the conductivity could be well accounted for by a modification of the Arrhenius equation generally known as the VTF equation which is applicable to all transport processes, y (e.g., viscosity, diffusion, conductivity)

$$y = A_y T^{-1/2} e^{-D_y T_0/(T-T_0)} \quad (1)$$

where A_y and D_y are constants specific to the process and T_0 is a constant characteristic of the liquid and common to all processes. The parameter T_0 is dominant and, as the present work will confirm, is closely related to the experimental glass transition temperature, T_g, as in the case of glass-forming nonpolymeric electrolyte solutions.[4-6] This fact alone establishes that the conduction mechanism is basically a liquidlike mechanism, as indeed is now generally agreed. The basic difference between polymer and nonpolymer electrolytes, as many workers have pointed out, is that the friction on the ion motion is determined by the microscopic rather than the macroscopic viscosity.[3,7-9]

While the microscopic friction, which is involved in the glass transition, is the dominant control on this conductivity, it is recognized that the conductivity is also strongly dependent on the proportion of the ions that are not bound up as ion pairs. Ion pairing, which is a minor effect in solutions of alkali-metal salts in water, is expected to be much more important in polymer solutions because of the low solvent dielectric constant, $\epsilon_0 \approx 5$. With such a value of ϵ_0 the electrical work of separating a pair of ions initially at contact to an infinite distance is a factor of $\sim 80/5$ greater than in aqueous solutions. Hence, in molecular solutions of $\epsilon_0 = 5$ it would be expected that dissociation comparable to that found in aqueous solutions would only be obtained at much higher thermal energies. However, in polymer solutions a further factor associated with the peculiarities of macromolecular solution thermodynamics[10,11] enters into consideration, and instead of increases in temperature causing the expected increases in dissociation, the reverse is observed.

The ion-pairing phenomenology can be studied quantitatively by spectroscopic methods that can distinguish between free anions and anions distorted by interactions with near-neighbor cations. Torell and co-workers,[12] using Raman spectral analysis, find the percentage of free ions in $NaCF_3SO_3$ solutions in PPG(4000), at a concentration of 30 ether oxygens (–O–) per cation (designated hereafter 1:30) to decrease from 85% at 186 K to 39% at the highest temperature of their study, 360 K. In the case of the stronger electrolyte $LiClO_4$ the corresponding values are reported as 96% at 200 K and 78% at 340 K. In both cases the free and

† Research contained in this paper was performed in partial fulfillment of the Ph.D. requirements in Physical Chemistry at Purdue University.

* To whom correspondence should be addressed at Arizona State University.

(1) Wright, P. V. *Br. Polym. J.* **1976**, *7*, 319.
(2) Armand, M. B.; Chabagno, J. M.; Duclot, M. J. In *Fast-Ion Transport in Solids*; Vashishta, P., Mundy, J. N., Shenoy, G., Eds.; North-Holland: Amsterdam, 1979; p 131.
(3) Berthier, C.; Gorecki, W.; Minier, M.; Armand, M. B.; Chabagno, J. M.; Riguad, P. *Solid State Ionics* **1983**, *11*, 19.
(4) Angell, C. A. *J. Phys. Chem.* **1966**, *70*, 3988.
(5) (a) Angell, C. A.; Bressel, R. D. *J. Phys. Chem.* **1972**, *76*, 3244. (b) Angell, C. A.; Pollard, L. J.; Strauss, W. *J. Solution Chem.* **1972**, *1*, 516.
(6) Papke, B. L.; Ratner, M. A.; Shriver, D. F. *J. Phys. Chem. Solids* **1981**, *42*, 493.
(7) Ratner, M. A. In *Polymer Electrolyte Reviews 1*; MacCallum, J. R., Vincent, C. A., Eds.; Elsevier: New York, 1988; Chapter 7.
(8) Cameron, G. G.; Ingram, M. D.; Sorrie, G. A. *J. Chem. Soc., Faraday Trans. 1* **1987**, *83*, 3345.
(9) Torell, L. M.; Angell, C. A. *Br. Polym. J.* **1988**, *20*, 173.
(10) Patterson, D. *Macromolecules* **1969**, *2*, 672.
(11) Nitzan, A.; Ratner, M. A. *Symp. Mater. Res. Soc.* **1991**, *210*, 203.
(12) (a) Kakihana, M.; Schantz, S.; Torell, L. M. *J. Chem. Phys.* **1990**, *92*, 6271. (b) Kakihana, M.; Schantz, S.; Mellander, B.-E.; Torell, L. M. In *Proceedings of the 2nd International Symposium on Polymer Electrolytes*; p 23.

0022-3654/91/2095-9464$02.50/0

ion-paired ion populations obey a van't Hoff equation with respect to temperature.[13]

It is of interest to see the extent to which these spectroscopic results are consistent with the results of more conventional electrochemical measurements such as the combination of solution conductivity and viscosity behavior embodied in the Walden rule[14]

$$\Lambda\eta = \text{const} \qquad (2)$$

where Λ is the equivalent conductivity and η is the shear viscosity. This rule should hold true for a given solution studied at different temperatures so long as the number of current carriers is constant and the frictional force impeding their motion is correctly represented by the macroscopic viscosity. While it is known that the macroscopic viscosity is not a relevant quantity for ion conductivity in high molecular weight polymer solutions (because the ions "see" a more local or microscopi viscosity[3,7-9]), this is not the case for unentangled polymers. For the molecular weights of 4000 and less discussed in the analysis of Torell and Angell,[9] the microviscosity seen by the ions, and the viscosity measured in a conventional viscometer, are related by a simple numerical constant proportional to the polymer molecular weight. Therefore, the conventional viscosity and in particular its temperature dependence can be expected to serve as a useful guide to the forces impeding the motion of ions present in the solutions, and differences in the temperature dependence of conductivity and viscosity should be interpretable in terms of changing free ion populations and hence be validly comparable to the results of the spectroscopic studies. On the basis of the above considerations, we have carried out a detailed study of conductivity and viscosity of various alkali-metal salts in PPO(4000), and in this first report we present results for the two solutions studied in detail by Torell and co-workers,[12-16] viz., $NaCF_3SO_3$ and $LiClO_4$ in PPO(4000). In subsequent papers we will compare cation and anion effects on the viscosity–conductance relations and will also examine the individual ion diffusion coefficients using chronoamperometric methods.

Experimental Section

The salts used in this work were $LiClO_4$ (Aldrich reagent grade) and $NaCF_3SO_3$ (Alfa reagent grade). Both were used without further purification. The polymer electrolyte solutions were prepared by vacuum drying of pure PPG(4000) obtained from the Polyscience Corp. at 65 °C for 5 h and then adding measured amounts of dried salts dissolved in acetonitrile. The acetonitrile was then quantitatively removed by vacuum oven drying until constant mass was achieved. The final weights of the solutions were generally within 1 wt % of the values calculated for complete removal of the acetonitrile. All samples had final masses that were slightly less than the calculated values due to a small but expected loss of the polymer itself by vaporization during the vacuum drying procedure.

Conductivities were measured in an all-metal conductivity cell with a low cell constant ($\sim$0.02 cm^{-1}). Measurements were made using an interfaced HP4192A impedance analyzer with automated Eurotherm temperature controller. Dc conductivities were determined from complex impedance plots, of which an example is shown in the Figure 6 inset. The precision is 2%.

Viscosities were determined with a digital Brookfield spindle viscometer with a precision of 0.2% of full scale and accuracy of 1% of full scale. The sample was contained in a Brookfield Thermosel accessory controlled to 0.1 °C by a Eurotherm temperature controller. The apparatus was enclosed in glovebag through which dry nitrogen flowed to protect the solutions from ambient moisture. Subambient temperatures to $\sim$−20 °C were achieved by enclosing the Thermosel attachment is an in-house-made polystyrene cooler in which dry ice was placed.

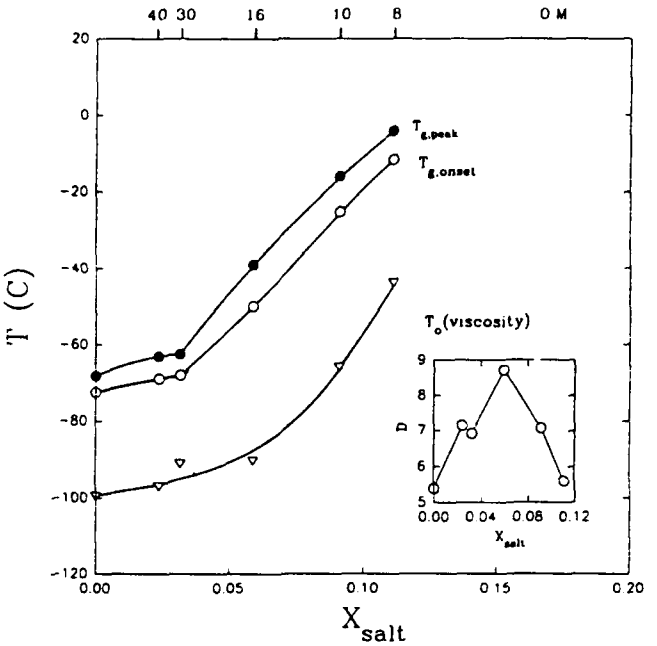

Figure 1. Onset and peak glass transition temperature, T_g, and ideal glass transition temperature, T_0 (from VTF fits of viscosity data), versus mole fraction salt for $LiClO_4$ PPG(4000) solutions. Inset: best-fit D parameter of the VTF equation for viscosity versus mole fraction salt for $LiClO_4$ PPG(4000) solutions.

Glass transition temperatures were determined by differential scanning calorimetry (Perkin-Elmer DSC-4) using 10 deg/min scans. Although we will discuss some of our conductivity results in terms of equivalent conductivities, we deemed it unnecessary to carry out the simple but time-consuming density measurements which in principle are needed for the conversion. This is because previous work[17] has shown that to within error limits of 3% (less than are detectable on the plots as we will present here) the molar volumes of salt and polymer are additive. Likewise, in consideration of the equivalent conductance at different temperatures, the differences in temperature dependence of specific and equivalent conductivities due to the temperature dependence of molar volume are negligible in comparison with the order of magnitude changes in conductivity we are dealing with in this work.

Results

Glass transition temperatures and their dependence on salt content for the $LiClO_4$–PPG(4000) and $NaCF_3SO_3$–PPG(4000) systems are shown in Figures 1 and 2. For these two systems, T_g appears to only depend on salt concentration in the 1:40–1:8 (M:O) regime. Both systems show pronounced variations, which are qualitatively similar for both salts (see Figure 3), in the temperature range over which the glass transition occurs. The range is reasonably narrow for the pure polymer and salt solutions up to concentrations of 1:30, but then the range becomes very broad at the 1:16 compositions. Both systems exhibit a gradual narrowing of the range as salt content increases for more concentrated solutions.

Glass transition temperatures reported in Figures 1 and 2 are somewhat lower (5–6 K) at 1:10 and 1:8 compositions than those previously reported by Stevens and Schantz[18] for the same compositions. It is unclear from their description if T_g was defined as in our figures or in some other way. Samples of 1:30 and 1:8 $NaCF_3SO_3$ PPG(4000) obtained from Schantz and measured by us gave results in excellent agreement (to 0.5 °C) with those of our own samples. Thus, differences in our sample preparation techniques evidently are not important with respect to transport properties.

(13) Schantz, S. *J. Chem. Phys.* **1991**, *94*, 6296.
(14) O'M. Bockris, J.; Reddy, A. K. N. In *Modern Electrochemistry*; Plenum Press: New York, 1970; Vol. 1, Chapter 4.
(15) (a) Schantz, S.; Sandahl, J.; Borjesson, L.; Torell, L. M.; Stevens, J. R. *Solid State Ionics* **1988**, *28/30*, 1047. (b) Schantz, S.; Torell, L. M.; Stevens, J. R. *J. Appl. Phys.* **1988**, *64*, 2038. (c) Sandahl, J.; Schantz, S.; Borjesson, L.; Torell, L. M.; Stevens, J. R. *J. Chem. Phys.* **1989**, *91*, 655.
(16) Torell, L. M.; Schantz, S. In *Polymer Electrolyte Reviews 2*; MacCallum, J. R., Vincent, C. A., Eds.; Elsevier: New York, 1989; Chapter 1.
(17) Moacanin, J.; Cuddihy, E. F. *J. Polym. Sci.* **1966**, *C14*, 313.
(18) Stevens, J. R.; Schantz, S. *Polym. Commun.* **1988**, *29*, 330.

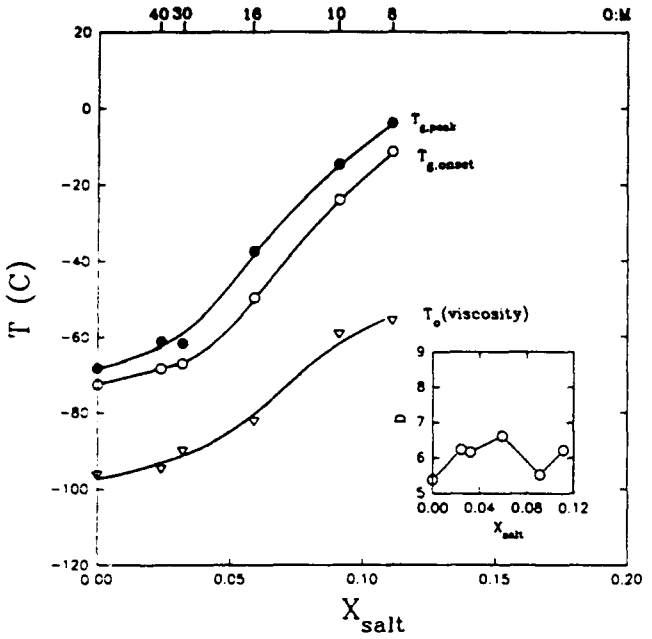

Figure 2. Onset and peak glass transition temperature, T_g, and ideal glass transition temperature, T_0 (from VTF fits of viscosity data), versus mole fraction salt for $NaCF_3SO_3$ PPG(4000) solutions. Inset: best-fit D parameter of the VTF equation for viscosity versus mole fraction salt for $NaCF_3SO_3$ solutions.

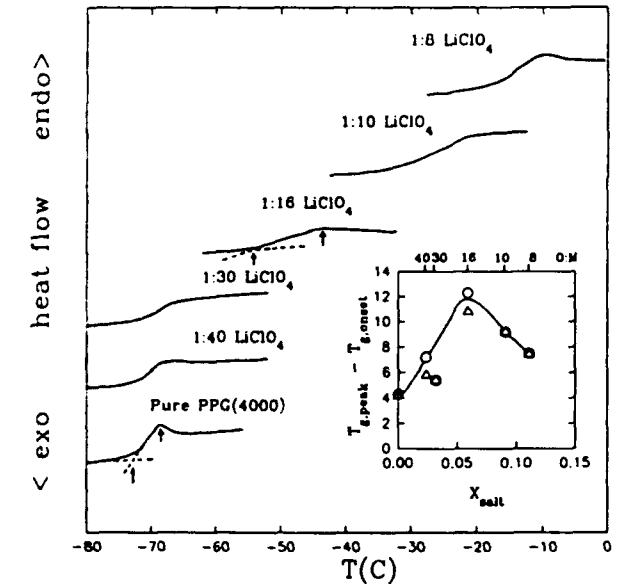

Figure 3. DSC traces for pure PPG(4000) and various compositions of $LiClO_4$ PPG(4000). Inset: difference between peak and onset glass transition temperatures versus mole fraction salt for $NaCF_3SO_3$ PPG(4000) (○) and $LiClO_4$ PPG(4000) (△).

As seen in previous studies of liquid PPO solutions,[19] the viscosities of both systems rise dramatically as salt concentration increases. At temperatures well above T_g, the viscosity of a $NaCF_3SO_3$ solution, at a given composition, is less than that of the corresponding $LiClO_4$ solution (see Figure 4). The difference is largest at subambient temperatures and gradually diminishes as temperature increases. In addition, the difference in viscosity between the systems at a given temperature increases as salt content increases.

The variation in specific conductivity with temperature and salt concentration is shown in Figure 5. At low temperatures the most dilute solutions are the best conductors, with the conductivity decreasing with salt concentration. At high temperatures, the

(19) (a) Watanabe, M.; Ikeda, J.; Shinohara, I. *Polym. J.* **1983**, *15*, 177. (b) Watanabe, M.; Ogata, N. *Br. Polym. J.* **1988**, *20*, 181.

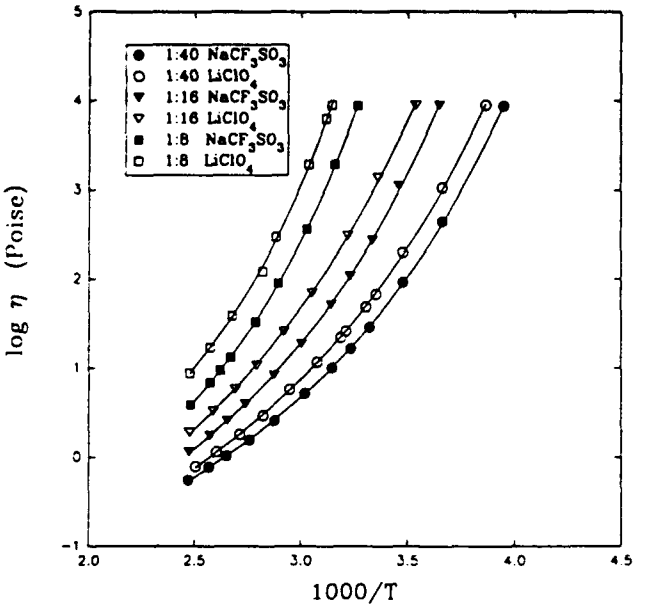

Figure 4. Arrhenius representation of viscosity data for 1:40, 1:16, and 1:8 (M:O) solutions of $LiClO_4$ PPG(4000) and $NaCF_3SO_3$ PPG(4000).

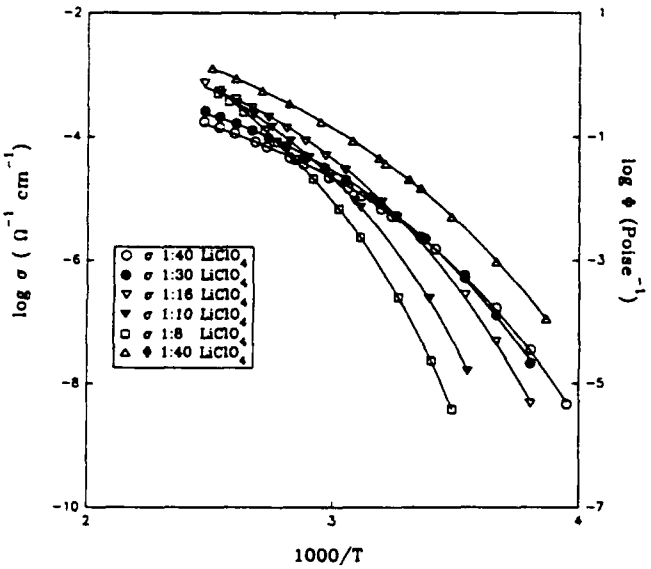

Figure 5. Arrhenius representation of specific conductivity, σ (Ω^{-1} cm^{-1}), for 1:40–1:8 (M:O) $LiClO_4$ PPG(4000). Also, included for comparison is an Arrhenius plot of fluidity, ϕ, data for 1:40 $LiClO_4$ PPG(4000) (△).

concentrated solutions are the better conductors. These conductivity crossovers indicate that a maximum exists in the variation of conductivity with salt content and that the maximum shifts to higher concentrations as temperature increases, see below, as in aqueous systems.[5]

The $NaCF_3SO_3$ solutions at a given concentration have conductivities that are greater than those for $LiClO_4$ solutions up to temperatures well above ambient (see Figure 6). At higher temperatures a crossover occurs, and the $LiClO_4$ solutions become the better conductors.

The dependence of viscosity and conductivity on mole fraction salt is shown in Figures 7 and 8. The aforementioned shifts in conductivity maxima with temperature are evident with the $NaCF_3SO_3$ system having the largest shifts. The salt content dependence of the viscosity is significantly larger for the $LiClO_4$ system than for the triflate system with the difference decreasing with temperature.

Discussion

In this section we will discuss, in three stages, the role played by the ions and the ion-pairing phenomenon in polymer solution

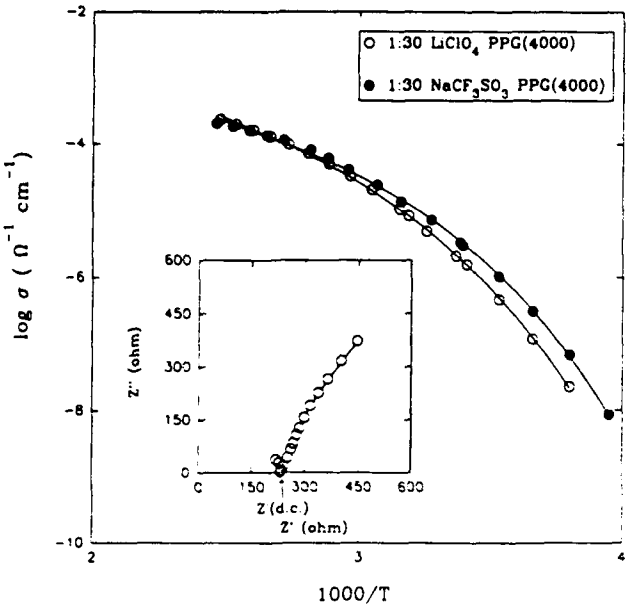

Figure 6. Arrhenius representation of conductivity data for 1:30 $LiClO_4$ PPG(4000) (○) and 1:30 $NaCF_3SO_3$ PPG(4000) (●). Inset: complex impedance plot for 1:30 $LiClO_4$ PPG(4000) at 80.2 °C, showing the definition of Z' (dc) used to calculate the dc conductivities plotted in Figures 5 and 6.

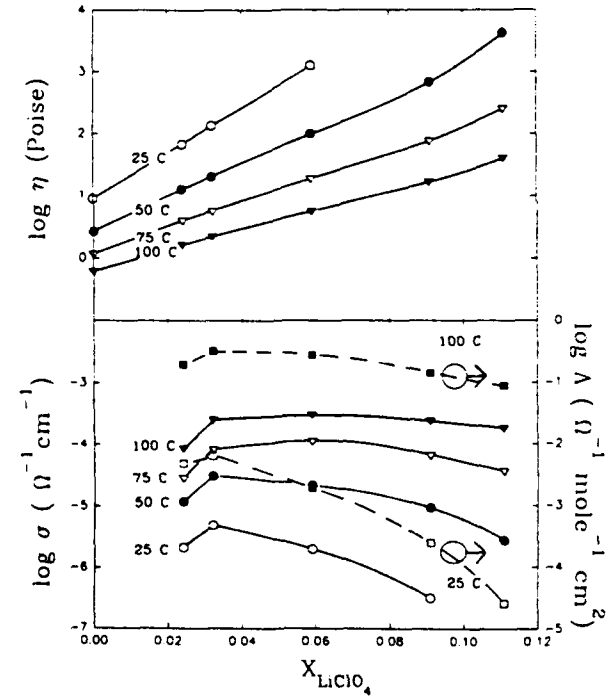

Figure 7. (top) log viscosity versus mole fraction salt for $LiClO_4$ PPG(4000) solutions at 25 (○), 50 (●), 75 (▽), and 100 °C (▼). (bottom) log σ versus mole fraction salt for $LiClO_4$ PPG(4000) solutions at 25 (○), 50 (●), 75 (▽), and 100 °C (▼). Also, included to show the effect of concentration changes is the equivalent conductivity, log Λ versus mole fraction salt for $LiClO_4$ PPG(4000) solutions at 25 (□) and 100 °C (■).

dynamics. We examine first the composition effects on viscosity alone, then consider the differences in viscosity and conductance behavior with changing composition and temperature, and finally examine the ion-pairing problem in what seems to be the most direct manner, through Walden plots. The latter analysis permits a direct comparison with the spectroscopic findings of Torell and co-workers.[12,13,15,16]

The dominance of ion mobility over charge carrier effects in polymer solution conductance is immediately conveyed by the large and comparable variations of conductivity and viscosity with temperature seen in Figures 4 and 5. This is seen most clearly

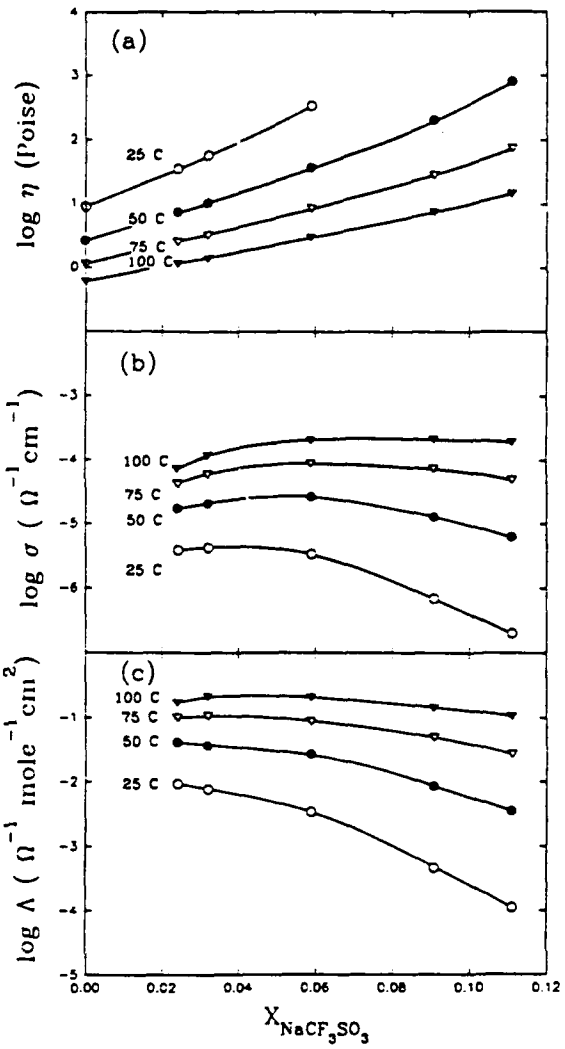

Figure 8. (a) log viscosity versus mole fraction salt for $NaCF_3SO_3$ PPG(4000) solutions at 25 (○), 50 (●), 75 (▽), and 100 °C (▼). (b) log σ versus mole fraction salt for $NaCF_3SO_3$ PPG(4000) solutions at 25 (○), 50 (●), 75 (▽), and 100 °C (▼). (c) log Λ versus mole fraction salt for $NaCF_3SO_3$ PPG(4000) solutions at 25 (○), 50 (●), 75 (▽), and 100 °C (▼).

by comparison of conductivity Arrhenius plot with the fluidity, ϕ ($\phi = 1/\eta$), plot included in Figure 5 for the composition 1:40 $LiClO_4$. The fluidity data are very well described by the VTF equation, eq 1, and the best-fit T_0 values closely parallel the measured T_g values, particularly for the $LiClO_4$ solutions, as seen in Figures 1 and 2. The corresponding values of the "strength" parameter,[20] D, are displayed in the insets. The parameter D determines the departure from Arrhenius behavior exhibited by the liquid or solution,[21] and so its composition dependence, and in particular the differences in its composition dependence for different solutions, is of interest. According to the insets of Figures 1 and 2, the $LiClO_4$ solutions show a return toward Arrhenius behavior as the salt content builds up whereas this is not seen in the more heavily ion-paired $NaCF_3SO_3$ case. This behavior is consistent with current ideas on non-Arrhenius behavior in liquids[20,22-24] and the suggestions of many authors that dissolved

(20) (a) Angell, C. A. In *Relaxations in Complex Systems*; Ngai, K., Wright, G. B., Eds.; National Technical Information Service, US Department of Commerce: Springfield, VA, 1985; p 3. (b) Angell, C. A. *J. Non-Cryst. Solids* **1991**, *131-133*, 13.

(21) At first sight it might seem that the reason for departure from Arrhenius behavior would lie in $T_0 \neq 0$ K. But the departure is conditioned very strongly by the B parameter of the unmodified VTF equation ($B = DT_0$), so that if B is large for a given T_0 the departure from Arrhenius behavior is small. In the modified form given in eq 1 all deviation from Arrhenius behavior is contained in the D parameter. The smaller D, the larger the departure and the closer T_g lies to T_0. At the limit of small D, $T_g/T_0 \rightarrow 1$; see ref 20.

cations act as transient cross-links in the polymer chain matrix,[3,6-9,25] since it is known that the closer to 3-D network conformation a liquid becomes the more nearly Arrhenius is its viscosity temperature dependence.[24] Thus, the Li^+ cations in $LiClO_4$, which are mostly free, can at least transiently cross-link the chains by including ether oxygens of adjacent chains in their first coordination shell to provide a network structure. The network would be less developed in the $NaCF_3SO_3$ case because more of the potential cross-links are tied up instead as ion pairs. This would also explain the greater viscosity of the perchlorate over triflate solutions despite their essentially identical glass transition temperatures. Unfortunately, this attractive interpretation may not hold up when other systems are examined in detail since conflicting variations of D are found in the cases of $NaClO_4$ and $NaCF_3SO_3$.[26] Furthermore, the A parameters of eq 1, which range from $\sim(1-3) \times 10^{-4}$ P, exhibit variations complementary to the D parameters. This aspect should be clarified by extended range viscosity measurements (up to 10^{12} P) to be reported.

To understand the return to "fragile" behavior[20] at high salt content, we must suppose that as the salt concentration reaches values where the majority of cations have other cations as their second nearest neighbors, the Coulomb forces become dominant and the fragile behavior typical of molten salts[22] and hydrate melts[23] is reestablished. Again, this would not be expected in the presence of extensive ion pairing or aggregation.

Turning now to the conductivity data, we find immediately the reason that, at a given stoichiometry, the triflate solution conductivity is higher at the lower temperatures. According to eq 1, for equal T_0 values, the ion mobility will be greater at a given T if D is smaller (as for the triflate). On the other hand, at high temperatures the exponential term in eq 1 is less important and the free ion concentration will be dominant. Hence, we can understand that at high temperatures the triflates are poorer conductors despite their lower viscosities.

To be more quantitative, we consider the solution of concentration 1:30 in which the conductivities are the same at 105 °C (see crossover in Figure 6). The viscosity of the triflate solution is lower by 52% at this temperature; so if the mobility of the ions scales with the viscosity, the number of free ions in the perchlorate would have to be greater by 52%. At this temperature we find by a short extrapolation of the data of Torell et al.[12] that the percentage of free ions is 62% in the perchlorate case and only 40% in the triflate case; i.e., the percentage of free ions in the perchlorate solution is greater by 55%.

Finally, we examine the temperature dependence of ion pairing in these solutions using the Walden rule approach.[19] For the ideal case in which the ionic concentrations are temperature invariant and the only temperature influence on the ion conductivity is through the viscosity to which the ionic motion is fully coupled, then the plot of log σ vs log $1/\eta$ should be a straight line of unit slope. If solutions of different concentration are to be compared, then it is appropriate to plot equivalent conductivity against the fluidity. Then, except for ionic interference (cation–anion friction) effects, all compositions should fall on the same line. On the other hand, if ion populations change with temperature or some decoupling of conductivity from viscosity occurs, then plots of different slope and position will be encountered.

To test the behavior of the present solutions, we plot the log equivalent conductivities obtained from measured σ using an additive molar volume assumption (see Experimental Section for justification) vs log $1/\eta$ for $LiClO_4$ solutions at different temperatures in Figure 9 and for $NaCF_3SO_3$ solutions at different

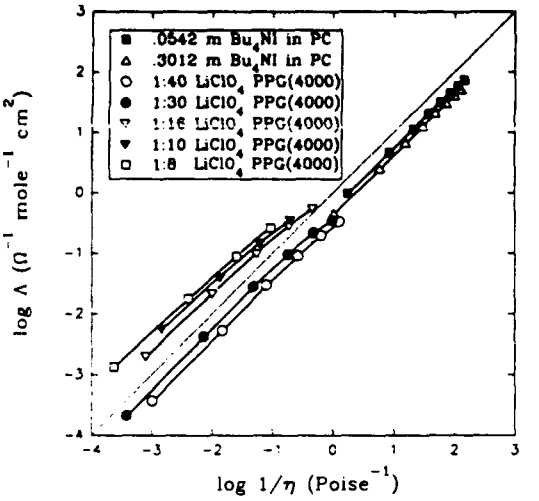

Figure 9. Walden plots of equivalent conductivity and viscosity for $LiClO_4$ solutions in the range 1:40–1:8 (M:O) in PPG(4000). Included in diagram are literature data on nonaqueous solutions (ref 25) which behave almost ideally. Dashed line has a slope of unity.

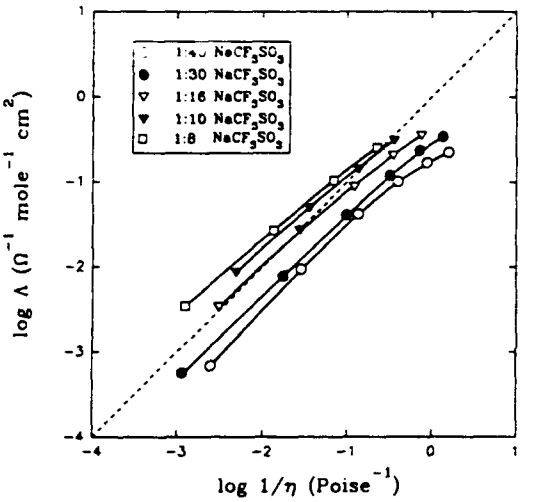

Figure 10. Walden plots for sodium triflate solutions in the range 1:40–1:8 (M:O) in PPG(4000). Dashed line has a slope of unity.

temperatures in Figure 10. We include in Figure 9 some very precise data[27] for a case in which conformity to the Walden rule would be expected (large ions, *tert*-butylammonium iodide, in low concentrations in an aprotic solvent, propylene carbonate), and these data are seen to form a natural extension to lower viscosities of the data for dilute $LiClO_4$ in PPO. The least-squares slopes for the two concentrations plotted, 0.0542 and 0.3012 m, are 1.018 and 0.983, respectively.

For the dilute perchlorate solutions in PPO the slope is also unity within experimental error, but for the higher concentrations, in which more ions are paired, the conductivity increases more slowly with increasing temperature than does the fluidity (slope <1). The vertical displacements with change of salt concentration are in opposite directions for the PC and PPO solutions, but the concentration ranges under study in each case are quite different. The deviations from unit slope are greater for triflate solutions than for perchlorate and are greatest for high concentrations of triflate, all of which is in accord with the findings of Torell and co-workers.[12] Thus, the anomalous ion dissociation temperature dependence of the polymer solutions, which culminates in some cases in the precipitation of salt from solution[28] (probably preceded

(22) Angell, C. A. *J. Non-Cryst. Solids* **1985**, *73*, 1.
(23) Elmroth, M.; Borjesson, L.; Torell, L. M. In *Proceedings in Physics: Static and Dynamic Properties of Liquids*; Davidovic, M., Soper, A. K., Eds.; Springer-Verlag: Berlin, Vol. 40, p 118.
(24) Tatsumisago, M.; Halfpap, B. L.; Green, J. L.; Lindsay, S. M.; Angell, C. A. *Phys. Rev. Lett.* **1990**, *64*, 1549.
(25) (a) LeNest, J. F. Ph.D. Thesis, INP Grenoble, 1985. (b) Cheradame, H.; LeNest, J. F. In *Polymer Electrolyte Reviews 1*; MacCallum, J. R., Vincent, C. A., Eds.; Elsevier: New York, 1987; Chapter 5.
(26) McLin, M. G.; Angell, C. A. To be published.
(27) Casteel, J.; Angel, J. R.; McNeely, H. B.; Sears, P. G. *J. Electrochem. Soc.* **1975**, *122*, 319.
(28) (a) Wintersgill, M. C.; Fontanella, J. J.; Greenbaum, S. G.; Adamic, K. J. *Br. Polym. J.* **1988**, *20*, 195. (b) Teeters, D.; Frech, R. *Solid State Ionics* **1986**, *18/19*, 271.

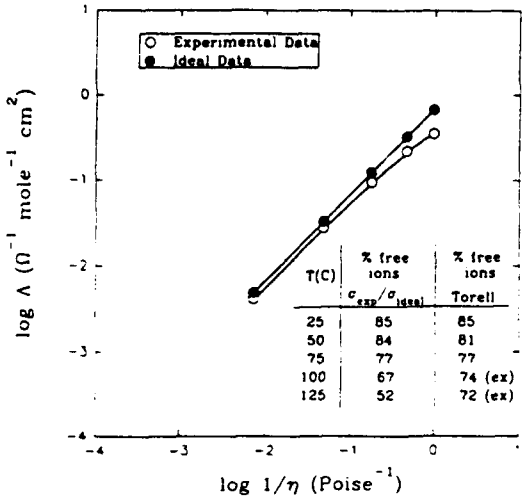

Figure 11. Walden plot comparison of experimental (O) and ideal (fully dissociated, viscosity-dominated) behavior (●) for 1:30 $LiClO_4$ PPG-(4000). Numerical evaluations of conductivity-based and spectroscopically evaluated (ref 12) percent free ions are given in the inset.

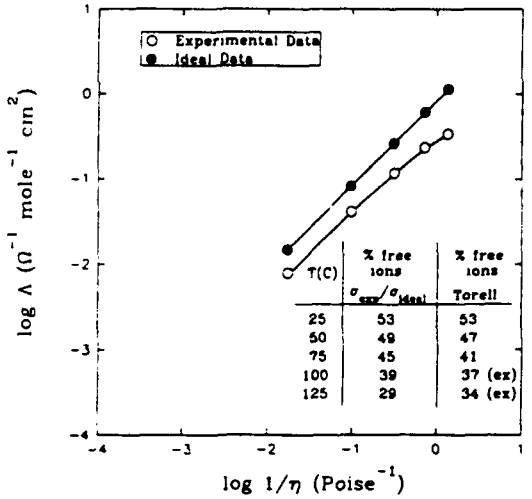

Figure 12. Walden plot of experimental (O) and ideal (●) behavior for 1:30 $NaCF_3SO_3$ PPG(4000). (For table, see Figure 11 caption.)

by liquid–liquid unmixing), is fully confirmed.

A more quantitative verification can be made as follows. Conductivities consistent with a line of unit slope through the 25 °C data point in the Walden plots of both 1:30 $LiClO_4$ and 1:30 $NaCF_3SO_3$ were calculated. These conductivities are appropriate to a system in which ionic content is temperature invariant and conductivity and viscosity remain fully coupled. Next, these conductivities were multiplied by a constant factor to raise the conductivity to that for a fully dissociated salt ("ideal" behavior). This factor was taken from ion pair concentrations at 25 °C from the data of Torell and co-workers.[12] The percentage of ions existing as pairs at different temperatures was then calculated from the ratio of the experimental and calculated ideal conductivities. The results for 1:30 $NaCF_3SO_3$ were within 4%, and for 1:30 $LiClO_4$ were within 3%, of the data of Torell and co-workers[12] up to ~75 °C, the high temperature limit of their data, and the procedure thus provides a basis for evaluating the degree of ion pairing up to temperatures of 125 °C. The results are summarized in the table insets in Figures 11 and 12. The numbers marked (ex) in the Torell column are based on extrapolation of their van't Hoff plot. Our data suggest that the van't Hoff equation may fail at high temperature, possibly becoming a power law as a coexistence line (miscibility gap) is approached. The differences in the extent of ion pairing in triflate vs perchlorate solutions are highlighted by the difference between the ideal and experimental Walden plots in Figures 11 and 12.

These findings are also consistent with the different temperature dependences for the composition of Λ_{max} for the $LiClO_4$ system (Figure 7) and the $NaCF_3SO_3$ system (Figure 8). In Figure 7 the composition of Λ_{max} for the $LiClO_4$ system exhibits essentially no temperature dependence between 25 and 100 °C. However, in the $NaCF_3SO_3$ system the shift is considerable as seen in Figure 8c. The differences between the two can be explained by differences in the relative importance of charge carrier number and ionic mobility with increasing temperature. Since the ion-pair concentration in $NaCF_3SO_3$ increase more rapidly with temperature than in $LiClO_4$, the decrease in the number of charge carriers and the concomitant rise in ion mobility (due to the decreased number of transient cross-links) results in a larger shift in Λ_{max} with salt concentration in the $NaCF_3SO_3$ system.

The consistency of spectroscopic and conductivity findings we have shown here must cast doubt on the interpretation of dilute solution conductivity studies[29] which invoke a ion triplet formation not observed spectroscopically[13] in this dilute concentration range.

The only feature in Figures 9 and 10 for which we do not have an immediate explanation is one also seen by Wantanabe,[19] viz., the upward displacement of the Walden curves with increasing concentration. This will be considered further in a subsequent paper in which we will introduce extended range viscosity data which will assist the interpretation.

Conclusion

We have shown that $NaCF_3SO_3$–PPG(4000) solutions are more ion paired than $LiClO_4$–PPG(4000) solutions and that ion pairing in these solutions increases with temperature, in agreement with independent spectroscopic data. In future papers we will examine systematically the influence of anion and cation types on ion pairing in polymer electrolyte solutions.

Acknowledgment. We are grateful for support of this work in its initial stages by the Office of Naval Research under Agreement No. N00014-87-K0417 and to the Department of Energy under whose auspices (DE-FG02-89ER453S398) it was completed. We also acknowledge helpful discussions and exchange of information with Prof. Lena Torell and her co-workers at Chalmers University of Technology, Gothenburg, Sweden, which was made possible by a National Science Foundation International Collaboration Grant (INT8619785).

(29) (a) MacCallum, J. R.; Tomlin, A. S.; Vincent, C. A. *Eur. Polym. J.* **1986**, *22*, 787. (b) Hall, P. G.; Davies, G. R.; Ward, I. M.; McIntyre, J. E. *Polym. Commun.* **1986**, *27*, 100.

(14)

Materials Science Forum Vols.32-33 (1988) pp.373-384

STRUCTURAL MOTIFS IN FLUORIDE GLASSES, AND THEIR INFLUENCE ON LIQUID AND GLASSY STATE PROPERTIES

C.A. Angell and C.C. Phifer
Department of Chemistry
Purdue University
West Lafayette, IN 47907, USA

ABSTRACT

We review the essential features of three complementary approaches — elastic scattering, spectroscopy, and computer simulation — to the study of structure in glasses, and discuss the alternative models of fluorozirconate glass structure which these approaches have suggested. A detailed review of the structures of some 97 known crystalline fluorozirconates lends strong support to one of the models and explains the origin of possible inaccuracies in others.

INTRODUCTION

The understanding of the atomic-level structure of heavy metal fluoride (HMF) liquids and glasses constitutes a challenge in the purely academic sense as well as in the practical materials science sense. The molten heavy metal fluorides are exceptional amongst the known glassforming ionic liquids, in that their liquid structural relaxation times exhibit[1,2] an extraordinary temperature dependence. They fall at the opposite extreme of behavior from that represented by the classical glassforming liquid silica and the related liquid silicates. The challenge is to understand what it is about the structure of these systems which causes them to be so different from the better-characterized silicate glasses. This is also a matter of great practical concern because of the problems in fiber-pulling caused by the very high temperature dependence of viscosity.

The same challenge is involved in understanding the relatively poor glassforming ability of the HMF systems. It can be argued that it is only this extremely rapid decrease in the relaxation times with increase of temperature above T_g which prevents the heavy metal fluoride glasses from being amongst the best of glassformers, since even in the very weakly glassforming system BaF_2-ZrF_4 the liquidus temperatures are unusually close to the glass transition temperatures ($T_m/T_g \approx 0.59$). In most systems this figure would imply a very high viscosity at the point where the crystal becomes thermodynamically stable, hence very slow crystallization kinetics and good glassforming ability. Because of the exceptional "fragility"[2] of the HMF liquid state, however, the liquids are relatively fluid at the liquidus temperature, hence crystallize rapidly despite considerable nucleation barriers. The proximity of T_m to T_g implies that the liquid state has been stabilized thermodynamically relative to the crystalline state,[3] presumably by the high degree of configurational degeneracy. But what does this imply? Evidently, a very broad distribution of different possible configurational ionic arrangements can be realized in the liquid

fluorozirconates. Presumably this is at least in part due to the ability of Zr^{4+} to adopt multiple coordination states so that there can be configurational degeneracy in the nearest neighbor shell as well as in the 2nd, 3rd, etc.

In view of the number of possible coordination states, it is not surprising that there has been controversy surrounding the best description of the basic fluoride glass systems, BaF_2-ZrF_4. The best known model for these systems is the one first put forward by Almeida and Mackenzie[4]. The essential feature of their model, which was based on comparison of Raman frequencies with those of a limited class of fluorozirconate crystals, invoked a chain-like structure involving six-coordinated corner-linked Zr-F polyhedra with barium ions occupying between-chain positions. This model was not supported by early computer simulation studies[5] which indicated a more three-dimensional linking of more highly coordinated Zr-F polyhedra, and a combination of more refined simulations and x-ray scattering data[6,7] led to a model in which the coordination of zirconium by fluorine was closer to eight with a mixture of single and double fluoride bridges. Most of the recent descriptions of fluoride glass structures[8–10] have contained the latter elements, though in general much credence still seems to be lent to the original Almeida-Mackenzie model.

In this paper, we will briefly review the different approaches to determining the structure of fluoride glass systems and will then provide, as a background for detailed structural studies to follow, a comprehensive review of the structural motifs and trends in fluorozirconate systems which are available from analysis and classification of the known crystalline fluoride structures.

There are three distinct and mutually reinforcing approaches to the study of glass structures which we will consider in the order (1) elastic scattering studies, (2) inelastic scattering or absorption spectroscopy studies, and (3) computer simulation studies. Of these the first gives the correct overall average structure but obscures details of particular significance because of overlapping of contributions to the total scattering function from the individual pairs. The second gives important detail but fails to give the overall picture, while the third gives, in principle, everything but is limited by the artificiality, or approximate nature, of the necessary input information in the form of pair (or sometimes manybody) interaction potentials of fundamental importance to the simulations.

(1) ELASTIC SCATTERING STUDIES

The elastic scattering studies of main importance to fluoride glass structure elucidation are those involving the scattering of neutrons and x-rays. The two approaches are complementary since the scattering powers of different atoms are quite different in the two cases. In the case of neutrons, certain nuclei may even have negative scattering cross-sections which is particularly useful for refined structure studies to be referred to below.

Primary experimental data are obtained in the form of scattered intensity vs. angle patterns which are related to the real space distribution of the atomic centers by a Fourier transformation, after appropriate weighting of atomic scattering powers.[12] The Fourier transformation introduces uncertainties into the real space information and may lead to artifacts which experts in the field are always concerned about.[12] Without concentrating on these problems, we note that the deduced radial distribution functions (RDF) are increasingly difficult to interpret, the larger the number of different atomic species present in the glass. Already in a two-component glass such as BaF_2-ZrF_4, there are difficulties in interpretation of the total RDF beyond the first two peaks,[13,14] and systems with several components are essentially impossible to study profitably

by the scattering methods in their straightforward forms.

An approach which is more fruitful, both for the simple and the complex systems, is to take advantage of the fact that different isotopes have different neutron scattering cross-sections and compare the neutron scattering patterns of glasses which are identical in all respects except for the isotopic composition. This approach,[15] called the difference neutron scattering method, has been extensively applied in the study of metal alloys and aqueous solutions, but has had only very limited application in the study of glassy structures so far.[16] The subtraction of one pattern from the other removes most of the complications of analysis of the real space radial functions, since the difference pattern contains only scattering from pairs containing the atom whose isotopes have been substituted with a third isotope, or isotope composition. *Second* order differencing is also possible (though with poorer signal/noise), and even greater structural detail can be deduced. Disadvantages of the technique are that the isotopes are often very expensive, and the analysis can be confused by even small departures from identical compositions and also, in the case of glasses, identical heat treatments. Hopefully, there will be developments based on the phenomena of "anomalous neutron scattering" and "anomalous x-ray scattering" techniques which utilize the possibility of scattering from the same sample using two different frequencies, one which is chosen to fall on a natural resonance of an atom of interest. Again taking the difference, one has the possibility of eliminating pairs other than those containing the "active" species. This technique has the advantage of demanding only one sample, but is beset with other technical problems and has not yet reached a high state of development.

(2) INELASTIC SCATTERING OR ABSORPTION SPECTROSCOPY STUDIES

This approach has a great many branches and it is not appropriate to attempt any sort of review in this contribution. Rather we will concentrate on the information available from *vibrational* spectroscopy and, to a lesser extent, *nuclear magnetic resonance* spectroscopy.

Among the former, studies of Raman-active and infrared-active modes have dominated the field of investigation. Raman spectra of fluorides tend to be problematical because of the relatively low scattering power (due to the small change of polarizability as fluoride ions vibrate against their neighbors) and there is a danger of artifacts (e.g. otherwise-weak "ghosts" becoming prominent because of the long counting periods required) or degradation of spectral quality due to surface scattering in powdered or microcrystalline samples. Infrared studies bring a different set of problems associated with the very high absorption intensity and the need to have very dilute mulls or very thin glass films. Notwithstanding these problems, a large number of spectra have been published[17–20] and have, for instance, provided the basis for one of the outstanding models of fluoride glass structure.[4] The principal point of the present contribution is to emphasize the need for caution in the interpretation of vibrational spectra of fluoride glasses. The usual technique of "fingerprinting," i.e. interpreting observations by reference to crystal spectra, can be deceptive if not practiced with a great deal of circumspection. Trends of observed frequency with coordination number seen in one class of crystals may be contradicted by those in a different group. Much depends not only on the coordination number, but also on the nature of the counter-cation, both its charge and size.

The major contribution of this article is to provide a detailed, and previously unavailable, background of trends in structural characteristics of fluorozirconate crystals and to discuss their relation to glass structure and glass vibrational spectra. We defer this to a concluding section.

Nuclear magnetic resonance spectroscopy offers an alternative and powerfully discriminating method of obtaining structural information with the special advantage that one can interrogate the different atomic species individually. Surprisingly little use of NMR has so far been made in HMF structure studies, despite the fact that ^{19}F is a very favorable nucleus. The main problem is that the "motional narrowing" phenomenon that makes it possible to obtain high resolution spectra in liquid samples does not occur in viscous liquids and glasses, and structural studies therefore require the less readily available high field NMR spectrometers and the "magic angle" spinning technique which permits the averaging out of chemical shifts and dipole coupling even in solid samples.

The resonance frequency observed for the nucleus in a given magnetic field depends on the electron density at the nucleus, which in turn depends on the chemical nature, number, and symmetry of its nearest (and to a lesser extent second nearest) neighbors in the glass structure. Since we expect (see below) three distinct "sorts" of fluoride ion in HMF structures, we should expect three distinct resonance frequencies, and in principle their intensities should give information on the respective populations.

Unfortunately the effects of different chemical, and symmetry or distance, characteristics may counteract each other such that two geometrically distinct fluorides could have the same or very similar resonance frequencies. Even here, however, NMR spectroscopy provides a resolution, because the species which are degenerate in frequency will frequently have very different relaxation times, i.e. different time scales on which the excited states induced by the RF field return to the ground state. This allows the frequency-degenerate sites in a structure to be distinguished by the simple device of making the observation at different times after the initial (pulsed) excitation.

In this manner, preliminary ^{19}F studies of a ZBLA glass have resolved three distinct resonances.[21] It seems clear that systematic studies using this technique could be very valuable to fluoride glass structure diagnosis and are strongly to be encouraged.

(3) COMPUTER SIMULATION STUDIES

Computer simulations of liquid and glass structures are concentrated into two groups. The first is based on the Monte Carlo approach, in which the stable structure is decided by testing random displacements of particles in an initial configuration and weighting the outcome of "successful" moves (i.e. those which lower the energy) by the Boltzmann factor. This approach leads to equilibrium structures under circumstances where the system is *ergodic*, but fails to give any information about the dynamics of structural change. The second approach, called Molecular Dynamics (sometimes Ion Dynamics) is based on the solution by fast computer of Newton's equation of motion for all particles in a primary sample of the system, the forces acting on the particles being assessed by the pairwise evaluation of the unbalanced force acting on each individual particle according to an assumed form of pair interaction potential. Details are given in the literature.[22] The advantage of this approach is that the diffusion mechanisms are obtained in addition to the average structures, energies, etc. and the loss of ergodicity, i.e. the glass transition, can be directly observed during cooling. This latter corresponds to a glass transition during an extremely fast quench and hence occurs at temperatures far above that of the laboratory glass transition, yet it is a related phenomenon consequent on the cessation of diffusion on the "experimental" time scale. In current developments[23] the dynamic structure can be depicted in three-dimensional images by projecting on the monitor screen dynamic images from different perspectives in different colors and using colored spectacles to produce the stereo impression. With the

option to "zoom" in on small ionic groupings within the primary box, the method offers a very powerful approach to visualizing in atomic detail the structure and dynamics of any system for which adequate pair potentials can be devised.

DISCUSSION OF STRUCTURAL MOTIFS IN FLUORIDE GLASSES AND RELATIONSHIP TO CRYSTAL DATA

The analysis of data acquired by the three different methods discussed above has led to the suggestion that the structure of fluoride glasses is to be understood in terms of the interplay of structural motifs of which a most important one is the edge-sharing or double fluoride bridging motif. The prevalence of this structural motif is found to depend on composition and on density.[18,19,24] One approach[6,7] focuses on this motif and regards the structure of the prototypical fluorozirconate glass as made up of modules of twin polyhedra joined by the double fluoride bridge and connected to other elements of the structure by single (corner-sharing) bridges. A more general model[7,25] recognizes the presence of varying proportions of three fundamental types of fluoride ion in the structure viz., (double, bridging E (edge), single, bridging C (corner), and non-bridging T (terminal)), and analyzes the different possible combinations of polyhedral linkages in a bulk (three-dimensional) fluoride glass. Examples of the unit polyhedra which may occur in the glass are given in Fig. 1(a) and identified by the crystalline fluorozirconates in which they are found. Additional polyhedra likely to be found in the glasses are shown in Fig. 1(b). Some of the different ways in which such polyhedra may be linked together in the liquid and glassy states may be seen in Ref. 7.

The highest fundamental Raman frequency is determined by the fluoride amongst the above which has the shortest Zr-F distance. This is invariably the non-bridging (or terminal) fluoride, which vibrates with a frequency determined by the other linkages in the polyhedron to which it belongs. It is possible to see how this will vary with structure by examining the distances characteristic of different fluorides in crystalline fluorozirconate compounds. We have researched the crystallographic literature and identified certain features amongst the crystals which are undoubtedly of primary importance to the structural characterization of glassy states containing fluorozirconate elements. We summarize these in the following tables and descriptive passages and look forward to incorporating the information in a broadly based Raman spectroscopic study of fluoride glasses and crystals in the future.

In the first place, we have identified in the literature 97 different fluorozirconates mostly with a single counter-cation species M (usually but not necessarily a metal ion), of which 63 have been characterized in sufficient detail that the Zr coordination number and ECT character (Fig. 1a, b) can be extracted. The polyhedra observed range from simple octahedra with all T-type fluorides to a limiting complexity in the compound $Rb_5 Zr_4 F_{21}$, which contains no less than four different polyhedra of coordination numbers ranging from six to eight, each displaying different ECT fluoride combinations.

The complete compilation showing Zr^{4+} and M^{n+} coordination numbers, and ECT character, will be reported elsewhere.[26] For the present purposes we extract from this mass of data, key information on structural motifs or polyhedral linkages, specifically, the Zr - Zr distances for corner- and edge-sharing linkages and the corresponding Zr - F - Zr angles, designated Zr - C - Zr for corner-linking and Zr - E - Zr for edge-linking. These are displayed in Table 1 for the 20 cases where sufficient crystallographic data are available for the quantities of interest to be calculated. Details on the analysis and literature references too numerous to include here are given elsewhere.[26] The outstanding feature of Table 1 is the contrast in regularity of the edge-sharing

and corner-sharing polyhedral linkages. The angles involved in corner-linking range from the linear (180°) in β–$Na_5Zr_2F_{13}$ to a strongly bent 143° in β–$BaZr_2F_{10}$. By contrast, in edge-sharing the Zr - F - Zr angle is remarkably constant, ranging only between 113° and 119° over a widely divergent series of compounds. The average value is 115 ± 2°. It is easy to accept, then, that edge-sharing when it occurs in glasses will be comparably well-defined. However, such tight constraints imply low entropy which suggests that the edge link may not be as prevalent in the glassy state as in the lower entropy crystalline state. It is here that a careful fluorine NMR study would be particularly useful.

The well-defined geometry of the edge-sharing motif discussed above does not necessarily indicate high stability. Because of the Zr^{4+} - Zr^{4+} repulsion the Zr - F bond length in the edge sharing unit is longer, Zr - E = 2.18 ± 0.02 Å, than the average for corner-sharing, Zr - C = 2.11 ± 0.04. Both are longer than the terminal Zr - F distance, Zr - T = 2.01 ± 0.05 Å. If bond-breaking is a mechanism for thermal excitation in the liquid state, as seems natural, then the probability of bond rupture should go as $\exp(-\varepsilon_b/\kappa T)$, where ε_b is the bond energy, neglecting entropic factors. On this basis alone the Zr - E bonds should be the most susceptible to rupture since ε_b must scale inversely with the bond length. When we take into consideration the above observation that rupture of the geometrically-constrained edge-sharing motif must be strongly favored entropically we must conclude that the break-up of edge-shared polyhedral linkages should be a dominant mode of thermal excitation. Indeed it may well be an important source of the exceptional fragility of the fluorozirconate liquids near T_g, the explanation of which we noted as an academic challenge in our opening remarks. Again solid state NMR of quenched and annealed glasses would provide critical evidence on this issue through the fictive temperature dependence of the E-fluoride population. Already it is known from Raman studies[27] in the liquid that the band we assign to edge sharing almost disappears with increasing temperature in the liquid, (though the bridging motif is still very prevalent in molecular dynamics "snapshots" of the high temperature liquid state[7–11]).

Thus our analysis of the fluorozirconate crystal literature has lent strong support to a model of fluoride glass structure in which edge-sharing polyhedra play a prominent role and has led to a suggestive qualitative interpretation of the outstanding feature of the liquid behavior near T_g.

In a less positive sense, the crystal data also provide strong reasons for believing that octahedral ZrF_6 groupings *are not* prevalent in barium fluorozirconate based glasses, and offer an alternative explanation of the vibrational frequency trends which led to that model in the first place. For this we turn to Table II which gives data on a series of isostructural metafluorozirconates containing octahedral ZrF_6 groups in which the divalent cation changes systematically in size. *The last of this group, and that which exhibits the longest Zr-F bond, of the group 2.09 Å is* $CaZrF_6$, *and it is metastable.* These are simple cubic compounds which can be easily computer modelled as infinite crystals using our ion dynamics programs. We find that the dynamic simulation using rigid ion pair potentials reproduces the crystal coordinates, and even the Raman spectrum, of $MgZrF_6$ (see Fig. 2). Isostructural crystals with M^{2+} larger than Sr^{2+} are absolutely (mechanically) unstable and spontaneously collapse (within 20 vibration periods) to disordered structures with larger Zr coordination numbers (but comparable Zr-F bond lengths). ZrF_6 octahedra and therefore unlikely to coexist in glasses with Ba^{2+} counter-cations. The high vibration frequencies which provided the argument for the ZrF_6-based linear chain model[4] seem to be a consequence of the redistribution of electron density in bridged 7- or 8-coordinate polyhedra such that the Zr-T bonds become as short or shorter than those found in some isolated octahedral groups. For instance some of the Zr-T bonds in $Rb_5Zr_4F_{21}$, which has

the polyhedron [ZrT_3E_4C], are 2.00 Å compared with the Zr-T length 2.04 Å in the ZrT_6 octahedra of Rb_2ZrF_6, and 2.016 Å in the octahedra of Li_2ZrF_6. In general, increasing bridging causes decreasing Zr-T distances in crystals, hence presumably higher vibration frequencies. This and other important correlations relevant to glass structure and vibrational spectroscopy will be described elsewhere.[26]

ACKNOWLEDGEMENTS

It is a pleasure to acknowledge the support of this work by the U.S. National Science Foundation under Solid State Chemistry Grant No. 8304887 and by the Office of Naval Research under Agreement No. N00014-84K0289

REFERENCES

1. Crichton, S.N.; Mossadegh, R.; Moynihan, C.T.; Gupta, P.K. and Drexhage, M.G.: Mat. Sci. Forum, 1987, *19-20*, 435.
2. Angell, C.A.: J. Non-Cryst. Solids, Kreidl Symposium, 1985, *73*, 1.
3. Angell, C.A.; Busse, L.E.; Cooper, E.E.; Kadiyala, R.K.; Dworkin, A.; Ghelfenstein, M.; Szwarc, H. and Vassal, A.: J. de Chim. Phys., 1985, *82*, 267.
4. (a) Almeida, R. and Mackenzie, J.D.: J. Chem. Phys., 1981, *74*, 5954.
   (b) Almeida, R. and Mackenzie, J.D.: J. Chem. Phys., 1983, *78*, 6502.
5. (a) Angell, C.A. and Cheeseman, P.A.: Abstract of 1st International Conference on Non-Oxide Glasses, Cambridge 1981.
   (b) J. de Phys., 1982, *43*, Cq. 381.
6. Lucas, J. and Angell, C.A.: Mat. Sci. Forum, 1985, *6*, 449.
7. Phifer, C.C.; Angell, C.A.; Laval, C. and Lucas, J.: J. Non-Cryst. Solids, 1987, *94*, 315.
8. Inoue, H.; Hasegawa H. and Yasui, I.: Phys. Chem. Glasses, 1985, *26*, 74.
9. Yasui, I. and Inoue, H.: J. Non-Cryst. Solids, 1985, *71*, 39.
10. Kawamoto, Y.; Horiska, T.; Hirao, K. and Soga, N.: J. Chem. Phys., 1985, *83*, 2398.
11. Hamill, L.T. and Parker, J.M.: Mater. Sci. Forum, 1985, *6*, 437.
12. Wright, A.C.: Adv. Struct. Res. Diffr. Meth., 1974, *5*, 1.
13. Coupe, R.; Louer, D.; Lucas, J. and Leonard, A.J.: J. Am. Ceram. Soc., 1983, *66*, 523.
14. Etherington, G.; Keller, L.; Lee, A.; Wagner, C.N.J. and Almeida, R.M.: J. Non-Cryst. Solids, 1984, *69*, 69.
15 (a) Derrien, Y. and Dupuy, J.: J. de Phys., Paris, 1975, *36*, 191.
   (b) Enderby, J.E. and Biggin, S.: Adv. Molten Salt Chem., 1983, *5*, 1.
16. Wright, A.C.; Etherington, G.; Erwin Desa, J.A. and Sinclair, R.N.: J. de Phys. Colloq., C9, Suppl. No. 12, 1982, *43*, C9-31.
17. Drexhage, M.G.; Bendow, B. and Moynihan, C.T.: Laser Focus, 1980, *10*, 62.
18. Banerjee, P.; Bendow, B.; Drexhage, M.G.; Goltman, J.; Mitra, S. and Moynihan, C.T.: J. de Phys., 1981, *42* Suppl. C6, 75.
19. Kawamoto Y. and Sakaguchi, F.: Bull. Chem. Soc. Jpn., 1983, *56*, 2138.

20. Bendow, B.; Banerjee, P.; Drexhage, M.G.; Goltman, J.; Mitra, S.S.; Moynihan, C.T.: J. Amer. Ceram. Soc., 1982, *65*, C8.
21. Taulelle, F. and Angell, C.A.: unpublished work.
22. Woodcock, L.V.: Adv. Molten Salt Chem., 1975, *3*, 1.
23. Kieffer, J. and Angell, C.A.: unpublished work.
24. Phifer, C.C. and Angell, C.A. to be published.
25. Phifer, C.C. and Lucas, J.: Mat. Sci. Forum, 1987, *19-20*, 111.
26. Phifer, C.C.: to be published.
27. Walrafen, G.E.; Hokmabadi, M.S.; Guha, S.; Krishnan, P.N. and Tran, D.C.: J. Chem. Phys., 1985, *83*, 4427.

Table I. Data pertaining to fluorozirconate crystals with bridging structures.

Compound	$(Zr–Zr)_C$	$(Zr–Zr)_E$	Zr-C-Zr	Zr-E-Zr
α–ZrF_4	4.105	3.565	154.7°	114.3°
β–ZrF_4	4.140	-	162°	-
γ–ZrF_4	?	?	?	?
α–$BaZrF_6$	-	3.724	-	115.3°
β–$BaZrF_6$	-	3.82	-	118°
α–$BaZr_2F_{10}$	-	?	-	?
β–$BaZr_2F_{10}$	3.917	3.617	143°	113°
$Cu_3Zr_2F_{14}\cdot 16H_2O$ (nc)	-	3.663	-	114.6°
α–$EuZrF_6$	-	3.76	-	119°
α–K_2ZrF_6	-	3.638	-	113.8°
$K_2CuZr_2F_{12}\cdot 6H_2O$ (nc)	-	3.636	-	114.8°
$LiTlZr_5F_{22}$*	4.121	-	152.4°	-
(1)	4.094	-	156.3°	-
(2)	4.129	-	151.5°	-
$(N_2H_6)ZrF_6$	-	3.68	-	113°
γ–Na_2ZrF_6	-	3.602	-	113.6°
β–$Na_5Zr_2F_{13}$	4.215	-	180°	-
$Na_7Zr_6F_{31}$	?	3.647	?	113.7°
$PbZrF_6$	-	3.77	-	119°
$Rb_5Zr_4F_{21}$**	4.158	3.635	157°	115°
(1)	4.147	3.631	156°	115°
(2)	4.210	3.635	162°	115°
(3)	4.164	-	157°	-
(4)	4.132	3.639	154°	115°
α–$SrZrF_6$	-	3.78	-	119°
$TlZrF_5$	4.193	3.676	160.3°	114.9°

nc = not colorless.

*There are two different ZrF_8 coordination polyhedra for this compound. They are treated separately in the two rows below this listing.

** There are four different ZrF_n coordination polyhedra for this compound. They are treated separately in the four rows below this listing.

Table II. The average Zr-F bond distances for a series of isostructural compounds with divalent countercations and isolated [ZrF_6^{2-}] ions.

	Compound	M CN	M radius	Zr-F	Refs.
	$NiZrF_6$	6	0.690	1.96	a,b
	$MgZrF_6$	6	0.720	1.96	a,c
	$CoZrF_6$	6	0.745	1.98	a,b
	$ZnZrF_6$	6	0.750	1.97	a,b
	$FeZrF_6$	6	0.780	2.00	a,b,d
	$MnZrF_6$	6	0.830	2.02	a,b
	$CaZrF_6$	6	1.00	2.09	a,c
Average				2.00	

References

a: Poulain, M. and Lucas, J.: Compt. Rend. 1970, *271*, 822.

b: Shannon, R. D. and Prewitt, C. T.: Acta Cryst. 1970, *B26*, 1046.

c: Shannon, R. D. and Prewitt, C. T.: Acta Cryst. 1969, *B25*, 925.

d: Mayer, H. W.; Reinen, D.; Heger, G.: J. Solid St. Chem. 1983, *50*, 213.

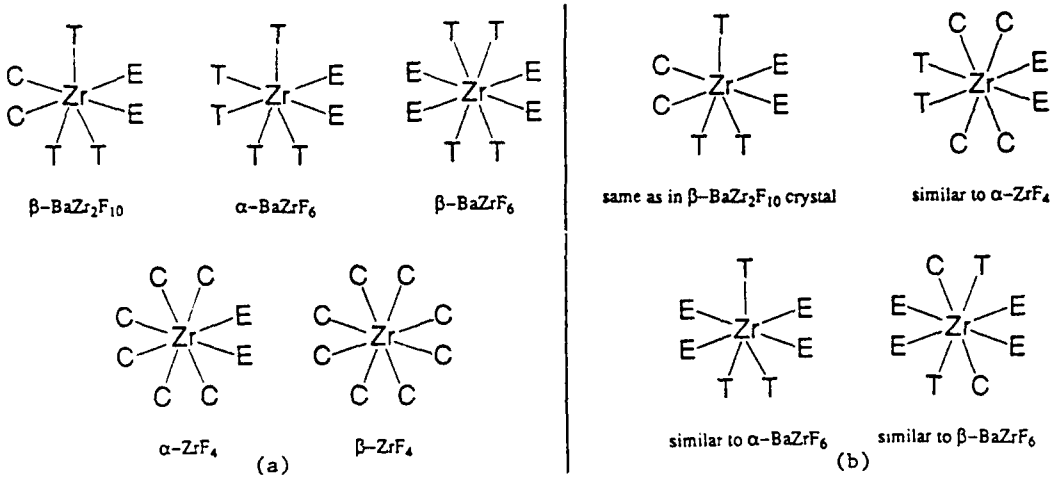

Fig. 1. Zr-F polyhedra with types of fluoride characterized as E, C, or T as found in fluorozirconate crystals (part (a)), or related to those found in crystals (part (b)).

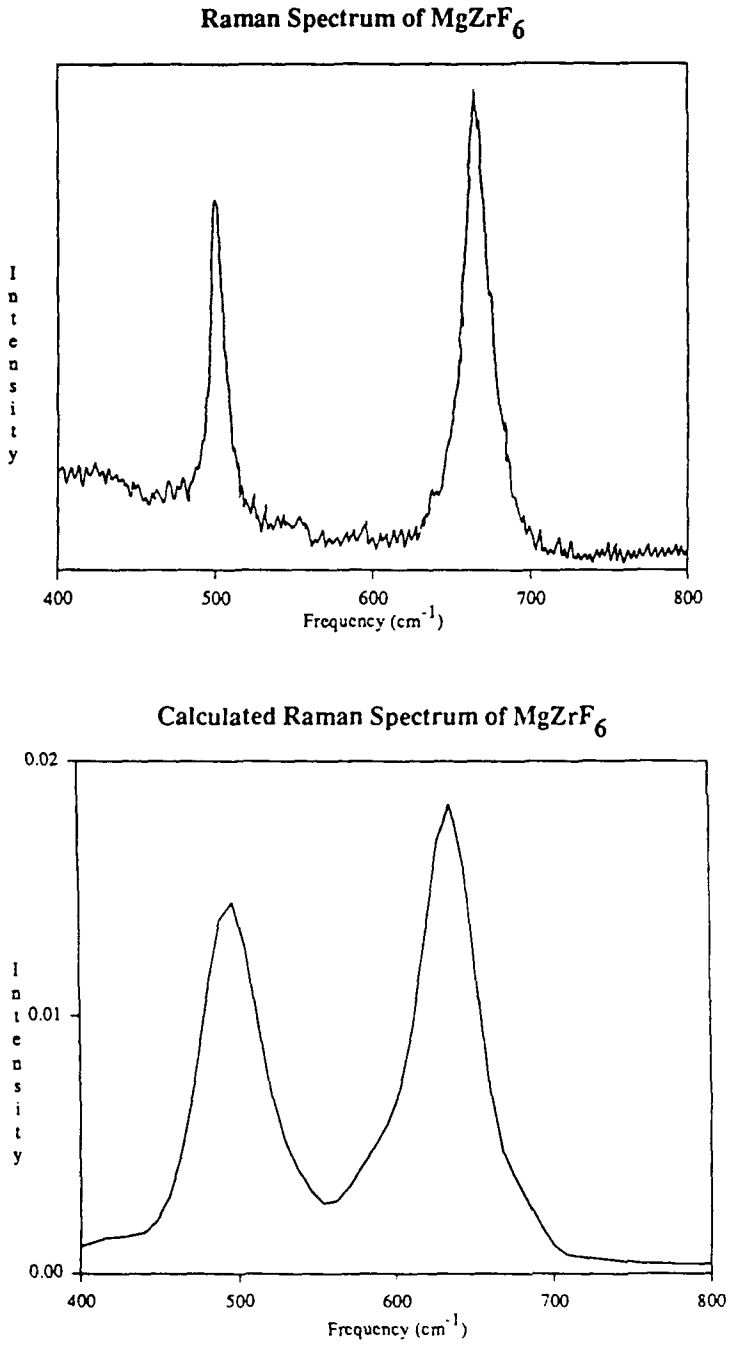

Fig. 2. Comparison of observed and computer-simulated Raman spectra for the crystal $MgZrF_6$.

Effects of coordination environment on the Zr–F symmetric stretching frequency of fluorozirconate glasses, crystals, and melts

Carol C. Phifer,[a] David J. Gosztola,[b] John Kieffer,[c] and C. Austen Angell[d]
Department of Chemistry, Purdue University, West Lafayette, Indiana 47907

(Received 11 April 1990; accepted 17 October 1990)

A treatment based on Badger's rule is used to estimate symmetric stretching frequencies ν_s of the nonbridging fluorides of various ZrF_n groups in the presence of divalent and monovalent countercations. New vibrational spectra of $MgZrF_6$, Ba_2ZrF_8, and β-$BaZr_2F_{10}$ are presented and incorporated into the method. The factors affecting ν_s are outlined and discussed in detail. Compilations of estimated frequencies are used to deduce the probable local structure around Zr ions in binary barium fluorozirconate glasses and in fluorozirconate melts containing lithium and sodium ions. It is concluded that the results of Raman spectroscopy indicate the presence of seven- and eight-coordinate Zr in some barium fluorozirconate glasses.

I. INTRODUCTION

The possible technological applications and the uncommon atomic structures of fluorozirconate glasses have provoked a considerable research effort in recent years. The nature of the fluoride-ion arrangements around zirconium has been much debated, but is still not known with certainty. Vibrational spectroscopy, especially Raman spectroscopy, has proved to be a sensitive indicator of the immediate environment of zirconium. In particular, the totally symmetric stretching frequency of the fluorides that are bonded to only one zirconium (the nonbridging, or terminal fluorides) has been used as a probe of the zirconium surroundings. Several aspects of the nearby solid-state environment can influence this symmetric stretch frequency, otherwise known as ν_s, but there has been no systematic attempt to categorize or to quantify these influences.

This paper describes a general semiquantitative scheme for predicting ν_s frequencies of various types of ZrF_n units. The success of the method depends on the reproducible contribution made by each of a number of factors. While the coordination number (CN) of Zr is an important one of these factors, it is by no means dominant, as has been assumed tacitly in some previous attempts to use crystal Raman spectra to deduce Zr coordination numbers in different media. As will be seen, ν_s also depends sensitively on the number and type of bridging fluorides in the ZrF_n polyhedron, as well as on the nature of the modifier cations.

In order to develop this correlation scheme, it has been necessary to obtain new Raman spectroscopic data on some key crystals of known structure. These results were used along with literature data on other fluorozirconate crystals to produce tables showing the frequency-structure relations. Finally, we have applied the results to the interpretation of the structures of fluorozirconate glasses whose Raman spectra have been published previously.

II. EXPERIMENTAL PROCEDURE

The fluorozirconate crystals were prepared by solid-state reaction of the appropriate proportions of starting materials (ZrF_4, MgF_2, and BaF_2). The 99% ZrF_4 obtained from Cerac was purified by sublimation before use. A sealed reaction vessel is required to prevent the loss of ZrF_4 during heating. The apparatus shown in Fig. 1 allowed the samples to be sealed into platinum pans without the need for welding. The powdered mixtures were pressed into disks and placed

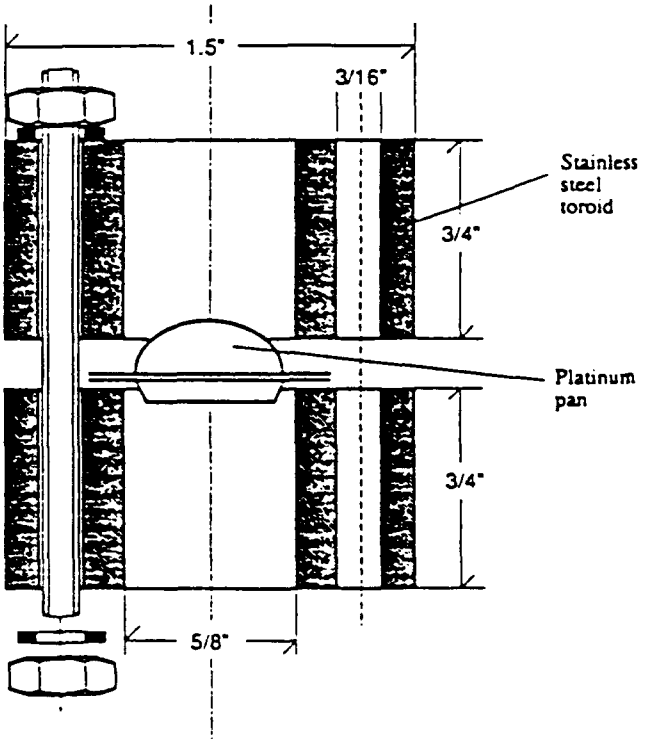

FIG. 1. Cross section of the assembly used to synthesize fluorozirconate crystals.

[a] Present address: Division 1845, Sandia National Laboratories, Albuquerque, New Mexico 87185.
[b] Present address: Department of Chemistry, Princeton University, Princeton, New Jersey 08544.
[c] Present address: Department of Materials Science and Engineering, University of Illinois, Urbana, Illinois 61801.
[d] Present address: Department of Chemistry, Arizona State University, Tempe, Arizona 85287.

 0021-9606/91/053440-11$03.00

between two shallow Pt pans, one inverted. The rims of the pans were sealed tightly together by two larger stainless steel rings connected by screws and bolts. During heating, the entire assembly was wrapped in Cu foil, which acted as an oxygen scavenger and slowed the corrosion of the steel. To further protect against oxidation of the steel, a small flow of N_2 was circulated through the furnace during runs. This simple method of synthesis appeared to work very well. There was no evidence of ZrF_4 loss from the reaction vessel.

The samples were heated according to schedules determined previously by other authors. Specifically, $MgZrF_6$ was prepared by heating to 850 °C for 24 h[1] and Ba_2ZrF_8 was obtained by heating to 530 °C for 48 h.[2] The sample of β-$BaZr_2F_{10}$ was kindly provided by Dr. J. P. Laval of the Université de Limoges in Limoges, France. The identities of the products were verified by x-ray diffraction.

Raman spectra were obtained using a Spectra Physics Model 165 Ar^+ laser, a Spex Industries model 1403 double monochromator, a cooled RCA C31034-02 photomultiplier tube (PMT), and standard photon counting electronics. The excitation geometry was such that the samples were illuminated with a focused (0.5 mm) beam of 514.5 nm light at a power of ~150 mW at an angle of 60° from the surface normal. Scattered radiation was collected with an $f/0.95$ camera lens (D. O. Industries) orthogonal to the incident light and focused onto the monochromator's entrance slit using f-matching achromatic optics. Spectra were typically recorded using a bandpass of 5 cm^{-1} determined by the exit slit, 2 s integration time, and a 0.5 cm^{-1} step size. Due to the polycrystalline nature of the samples, it was not possible to obtain polarization information.

III. RESULTS

The Raman spectra of $MgZrF_6$, Ba_2ZrF_8, and β-$BaZr_2F_{10}$ are shown in Figs. 2, 3, and 4, respectively. The Raman spectrum of $MgZrF_6$ exhibits a very high totally symmetric stretching frequency ν_s. Its value of 669 cm^{-1} is the highest frequency yet reported for a fluorozirconate compound. The identification of this peak as the ν_s is not completely unequivocal, due to the near impossibility of obtaining polarization information from polycrystalline samples, but its high frequency, strong intensity, and narrow bandwidth agree with the hallmarks of fluorozirconate ν_s peaks.[3] The ν_s peak of Ba_2ZrF_8 occurs at 544 cm^{-1} and the ν_s of β-$BaZr_2F_{10}$ is 590 cm^{-1}. The differences between the prototypical dizirconate glass spectrum (see Fig. 7) and the

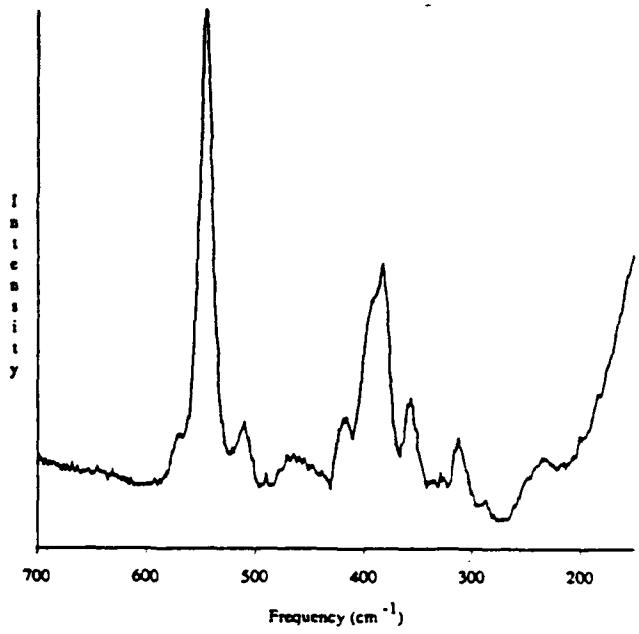

FIG. 3. Raman spectrum of Ba_2ZrF_8.

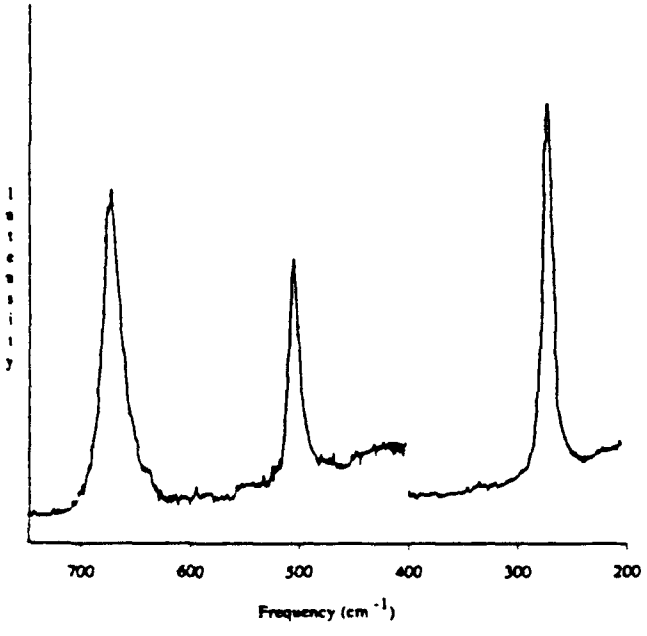

FIG. 2. Raman spectrum of $MgZrF_6$. The intensity of the portion of the spectrum below 400 cm^{-1} is plotted at half scale.

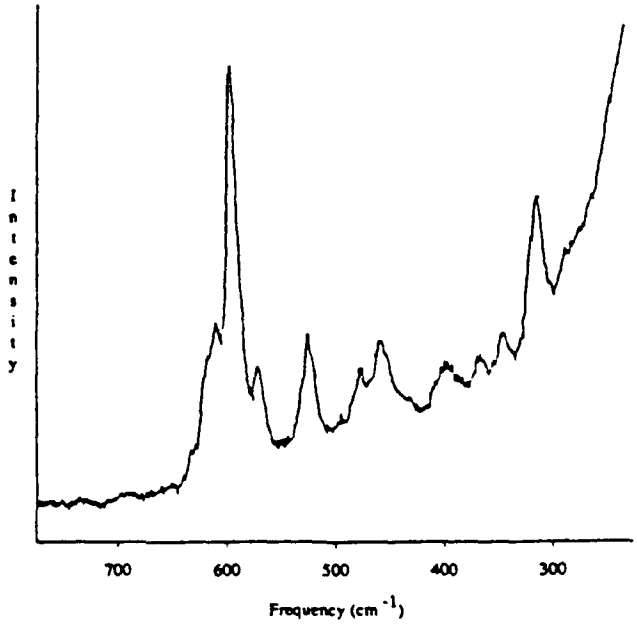

FIG. 4. Raman spectrum of β-$BaZr_2F_{10}$.

β-$BaZr_2F_{10}$ spectrum lend further support to the idea that the structures of the glass and crystalline forms of this composition are significantly different.[4,5]

IV. METHOD FOR ESTIMATING FREQUENCIES

The five factors influencing the ν_s frequency are: (1) the radius of the countercation (e.g., Ba^{2+}); (2) the coordination number of the countercation; (3) the degree of bridging between Zr ions; (4) the CN of Zr; and (5) the charge on the countercation. The effects of these conditions will be discussed individually after the development of some empirical relationships between force constants, the nature of the countercation, and bond strengths.

Badger[6] reported an empirically derived equation relating force constants of diatomic molecules to internuclear separation

$$k^{-1/3} = a_{ij} \cdot r_e - b_{ij}, \tag{1}$$

where k is the force constant, r_e is the internuclear distance, and a_{ij} and b_{ij} are constants for all diatomic molecules with one element from the ith row and one element from the jth row of the periodic table. The value of a_{ij}, the slope of the equation, is not very variable. In fact, since plots of $k^{-1/3}$ vs r_e give straight, almost parallel lines for many different types of diatomics, a_{ij} was originally described[7] as a universal constant over all molecules. Badger's equation has proved to be remarkably accurate in its predictions. Waser and Pauling[8] showed that it can be applied to the solid state.

As stated above, the variable r_e in the Badger rule refers to internuclear separation. A more general measurement is needed, for two reasons: (1) there are not many crystal data available for fluorozirconates and (2) we wish to extend the approach to estimate frequencies of structures which are not known to occur in crystals. The more general variable r_M, the radius of the countercation, shows a definite correspondence with r_e for the Zr–T (T = terminal fluoride) separation, as shown in Fig. 5 for some sets of isostructural divalent and isostructural trivalent fluorozirconate crystals. (All ionic radii used in this paper are taken from or calculated from data reported in Ref. 9.) Equation (1) may therefore be written as

$$k_T^{-1/3} = A \cdot r_M + B, \tag{2}$$

where k_T is the force constant associated with the terminal-fluoride stretch, and A and B are constants for related sets of compounds. The values of A and B are determined by the effects of the particular factor influencing ν_s. For example, if a decrease in the countercation radius increases ν_s, the slope of the equation describing this effect will be positive. For a given parameter, the slope A would be expected to be relatively invariant for different sets of compounds.

An approximation to k_T can be calculated directly from ν_s using the relation

$$\nu_s = \frac{1}{2\pi c}\left(\frac{k_T}{m_F}\right)^{1/2}, \tag{3}$$

where ν_s is in wavenumbers, c is the speed of light in cm/s, k_T is in dyn/cm, and m_F is the mass of a fluorine atom in grams. It is assumed that there is no motion of Zr atoms during the symmetric stretching vibration.

Equation (3) is strictly applicable only for the case of harmonic motion in diatomic molecules. In more complex molecules, observed frequencies correspond to more complex vibrations that depend on several force constants. This means that the absolute magnitudes of the k_T values calculated from Eq. (3) are not accurate. However, in the absence of normal coordinate analyses, we will use Eq. (3) as a way of monitoring trends in the data. In other words, the relative values of k_T values will be used as a reference framework.

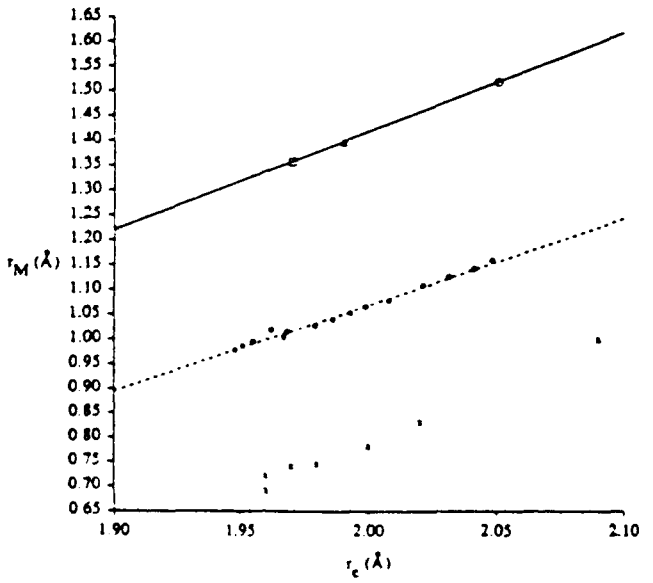

FIG. 5. Plot of countercation radius vs Zr–T internuclear separation for some isostructural fluorozirconate crystals. For the solid line, the circle represents β-$BaZrF_6$, the triangle is $PbZrF_6$, and the square is α-$SrZrF_6$ (r_e values from Ref. 25). The dashed line refers to $LnZrF_7$ compounds, where Ln is an eight-coordinate lanthanide ion (r_e values calculated from data in Refs. 42 and 43). The dotted line contains points for cubic $MZrF_6$ compounds, where M is a six-coordinate divalent ion (r_e values calculated from data in Refs. 1 and 44).

A. Effect of countercation radius on force constant

In a set of isostructural crystals, the Zr–T ν_s values increase as the countercation size decreases. This effect can be seen from Table I, which lists the k_T and r_M values for some isostructural fluorozirconates.

The structure of the crystals in Table I can be written in a "shorthand" manner as $M^{II}\{10\}ZrT_4E_4$, indicating that the countercation is divalent with a CN of 10 and that the Zr is eight-coordinate, with four terminal fluorides and four edge (doubly bridging) fluorides. Using the information shown in Table I, the effects of different countercations on k_T can be written as

$$k_T^{-1/3} = 0.0660 \cdot r_M + 0.557 \tag{4}$$

for the $M^{II}\{10\}ZrT_4E_4$ type of structure. In analogy with the Badger rule, the slope of this equation should be nearly the same for other isostructural crystals differing only in the identity of the countercation. This is seen to be the case for the alkali fluorozirconate crystals listed in Table II.

TABLE I. Data for isostructural fluorozirconate crystals containing divalent countercations. The ν_s values are from Ref. 10.

	ν_s (cm^{-1})	k_T (mdyn/Å)	r_M (Å)
α-$SrZrF_6$	578	3.74	1.36
$PbZrF_6$	567	3.60	1.40
β-$BaZrF_6$	562	3.54	1.52

The equation is

$$k_T^{-1/3} = 0.0596 \cdot r_M + 0.534 \quad (5)$$

for the $(M^I\{12\})_2ZrT_6$ type of structure. The coordination number of M^I is $9+3$, and 12 is an acceptable description.[13,14]

Since the ν_s and the r_M values for $MgZrF_6$ are known (Sec. III), it would be possible to estimate from an appropriate equation the frequency expected for an isostructural crystal containing Ba rather than Mg, even though such a crystal does not exist. If an average of the slopes of Eqs. (4) and (5) is used for the new equation, we obtain

$$k_T^{-1/3} = 0.0628 \cdot r_M + 0.539 \quad (6)$$

for the $M^{II}\{6\}ZrT_6$ structure type (r_M for six-coordinate Mg^{2+} is 0.720 Å). This yields a value of 606 cm^{-1} for the frequency of the hypothetical six-coordinate Ba crystal, whose r_M value is 1.35 Å. [The information from Eqs. (4)–(6) is graphed in Fig. 6.]

However, the Ba CN in glasses is almost certainly higher than 6. The results of Shafer and Perry[15] indicate a value of 12, and the most common Ba CN in the known barium fluorozirconate crystals is 11.[16] For comparison with glass spectra, it will therefore be necessary to determine the frequency for a Ba crystal with a higher Ba CN.

B. Effect of countercation coordination number

Equations (4)–(6) apply to the case of substituting countercations of different sizes into isostructural crystals. The effect on ν_s of changing the coordination number of a given countercation is a separate problem. The force constant expected for a hypothetical Li fluorozirconate crystal isostructural with the compounds listed in Table II (i.e., containing 12-coordinate Li) can be calculated from Eq. (5).

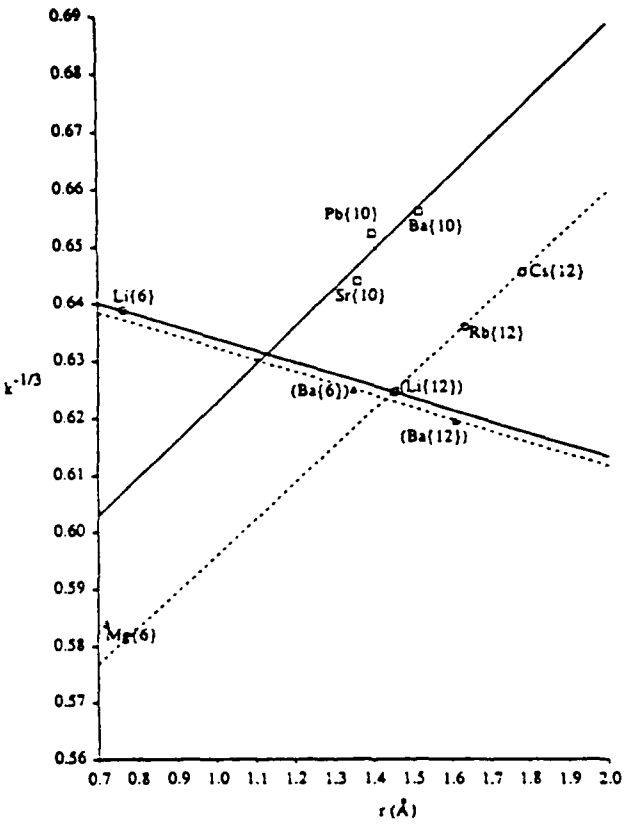

FIG. 6. The lines with positive slope are plots of $k^{-1/3}$ vs countercation radius for different sets of isostructural fluorozirconate crystals. Following the notation used in the text, the solid line refers to $M^{II}\{10\}ZrT_4E_4$, the dashed line to $(M^I\{12\})_2ZrT_6$, and the dotted line to $M^{II}\{6\}ZrT_6$. The lines with negative slope are plots of $k^{-1/3}$ vs countercation CN (converted to radius using Ref. 9). The solid line refers to $(Li\{CN\})_2ZrT_6$ and the dashed line to $Ba\{CN\}ZrT_6$. The parentheses indicate calculated values.

When the data for the crystal with 12-coordinate Li are compared with the information for a crystal containing six-coordinate Li, as in Table III, the following equation for $(Li\{CN\})_2ZrT_6$ results:

$$k_T^{-1/3} = -0.0275 \cdot r_M + 0.660. \quad (7)$$

This equation shows the effects of changing the countercation CN, which has been converted to r_M using Ref. 9. It can be seen that ν_s is expected to increase as the countercation CN increases. Equation (7) may be adapted to the case of $Ba\{CN\}ZrT_6$ by using the same slope and calculating a new intercept based on the value of 606 cm^{-1} calculated from Eq. (6) for the hypothetical $Ba\{6\}ZrT_6$ crystal. This yields

$$k_T^{-1/3} = -0.0275 \cdot r_M + 0.661. \quad (8)$$

TABLE II. Data for isostructural fluorozirconate crystals containing monovalent countercations. The ν_s values for the Rb and Cs compounds are from Refs. 11 and 12, respectively.

	ν_s (cm^{-1})	k_T (mdyn/Å)	r_M (Å)
β-Rb_2ZrF_6	589	3.89	1.72
β-Cs_2ZrF_6	576	3.72	1.88

TABLE III. Data for lithium fluorozirconate crystals containing lithium with different coordination numbers. The ν_s value for the compound with six-coordinate Li is from Ref. 17, and the r_M value for a hypothetical 12-coordinate Li is from an exponential fit of data found in Ref. 9.

	Li CN	ν_s (cm^{-1})	k_T (mdyn/Å)	r_M (Å)
Li_2ZrF_6	12	(606)	(4.12)	(1.45)
Li_2ZrF_6	6	585	3.84	0.76

This means that the $BaZrT_6$ crystal with a Ba CN of 12 ($r_M = 1.61$ Å) would exhibit a ν_s of about 616 cm^{-1}. Figure 6 shows Eqs. (4)–(8) graphically.

This calculated ν_s of 616 cm^{-1} may be compared with the results from Raman studies of a series of $BaM^{IV}T_6$ compounds containing 12-coordinate Ba. The ν_s information in Table IV is from Ref. 18. The ν_s value for $BaSnF_6$ was not included because there is disagreement as to whether it is isostructural with the three compounds listed.[19,20] The original form of the Badger rule [Eq. (1)] could be used for the calculation of ν_s for an isostructural $Ba\{12\}ZrT_6$ crystal, but $r_{M(IV)}$ [where M(IV) refers to the central cation] will be used rather than r_e because there are no consistent r_e data for all three substances. The equation is

$$k_T^{-1/3} = 0.148 \cdot r_{M(IV)} + 0.522. \quad (9)$$

This leads to a value of 600 cm^{-1} for the hypothetical isostructural $Ba\{12\}ZrT_6$ crystal ($r_{M(IV)} = 0.72$ Å). Both of the methods used for calculating the ν_s of this crystal are necessarily in error to some degree. Since it is not known which value is "better," we will use the average of the two 608 cm^{-1} in subsequent calculations.

C. The relation between force constant and bond strength

The concept of bond strength, or bond valence, in inorganic compounds was first described by Pauling.[21] If Z is the charge on a cation and CN is its coordination number, then the average bond strength s is given by

$$s = \frac{Z}{CN}. \quad (10)$$

In other words, the sum of the bond strengths around a cation is equal to the charge on the cation. Brown and Altermatt[22] devised an empirical relation between bond strength and r_e:

$$s = e^{(1.846 - r_e)/0.37}. \quad (11)$$

The above equation contains constants specific to the case of Zr bonded to F. Equations (1) and (11) may be combined to yield

$$k^{-1/3} = C \ln s + D. \quad (12)$$

The terminal bond strength for a F-about-Zr structure may be obtained by assuming that the bridging bond strength is a certain fraction of the terminal bond strength. Other authors[23,24] have observed that bridging force constants k_B for halogen-bridged complexes are about 50%–75% of the terminal force constant k_T. For the barium fluorozirconate crystals known to contain bridging fluorides,[5,25,26] the s_C/s_T ratio is 0.763 and the average s_E/s_T ratio is 0.607, as calculated from Eq. (11). For generality, we will adopt an average s_B/s_T ratio of 0.685, where B signifies a bridging fluoride (corner or edge). Equation (10), which is valid if all bonds around the central cation are of the same type, can be rewritten as

$$n_T s_T + n_B s_B = Z \quad (13)$$

when there are different types of bonds around the cation. In Eq. (13), n_T and n_B are respectively the numbers of terminal fluorides and bridging fluorides per Zr, and $n_T + n_B = CN$. The values of s_T for the different F-about-Zr structures shown in Table V were obtained by substituting $s_B = 0.685 s_T$ and $Z = 4$ into Eq. (13).

The values of s_T from Table V will now be used to predict frequencies for various ZrF_n polyhedra as a function of the Zr CN and of the degree of bridging around Zr. For the compound Ba_2ZrF_8, which is nonstoichiometric and contains some fluoride-ion vacancies,[27] a bond strength of 0.5130 calculated from Eq. (11) and the Zr–T r_e of ~2.093 Å was used rather than the value of 0.5000 expected for an ideal crystal.

From the data of Table VI we can write

$$k_T^{-1/3} = -0.0874 \ln s_T + 0.612, \quad (14)$$

which gives the effect of bridging on k_T for barium fluorozirconates containing eight-coordinate Zr. Increased bridging on Zr for a given CN should increase ν_s.

The data of Table VII yield the equation

$$k_T^{-1/3} = -0.183 \ln s_T + 0.549, \quad (15)$$

which describes the effect of changing the Zr CN. This effect is larger than that due to bridging—the slope of Eq. (15) is about twice that of Eq. (14). From Eq. (15), the ν_s frequen-

TABLE IV. Data for $BaM^{IV}T_6$ crystals containing barium in 12 coordination. The $r_{M(IV)}$ values here refer to the central cation rather than the countercation.

	ν_s (cm^{-1})	k_T (mdyn/Å)	$r_{M(IV)}$ (Å)
$BaSiT_6$	675.4	5.106	0.400
$BaGeT_6$	640.0	4.585	0.530
$BaTiT_6$	626.2	4.389	0.605

TABLE V. Zr–T bond strengths (s_T) for different types of ZrF_n polyhedra. Terminal and bridging (corner or edge) fluorides are denoted by T and B, respectively. The degree of bridging increases down a column in the direction from a to h.

Zr CN →	6	7	8
a	ZrT_6	ZrT_7	ZrT_8
	0.6667	0.5714	0.5000
b	ZrT_5B	ZrT_6B	ZrT_7B
	0.7036	0.5984	0.5205
c	ZrT_4B_2	ZrT_5B_2	ZrT_6B_2
	0.7449	0.6279	0.5427
d	ZrT_3B_3	ZrT_4B_3	ZrT_5B_3
	0.7913	0.6606	0.5670
e		ZrT_3B_4	ZrT_4B_4
		0.6969	0.5935
f		ZrT_2B_5	ZrT_3B_5
		0.7373	0.6226
g			ZrT_2B_6
			0.6547
h			$ZrTB_7$
			0.6903

TABLE VI. Data for barium fluorozirconate crystals containing eight-coordinate Zr and different degrees of bridging between Zr ions. The ν_s value for β-$BaZrF_6$ (Ba CN = 10) has been increased from 562 cm^{-1} to reflect 12-coordination of Ba.

	ν_s (cm^{-1})	k_T (mdyn/Å)	s_T
β-$BaZrF_6$	565	3.57	0.6223
Ba_2ZrF_6	544	3.31	0.5130 (from r_e)

TABLE VIII. Data for barium fluorozirconate crystals containing seven-coordinate Zr and different degrees of bridging between Zr ions. The ν_s value for β-$BaZr_2F_{10}$ (Ba CN = 11) has been changed from 590 cm^{-1} to reflect 12-coordination of Ba.

	ν_s (cm^{-1})	k_T (mdyn/Å)	s_T
β-$BaZr_2F_{10}$	592	3.92	0.6969
$Ba_{1.5}ZrT_7$	(569)	(3.62)	0.5714

cy for the hypothetical $Ba_{1.5}ZrT_7$ crystal, which has bond strengths of $4/7 \approx 0.5714$, is 569 cm^{-1}.

From the data in Table VIII, the effect of bridging on seven-coordinate Zr units can be written in the following form:

$$k_T^{-1/3} = -0.0842 \ln s_T + 0.604. \quad (16)$$

The average of the slopes of Eqs. (14) and (16) can be used to obtain the equation describing the effect of bridging in compounds containing six-coordinate Zr

$$k_T^{-1/3} = -0.0858 \ln s_T + 0.588. \quad (17)$$

Obviously, the sparse amount of data available for crystalline fluorozirconates limits the accuracy of the above method. However, the qualitative trends seem to be clear. If other factors are equal, ν_s increases with decreasing countercation radius, increasing countercation CN, decreasing Zr CN, and increasing degree of bridging. Table IX is the result of attempts to quantify the separate effects of these influences and should be correct in at least the *relative* magnitudes of the frequencies shown.

D. Effect of countercation charge

The charge on the countercations surrounding a given type of ZrF_n group can have a considerable effect on the symmetric stretching frequency. As an example, Li_2ZrF_6 and $MgZrF_6$ have the same Zr CN (6) and F-about-Zr arrangement (discrete ZrT_6^{2-} anions), the same countercation CN (6), and almost the same countercation radius (0.76 Å for Li vs 0.72 Å for Mg). However, the ν_s for Li_2ZrF_6 is 585 cm^{-1},[17] and for $MgZrF_6$ it is 669 cm^{-1}. The size difference is very small and would account for only about 4 cm^{-1} of the difference in frequency.

Although it seems that the substitution of monovalent countercations for divalent ones serves to decrease ν_s, there is apparently no systematic way to predict directly the effects of substitution; rather, the two classes of crystals must be considered separately. A table analogous to Table IX can be constructed for the case of a monovalent cation. We will use eight-coordinate Na^+ and six-coordinate Li^+ as the base countercations. The slopes of Eqs. (7) and (8) are applicable to monovalent fluorozirconates, because they were derived for crystals which have similar structures and differ only in countercation size or CN. Equations (14)–(17), on the other hand, apply to crystals with the same countercation, but with ZrF_n units differing in degree of bridging or in Zr CN. Therefore, Eqs. (14)–(17) apply specifically to 12-coordinate Ba and would be expected to have different slopes when determined for monovalent countercations.

To illustrate, the frequency for $(Na\{6\})_2ZrT_6$ (which is not known to exist) can be calculated from the $(Li\{6\})_2ZrF_6$ frequency from the following equation, which has the same slope as Eq. (6):

TABLE VII. Data for barium fluorozirconate crystals with different Zr coordination numbers. The k_T value for the hypothetical $BaZrT_6$ crystal with 12-coordinate Ba was calculated previously.

	ν_s (cm^{-1})	k_T (mdyn/Å)	s_T
$BaZrT_6$	(608)	(4.14)	0.6667
Ba_2ZrT_6	544	3.31	0.5130 (from r_e)

TABLE IX. Estimated barium fluorozirconate frequencies in cm^{-1} for different types of ZrF_n polyhedra in the presence of 12-coordinate Ba ions. Terminal and bridging (corner or edge) fluorides are denoted by T and B, respectively. Diagonal lines enclose structures with the same composition. The compositions are given in mole percent ZrF_4.

Zr CN →	6	7	8	
a	ZrT_6 608	ZrT_7 569	ZrT_8 541	33.3 % ZrF_4 F/Zr = 8.0
b	ZrT_5B 615	ZrT_6B 574	ZrT_7B 545	36.4 % ZrF_4 F/Zr = 7.5
c	ZrT_4B_2 622	ZrT_5B_2 579	ZrT_6B_2 550	40.0 % ZrF_4 F/Zr = 7.0
d	ZrT_3B_3 630	ZrT_4B_3 585	ZrT_5B_3 554	44.4 % ZrF_4 F/Zr = 6.5
e		ZrT_3B_4 591	ZrT_4B_4 559	50.0 % ZrF_4 F/Zr = 6.0
f		ZrT_2B_5 598	ZrT_3B_5 564	57.1 % ZrF_4 F/Zr = 5.5
g			ZrT_2B_6 570	66.7 % ZrF_4 F/Zr = 5.0
h			$ZrTB_7$ 576	80.0 % ZrF_4 F/Zr = 4.5

TABLE X. Estimated fluorozirconate frequencies in cm^{-1} for different types of ZrF_n polyhedra with monovalent countercations. Two frequencies immediately below a ZrF_n unit refer respectively to Na{8} and Li{6} ions, and a frequency in brackets is the frequency calculated for a Na/Li mole ratio of 0.535/0.465. Terminal and bridging (corner or edge) fluorides are denoted by T and B, respectively. Diagonal lines enclose structures with the same composition. The compositions are given in mole percent ZrF_4.

Zr CN →	6	7	8	
a	ZrT_6 567,585 [575]	ZrT_7 558,576 [566]	ZrT_8 550,568 [558]	20.0 % ZrF_4 F/Zr = 8.0
	ZrT_5B [>575]	ZrT_6B [~566]	ZrT_7B [~558]	22.2 % ZrF_4 F/Zr = 7.5
c	ZrT_4B_2 [>575]	ZrT_5B_2 [~566]	ZrT_6B_2 [~558]	25.0 % ZrF_4 F/Zr = 7.0
d	ZrT_3B_3 [>575]	ZrT_4B_3 [~566]	ZrT_5B_3 [~558]	28.6 % ZrF_4 F/Zr = 6.5
e			ZrT_4B_4 [~558]	33.3 % ZrF_4 F/Zr = 6.0
f			ZrT_3B_5 [~558]	40.0 % ZrF_4 F/Zr = 5.5

$$k_T^{-1/3} = 0.0628 \cdot r_M + 0.592. \quad (18)$$

This yields a frequency of 562 cm^{-1}. In order to change six-coordinate Na ($r_M = 1.02$ Å) to eight-coordinate ($r_M = 1.18$ Å), we use an equation with the slope of Eq. (7):

$$k_T^{-1/3} = -0.0275 \cdot r_M + 0.685. \quad (19)$$

This gives 567 cm^{-1} for the 6a position of the new table (Table X). The crystal Na_3ZrF_7 contains seven-coordinate Na ($r_M = 1.12$ Å) and has a ν_s of 556 cm^{-1}.[17] Its analog with eight-coordinate Na would have a frequency of 558 cm^{-1}. We can now calculate the equation analogous to Eq. (15)

$$k_T^{-1/3} = -0.0549 \ln s_T + 0.629. \quad (20)$$

As expected, the slope of the equation for Zr CN dependence is different for the cases of monovalent and divalent countercations. In fact, the slope of Eq. (20) (monovalent) is only about 30% that of Eq. (15) (divalent). Using Eq. (20), we obtain an estimated ν_s of 549 cm^{-1} for $(Na\{8\})_4ZrT_8$.

To investigate the effect of bridging, it is necessary to know the ν_s for a sodium fluorozirconate with bridging fluorides. The compound $Na_7Zr_6F_{31}$ contains Na with an average CN of 10.3 and eight-coordinate Zr with six bridging fluorides (F/Zr ratio = 5), but there is an "extra," non-bonded fluoride for every six Zr ions.[28] This probably serves to make the known frequency of 548 cm^{-1} artificially low. (It would be even lower when adjusted to eight-coordinate Na.) Instead, the ν_s of 525 cm^{-1} for $(K\{8\})_2ZrT_4E_4$ from Ref. 17 will be adjusted to the frequency appropriate to $(Na\{8\})_2ZrT_4E_4$—i.e., 550 cm^{-1}. This means that, within the limitations of the very approximate framework outlined above, the effect of bridging on ν_s in fluorozirconates containing monovalent countercations is essentially negligible. This result agrees with the Raman spectra of lithium/sodium fluorothorate melts, which showed no effect on ν_s as bridging increased around the seven-coordinate Th ions.[29]

In analogy with the behavior of divalent fluorozirconates, it is probable that there is actually a small increase due to bridging in monovalent fluorozirconates. This increase would be more pronounced for lower coordination numbers. As shown in Table V, terminal bond strengths increase more rapidly with bridging as the Zr CN is decreased. Table X summarizes the estimated frequencies for sodium and lithium fluorozirconates.

V. DISCUSSION

A. Origins of environmental effects

1. Countercation radius

The general trend of an increase in frequency with decreasing size of countercation in infrared spectroscopy has been noted by Adams[23] and by Ferraro.[30] The same trend is observed in Raman spectra of fluorothorate melts[29] and fluoroberyllate crystals and melts.[31] The substitution of smaller countercations requires that the ZrF_n species be packed together more closely. Apparently, the presence of smaller countercations increases ν_s because of increased fluoride–fluoride short-range repulsions between the more closely packed ZrF_n units.[31]

2. Countercation coordination number

As the countercation coordination number is increased, it is expected that the packing around the countercations would become more efficient, leading to greater fluoride-fluoride repulsions between neighboring ZrF_n units and an increase in ν_s, as in the case of smaller countercations discussed above. This is seen to be the case, but the effect is not very pronounced. The magnitude of the slope of Eq. (6) (radius) is about three times the magnitude of the slope of Eq. (7) (CN).

3. Zirconium coordination number

The CN of the central cation is known to exert a predictable and significant effect on Raman stretching frequencies.[23] An increase in CN always leads to a decrease in frequency due to the decrease in bond order, as seen from Tables V and IX. The effect of changing the zirconium coordination number in fluorozirconates is larger than the effect of bridging. The slope of Eq. (15) (Zr CN) is about twice times that of Eq. (14) (bridging).

4. Degree of bridging about zirconium

The occurrence of bridging around Zr (with the CN kept constant) leads to an increase in ν_s. It is known from fluorozirconate crystal chemistry that bridging gives rise to shorter terminal bonds.[32] As Zr–T bonds are replaced by longer, weaker Zr--B bonds, electron density on the Zr is shifted to the remaining Zr–T bonds. So, even though the *average* bond order as defined by Eq. (10) does not change, the *terminal* bonds (which are the source of the ν_s band[33]) are stronger than before. In addition, the average strength of a bridging bond (assumed earlier to be a certain fraction of the terminal bond strength) increases with increased bridging. These trends were recognized by Almeida and Mackenzie,[33] who studied fluorozirconates and fluorohafnates.

The manifestation of the decrease in Zr–T bond length in the form of ν_s requires the assumption of separability of the motions of the different types of fluorides (bridging or nonbridging) about the Zr ion. In other words, separability of fluoride-ion movements means that a normal mode of vibration can be approximated as involving primarily one type of fluoride-ion movement. Any cooperative movement between different types of fluorides would necessarily entail the movement of the zirconiums. Since a zirconium ion is about five times heavier than a fluoride ion, the Zr ions can be considered to remain motionless on the time scale of fluoride-ion movements, and the approximation of separability is acceptable in this case. In fact, the ν_s peak (due to terminal fluorides) disappears completely for crystalline HfF_4 and β-ZrF_4, which contain only bridging fluorides.[34,35] Crystalline chlorocadmates (Cd/Cl weight ratio is ~ 3) show the same trend of increased terminal-ligand frequency with increased bridging.[36]

For lighter central cations, however, this picture is inadequate. In the case of melts containing beryllium fluoride, Toth *et al.*[37] have shown that increased bridging about Be leads to a decrease in the totally symmetric stretching frequency. Separability cannot be assumed in this case because the weight of a Be ion is about half that of a fluoride ion, and Be is therefore ineffective in behaving as a "buffer" between movements of different types of fluorides. The Raman bands

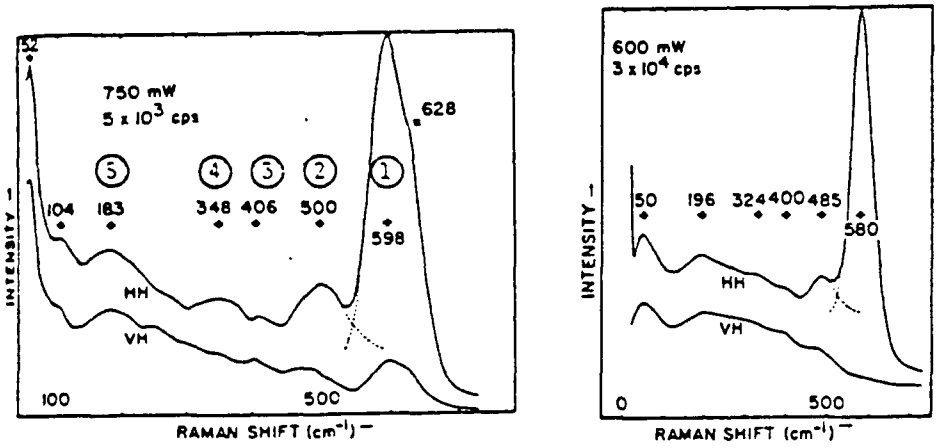

74 mol % ZrF_4 64 mol % ZrF_4

FIG. 7. Raman spectra of some barium fluorozirconate glasses (adapted from Ref. 3). The high-frequency peaks are the source of the ν_s frequencies. The ν_s peak for the 74 mol% ZrF_4 composition is labeled "1."

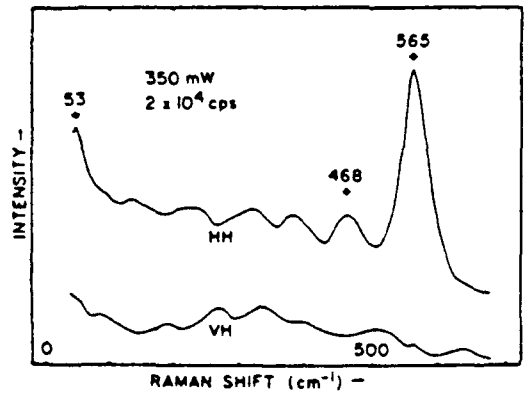

52 mol % ZrF_4

are due to normal modes involving the Be_xF_y polymeric unit as a whole. The decrease in frequency is due, not to a decrease in overall bond order, but to a greater value of the reduced mass of the vibrating species.

5. Countercation charge

The effect of the countercation charge on ν_s is related to the packing effect mentioned above. For a given F-to-Zr ratio, the number of monovalent countercations needed for charge balancing is twice the number necessary for divalent countercations. This means that if all other factors are equal, i.e., countercation radius, countercation CN, Zr CN, and degree of bridging, then the packing requirements will be more stringent in the case of divalent countercations, and the ν_s will be higher. The extra monovalent cations provide more shielding between the ZrF_n units. Perhaps the effectiveness of monovalent countercations in separating the ZrF_n groups helps to explain the greatly lessened consequences of bridging and Zr CN on the ν_s frequencies of monovalent fluorozirconates as compared to divalent fluorozirconates.

B. Application to interpretation of glass spectra

Assuming that the frequencies presented in Table IX are roughly correct, some possible structures for a fluorozirconate glass with a given composition are immediately precluded. Figure 7 shows the Raman spectra obtained by Almeida and Mackenzie[3] for three binary barium fluorozirconate glass compositions. For the composition containing 64 mol% ZrF_4 (referred to as the dizirconate composition), the measured ν_s value is 580 cm^{-1}. From a comparison with the ν_s of 585 cm^{-1} of Li_2ZrF_6, the authors concluded that the Zr ions were six-coordinate. From the F-to-Zr ratio of the composition, they added the requirement that two of the six fluorides be bridging. This structure corresponds to the ZrT_4B_2 unit in position 6c of Table IX. However, Table IX predicts an approximate ν_s of 622 cm^{-1} for this proposed structure in the presence of 12-coordinate Ba^{2+} countercations. For the dizirconate composition, the structures possessing the closest frequencies to the experimental one are found in positions 8g and 7e—in other words, in the columns containing seven- and eight-coordinate Zr.

It is reasonable that the ZrT_4B_2 structure would have such a high frequency, since it applies to six-coordinate Zr with divalent countercations (recall the ν_s of 669 cm^{-1} for $MgZrF_6$). In addition, there is bridging in the structure, a condition which serves to increase the frequency. So even if the predicted frequency of 622 cm^{-1} is too high by a relatively large amount, even say 30 cm^{-1}, the ν_s frequency of a barium fluorozirconate glass with ZrT_4B_2 units would still be expected to be much higher than the observed frequency of 580 cm^{-1}. Almeida and Mackenzie reject the idea of eight-coordinate Zr in the glasses on the basis of the ν_s of only 525 cm^{-1} for α-K_2ZrF_6, which is known to contain Zr in eight coordination, but, as discussed in Sec. V A, the effects of raising the countercation CN and replacing monovalent cations by divalent ones both contribute to a higher ν_s. Also, since α-K_2ZrF_6 has a F-to-Zr ratio of 6, an additional two fluorides would have to be bridging in order to satisfy the dizirconate F-to-Zr ratio of 5; this would lead to an even higher value of the expected frequency. In the end, the predicted frequency of the ZrT_2B_6 unit in Table IX is 570 cm^{-1}, not too far from the observed ν_s of 580 cm^{-1} for the dizirconate glass.

The ν_s value of 565 cm^{-1} for the 52 mol% ZrF_4 glass in Fig. 7 coincides with the expected frequency for bridged, eight-coordinate Zr ions. Table IX predicts a value of about 559 cm^{-1} for the unit in position 8e.

The glass with 74 mol% ZrF_4 has a ν_s of 598 cm^{-1} and Table IX gives an interpolated frequency of about 573 cm^{-1} for eight-coordinate ZrF_n units. To account for the higher measured frequency, it must be assumed that the Zr atoms containing nonbridging fluorides are mainly seven coordinate. The interpolated frequency from Table IX for seven-coordinate Zr polyhedra at a composition of 74 mol% ZrF_4 is 595 cm^{-1}. Note that this does not necessarily mean that the predominant overall CN of Zr in the glass is 7. As the percentage of ZrF_4 becomes large, there will be fewer zirconiums with terminal fluorides, so the environment around these Zr atoms will be disproportionately represented in the value of ν_s.

An interesting sideline about the utility of Table IX is its interpretation of the origin of the high-frequency shoulder at about 628 cm^{-1} in the spectrum of the 74 mol% ZrF_4 glass in Fig. 7. Almeida and Mackenzie attributed this feature to the presence of five-coordinate Zr in the glass, even though five-coordination of Zr has never been observed in fluorozirconate crystals. The frequency agrees with the interpolated ν_s of 626 cm^{-1} for a mixture of the six-coordinate ZrT_4B_2 and ZrT_3B_3 units of Table IX.

C. Application to interpretation of crystal spectra

Another point can be made in the application of Table IX to the explanation of the ν_s value (560 cm^{-1}) of the α-$BaZrF_6$ crystal. In the report of the crystal structure of this polymorph,[26] it was mentioned that the ZrT_5B_2 structure of α-$BaZrF_6$ is clearly more irregular than that found in $K_2Cu(ZrF_6)_2 \cdot 6H_2O$ and that the crystal can alternatively be described as containing eight-coordinate Zr units connected together in zigzag chains. In this case, Table IX predicts a frequency of 559 rather than the 579 cm^{-1} expected for seven coordination. However, the inclusion of the eighth relatively distant F from a neighboring ZrF_n group does not alter the essential character of the basic ZrT_5B_2 unit and may therefore lead to a "quasi-ZrT_5B_3" structure, as viewed by Raman spectroscopy. Table IX shows a ν_s of 554 cm^{-1} for this structure. This interpretation explains the otherwise puzzling relative order of the ν_s values of β-$BaZrF_6$ (562 cm^{-1}, Ba CN of 10, Zr CN of 8) and α-$BaZrF_6$ (560 cm^{-1}, Ba CN of 11, ostensible Zr CN of 7).

D. Application to interpretation of melt spectra

Toth *et al.*[17] obtained Raman spectra for fluorozirconate melts containing Li and Na as countercations. They concluded that the melts contained discrete ZrF_n^{4-n} complex ions, where n is between 5 and 8 (and perhaps can be 4).

Table X, prepared for the case of ZrF_n units in the presence of eight-coordinate Na or six-coordinate Li, is applicable to the interpretation of melt spectra if it is assumed that the frequencies do not change drastically with increasing temperature (a justifiable assumption, according to Toth *et al.*[17]) and that Na is close to eight coordinate in the melt. It will also be assumed that Li is six coordinate in the melt and that the ν_s values can be calculated from 0.535 times the Na value plus 0.465 times the Li value, in accordance with the mole ratios of these ions in the melts.

Toth *et al.* assumed the existence of eight-coordinate Zr in the melt when the F/Zr ratios were very high (between 8 and ~10). This seems to be a viable assumption; they observed melt frequencies of 555 and 554 cm^{-1}, and the frequency from Table X for ZrF_8^{4-} is 558 cm^{-1} for a F/Zr ratio of 8. As the F/Zr ratio is decreased, the ν_s values increase. This was interpreted by Toth *et al.* as evidence for a decrease in the average Zr CN and this also seems reasonable. Table X predicts frequencies of 566 and 575 cm^{-1} for ZrF_7^{3-} and ZrF_6^{2-} anions, respectively.

The lowering of the melt F/Zr ratio below 6 seems to have caused a somewhat abrupt jump in the ν_s, as well as the appearance of a new low-frequency band at 165 cm^{-1}. For the 40 mol% ZrF_4 melt (F/Zr ratio of 5.5), Toth *et al.* conclude from the relatively high frequency of 593 cm^{-1} that species with four- or five-coordinate Zr are present. The existence of neutral ZrF_4 molecules in the melt would be a little surprising, considering the well-known volatility of ZrF_4 at elevated temperatures, but five-coordinate Zr has been indicated previously in surface-tension measurements of fluorozirconate melts containing monovalent counterions.[38] The value of ν_s predicted for ZrF_5^- is 586 cm^{-1}, which is somewhat low. Although the presence of some four-coordinate Zr cannot be ruled out, it is also possible that a higher ν_s could be due to the formation of $Zr_2F_9^-$ dimers. It is conceivable that the occurrence of bridged five-coordinate ZrF_n groups would lead to an extra feature in the bending region of the spectrum; this would explain the 165 cm^{-1} peak. The experimental and calculated frequencies are compared in Table XI.

The effects of bridging, if present, would be expected to be much more pronounced in the divalent-countercation melts. Because of this phenomenon, Raman spectroscopy would be expected to yield detailed information concerning the extent of bridging in fluorozirconate melts containing only divalent countercations. Currently, there are very few experimental data on this subject, but the higher viscosities of the melts with divalent cations as opposed to monovalent cations[39,40] may indicate an increased occurrence of bridging. Spectroscopic studies focusing on variations in composition and temperature of fluorozirconate melts would be very useful. A better understanding of the melt structure would elucidate the properties of "fragile" liquids (as described by Angell[41]) and would probably lend insight into glass formation in these systems.

TABLE XI. Measured Raman frequencies for LiF–NaF–ZrF_4 melts at a constant LiF–NaF ratio of 0.465/0.535. Experimental data are taken from Ref. 17.

Mol% ZrF_4	F/Zr ratio	Measured ν_s (cm^{-1})	Calculated ν_s (cm^{-1})	Species present
14	10.14	555	558	ZrF_8^{4-}
20	8.00	554	558	ZrF_8^{4-}
25	7.00	568	566	ZrF_7^{3-}
29	6.45	573	571	ZrF_7^{3-} + ZrF_6^{2-}
33	6.03	577	575	ZrF_6^{2-}
40	5.50	593	?	ZrF_6^{2-} + ZrF_5^- + $Zr_2F_9^-$? + ZrF_4 ?

VI. SUMMARY AND CONCLUSIONS

This paper has presented a frequency-structure correlation scheme derived from Raman spectroscopy results. It resolves a long-standing controversy over the Zr coordination number in barium fluorozirconate glasses as measured by x-ray experiments[45,46] and from previous interpretations of Raman spectroscopy results.[3,47] Specifically, for the prototypical dizirconate ($BaZr_2F_{10}$) glass composition, x-ray results indicate a CN between 7 and 8 for Zr, and the Raman results were interpreted as indicating a Zr CN of 6. In the present treatment, the reinterpretation of the Raman data reveals that the Zr CN is between 7 and 8 (~7.5) for the dizirconate composition, in agreement with x-ray information.

For the 52 mol% ZrF_4 composition, the present paper concludes that the Zr CN is about 8, and the CN of Zr atoms with one or more terminal fluorides in the 74 mol% ZrF_4 glass is mostly 7, with some six coordination. As with the dizirconate composition, these coordination numbers are higher than those deduced by Almeida and Mackenzie[3]—7 for the 52 mol% ZrF_4 glass, and 6 plus some five coordination for the 74 mol% ZrF_4 glass.

As discussed in Sec. V B, the key problem in the previous Raman interpretations stemmed from the use of a fluorozirconate crystal containing *monovalent* countercations as the basis for comparison with the spectra of glasses containing *divalent* countercations. This paper has shown that variations in the countercations in fluorozirconate glasses or crystals can cause marked changes in the ν_s frequencies. It is therefore very important to compare similar compositions when attempting to interpret fluorozirconate glass structure from vibrational spectra.

Walrafen *et al.*[48] have interpreted their Raman data for many fluorozirconate glasses solely in terms of the stoichiometric F/Zr ratio. In other words, their treatment was essentially based on only one variable, the CN of Zr. They compared several quite disparate compositions in spite of the possibility for serious complications in interpretation. Their choice of compositions included somewhat random mixtures of monovalent, divalent, and trivalent countercations, and even a combination of network formers (ZrF_4 and ThF_4) was used. Their assumption that bridging has almost no effect on ν_s was based on the fact that the measured ν_s for their glass with a F/Zr ratio of 6 is similar to the frequencies observed for an aqueous solution of Na_2ZrF_6 and a melt of unreported composition, neither of which is expected to ex-

hibit substantial bridging. However, the glass chosen for comparison contains much more BaF_2 than NaF, and its frequency cannot be directly compared with the solution and melt data. It seems that the agreement among the three frequencies may be simply fortuitous.

It is also to be noted that the method presented here can be related to bond lengths through its connection to bond strengths [Eq. (11)]. This means that results from experimental methods which yield information in terms of bond lengths [such as extended x-ray-absorption fine-structure spectroscopy (EXAFS)] should be interpreted with the same care as the frequencies from Raman spectroscopy. In other words, comparison of barium fluorozirconate glass EXAFS spectra with those from alkali-metal fluorozirconate crystals is not advised and can lead to wrong conclusions, as we believe is the case in Ref. 49. In addition, only average bond lengths are obtained from EXAFS. This means that if bridging is involved, the interpretation of results becomes even more ambiguous.

In summary, the approach outlined in this paper is approximate and involves many assumptions. Even so, it appears to provide a plausible explanation for the observed ν_s frequencies in binary barium fluorozirconate glasses and crystals, as well as monovalent-countercation fluorozirconate melts. If there are inaccuracies in the absolute magnitudes of the predicted frequencies for given structures, it is at least probable that the relative magnitudes are correct. In spite of the paucity of available data, there are definite, identifiable trends in the effects of certain variables on the ν_s frequencies. We have attempted to analyze and quantify these trends in order to clarify the murky situation which has surrounded the interpretation of fluorozirconate glass data for some time. As an example, we quote Kawamoto[10]: "...no consistent correlation can be deduced between the ν_s and the F coordination number of Zr in fluorozirconate compounds... . Moreover, when bridging takes place between the F complex ions, it should give many complicated effects on the ν_s vibrations... . The above concludes that the Raman ν_s frequency cannot be utilized as a reliable guide for identifying the F coordination number of Zr in a fluorozirconate complex with unknown structure." We hope to have disproved these statements, at least to some degree.

ACKNOWLEDGMENTS

This work has been supported by the Office of Naval Research under Agreement No. N00014-84K0289. We are indebted to Professor M. Weaver for his willingness to allow the use of his excellent Raman facilities in the execution of part of this research and for his overall encouragement in the project.

[1] M. Poulain and J. Lucas, C. R. Acad. Sci. Ser. C, 271, 822 (1970).
[2] J.-P. Laval, B. Frit, and B. Gaudreau, Rev. Chim. Min. 16, 509 (1979).
[3] R. M. Almeida and J. D. Mackenzie, J. Chem. Phys. 74, 5954 (1981).
[4] C. C. Phifer, C. A. Angell, J.-P. Laval, and J. Lucas, J. Non-Cryst. Solids 94, 315 (1987).
[5] J.-P. Laval, B. Frit, and J. Lucas, J. Solid State Chem. 72, 181 (1988).
[6] R. M. Badger, J. Chem. Phys. 3, 710 (1935).
[7] R. M. Badger, J. Chem. Phys. 2, 128 (1934).
[8] J. Waser and L. Pauling, J. Chem. Phys. 18, 747 (1950).
[9] R. D. Shannon, Acta Crystallogr. Part A 32, 751 (1976).
[10] Y. Kawamoto and F. Sakaguchi, Bull. Chem. Soc. Jpn. 56, 2138 (1983).
[11] I. W. Forrest and A. P. Lane, Inorg. Chem. 15, 265 (1976).
[12] P. A. W. Dean and D. F. Evans, J. Chem. Soc. A 1967, 698.
[13] J. L. Hoard and W. B. Vincent, J. Am. Chem. Soc. 61, 2849 (1939).
[14] S. Siegel, Acta Crystallogr. 5, 683 (1952).
[15] M. W. Shafer and P. Perry, Mater. Res. Bull. 14, 899 (1979).
[16] C. C. Phifer, Ph.D. thesis, Purdue University, December 1988.
[17] L. M. Toth, A. S. Quist, and G. E. Boyd, J. Phys. Chem. 77, 1384 (1973).
[18] D. Breitinger and U. Kristen, J. Solid State Chem. 22, 233 (1977).
[19] R. Hoppe, Rec. Trav. Chim. 75, 569 (1956).
[20] B. Cox, J. Chem. Soc. 1956, 876.
[21] L. Pauling, J. Am. Chem. Soc. 51, 359 (1929).
[22] I. D. Brown and D. Altermatt, Acta Crystallogr. Part B 41, 244 (1985).
[23] D. M. Adams, *Metal–Ligand and Related Vibrations* (St. Martin's, New York, 1968).
[24] D. M. Adams and R. G. Churchill, J. Chem. Soc. A 1968, 2141.
[25] J.-P. Laval, D. Mercurio-Lavaud, and B. Gaudreau, Rev. Chim. Min. 11, 742 (1974).
[26] J.-P. Laval, R. Papiernik, and B. Frit, Acta Crystallogr. Part B 34, 1070 (1978).
[27] J.-P. Laval and B. Frit, Acta Crystallogr. Part B 36, 2533 (1980).
[28] J. H. Burns, R. D. Ellison, and H. A. Levy, Acta Crystallogr. Part B 24, 230 (1968).
[29] L. M. Toth and G. E. Boyd, J. Phys. Chem. 77, 2654 (1973).
[30] J. R. Ferraro, *Low-Frequency Vibrations of Inorganic and Coordination Compounds* (Plenum, New York, 1971), p. 7.
[31] J. B. Bates and A. S. Quist, Spectrochim. Acta Part A 31, 1317 (1975).
[32] I. P. Kondratyuk, M. F. Eiberman, R. L. Davidovich, M. A. Medkov, and B. V. Bukvetskii, Koord. Khim. 7, 1109 (1981).
[33] R. M. Almeida and J. D. Mackenzie, J. Chem. Phys. 78, 6502 (1983).
[34] M. Goldstein, R. J. Hughes, and W. D. Unsworth, Spectrochim. Acta Part A 31, 621 (1975).
[35] Y. Kawamoto, Phys. Chem. Glasses 25, 88 (1984).
[36] J. H. R. Clarke, P. J. Hartley, and Y. Kuroda, J. Phys. Chem. 76, 1831 (1972).
[37] L. M. Toth, J. B. Bates, and G. E. Boyd, J. Phys. Chem. 77, 216 (1973).
[38] G. W. Mellors and S. Senderoff, J. Electrochem. Soc. 111, 1355 (1964).
[39] H. Hu and J. D. Mackenzie, J. Non-Cryst. Solids 54, 241 (1983).
[40] J. E. Shelby, C. G. Pantano, and A. A. Tesar, J. Am. Ceramic Soc. 70, C-164 (1970).
[41] C. A. Angell, in *Relaxations in Complex Systems*, edited by K. Ngai and G. B. Wright (National Technical Information Service, U.S. Dept. of Commerce, Springfield, Va., 1985).
[42] M. Poulain, M. Poulain, and J. Lucas, Mater. Res. Bull. 7, 319 (1972).
[43] M. Poulain, M. Poulain, and J. Lucas, J. Solid State Chem. 8, 132 (1973).
[44] H. W. Mayer, D. Reinen, and G. Heger, J. Solid State Chem. 50, 213 (1983).
[45] R. Coupé, D. Louër, J. Lucas, and A. J. Léonard, J. Am. Ceramic Soc. 66, 523 (1983).
[46] G. Etherington, L. Keller, A. Lee, C. N. J. Wagner, and R. M. Almeida, J. Non-Cryst Solids 69, 69 (1984).
[47] R. M. Almeida and J. D. Mackenzie, J. Chem. Phys. 78, 6502 (1983).
[48] G. E. Walrafen, M. S. Hokmabadi, M. R. Shariari, G. H. Sigel, Jr., R. Pafchek, A. Elyamani, and M. Poulain, Proc. SPIE 929, 133 (1988).
[49] F. Ma, Z. Shen, L. Ye, M. Zhang, K. Lu, and Y. Zhao, J. Non-Cryst. Solids 99, 387 (1988).

Journal of Non-Crystalline Solids 140 (1992) 350–358
North-Holland

JOURNAL OF
NON-CRYSTALLINE SOLIDS

Vibrational spectra in fluoride crystals and glasses at normal and high pressures by computer simulation

B. Boulard [1], J. Kieffer [2], C.C. Phifer [3] and C.A. Angell
Arizona State University, Department of Chemistry, Tempe, AZ 85287-1604, USA

Molecular dynamics computer simulation methods to obtain the infrared and Raman spectra of ionic liquids and glasses are described. These methods are applied to two problems: (1) the simulation and interpretation of the vibrational spectra of heavy metal fluoride glasses, and (2) the problem of reversible collapse of network glasses and the dramatic spectroscopic consequences of this collapse observed in recent experiments on SiO_2-like glasses. As a contribution to this latter problem, the case of BeF_2, for which our rigid ion potentials should be good approximations to the actual interactions, is studied. In the spectra, an initial network stiffening with increase of pressure, followed by rather sudden collapse to a spectrum characteristic of a higher coordinated state, is observed. This is correlated with a sudden increase in average coordination numbers. The changes are mostly reversible on decompression, so the behavior is reminiscent of the transition between 'vitreous polymorphs' observed in the case of vitreous water and vitreous silica.

1. Introduction

In the development of models for the structure of fluoride glasses, vibrational spectroscopy has played an important and often controversial role [1–6]. A key problem has been [6] the proper accounting for all the structural factors which can affect the frequency of the most prominent Raman spectroscopic feature, the symmetric stretching mode involving the terminal fluoride ions in the Zr coordination shell. An obvious way of obtaining definitive information on the relation between structure and vibrational spectra is to calculate both simultaneously for a series of glass structures obtained by the method of molecular dynamics computer simulations. In this laboratory, computer simulations, which have played an important role in the development of some current models for fluoride glass structures [7–9], have been in progress for a number of years. However, it is only recently that the programs necessary to calculate and Fourier transform the time correlation functions appropriate to the standard infrared and Raman spectra have been developed. In this contribution, we present first some tests of the ability of these calculations to reproduce the characteristic spectral frequencies of simple crystalline compounds, and then use them to simulate the spectra of both heavy metal fluoride and BeF_2 glasses. Finally we examine the spectroscopic consequence of major structural change induced by compression of the BeF_2 glass, and compare this with results of recent diamond cell studies on analog oxide glasses.

A key paper in this area is that of Brawer [10], who compared two alternative approaches to the calculation of Raman and infrared spectra by computer simulation methods and showed that they yielded comparable results. The first method involves the use of either of the molecular dynamics or Monte Carlo methods to obtain an equilibrium liquid or a frozen glassy structure and also the forces acting between particles in this

[1] Present address: Laboratoire des Fluorures, UA 449, Faculté des Sciences, Universite du Maine 72017, Le Mans Cedex, France.
[2] Present address: Department of Materials Science, University of Illinois at Urbana, Champaign-Urbana, IL 61801, USA. Sandia National Laboratories, Division 1845, Albuquerque, NM 87185, USA.
[3] Present address: Sandia National Laboratories, Division 1845, Albuquerque, NM 87185, USA.

particular structure, and then to diagonalize the dynamical matrix for the structure to find the eigenfrequencies. The second method, which we have adopted in this work, uniquely utilizes the molecular dynamics method to calculate the time correlation function for the dynamical property appropriate to the spectrum of interest, and then obtains the spectrum by carrying out the appropriate Fourier transformation from time to frequency domains. Since this procedure invokes none of the quantum mechanical matrix elements which determine, for example, the Raman scattering cross-section in real laboratory systems, no reliable information on spectral intensities can be expected. However, if the potential functions employed in the simulations are adequate, then the frequencies of absorption peaks should be more or less correct.

2. Computational procedures

In this work, we have obtained the infrared spectrum by Fourier transforming the dipole moment correlation function according to

$$I(\omega) = \int_0 \mathrm{d}t \langle M(0)M(t)\rangle \, \mathrm{e}^{-\mathrm{i}\omega t}, \qquad (1)$$

where $M(t) = \sum \mu_i(t)$ is the total dipole moment of the configuration at time t. The simplest way of obtaining μ_i is to consider a charge q_i to be located at the center of mass r_i of an ion and then sum over all ions $M(t) = \sum q_i r_i(t)$. The program actually sums $q_i v_i(t)$ over all particles, which results in the evaluation of the electrical flux–flux correlation function, FFCF. This procedure makes the recorded signal independent of the spatial origins. It differs from the previous signal only by its magnitude and by a phase angle of 90°. Actually, the FFCF is in phase with the electric field vector of the electromagnetic wave emitted by an oscillating dipole:

$$C(t) = \sum_i v_i q_i(t), \qquad (2)$$

$$\mathrm{FFCF} = \langle C(0)C(t)\rangle. \qquad (3)$$

The angular brackets represent an average taken over all time origins from $t = 0$ to $= t_{\max}$. $t_{\max}$ is the total duration of the simulation minus t_c, where t_c is the time span over which correlation effects are observed and corresponds to the period of the vibrational mode with the lowest frequency. The resulting correlation function is independent of time origins.

For the Raman spectrum, there is some debate about the most appropriate time correlation function to transform. We will not discuss the alternatives for lack of space but simply state the choice we have made (the results for other choices are compared in a more detailed report to be published elsewhere [11]). We concentrate here on the high frequency modes involving bond stretching rather than bond bending, so the Raman spectrum is calculated by Fourier transformation of 'the total bond stretching autocorrelation function' obtained by summing the 'group breathing correlation functions' GBCF ($C_j(t)$), defined below, over a number of groups. The GBCF is obtained for each 'group' – consisting of a central particle i and its j nearest neighbors within a cut-off distance r_{ij} (max) – by projecting the velocity differences $v_i - v_j$ between central and neighbor particles onto the bond direction r_{ij}; thus,

$$C_j^{\xi}(t) = \sum_{i=1} \left(v_j^{\xi}(t) - v_j^{\xi}(t)\right) r_{ij}^{\xi}(t), \quad \xi = x, y, z, \qquad (4)$$

and

$$\mathrm{GBCF} = \langle C(0)C(t)\rangle, \qquad (5)$$

For lower frequency Raman bands, one would have to examine the angular momentum correlation functions which we will not consider here.

2.1. Damping and averaging

In any large collection of particles, even in the crystalline state, time correlation functions such as we discuss here should decay to zero within a small number of vibration periods – by vibrational dephasing if not by anharmonic damping. However, in simulations on small numbers of particles it is normal to obtain functions which continue to oscillate about zero out to long times. The low amplitude oscillations are effectively ar-

tifacts which are partly due to boundary conditions and partly due to small number effects. They must be removed before Fourier transformation or they cause unphysical ripples and spikes in the simulated spectra. Two methods are effective in removing them. One is to average together several individual correlation functions from quite different (statistically independent) portions of the same production run, in which case the nonphysical part of the correlation function averages to zero. The second is to apply a damping function

$$\phi(t) = \exp(-\alpha t^2) \tag{6}$$

to the correlation function, choosing the parameter α such that the amplitude reduces to zero in a time interval of order 0.5 ps. Thus for the spectral intensity $I(\omega)$, we have

$$I(\omega) = \int_0 \mathrm{d}t \langle C(t)(O) \rangle \, \mathrm{e}^{-(\alpha t)^2} \, \mathrm{e}^{-\mathrm{i}\omega t}. \tag{7}$$

The former is preferable, although more time consuming, and is probably essential in cases where the structural correlations are relatively long-ranged as in tetrahedral networks such as SiO_2 and BeF_2. In these cases the primary box structure at one instant is not fully representative of the liquid unless boxes larger than economi-

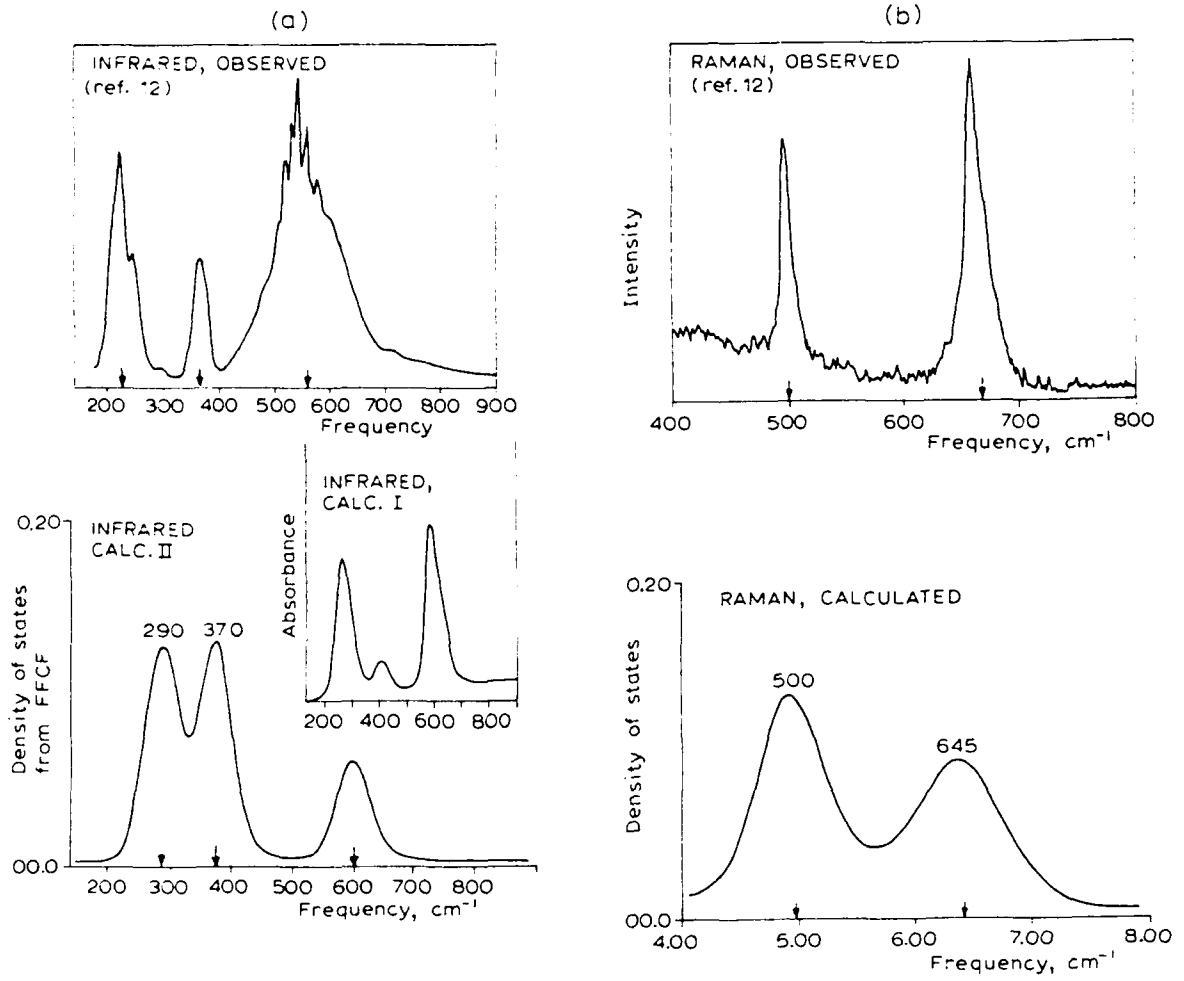

Fig. 1. (a) Observed and calculated IR spectra for $MgZrF_6$ crystal at 300 K: calculations from flux-flux correlation functions (two completely independent attempts). (b) Observed and calculated Raman spectra for $MgZrF_6$ crystal at 300 K (two completely independent attempts): calculations from structure breathing correlation function.

Table 1
Potential parameters used for computation: $A_{ij} = 0.19 \times 10^{-12}$ erg; $b_{ij} = 34.484$ nm^{-1}

Element	z_i (e.u.)	n_i	σ_i (nm)
Zirconium	+4.0	8.0	0.1517
Magnesium	+2.0	8.0	0.1230
Barium	+2.0	8.0	0.1854
Beryllium	+2.0	2.0	0.0934
Fluorine	−1.0	8.0	0.1237

cally convenient are used. Brawer [10] encountered the same problem and adopted the averaging procedure to compensate. The parameters used in the two term rigid ion potentials, whose form has been given in our many earlier papers. are presented in table 1.

3. Results

3.1. Crystals – $MgZrF_6$

Trial runs were conducted on the cubic crystal $MgZrF_6$, for which both IR and Raman spectra are available [5,6], and have simple forms. The observed and calculated IR spectra are shown in fig. 1(a) and the observed and calculated Raman spectra are shown in fig. 1(b). The results for the Raman spectrum accord rather closely with the experimental findings although the frequency calculated for the Mg–F stretch 640 cm^{-1} is low by about 30 cm^{-1}. The highest frequency mode in the simulated infrared spectrum, 600 cm^{-1}, on the other hand is slightly higher than the center of the broad observed high frequency mode, ~ 560 cm^{-1}. The simulation agrees exactly with experiment for the intermediate IR band (370 cm^{-1}) but seriously overestimates the lowest frequency band (290 cm^{-1} vs. experiment 240 cm^{-1}). All-in-all, however, the results are quite pleasing and encourage the application of the method to other structures.

3.2. Fluorozirconate glasses

The fluorozirconate glass most appropriate for study is the $BaF_2 \cdot 2ZrF_4$ composition which can be obtained as both crystal and glass in the laboratory, and which has been the composition accorded most attention in attempts to model the glass structure. The crystal of this composition is unfortunately not of cubic symmetry and therefore cannot be simulated using our current MD program. (Interestingly enough it is also not possible to simulate a crystal with the $MgZrF_6$ structure in which Mg^{2+} is replaced by a significantly larger divalent cation, such as Ca^{2+}. The initial crystal configuration spontaneously disorders to an amorphous form in a few vibration periods.) Thus we perform the spectral simulations on glassy configurations obtained by 4 ps (2000 timestep) simulations at high temperatures, 1300 K (where complete structural equilibrium is obtained in a few hundred timesteps), for a few hundred timesteps, followed by instantaneoulsy quenching to 300 K, where the run is continued for a further 4 ps to acquire the dynamic record on which the spectral calculations are performed. Because we are seeking information on quite a complex system using a rather small sample, in most cases it is likely that all configurations characteristic of the experimental substance may not be sampled. To estimate the importance of such effects, some structural analyses were performed on structures obtained with three different sam-

Table 2
Disposition of fluorides in the structures in different box sizes

Boxside (nm)	Zr	CN	Terminal	Corner	Edge	Free F
1.375	22	7.41	50.0	36.4	12.7	1
1.732	44	7.41	47.3	41.6	9.1	5
1.983	66	7.27	50.6	40.6	7.3	5
Crystal	–	7.0	60.0	20.0	20.0	–

ple sizes at the same density. It was found that the intermediate range order was sensitive to primary sample size because Zr–Zr radial distribution functions showed different splittings [11], indicating different proportions of edge and corner-linking modes for the ZnF_n polyhedra. The structures were examined quantitatively for differences in polyhedral linkage types. The results are summarized in table 2 which shows that in larger primary boxes the proportion of edge-sharing polyhedra is diminished in favor of corner-sharing polyhedra. The proportion seems to be stabilizing for boxes with 50 or more Zr ions.

The laboratory IR [12] and Raman [1] spectra are compared in fig. 2 with simulated spectra obtained from small box simulations both for an average of four almost unsmoothed ($\alpha = 2$) runs and for single runs smoothed by use of eq. (6) with $\alpha = 12$. The calculated IR spectral frequencies are in rather good agreement with experiment, none of the three bands differing by more than 30 cm^{-1} from its laboratory equivalent.

3.3. BeF_2 glass at normal and high densities

In order to study the effect of coordination number changes induced by changes in pressure at constant composition rather than by composition at constant pressure (and at the same time to obtain insight into the origin of major but re-

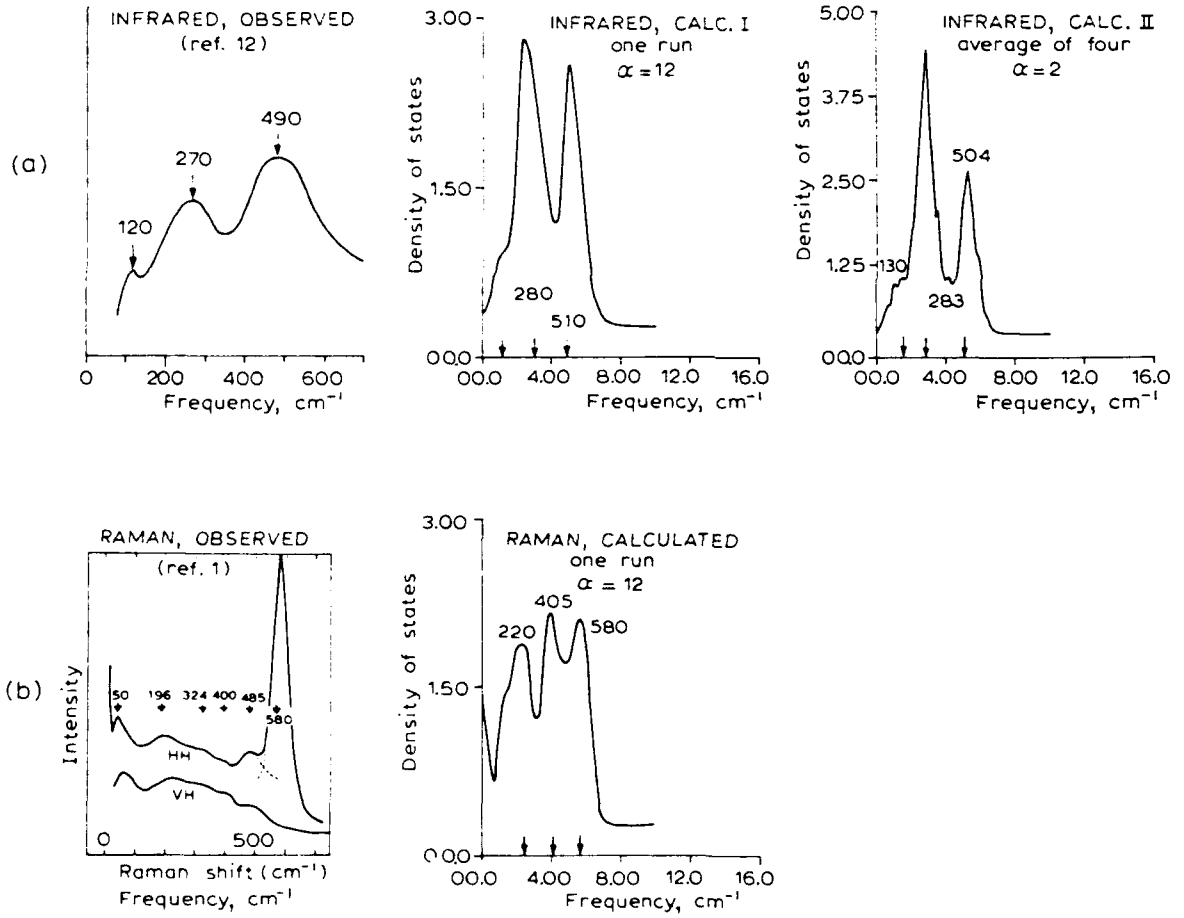

Fig. 2. BaF_2–$2.2ZrF_4$ spectra: (a) IR spectra, observed and calculated (single run smoothed with $\alpha = 12$ and average of four runs each smoothed with $\alpha = 2$). (b) Raman spectra, observed and calculated (one run smoothed with $\alpha = 12$).

versible spectral intensity shift with pressure in oxide network glasses studied in diamond anvil high pressure cells [13–15]), we have chosen to study the simplest available fluoride glass, BeF_2.

Since Brawer found it necessary to average results of several independent runs in order to obtain simulated spectra which were comparable with laboratory results (implying that long range correlations exceed computational box dimensions), we have conducted test calculations on samples of two different box sizes containing 40 and 130 BeF_2 units (the same size used by Brawer) in addition to employing averaging procedures. Interestingly enough, the results for the smaller box correspond more closely with experiment, in particular with respect to the reproduction of a sharp IR mode at 400 cm^{-1} which is almost lost from the spectrum obtained for the larger box (see fig. 3(a)).

In fig. 4 we show results of the simulated IR spectrum of BeF_2 glass (in small box) at various isothermal (300 K) compressions as indicated by the initial-to-final volume ratio on each curve. Note how the initial increase of peak frequency is followed by a rather sudden change of spectral character between $V_0/V = 1.2$ and 1.6 in which the sharp Be rattling mode is 'smeared-out' into a broad band whose centroid then moves to lower frequencies with even higher compression up to $V_0/V = 1.8$, where the structure change is pre-

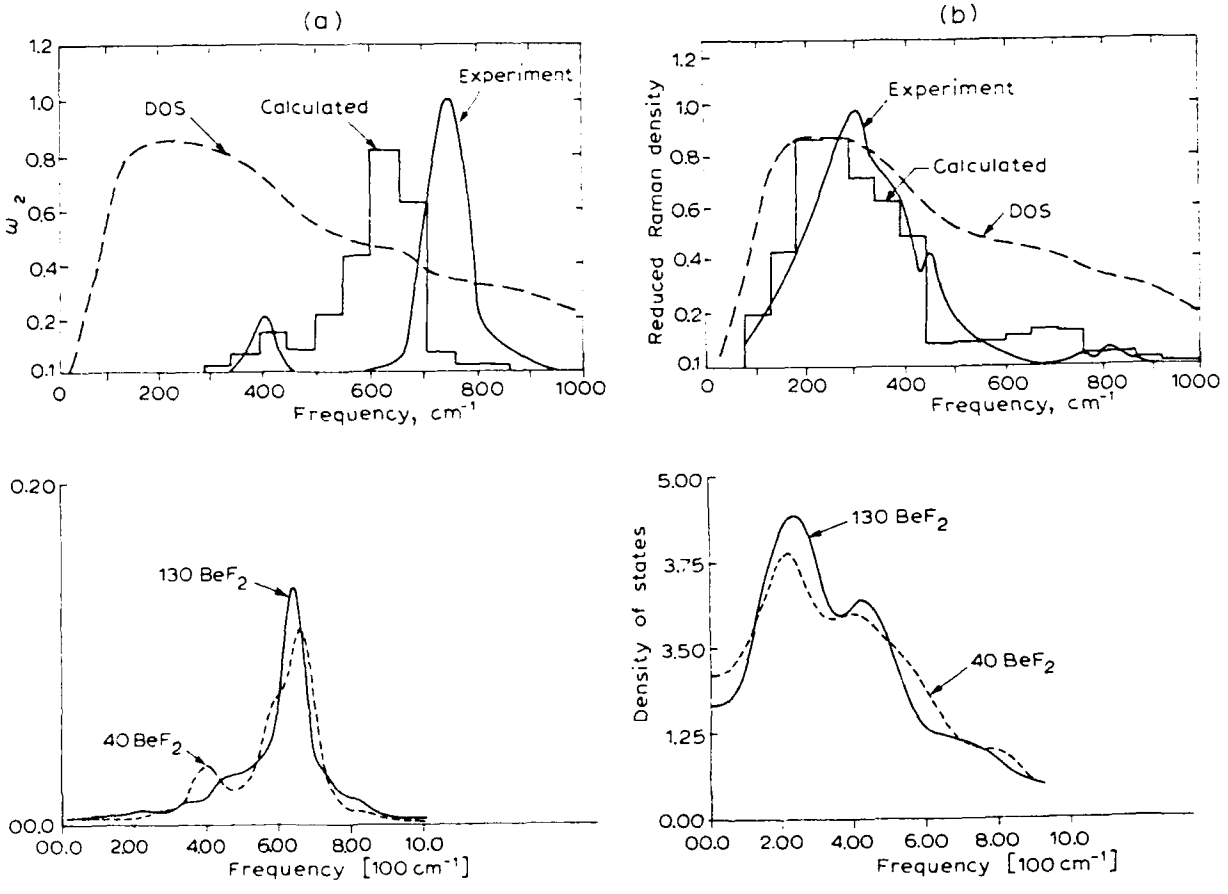

Fig. 3. BeF_2 glass spectra. (a) Observed and calculated infrared spectra. (b) Observed and calculated Raman spectra. The laboratory data are taken from figs. 2 and 3 in Brawer's paper [10] which contains histograms calculated by him by the dynamical matrix method.

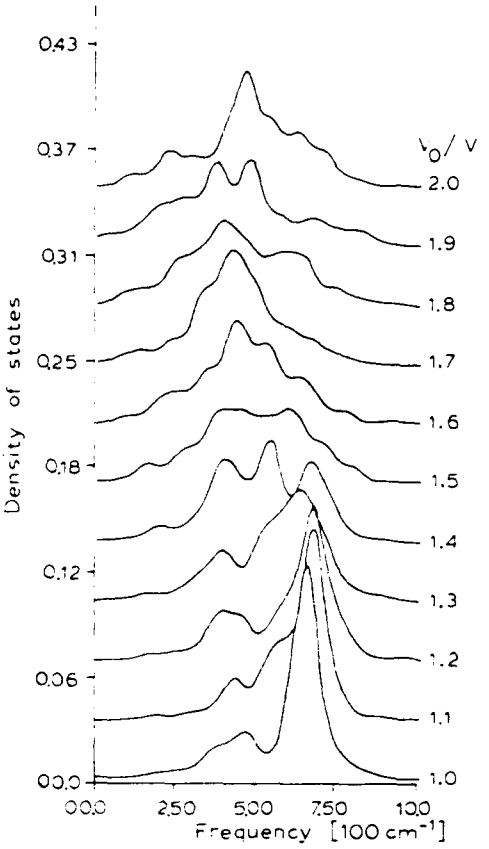

Fig. 4. IR spectra for BeF_2 glass calculated for different volume compressions expressed as volume ratios, V_0/V.

sumably complete. After this a shift to higher frequencies with further compression is observed. These shifts are interpreted in the discussion section.

4. Discussion

We briefly discuss reliability of the simulated fluoride glass spectra and means of improving their interpretation, and then interpret the pressure induced-effects in BeF_2 glass.

Although the elimination of Fourier transform artifacts in the simulated spectra by averaging of several independent CFs is in principle preferable to smoothing a single CF, fig. 2(a) shows that appropriate smoothing of a single run yields almost the same results. The agreement of simulated IR spectral frequencies with experimental values is encouraging. Future studies, in which the mass of one species, e.g. Ba^{2+}, is changed at constant potential, should help decide whether individual IR peaks may be associated with particular cation–anion quasilattice vibrations, e.g. Ba vs. F and Zr vs. F, or whether the interspecies couplings are too important to permit such a simple description.

The difference between the simulated and observed Raman spectra is more important. The experimental spectrum is non-descript except for the intense band at 580 cm^{-1} which dominates the HH spectrum. Lacking any scattering enhancement mechanism, the simulation could not be expected to reproduce the dominance itself, but the band frequency is well reproduced. The simulated spectrum also has features covering the same spectral range as the experimental spectrum but is missing the second band at 485 cm^{-1}. This is disconcerting since elsewhere [5] we have associated this band with the

$$Zr \begin{matrix} F \\ F \end{matrix} Zr$$

linkage which is one of the key structural features of current models of fluorozirconate glasses [5,9]. In some further simulations performed since this work was submitted, a weak band between the highest two peaks in fig. 2(b), i.e., at the correct frequency, has in fact been present but is not a robust feature. A decision on this aspect of the spectrum will have to await the results of current work in which the potentials are modified to enhance the population of double bridges and therefore also the associated spectral features.

Turning to the studies of BeF_2 under compression, we refer to the dramatic change in the simulated IR spectrum which occurs at compressions (V_0/V ratios) exceeding 1.2. This change is very similar to changes observed in the experimental IR spectrum of SiO_2 and analogs compressed in the diamond anvil cell [13–15]. In our case, we can link the spectral change directly to changes in nearest neighbor populations which occur systematically above compressions of 1.2. Figure 5 shows the distribution of near-neighbor coordination numbers in BeF_2 as a function of

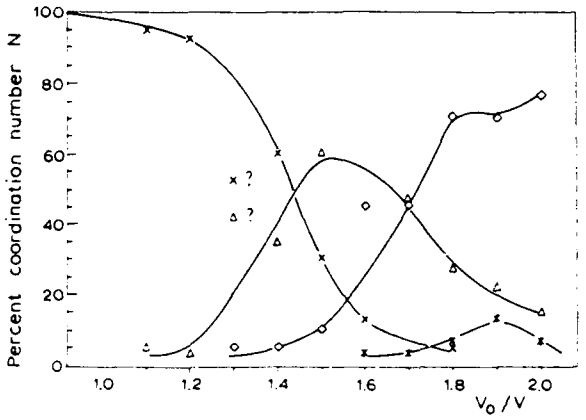

Fig. 5. Distribution of near neighbor coordination numbers for Be in BeF_2 glass as function of compression V_0/V. N:*, CN = 7; ◇, CN = 6; △, CN = 5; ×, CN = 4.

compression. The percentage of four-coordinated Be atoms drops from nearly 100 at $V_0/V = 1.2$ to almost 0 at 1.7. The population of six-coordinated Be on the other hand flattens out at $V_0/V = 1.8$ where the low frequency feature reverses pressure dependence. In between, the number of five-coordinated Be atoms maximizes at 1.5 where the spectrum is broadest. Other spectroscopic and structural observations will be reported in more detail separately [11]. Here we only note that, as in the case of SiO_2, in the laboratory [13,14], release of pressure at ambient temperatures results in a reversal of most of the structural (and spectroscopic) changes observed on compression. This inability to preserve a history was first observed in simulated SiO_2 glass [16]. As in that case, there is some residual densification of the four-coordinated glass, as indeed is observed in practice for SiO_2. Interestingly enough, the behavior is only marginally different when the compression is carried out in the *liquid*, as opposed to the glassy, state.

5. Conclusions

The ion dynamics method shows considerable promise for reproducing and hence interpreting the vibrational spectra of ionic glasses. Of the spectra simulated here, the IR spectrum of the laboratory glass is better reproduced than the Raman spectrum. More development work is needed in each case. Spectroscopic evidence for double fluoride bridges between Zr^{4+} centres remains indefinite.

In BeF_2 glass, sudden changes in simulated IR spectra correlate with sudden changes in coordination numbers. Over a narrow range of densities, complete and quasi-reversible changes from a four-coordinated to a six-coordinated glass occur. "The question raised here is whether or not it is proper to think in terms of vitreous polymorphs of a substance, i.e., whether long-range disordered substances can generate sufficient differences in their short-range order, when prepared under different conditions, to have distinct and different thermodynamic properties which are maintained above the glass transition (when the amorphous is in internal equilibrium) for a finite temperature interval." [17]. Even if the latter restriction is lifted, it seems, in view of the interconvertibility of the two distinct short-range ordered forms in the *glassy* state observed here and in the laboratory, that the concept of 'vitreous polymorphs' [18] is a reasonable one worthy of further refinement.

The authors are grateful for the support of this work by the Office of Naval Research under Agreement No. N00014-84-K-0289 and by the French Centre Nationale de Recherches Scientifiques for support of one of us (B.B.) during the period of this research. Carol Scamehorn is thanked for assistance with computational procedures.

References

[1] R. Almeida and J.D. Mackenzie, J. Chem. Phys. 74 (1981) 5954.
[2] R. Almeida and J.D. Mackenzie, J. Chem. Phys. 78 (1983) 6502.
[3] Y. Kawamoto, Phys. Chem. Glasses 25 (1984) 6502.
[4] G.E. Walrafen, M.S. Hokmabodi, S. Guha, P.A. Krishan and D.C. Tran, J. Chem. Phys. 83 (1985) 4427.
[5] C.A. Angell and C.C. Phifer, Mater. Sci. Forum 32&33 (1988) 373.

[6] C.C. Phifer, D.J. Gosztola, J. Kieffer and C.A. Angell, J. Chem. Phys. 94 (1991) 3440.
[7] (a) H. Inoue, H. Hasegawa and I. Yasui, Phys. Chem. Glasses 26 (1985) 74.
(b) H. Inoue, T. Namba, H. Hagihara, T. Kanzawa and I. Yasui, Nat. Sci. Forum 32&33 (1988) 403.
[8] Y. Kawamoto, T. Horisaka, K. Hirao and N. Soga, J. Chem. Phys. 83 (1985) 2398.
[9] C.C. Phifer, J. Lucas, J.P. Laval and C.A. Angell, J. Non-Cryst. Solids 94 (1987) 315.
[10] S.A. Brawer, J. Chem. Phys. 79 (1983) 4529.
[11] B. Boulard, J.A. Kieffer and C.A. Angell, to be published.
[12] C.C. Phifer, PhD thesis, Purdue University (1988).
[13] R. Hemley, H.K. Mao, P.M. Bell and B.O. Mysen, Phys. Rev. Lett. 57 (1986) 747.
[14] Q. Williams and J. Jeanloz, Science 239 (1988) 902.
[15] G.H. Wolf and D. Durben, J. Phys. Rev. B43 (1991) 2365.
[16] L.V. Woodcock, C.A. Angell and P.A. Cheeseman, J. Chem. Phys. 65 (1976) 1565.
[17] C.A. Angell and E.J. Sare, J. Chem. Phys. 52 (1970) 1058, footnote 39.
[18] M. Grimsditch, Phys. Rev. Lett. 52 (1984) 2379.

(17)

Fragility of Ge-As-Se Glass-Forming Liquids in Relation to Rigidity Percolation, and the Kauzmann Paradox

M. Tatsumisago,[1] B. L. Halfpap,[2] J. L. Green,[1] S. M. Lindsay,[2] and C. A. Angell[1]

[1]*Department of Chemistry, Arizona State University, Tempe, Arizona 85287-1604*

[2]*Department of Physics, Arizona State University, Tempe, Arizona 85287-1604*

(Received 18 December 1989)

The concept of mean-field rigidity percolation at average coordination number $\langle r\rangle = 2.4$ in covalently bonded inorganic glasses is shown to be relevant to the liquid-state behavior of glass-forming chalcogenide systems. In particular it correlates with remarkable variations in "fragility" and excess heat capacity which we observe in the model ternary system Ge-As-Se. Except near As_2Se_3, T_g itself depends only on $\langle r\rangle$ anywhere in the system up to $\langle r\rangle = 2.5$. These findings provide an important link between key structural concepts of glass science, the relaxation phenomena, and the thermodynamic problem embodied in the Kauzmann paradox.

PACS numbers: 61.42.+h

The notion that covalent bonding in glasses may be optimized when the average coordination number ($\langle r\rangle$) is 2.4 was advanced first by Phillips[1] to explain the strong glass-forming propensity of some chalcogenide systems. It was later refined by Thorpe,[2] who predicted, for the mean-field case, a sudden rise in bulk modulus as the composition in binary or multicomponent systems passes through the "rigidity percolation" (or vector percolation) threshold at this same coordination number.

Some sound-velocity-based observations supporting the idea of rigidity percolation were presented in an earlier Letter on the model system Ge-As-Se.[3] This system was chosen because the bonding numbers (valences) of 4, 3, and 2, respectively, permit realization of $\langle r\rangle = 2.4$ at many different chemical compositions ($\langle r\rangle = 4X_{Ge} + 3X_{As} + 2X_{Se}$, where X is mole fraction). This permits separation of connectivity effects from chemical effects.[3] However, these early measurements were later found to be affected adversely by oxide contamination of the samples. In fact, the absence of a transition at $\langle r\rangle = 2.4$ has recently been reported,[4] in accord with Thorpe's[5] subsequent prediction that for real systems with van der Waals interactions between unbonded neighbors, the rigidity-percolation phenomena would be smeared out. With an interest in checking this prediction, and also in testing our suspicion that the vector-percolation concept might be more sensitively investigated in the *liquid* state of this system, we have extended the original study not only in composition range but also in temperature and variety of properties investigated. In particular, we have now included measurements of (i) the glass transition temperature T_g, (ii) changes in thermodynamic properties (expansivity α and heat capacity C_p) at T_g, and (iii) viscosity (the key liquid-state property) with striking results.

Most of the measurements reported will concern the pseudobinary join $Se_{(1-x)}(As_{0.5}Ge_{0.5})_x$, chosen by us to maximize the likelihood of random bonding, and hence conformity to mean-field arguments. In this study, our original sample preparation techniques have been refined in order to eliminate the oxygen contamination which vitiated the earlier results. High-purity lump elements (99.9999%) were melted together in evacuated silica tubes at 600–1150 °C, depending upon composition, for 24 h. They were then cooled at ~15 K/min. Prior to loading the tubes, the arsenic was placed in an evacuated chamber, the bottom of which was heated to 350 °C while the top was kept at 25 °C. This distilled off arsenic oxide contamination. The resulting samples, 65 in all, contained 100- to 200-ppm oxygen as determined by infrared spectroscopy.[6] They exhibited no evidence of crystallization in differential-scanning-calorimeter (DSC) thermograms.

Elastic constants were determined from sound-velocity measurements as described before,[3] but with an improved precision of 0.1%. Thermal-expansivity (α) measurements were made using a Perkin-Elmer model TMS-2, scanning at 2.5 K/min. The same instrument was used, with a beam-bending attachment, to determine the viscosity in the range 10^9–10^{13} Pas with a precision *and* accuracy of ±5% (based on measurements made on BS710 standard glass). Heat-capacity C_p and enthalpy-relaxation measurements were made using the Perkin-Elmer DSC-4 differential scanning calorimeter at scan rates between 2.5 and 40 K/min.

The absence of universal or dramatic behavior of the longitudinal mechanical modulus C_{11} as the mean-field percolation threshold is crossed[4] is confirmed in this work for all $Se_{(1-x)}(Ge_yAs_{1-y})_x$ cuts across the ternary system. The results are more definitive than in binary systems[4] because of the extended $\langle r\rangle$ range available. In the As-Se binary and in Ge-poor glasses, we even observe[7] a contradictory maximum in C_{11} at or near $\langle r\rangle = 2.4$. Clearly the study of C_{11} at ambient temperature is not fruitful in the present context.

Turning to T_g (defined as the onset of the rises in C_p or α, as ergodicity is restored during heating at 20 K/min [see Fig. 1, inset (b)]), we observe more promising phe-

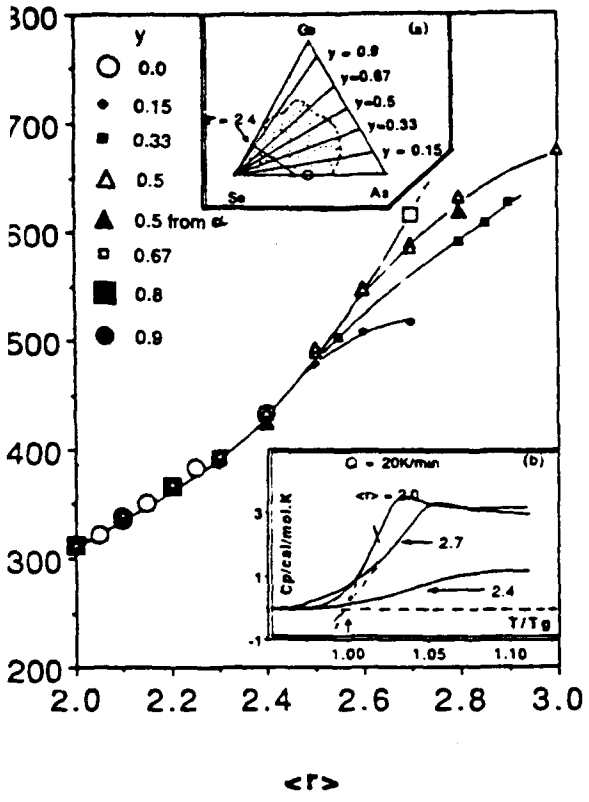

FIG. 1. $\langle r\rangle$ dependence of T_g from DSC and α, for Ge-As-Se glasses along various pseudobinary cuts $Se_{(1-x)}(Ge_ySe_{1-y})_x$ as indicated in inset (a). Inset (b) shows behavior of the heat capacity C_p through the glass transition for $\langle r\rangle$ values at, and on either side of, the rigidity-percolation threshold along the $y=0.5$ join.

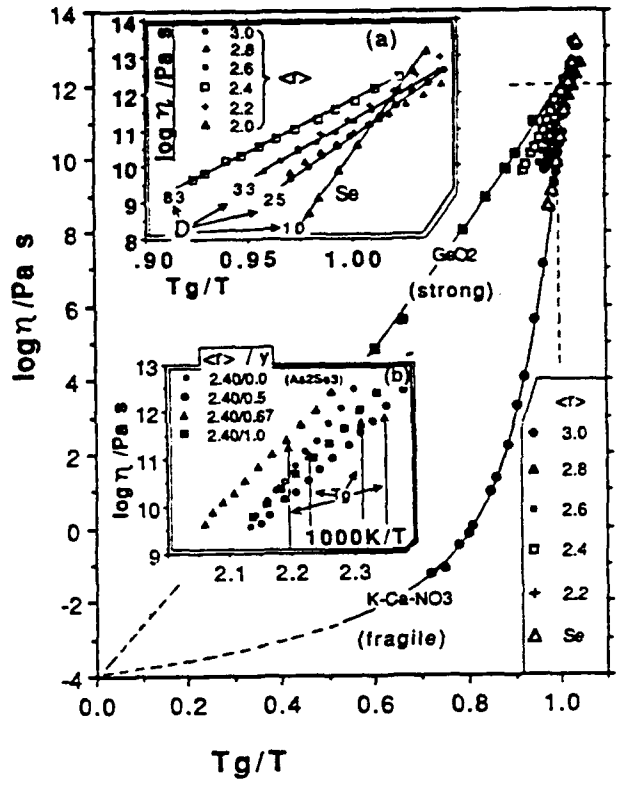

FIG. 2. Comparison of viscosities of pseudobinary ($y=0.5$) Ge-As-Se liquids near T_g, with the "strong" (GeO_2) and "fragile" [$2Ca(NO_3)_2\cdot 3KNO_3$] extremes of the liquid pattern (Ref. 8) from literature data, using a T_g-scaled Arrhenius plot. Inset (a) shows present results in more detail (note strong behavior at $\langle r\rangle=2.4$). Equation (2) D values marked on plots are based on measured slopes (Arrhenius: $D=\infty$, slope $=16$). Inset (b) shows how strength is maintained at other $\langle r\rangle=2.4$ points in ternary systems (As_2Se_3 is exceptional, see text).

nomena. Figure 1 shows that T_g is a universal function of $\langle r\rangle$ up to and somewhat beyond the percolation threshold. It is only above $\langle r\rangle=2.5$ that composition-specific effects enter, as different ways of disposing of the superfluous bonds are explored. There is, however, no sudden upturn in the $\langle r\rangle$ dependence of T_g to signal a threshold crossing. On the other hand, note the contrast in shapes of the heat-capacity scans at the threshold $\langle r\rangle$ value, and on either side of it: The heat-capacity "jump" at T_g in the vicinity of $\langle r\rangle=2.4$ is so small and smeared out that we at first believed the sample had crystallized.

A small heat-capacity jump at T_g implies a strong resistance to structural degradation in the liquid state, and has been correlated with a minimum "fragility" (i.e., departure from Arrhenius viscosity behavior) in the overall pattern of viscous-liquid behavior.[8] (Fragility is a term being used[8-11] to characterize and quantify the anomalous non-Arrhenius transport behavior which develops in most glass-forming liquids as they approach the ergodicity-breaking[11] glass transition.) This interesting possibility stimulates three related questions to which we provide answers in Figs. 2 and 3. The first is, of course, whether the viscosity indeed passes through a fragility minimum at $\langle r\rangle=2.4$, as implied by Fig. 1, inset (b). The second is whether this is also evidenced in a comparable minimum in the fragility behavior of the more fundamental enthalpy-relaxation time, τ_H (the time scale on which the system relaxes towards the state of zero excess entropy at T_K, the Kauzmann[12] temperature), and the third is whether or not the volumetric behavior through T_g, i.e., $\Delta\alpha$, will mimic the heat-capacity changes, ΔC_p. If $\Delta\alpha/\Delta C_p$ at the glass transition is *not* constant for all $\langle r\rangle$, then this system may also provide a test case for distinguishing between "free volume" and "entropy" theories for liquid relaxation processes.[13-15]

The inset (a) in Fig. 2 represents viscosity data on five of twelve compositions studied along the join $Se_{(1-x)}(As_{0.5}Ge_{0.5})_x$, plotted in scaled Arrhenius form where the scaling temperature is the calorimetric T_g of Fig. 1. Within the error of the measurements, the results can be represented by straight lines in apparent conformity with the Arrhenius law but with wide variations in

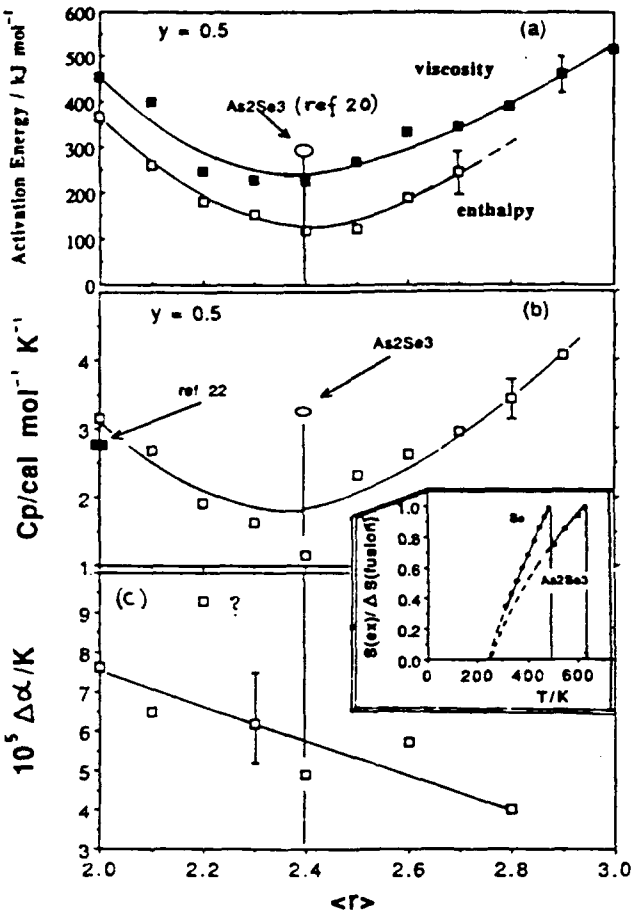

FIG. 3. $\langle r\rangle$ dependence of key relaxational and thermodynamic properties of $Se_{(1-x)}(Ge_yAs_{1-y})_x$ liquids at $y=0$ and 0.5: (a) Dependence of activation energies for viscosity and enthalpy relaxation. (b) Excess heat capacity ΔC_p measured at T_g showing minima in each case at the rigidity-percolation threshold $\langle r\rangle=2.4$. (c) Excess expansion coefficient $\Delta\alpha$ showing *absence* of anomaly at $\langle r\rangle=2.4$. Inset: Kauzmann plots for excess entropy in the cases $\langle r\rangle=2.0$ (pure Se) and $\langle r\rangle=2.4$ (pure As_2Se_3). Note how T_g/T_K differs according to liquid "strength." The values of T_g/T_K are predictable from Eq. (2) using D values based on the position of liquid in the strong-fragile classification.

viscosity preexponent as well as activation energy. However, when the same data are presented on the larger scale of T_g/T and compared with literature data covering a wider range of viscosities and temperature dependences, it can be seen that the present results simply represent the high-viscosity end of the same pattern of liquid behavior which has provided the basis for the "strong" and "fragile" liquids classification for which theoretical interpretations are currently being sought.[9,10,16] The remarkable thing is that compositions along a *single* pseudobinary cut in the present system cover almost the whole spectrum from strong to fragile behavior previously mapped out by combinations of data from many different liquid systems studied in a very wide range of temperatures.[8]

Of special interest in Fig. 2, of course, is the fact that the minimum fragility (minimum Arrhenius slope at $T_g/T=1$) observed in the present study occurs not at the highest value of $\langle r\rangle$ but rather at $\langle r\rangle=2.4$, the rigidity-percolation threshold. Evidently at higher $\langle r\rangle$ values, specific chemical effects such as the occurrence of double Se bridges

$$>\mathrm{Ge}<\begin{matrix}\mathrm{Se}\\ \mathrm{Se}\end{matrix}>\mathrm{Ge}<$$

[known to occur in pure $GeSe_2$ (Ref. 17)] enter into consideration. These are fragile structural elements.[18]

The inset (b) in Fig. 2 shows that the same low fragility is obtained for other ternary compositions with $\langle r\rangle=2.4$, lending credibility to the idea[1,2] of constraint counting involving *both* bond distances and angles[11,19] in these systems. The binary glass of $\langle r\rangle=2.4$, As_2Se_3 is, however, atypical according to Fig. 2, inset (b), having a more fragile character. It also has a larger enthalpy-relaxation activation energy, E_H (Ref. 20), and larger ΔC_p (Ref. 20) (see below). This is probably associated with its topological reorganization to give "raft"-like structures[21] of two-dimensional aspect.

Concerning our second question, the minimum in the "activation energy" seen at $\langle r\rangle=2.4$ for viscosity data is indeed also seen in the enthalpy-relaxation phenomena which determines the form of the heat-capacity scan. Using Moynihan's method of scan-rate-dependent T_g,[20] we obtain $E_H=Rd(\ln Q)/d(T^{-1})$, where Q is the scan rate. This quantity, for each of the glasses for which viscosity data were presented in Fig. 2, is plotted together with the viscosity activation energy E_η in Fig. 3(a). The minimum at $\langle r\rangle=2.4$ is even better defined for E_H, though the experimental precision of E_H is smaller.

We now return to the initial observation of Fig. 2 that the heat-capacity jump at T_g, ΔC_p, is remarkably small at $\langle r\rangle=2.4$ compared with the values at higher and lower $\langle r\rangle$. Figure 3(b) shows this quantity, obtained semiquantitatively ($\pm 10\%$), as a function $\langle r\rangle$ for all the $x=0.5$ glasses, together with a value for pure Se from Ref. 22. The correlation of a minimum in fragility with a minimum in ΔC_p is to be expected from the Adam-Gibbs equation,[14]

$$\eta=\eta_0\exp(C/TS_c). \qquad (1)$$

This is because, when ΔC_p is very small, S_c [$S_c=\int_{T_K}^{T}(\Delta C_p/T)dT$, where T_K is the Kauzmann liquid-crystal isoentropy temperature[11]] is almost temperature independent and Eq. (1) becomes equivalent to the Arrhenius law with the strong-liquid preexponent. The great differences in departures from Arrhenius behavior seen in Fig. 2 then suggest that a further (and very important) correlation be sought, as follows.

The pattern of viscosity behavior leading to the strong- and fragile-liquid classification can be reproduced by a modification, Eq. (2), of the famous Vogel-Tammann-Fulcher (VTF) equation in which the VTF B parameter

is replaced by DT_0,

$$\eta = \eta_0 \exp[DT_0/(T-T_0)]. \quad (2)$$

The "strength" of the liquid goes as the parameter D in Eq. (2). This equation [which is easily derived from Eq. (1) when $\Delta C_p = K/T$ (Ref. 15)] requires that T_g lie far above T_0 for strong liquids whereas for highly fragile liquids T_g/T_0 *approaches unity.*[8,9] From Fig. 3, therefore, we would predict that T_K ($\equiv T_0$) values for fragile Se and stronger As_2Se_3 ($\langle r\rangle = 2.4$) will be much more similar than are their T_g values (307 and 455 K, respectively). Since these are both *congruently melting* compounds, T_K can be assessed by the purely thermodynamic route described by Kauzmann.[12] The data necessary to check this expectation are available.[22,23] We obtain for Se, $T_K = 240 \pm 10$ K.[22] This is demonstrated by the Kauzmann plot, inset to Fig. 3. The value of T_K for As_2Se_3 is found to be 236 ± 10 K (Ref. 22) (As_2S_3, $T_K = 265$ K), also demonstrated in the inset to Fig. 3. Thus our expectation is confirmed, though the near identity of T_K values was unexpected. It is reminiscent of the behavior of systems such as $ZnCl_2$-KCl and SiO_2-Na_2O in which the T_0 of Eq. (2) is invariant during network breaking.[24]

Using these results, we find that T_g/T_K values for these two compositions are 1.23 and 1.90. From Eq. (2), these values go with D values of 8.5 and 33, which may be compared with the observed extremes for all liquids of 3.5 and ~ 100.[9,25] The slopes of the scaled Arrhenius plots at T_g, given by $(DT_K/2.3T_g)(1-T_K/T_g)^{-2}$, are predicted from the T_g/T_K values to be 85.9 and 33.7. These are in good agreement with the values observed in Fig. 2 (76.6 and 34.3)—perhaps fortuitously so considering the extrapolations (to get T_K) and approximations [to get Eq. (2) from Eq. (1)].

Thus, on a semiquantitative level, we have correlated the bond connectivity in the model covalent *liquid* system Ge-As-Se with two of the key viscous-liquid experimental observations, viz., strong-to-fragile (variably non-Arrhenius) transport behavior, and the Kauzmann vanishing-excess-entropy conundrum. It remains to examine systematically the relation to $\langle r\rangle$ of the *nonexponentiality* of relaxation described by the Kohlrausch function $\exp(-[t/\tau_0]^{\beta})$,[26] and of the *nonlinearity* of the various relaxation processes.[27] Here we note that a T_K value identical with ours has been obtained by Hodge[28] from an Adam-Gibbs-based analysis of nonlinear enthalpy relaxation. This is the subject of continuing investigation. We expect the technologically important low-loss characteristics of these glasses at $\langle r\rangle > 2.4$ (Ref. 29) will find a natural explanation in terms of the removal of "floppy" modes.[2]

We will discuss elsewhere how the finding $\Delta\alpha/\Delta C_p \neq$ const for $\langle r\rangle > 2.4$ seen in Fig. 3(c) (i.e., the answer to our third question) favors entropy-based, over free-volume–based, interpretations of viscous-liquid transport and relaxation data.[13-15]

This work has been supported by the Office of Naval Research under Contract No. N00014-87-K-0471 and N0014-84-K-0289.

[1]J. C. Phillips, J. Non-Cryst. Solids **34**, 153 (1979).

[2]M. F. Thorpe, J. Non-Cryst. Solids **57**, 355 (1983); J. C. Phillips and M. F. Thorpe, Solid State Commun. **53**, 699 (1985).

[3]B. L. Halfpap and S. M. Lindsay, Phys. Rev. Lett. **57**, 847 (1986).

[4]S. S. Yun, Hui Li, R. L. Cappelletti, R. N. Enzweiler, and P. Boolchand, Phys. Rev. B **39**, 8702 (1989); B. Swiler and A. Varshneya, in Proceedings of the American Ceramic Society 1989 Fall Meeting, Glass Division (American Chemical Society, Washington, DC, to be published), Abstract No. 31-G-89F.

[5]M. F. Thorpe (private communication); H. He and M. F. Thorpe, Phys. Rev. Lett. **54**, 2107 (1985).

[6]D. S. Ma, P. S. Danielson, and C. T. Moynihan, J. Non-Cryst. Solids **37**, 181 (1980).

[7]B. L. Halfpap and S. M. Lindsay (to be published).

[8]C. A. Angell, J. Non-Cryst. Solids **73**, 1 (1985).

[9]J. Setthna, Europhys. Lett. **6**, 529 (1988).

[10]F. H. Stillinger, J. Chem. Phys. **88**, 7818 (1988).

[11]D. Stein and R. Palmer, in *Complex Systems*, Santa Fe Institute Studies in the Science of Complexity, edited by D. Stein (Addison-Wesley, Reading, MA, 1989), p. 759.

[12]W. Kauzmann, Chem. Rev. **43**, 219 (1948).

[13]M. H. Cohen and D. Turnbull, J. Chem. Phys. **31**, 1164 (1959); M. H. Cohen and G. S. Grest, Phys. Rev. B **20**, 1077 (1979).

[14]G. Adam and J. H. Gibbs, J. Chem. Phys. **43**, 139 (1965).

[15]C. A. Angell and W. Sichina, Ann. N.Y. Acad. Sci. **279**, 53 (1976).

[16]G. Frederickson, Ann. Rev. Phys. Chem. **39**, 149 (1988); K. L. Ngai, J. Non-Cryst. Solids **95 & 96**, 969 (1987).

[17]A. C. Wright (private communication).

[18]C. A. Angell and C. C. Phifer, Mater. Sci. Forum **32-33**, 373 (1988).

[19]P. Boolchand, J. Grothaus, and J. C. Phillips, Solid State Commun. **45**, 183 (1983); J. C. Phillips, Solid State Commun. **47**, 203 (1983).

[20]C. T. Moynihan, A. J. Easteal, J. Wilder, and J. C. Tucker, J. Phys. Chem. **78**, 2673 (1974).

[21]P. Boolchand, W. J. Bresser, and P. Suranyi, Hyperfine Interact. **27**, 385 (1986).

[22]S. S. Chang and A. B. Bestul, J. Chem. Thermodyn. **6**, 325 (1974); S. S. Chang (private communication).

[23]M. B. Myers and E. J. Felty, J. Electrochem. Soc. **117**, 818 (1970); A. J. Easteal, J. Wilder, R. K. Mohr, and C. T. Moynihan, J. Am. Ceram. Soc. **60**, 134 (1977).

[24]C. A. Angell, J. Am. Ceram. Soc. **51**, 124 (1968); A. J. Easteal and C. A. Angell, J. Phys. Chem. **74**, 3987 (1970).

[25]C. A. Angell, J. Phys. Chem. Solids **49** 863 (1988).

[26]M. Shlesinger, Ann. Rev. Phys. Chem. **39**, 269 (1988).

[27]C. T. Moynihan *et al.*, Ann. N.Y. Acad. Sci. **279**, 15 (1976).

[28]I. M. Hodge (private communication).

[29]J. T. Krause, C. R. Kurkjian, D. A. Pinnow, and E. A. Sigerty, Appl. Phys. Lett. **17**, 367 (1970).

(18)

Correlations of the non-exponentiality and state dependence of mechanical relaxations with bond connectivity in Ge-As-Se supercooled liquids

Roland Böhmer
Institut für Physik, Johannes Gutenberg-Universität, D6500 Mainz, Germany
and
C. Austen Angell
Department of Chemistry, Arizona State University
Tempe, AZ 85287-1604, USA

Abstract

We have studied the mechanical responses of supercooled Ge-As-Se liquids to flexural strains and temperature steps. The departures from exponential relaxation correlate well with the variations in connectivity. The structural state dependence of the mechanical relaxation, detected in pure and weakly crosslinked Se, is completely suppressed at the percolation threshold $\langle r_c \rangle$ where the liquid fragility is minimum. The shapes of the decay functions of samples with $\langle r_c \rangle$ but different compositions are not universal at T_g probably due to chemical effects near the binary edges of the ternary system.

PACS numbers: 62.40.ti, 64.70.Pf

By setting off the number of degrees of freedom in a covalently bonded network glass against the number of its bonding constraints, Phillips[1] predicted a threshold of mechanical stability at average coordination numbers of $\langle r_c \rangle = 2.4$. These considerations stimulated a number of ultrasonic experiments in binary[2-5] and ternary[6] chalcogenide systems. However no evidence for anomalous elastic behavior at $\langle r_c \rangle$ could be obtained. Later on Thorpe[7] recognized that the qualitative Phillips theory can be formulated rigorously as a problem of rigidity percolation. Several refined analytical and numerical calculations based on these topological ideas suggested that below $\langle r_c \rangle$ an increasing number of floppy modes should be detectable.[8] Experimental results from vibrational,[9] neutron,[10] and Mössbauer[11] spectroscopies seemed to confirm this prediction.

It was also shown that topological effects rather than chemical ones must be considered to explain the energetical relaxations among glassy configurations in Ge-As-Se chalcogenides as probed by infrared hole burning at cryogenic temperatures.[12] The relevance of the concept of connectivity has also been explored in the *liquid* state.[13,14] A recent study[14] of ternary chalcogenide alloys provided evidence for a correlation between the rigidity percolation, the strength of the entropy crisis near their glass transition, and the departure from Arrhenius behavior, i. e. the fragility. This raises the question of whether the other two key aspects of the vitrification process, viz. the relaxation following external perturbations and the non-linear effects found when relaxation occurs far from thermal equilibrium, also show systematic composition dependences in this model system.

There have been experimental[15,16] and theoretical[17] indications that fragile glass formers relax less exponentially than strong ones, i. e. those for which the mean relaxation times or the viscosities follow simple Arrhenius laws in the whole range. On the other hand there are several examples which seem in conflict with any such simple generalization.[18,19]

To obtain additional systematic data on this question, we have studied the time dependent stress relaxation of Ge-As-Se

glassformers after exposing them to flexural strains and temperature steps. This allowed us to monitor the linear mechanical response as well as the non-linear structural response.

The melt cooled $Ge_aAs_bSe_c$ samples used for this study were taken from batches which had been prepared and characterized previously.[14] From the mole fractions a, b, and c the average coordination number can be calculated by $\langle r \rangle = 4a + 3b + 2c$; at constant connectivity the composition is further specified by the fraction $y = a/(a + b)$. Most experiments have been performed on samples along pseudo-binary cuts in the ternary system with either $\langle r \rangle$ (= 2.4) or y (= 0.5) being constant.

Preliminary tests have shown that the viscoelastic properties of these samples depend to some extent on their geometry.[20] Therefore, unless otherwise stated all measurements were taken on bar samples cut to identical sizes (1 x 1 x 5 mm^3). The tensile stress relaxation at constant strain was monitored in the flexural (three point bending) conformation. Data were recorded automatically[21] in the time range 10^{-1} s < t < 10^5 s and for temperatures between 300 and 600 K. Since the relaxation time for a liquid in the glass transformation range usually depends on its structural state (fictive temperature) as well as the actual temperature,[22] we have repeated the runs after various equilibration times both to ensure equilibration is reached and to acquire data on this non-linear aspect of the phenomenon.

Figure 1 shows typical results for an equilibrated $Ge_{10}As_{10}Se_{80}$ sample ($\langle r \rangle = 2.3$, $y = 0.5$) in its glass transformation range. With increasing temperature the S - shaped stress relaxation curves shift to smaller and smaller times and their maximum steepness increases. This means that the mechanical relaxation of this sample is the closer to exponential the higher the temperature is. Similar quality data could be obtained for six other compositions at constant $y \approx 0.5$, and for two at $\langle r \rangle = 2.4$ but $y \neq 0.5$. A good quantitative description of these data was achieved using the stretched exponential function[23]

$$Y(t) = Y(t=0) \exp\ [-(t/\tau)\ \beta]. \qquad (1)$$

Here β characterizes the broadening and $\langle\tau\rangle_Y = \tau\Gamma(1+1/\beta)$ the average relaxation time of the tensile stress autocorrelation function. Although other fitting procedures are usually also applicable to this type of relaxation function,[24,25] Fig. 1 shows that a three parameter expression is sufficient to provide an excellent fit to our data. High quality fits with Eq. (1) were also obtained for the viscoelastic decay functions of samples with $\langle r\rangle > 2.1$, i. e. except for pure and weakly crosslinked amorphous selenium (a-Se). In these cases the stress decay was composed of two contributions with distinctly separated average time scales. The relative strength of the two relaxation processes was found to be temperature dependent for a-Se.[26] In the vicinity of the glass transition the faster process, which was ascribed to localized modes,[26] relaxed more than 50% of the initial stress. For the $\langle r\rangle = 2.1$ sample the short time relaxation was responsible for no more than 5% of the total stress decay. In each case the slower relaxations could be parameterized satisfactorily using Eq. (1).

The temperature dependences of $\langle\tau\rangle_Y$ from all our samples within experimental uncertainty were found to comply with the Arrhenius law $\langle\tau\rangle_Y = \tau_0 \exp [E/(RT)]$ but with unphysical τ_0. In Fig. 2a the connectivity dependence of the apparent energy barriers E_Y from these fits is shown together with that determined from viscosity measurements[14] (E_η) on the same samples. Near $\langle r\rangle = 2.4$ a well defined minimum shows up for both sets of results. For $\langle r\rangle \leq 2.1$ the activation energies E_Y (for the slow processes) are substantially higher than E_η. We note however that for a-Se the energy barrier of the short time process within experimental error agrees with E_η[14] raising the possibility that the "constant velocity" condition used in the viscosity determination may have been located in the initial relaxation regime. The Arrhenius law when plotted as log t versus T_g/T and with $T_g = T(\langle\tau\rangle=\tau_g)$ exhibits a slope

$$m = d \log \langle\tau\rangle / d (T_g/T) = E/[\ln(10)\ R\ T_g] = \log \tau_g/\tau_0. \qquad (2)$$

The latter equality is simply a rewriting of the Arrhenius law for $T = T_g$. The quantity m has been called variously the "fragility"[27] and more recently the "steepness index".[17]

In calorimetric experiments the T_g is usually determined by heating or cooling the specimens with rates of 10 K/min thereby defining the relaxation time $\tau_{g,cal}$ to be 200 s.[22] By adopting this convention for τ_g we have calculated the slopes m for the various average coordination numbers from the present data and plotted them in Fig. 2b. This plot demonstrates that the fragility of the Se rich alloys decreases with increasing crosslinking. The minimum of m at $\langle r_c \rangle = 2.4$ is very shallow however and the increase of this figure is very slight at large $\langle r \rangle$. This is because beyond the percolation threshold $\langle r_c \rangle$ the increase in the apparent activation energies is compensated by increases in T_g.[14,28] Note that the minimum value m can reasonably have with the above definition of τ_g is when τ_o is the inverse of a vibration frequency, whence $m \approx 16$ (as indicated by the dashed line in Fig. 2).

Several samples with $\langle r \rangle = 2.4$ but different compositions (y = 0.2, 0.5, and 1.0) were investigated. For these, $m = 29 \pm 2$ was found to be constant. From the viscosity data of Ref. 14 for As_2Se_3 ($\langle r \rangle = 2.4$, y = 0) a larger slope (m = 37) was calculated. As has been pointed out previously[14] this higher fragility which is also reflected by a relative large calorimetric anomaly at T_g, is probably due to non-random bonding distributions in this compound.

In the final part of Fig. 2 we present the variations of the Kohlrausch exponent β with the average coordination as determined at T_g of various samples with y = 0.5. The relaxation of a-Se is the most non-exponential ($\beta = 0.42$). With increasing crosslinking β assumes larger values and for $\langle r \rangle \geq 2.3$ is roughly constant at 0.63. By comparing Figs. 2b and 2c it is clear that the increase in the fragility m is accompanied by a decrease in non-exponentiality. Figure 2c also shows that $\beta(T_g)$ for several compositions at the constant average coordination number 2.4 is not universal. Chemical effects probably play an important role for compositions close to the binary As-Se and Ge-Se edges, i.e. for samples with $y \approx 0$ (as discussed above[29]) and y = 1. Several authors have pointed out that a nanoscale (50 Å) phase separation (into Se chains and $GeSe_2$ "outrigger rafts") may take place in the germanium-selenium system at $\langle r \rangle = 2.4$.[9,30]

It is important to note that the detailed shape of the β versus $\langle r \rangle$ curve (Fig. 2c) depends on the definition of T_g, which is arbitrary. By requiring the glass transition to correspond to a much longer relaxation time than $\langle \tau_g \rangle$, a slight maximum at $\langle r \rangle = 2.4$ would show up in Fig. 2c, which by extrapolation would become more pronounced as the Kauzmannn temperature is approached.. This is because the fractional exponents necessary to describe the viscoelastic spectra of our samples show a T dependence which is interesting and which we now discuss.

In Fig. 3 we have plotted the scaled exponents $\beta(T)/\beta(T_g)$ versus the temperature T/T_g for samples with constant $y = 0.5$ (Fig. 3a) and $\langle r \rangle = 2.4$ (Fig. 3b). Although thermorheological simplicity [or $\beta(T) = \text{constant}$] is an assumption that has widely been made in the interpretation of viscoelastic (and scanning calorimetry) experiments, numerous relaxation studies, carried out over wide enough temperature ranges, have shown that the spectral shape of mechanical correlation functions in general depend on T. This is also expected since in the normal (low viscosity) liquid state the relaxation should be close to exponential. On the other hand it has been shown for the entropy relaxation of several organic liquids[16,30] that $\beta(T)$ extrapolates to zero at the "ideal" glass transition temperature T_K, i. e. the one which asymptotically would be reached at infinitely small cooling rates. The ratio of the conventionally defined glass transition to the Vogel-Fulcher temperature T_0 decreases with increasing fragility according to (Eq. 8 in Ref. 26)

$$T_g/T_0 = (1 - 16/m.)^{-1} \qquad (3)$$

Hence for the strong glass formers the degree of non-exponentiality should not be very (if at all) temperature dependent. Similar conclusions have been drawn more rigorously by Ngai *et al.* who used arguments based on the Adam-Gibbs equation and a coupling scheme.[32] Consistent with these ideas we find the fractional exponent of our strongest case, $Ge_{15}As_{15}Se_{70}$ (with $\langle r \rangle = 2.4$ and $y = 0.5$), exhibits the weakest T dependence as compared with other samples along both the $\langle r \rangle = 2.4$ and $y = 0.5$ pseudobinary cuts (see Fig. 3).

By extrapolating the β values of Fig. 3 linearly (on T or 1/T scales) to smaller values we have determined that the temperatures $T_{\beta->0}$ are roughly 1.5 times larger than the T_0's as calculated from the data given in Fig. 2 using Eqs. (2) and (3). We suspect that this lack of coincidence of T_0 and $T_{\beta->0}$ is at least partly due to the fact that any temperature dependence of the Kohlrausch exponent β as determined from the (simpler and possibly more fundamental) shear relaxations in the glass transformation range will appear to be more pronounced than those obtained from measurements of the tensile mechanical response.[26]

The results presented and discussed so far have been taken on structurally equilibrated samples, i. e. those which within experimental uncertainty yielded identical stress relaxations in successive runs. It is well known however, that after changing the temperature of a supercooled liquid it may take some time for its structure to reach thermal equilibrium. For instance, the time constant characterizing this stabilization process was found to be roughly ten times larger than the equilibrium $\langle\tau\rangle_Y$ in a fragile nitrate melt[33] and $(7 \pm 2)\langle\tau\rangle_Y$ in a-Se.[26] In those experiments the samples were quenched from well above T_g to a temperature at which (for experimental convenience) the average relaxation time is larger than 10^3 s. The temperature steps employed in those studies (and also in the present work) typically were as large as some tens of degrees. Under these circumstances the structural equilibration times should depend on the sign as well as the magnitude of the perturbation, i. e. the T step.[34] These are the hallmarks of the non-linear response regime.

The evolution of the average non-equilibrium stress relaxation times $\langle\tau_n\rangle_Y$ recorded during the isothermal stabilization of $(Ge_{0.5}As_{0.5})_{1-x}Se_x$ samples with $\langle r\rangle$ = 2.1 and 2.4 is depicted in Fig. 4. For the latter sample no change of $\langle\tau_n\rangle_Y$ could be detected. Note that in these experiments it is not possible to record the initial part of the structural relaxation, i. e. the one which occurs before the stabilization of the final temperature (about 15 min) is complete. The absence of pronounced changes during the annealing of the strong $\langle r\rangle$ = 2.4 liquid is compatible with its weak calorimetric anomaly at T_g.[14]

In the fragile <r> = 2.1 sample large changes in $<\tau_n>_Y$ were observed. However in contrast to the <r> = 2.0 case the structural equilibration, surprisingly, now proceeds faster than the relaxation following a bending strain. Therefore the first few <r> = 2.1 points in Fig. 4 are based on stress relaxation curves which have only been recorded down to 30 - 50% of the initial stress. We observed that the spectral width of the autocorrelation functions broaden on annealing (as seen earlier[35]). However no quantitative analysis of this effect was attempted because it is very likely that the effective spectral width was not even constant during each single run.

To summarize we have shown that Ge-As-Se compositions with low connectivity, typical of fragile liquids, show very non-exponential and state-dependent mechanical stress relaxations. Conversely at the vector percolation threshold $<r_c>$ the non exponentiality is small and also weakly temperature dependent, and a state dependence cannot be detected. In overconstrained conditions the temperature dependance of β, like the larger excess heat capacity[14], returns. However at $<r_c>$, β is not solely determined by <r>, probably because bonding is non-random for high, or low, Ge:Se.

We thank B. L. Halfpap for providing the glass ingots and Q. Zheng for helping with sample preparation. Stimulating discussions with R. V. Chamberlin, C. R. Kurkjian, and S. M. Lindsay are also acknowledged. This work has been supported by the Office of Naval Research under Agreement No. N00014-84-K-0289 and the Department of Energy under DE-FG02-89ER45398.

References

1 J. C. Phillips, J. Non-Cryst. Solids **34**, 153 (1979).

2. K. S. Gilroy and W. A. Phillips, Phil. Mag. B **47**, 655 (1983).

3. J. Y. Duquesne and G. Bellessa, J. Physique. **46**, C10-445 (1985).

4 S. S. Yun, H. Li, R. L. Cappelletti, R. N. Enzweiler, and P. Boolchand, Phys. Rev. B **39**, 8702 (1989).

5. S. Etienne, J. Perez, S. Peytavin, and M. Ribes (unpublished).

6. B. L. Halfpap and S. M. Lindsay, Phys. Rev. Lett. **57**, 847 (1986) and unpublished.

7. M. F. Thorpe, J. Non-Cryst. Solids **57**, 355 (1983).

8. J. C. Phillips and M. F. Thorpe, Solid State Commun. **53**, 699 (1985); H. He and M. F. Thorpe, Phys. Rev. Lett. **54**, 2107 (1985).

9. for a review see, J. C. Phillips, Phys. Rev. B **31**, 8157 (1985).

10. P. Boolchand, R. N. Enzweiler, R. L. Cappelletti, W. A. Kamitakahara, Y. Cai, and M. F. Thorpe, Solid State Ionics **39**, 81 (1990).

11. W. Bresser, P. Boolchand, and P. Suranyi, Phys. Rev. Lett. **56**, 2493 (1986).

12. S. P. Love, A. J. Sievers, B. L. Halfpap, and S. M. Lindsay, Phys. Rev. Lett. **65**, 1792 (1990).

13. Y. Tsuchiya, J. Non-Cryst. Solids **122**, 205 (1990).

14. M. Tatsumisago, B. L. Halfpap, J. L. Green, S. M. Lindsay, and C. A. Angell, Phys. Rev. Lett. **64**, 1549 (1990).

15. C. A. Angell, in *Relaxations in Complex Systems* edited by K. L. Ngai and G. B. Wright (Naval Research Laboratory, Washington, DC, 1984) p. 3-11.

16. P. K. Dixon and S. R. Nagel, Phys. Rev. Lett. **61**, 341 (1988).

17. D. J. Plazek and K. L. Ngai, Macromolecules **24**, 1222 (1991).

18. K. L. Ngai, J. Non-Cryst. Solids **95&96**, 969 (1987).

19. L. M. Torrell, L. Börjesson, and M. Elmroth, J. Phys. - Condensed Matter **2**, SA207 (1990).

20. From one glass ingot four samples were cut with identical lengths but cross-sections varying by factors of up to 14. As a preliminary result we find that at a given temperature the stress relaxation in the thicker samples was slower and more exponential. More detailed investigations of this sample size effect are currently underway in this laboratory. Unusual geometry effects in three and four point bending experiemnts have also been found by E. Suhir and C. R. Kurkjian (unpublished).

21. R. Böhmer, H. Senapati, and C. A. Angell, J. Non-Cryst. Solids (1991).
22. C. T. Moynihan et al., Ann. N. Y. Acad. Sci. **276**, 15 (1976).
23. F. Kohlrausch, Pogg. Ann. Phys. **119**, 337 (1863).
24. R. V. Chamberlin and D. N. Haines, Phys. Rev. Lett. **65**, 2197 (1990).
25. S. M. Rekhson, in *Glass Science and Technology* edited by D. R. Uhlmann and N. J. Kreidl (Academic, Orlando, 1986), vol. 3: Viscosity and Relaxation, chap. 1.
26. R. Böhmer and C. A. Angell, Phys. Rev. A (submitted).
27. M. Tatsumisago and C. A. Angell, in The Proceedings of the 30th Glass Conference, Japan, September 1989 (unpublished).
28. P. J. Webber and J. A. Savage, J. Non-Cryst. Solids **20**, 271 (1976); U. Tille, G. H. Frischat, and K. J. Leers, in *Non-Crystalline Solids* edited by G. H. Frischat (Trans Tech Publications, Aedermannsdorf/Switzerland, 1977), pp. 631-638; Z. U. Borisova, *Glassy Semiconductors* (Plenum, New York, 1981) pp. 261-274.
29. Due to the larger fragility of As_2Se_3 one would probably have expected a smaller β for samples close to this composition. We note however that the fractional exponent from the enthalpy relaxation of As_2Se_3 is found to be β = 0.67 (Ref. 22). This is another example of the danger of generalizations concerning the relation of β and fragility.
30. A. Feltz, H. Aust, and A. Blayer, J. Non-Cryst. Solids **55**, 179 (1983).
31. M. Oguni, H. Hikawa, and H. Suga, Thermochim. Acta **158**, 143 (1990); P. K. Dixon, Phys. Rev. B **42**, 8179 (1990).
32. K. L. Ngai, R. W. Rendell, and D. J. Plazek, J. Chem. Phys. **94**, 3018 (1991).
33. C. A. Angell, J. Non-Cryst. Solids **102**, 205 (1988).
34. e. g. R. W. Rendell, K. L. Ngai, G. R. Fong, and J. J. Aklonis, Macromolecules **20**, 1070 (1987).

Figure Captions

FIG 1. Stress relaxation $Y(t)/Y(t = 0)$ for $Ge_{10}As_{10}Se_{80}$ ($\langle r \rangle = 2.3$, $y = 0.5$) recorded at the temperatures (from left to right): 433.4, 422.6, 413.3, 403.7, 394.5, and 385.3 K. The lines are fits using Eq. (1) and the parameters displayed in Figs. 2 and 3.

FIG. 2. Connectivity ($\langle r \rangle$) dependence of (a) apparent energy barriers E, (b) fragilities m, and (c) fractional exponents β as determined at their glass transition temperatures T_g. The squares represent results from measurements of the viscosity on samples with $y = 0.5$ (taken from Ref. 14). The present stress relaxation experiments yielded data on alloys with $y = 0.5$ (circles) and off that pseudo-binary cut with y given near the plusses. The fractional exponent at $\langle r \rangle = 2.2$ was extrapolated[20] from a measurement of a thicker ($2.5 \times 2.5 \times 5$ mm^3) sample. The dashed line indicates the minimum fragility. The solid lines are guides to the eye only.

FIG. 3. Scaled Kohlrausch exponents $\beta(T)/\beta(T_g)$ versus scaled temperatures T/T_g for constant y [= 0.5, (a)] and $\langle r \rangle$ [= 2.4, (b)]. The straight lines represent linear least square fits.

FIG. 4. Evolution of the mean relaxation time on annealing for two different samples with $y = 0.5$. Prior to taking these data the samples were cooled with rates of several degrees per minute to the temperatures given near the curves. The dashed lines indicate the equilibrium relaxation times calculated using the parameters given in Fig. 2. The solid line is a guide to the eye only.

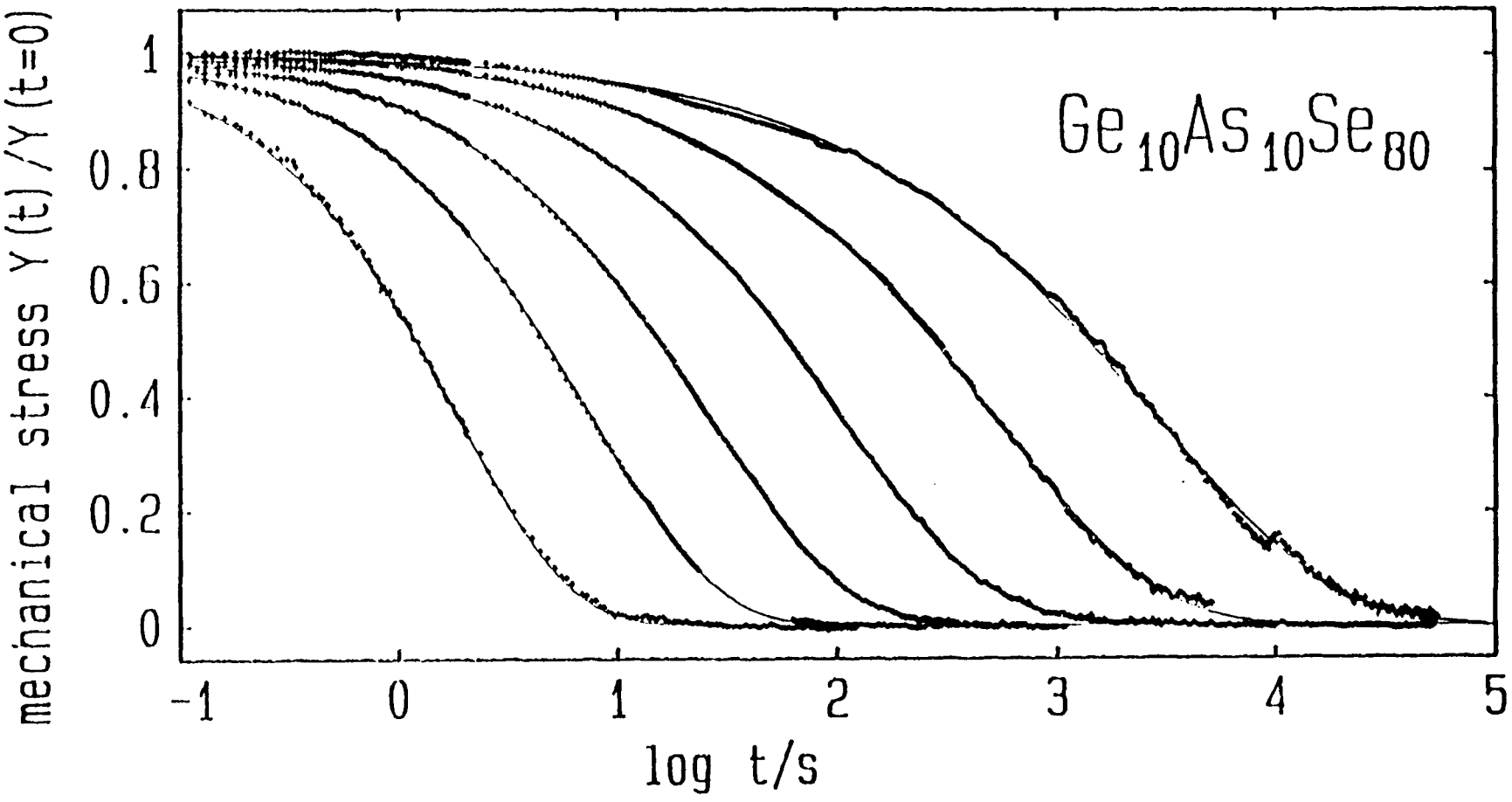
mechanical stress Y(t)/Y(t=0)
1
0.8
0.6
0.4
0.2
0
-1
0
1
2
3
4
5
log t/s
Ge10As10Se80

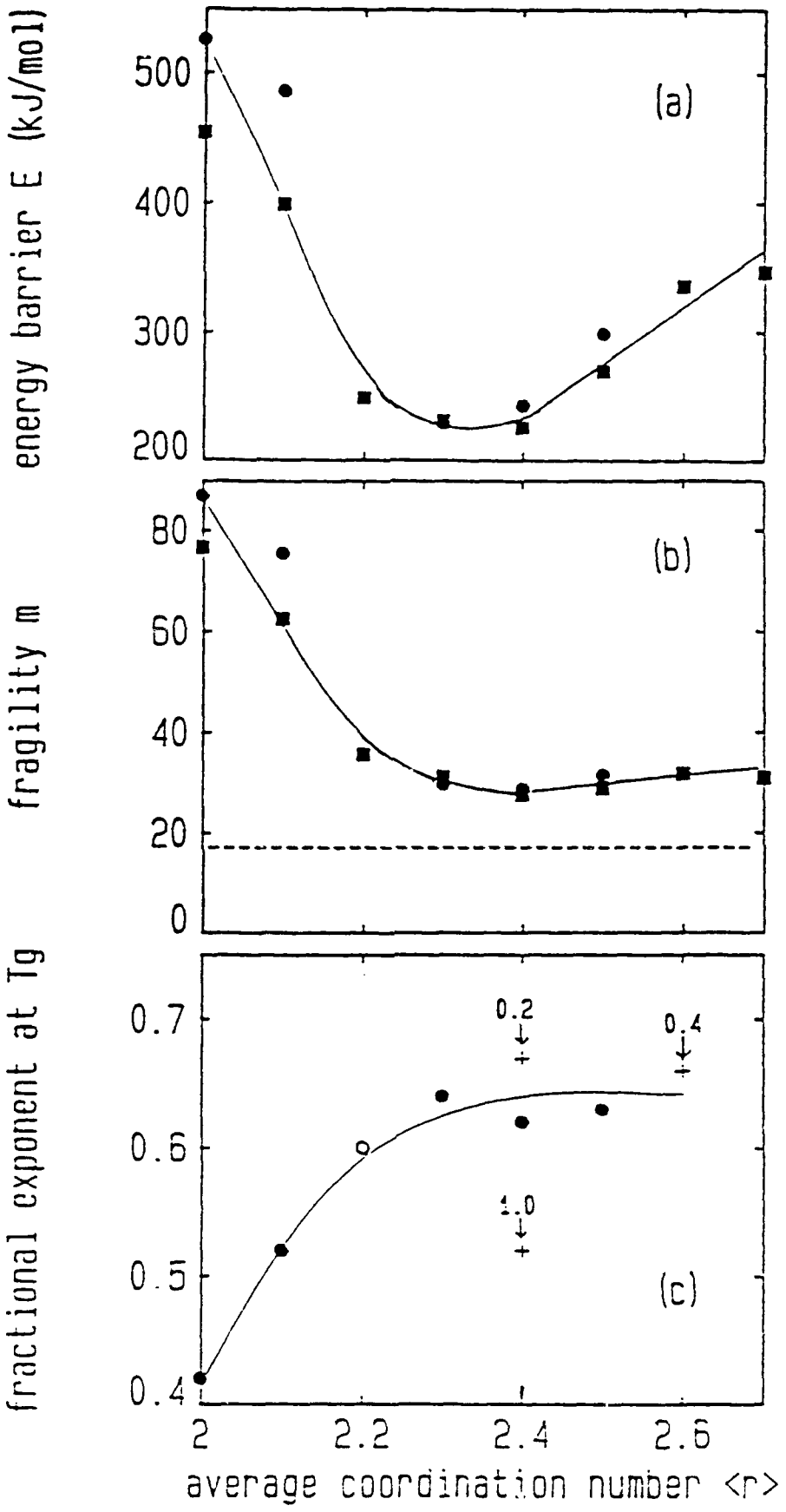
energy barrier E (kJ/mol)
500
400
300
200
(a)
fragility m
80
60
40
20
0
(b)
fractional exponent at Tg
0.7
0.6
0.5
0.4
0.2
0.4
1.0
(c)
2
2.2
2.4
2.6
average coordination number <r>

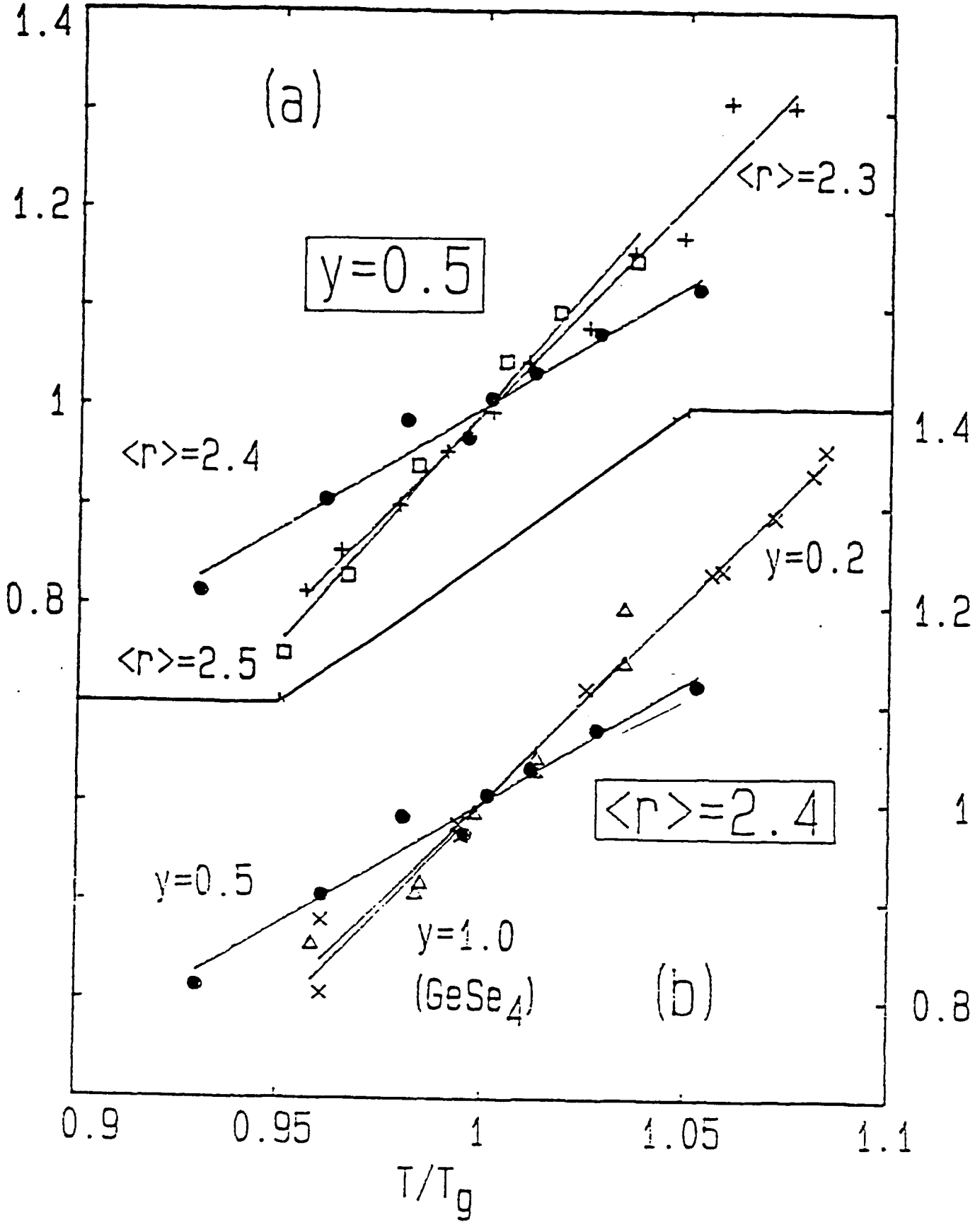
(a)
y=0.5
<r>=2.3
<r>=2.4
<r>=2.5
(b)
<r>=2.4
y=0.2
y=0.5
y=1.0
(GeSe4)
1.4
1.2
1
0.8
0.9
0.95
1
1.05
1.1
T/Tg

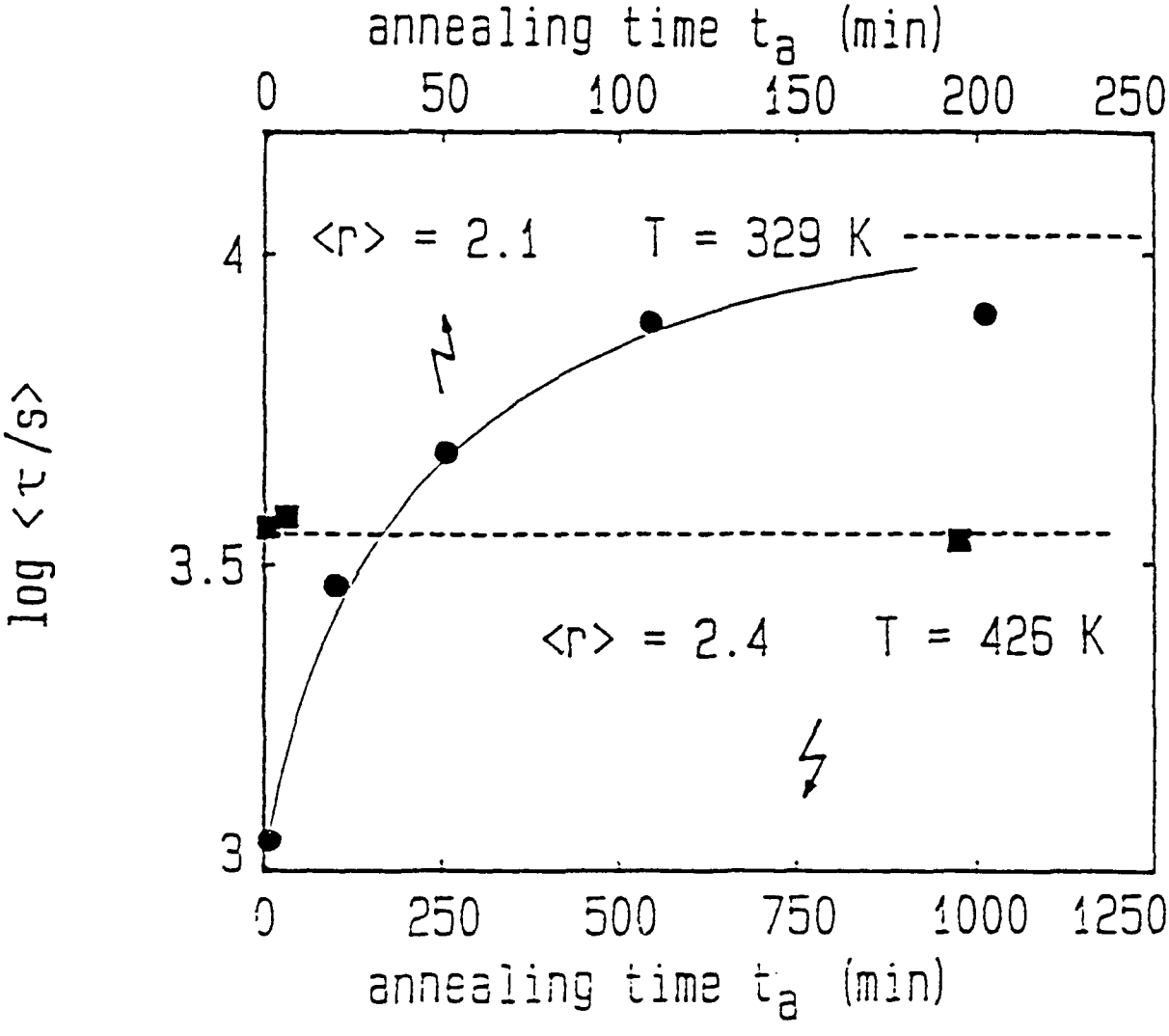
annealing time t_a (min)
0
50
100
150
200
250
4
3.5
3
log <τ/s>
<r> = 2.1
T = 329 K
<r> = 2.4
T = 425 K
0
250
500
750
1000
1250
annealing time t_a (min)

(19)

Elastic and viscoelastic properties of amorphous selenium: Possible identification of the elusive phase transition

R. Böhmer and C. A. Angell*
Department of Chemistry, Arizona State University
Tempe, AZ 85287-1604, USA

Abstract

Using a broadband mechanical spectrometer, the tensile modulus and stress relaxation of amorphous selenium was studied in the glass transformation range. Bimodal spectra were recorded under isothermal conditions in the time range 10^{-1} s < t < 10^{5} s. It was found that the structural equilibrations of the two contributions to the stress decay proceed independent of one another. The mechanical correlation functions of stabilized supercooled liquid Se could be described using a weighted sum of two stretched exponentials. The temperature dependences of the relative relaxation strengths were compared with results from a rotational isomeric state model. They are consistent with the existence of a sulfur-like polymerization transition temperature, which has been kinetically inaccessible to previous measurements, near 305 K.

PACS numbers: 62.40.ti, 64.70.Pf, 81.40.Ef

* present address: Institut für Physik, Johannes Gutenberg-Universität, D 6500 Mainz, Germany

I. Introduction

Amorphous selenium (a-Se) has been referred to as one of the best studied of all substances.[1] Among the reasons that have stimulated the intense interest in this material are not only its enormous technical importance, e. g. as a photoconductor,[2] but also the notion that glassy selenium may constitute one of the simplest polymers possible. For a long time it has been believed that, by analogy to liquid sulfur,[3] the *supercooled* liquid state of selenium contains polymeric chains and eight membered rings, in proportions which depend on temperature[4] as well as on thermal history.[5] These beliefs have in part been based on the thermodynamic arguments developed (in analogy to liquid sulfur[6]) by Eisenberg and Tobolsky.[7] A number of experiments were interpreted in the spirit of these arguments.[8,9] In particular results from infrared (IR) and Raman spectroscopy seemed to confirm the notion of a ring-chain equilibrium.[10,11] The analysis of these measurements was based on the comparison of the vibrational spectra of a-Se with those of its trigonal[12] (sometimes called hexagonal) or monoclinic[13] modifications. These crystalline structures are built from helical chains (the trigonal form) or contain eight membered rings (the monoclinic form).

Later evidence from IR, Raman,[14] and neutron[15] scattering experiments indicated that the atomic level structure of amorphous selenium is more complex than that of liquid sulfur. A refinement of the simple ring-chain picture is due to Misawa and Suzuki who developed the disordered chain model for a-Se.[16] This variety of the rotational isomeric state model[17] assumes that amorphous Se is not simply a mixture of cyclooctaselenium and polymeric chains but "includes a molecule having both ring and chain conformations of Se in a single molecule".[16] It remained an open question however whether the molecular interaction parameters used for this model are temperature independent. In fact, it has been speculated[16] that increasing molecular cooperation which can be expected to show up in the vicinity of the glass transition should modify the predictions of the Misawa-Suzuki model in this temperature range. Despite

numerous efforts to identify a sulfur-like polymerization transition in selenium no unambiguous experimental evidence has been obtained so far.

Another topic of continuing interest has been the study of stabilization of selenium glass, which obviously is of great technical importance. The effects of structural state dependence, although a general feature of the glass transformation range,[18] has received special attention in the case of a-Se because of the proximity of its calorimetric glass temperature T_g = 310 K to ambient.[19] In a-Se the structural relaxation has been investigated by a number of means including calorimetric,[20] viscosimetric,[21] dilatometric,[22] ultrasonic,[23-25] and dielectric[26] techniques. One of the most direct ways to monitor structural equilibration may be mechanical stress relaxation as employed in the present study. We have used a broadband spectrometer also in order to check whether the stress decay is bimodal as has been suggested previously.[27,28]

II. Experiments and analyses

The amorphous selenium used for this study was taken from the same batch which has been characterized earlier using calorimetric and viscosimetric experiments.[29] It was prepared by B. L. Halfpap using high purity starting material (99.9999%) as described in Ref. 29.

Details of the transient viscoelastometer and of experimental procedures and checks that have been performed are given elsewhere.[30] Tensile mechanical stress autocorrelation functions of a-Se have been recorded in the time range 10^{-1} s < t < 10^5 s. In this paper the decay functions are given in normalized form thus avoiding numerical uncertainties introduced by the geometric form factor.[30] In addition stress vs. strain curves have been recorded at several temperatures in and below the glass transformation range. The time used to built up the total strain (10 - 50 μm) was of the order of 1 s so the measurements and the linear behavior needed to yield Young's modulus at each temperature could be observed up to temperatures somewhat above the calorimetric glass point at which the average relaxation time is of the order of 200 s.

A. Elastic properties

Using ultrasonic measurements in the 1 - 20 MHz range, the elastic constants of a-Se have been determined by numerous researchers.[31] At low frequencies ($f \leq 1$ Hz) only shear moduli have been reported as a function of temperature[27,32] or frequency.[28] In Fig. 1 we compare the temperature dependence of the tensile (or Young's) modulus Y(T) from the present study with the shear constants G(T) obtained by Eisenberg and Tobolsky using a 5s experimental timescale.[27] In Fig. 1 the shear modulus commences its fall towards zero with increasing temperatures before the tensile modulus. Although some difference would be expected from the fact that the timescale used for the determination of Y(T) is shorter by a factor of approximately five it seems from results discussed later in Sec II.C that the differences in the temperatures where the falls start is not primarily a time scale effect. It is quite possible that the complex microstructure of amorphous selenium, leading to the bimodal stress relaxation spectra presented below, also gives rise to rather different response times to external shear strains and bulk compressions.

It is noted that the tensile moduli presented in Fig. 1 reflect equilibrium values. We observed that samples quenched from above the glass transition got stiffer on annealing below T_g. This can be viewed as a confirmation of earlier ultrasonic experiments: Here an increase in the sound velocity with time has been reported for quenched a-Se samples.[24] Fictive temperature effects which are a general feature of glass-formers far from structural equilibrium are discussed in more detail in the following section.

B. Structural equilibration

Amorphous selenium samples were kept at 335 K for at least 30 min in accordance with the suggestions by Chang and Bestul.[33] These authors noted that heating of a-Se to temperatures above 310 K ($=T_g$) lead to a completely equilibrated state irrespective of the previous thermal history. After annealing the samples they were cooled to several temperatures between 300 and 308 K with rates of

1-2 K/min while carefully excluding light.[34] Immediately after temperature stabilization an initial stress relaxation measurement was made followed by repeat runs after various holding (annealing) periods at the same temperature. Figure 2 shows the results obtained at an annealing temperature of T = 300.5 K. It is clear that the time required to relax the initial stress increases rapidly with annealing time t_a.

For a quantitative description of the stress relaxation the Kohlrausch function[35]

$$Y(t) = Y \exp\,[-(t/\tau)^{\beta}] + Y_0\,, \qquad (1)$$

was used. Here the relaxation of the tensile stress is characterized by a relaxation time τ and a fractional exponent $\beta \leq 1$. Y and Y_0 denote Young's moduli for $t \to 0$ (as presented in Sec. II.A) and $t \to \infty$, respectively. In the glass transformation range of viscoelastic bodies, Y_0 usually approaches zero for long times. It may be non-zero however in crystalline solids[36] and polymeric substances which show a rubbery plateau.[37] The best least squares fit to the $t_a = 0$ curve in Fig. 2 yielded $Y_0 = 0.03Y$. Good fits were also obtained using $Y_0 = 0$ (see Fig. 2).

In Fig. 3 structural equilibration data for T > 304 K are displayed as $\log[-\ln Y(t)/Y]$ vs log t (log denotes the logarithm to the base 10). This representation gives a straight line if Eq. (1) [with $Y_0 = 0$] is obeyed. For T = 304.6 K this is indeed the case. The slope of these curves give the fractional exponent β.

The changes of the time constants $\Delta \log \tau$ used to characterize the stress decay on annealing at T = 300.5 K and 304.6 K are summarized in Fig. 4. One notes that the total change $\Delta \log \tau$ or the change in the fictive temperature T_F[38] is larger for the stabilization at the lower temperature. This is expected because in both runs the samples were quenched using similar cooling rates and hence must haven fallen out of thermal equilibrium at about the same temperature. The relaxation of the fictive temperature has previously been described with Eq. (1) also.[39] The quality of the results presented in Fig. 4 does however not allow us to draw any

conclusions about the functional form of the temporal relaxation of T_F in a-Se. In order to estimate the time constant which governs this process, we have chosen a single exponential decay. The relaxation times obtained by this procedure are by factors of 5 and 9 larger than the equilibrium relaxation times $<\tau_s>$ extrapolated from Fig. 7 below for T = 304.6 K and 300.5 K, respectively. A similar ratio of equilibration to stress relaxation time (~ 10) has been obtained previously for a nitrate melt.[40]

The stress relaxation curves obtained at 307.5 K do not give a straight line in the representation of Fig. 3. Apparently an additional relaxation process shows up at long times. At first glance the change in slope suggests that this relaxation is characterized by a smaller β. It is however noted that the linearization procedure described above is expected to work only if the decay function is properly normalized [Y(t)/Y should go from 1 to 0 as t goes from 0 to -> ∞]. This condition is met for neither of the two relaxation processes. A remarkable feature of these spectra is that the equilibration of the long time decay is still progressing while the structural relaxation associated with the faster process is already complete. This observation suggests that the relaxations have different microscopic origins.

C. Stress relaxation at structural equilibrium

Figure 5 shows the time dependence of the normalized tensile stress of carefully equilibrated amorphous selenium. The wide spectral range of almost six decades accessible with the transient viscoelastometer used for this work allowed the full detection of bimodal decays at several temperatures. Indications for such a composite relaxation have existed before from measurements of the tensile[27] and shear moduli.[28] As shown in Fig. 5 the spectral shapes of the mechanical correlation functions change with T. This casts doubts on the validity of the thermorheological simplicity assumption, used in Ref. 27. While the time-temperature superposition principle has been demonstrated to hold for the electrical relaxation,[41] it seems to be more appropriate to describe

the mechanical properties of a-Se in terms of two independent processes, weighted by a coefficient z

$$Y(t) = Y[\exp\{-(t/\tau_S)^{\beta_S}\} + z \exp\{-(t/\tau_L)^{\beta_L}\}]. \quad (2)$$

The subscripts S and L stand for *s*hort and *l*ong time contributions to the Young modulus, respectively. The quality of the fits using Eq. (2) is demonstrated in Fig. 5. In the inset of this figure we plotted the derivative -d[Y(t)/Y] / d[log t/s] of the theoretical curve for T = 307.5 K. It gives a good impression of the separation of the average time scales of the two processes, and also of their relative widths.

At lower temperatures the slow relaxation appeared to be well outside our spectral range. If we assume $\tau_S << \tau_L$ then the second exponential in Eq. (2) can be approximated by unity in our time window. Thus, Eq. (1) is recovered and the weighting factor for a seemingly unimodal decay function is given by

$$z \approx Y_0/Y. \quad (3)$$

We will show in the discussion section that z, rather than being a mere fitting parameter may reflect a pivotal material characteristic viz. the fraction of Se atoms present in chain conformations. In Fig. 6 the coefficient z, as determined using Eqs. (1) and (2) is seen to decrease with temperature and approaches zero at low T. Also the fractional exponent β_S which characterizes the faster relaxation process strongly depends on temperature (Fig. 6). If $\beta_S(T)$ is linearly extrapolated (on a T or a 1/T scale) to lower T it crosses zero at $T_{\beta->0}$ = 270 ± 10 K. The shape parameter for the long time process is found to be β_L = 0.42 ± 0.1 but the temperature dependence could not be detected.

From the fits to our stress relaxation curves the average relaxation times[42]

$$\langle\tau\rangle = \tau\Gamma(1+1/\beta), \quad (4)$$

have been calculated for both long and short processes and are given in an Arrhenius plot (Fig. 7). This plot also contains relaxation times calculated from the maxima of the frequency dependent internal friction measured in shear[28] and from creep data.[21] The relaxation times determined in susceptibility (or creep J) experiments can be transformed into modulus (M) relaxation (or retardation) times according to $\tau_M/\tau_J = J_{t=0}/J_{t->\infty}$ ($= M_{t->\infty}/M_{t=0}$).[43] From the longitudinal sound velocities v of the liquid[44] extrapolated to T_g and the glass,[25] it is found that $\tau_M \approx \tau_J(v_{liq}/v_{glass})^2 \approx 2.7\tau_J$. The time constants determined from internal friction peaks are also expected to be larger than τ_M (but smaller than τ_J). However no transformation procedure similar to the one given above is known to us. From Fig. 7 one notes good agreement of the relaxation times $<\tau_s>$ obtained in the various experiments. We parameterized our results for both long and short time processes in terms of an Arrhenius law

$$<\tau_s> = A_s \exp(E_s/RT), \quad (5a)$$

$$<\tau_L> = A_L \exp(E_L/RT), \quad (5b)$$

where A is a prefactor. The apparent activation energy E_s used to describe the tensile relaxation times $<\tau_s>$ in the glass transformation range is E_s = 485 kJ/mol. R. This value is somewhat larger than that determined in creep (see Fig. 7), specific heat,[21] and viscosity[29] measurements none of which distinguish long from short time processes. However the large value of E_s and the unphysical value of log A_s = -80 imply that the process under study is highly cooperative. Indeed, if viscosities over an extended temperature range are taken into account, deviations from the seemingly thermally activated behavior become apparent.[45]

We note that the relaxation times determined in dielectric experiments[41] when extrapolated to sub-audio frequencies are significantly longer than those presented in Fig. 7. Decoupling of mechanical (and structural) degrees of freedom is a well known phenomenon in many solids (including ion conductors[46] as well as disordered crystals[47]). It seems to be a peculiarity of (the) amorphous (semiconductor) selenium that the electrically active

modes freeze first on cooling. These modes presumably involve electron hops between chain end radicals.[41]

An accurate analysis of the longer relaxation times is hampered by a considerable experimental uncertainty. From Fig. 7 it is however clear that the apparent hindering barrier E_L necessary to parameterize the slower process is slightly larger than E_S and in fact may be only the average of a diverging process related to the phase transition.

III. Discussion

The bimodal spectra of a-Se obtained in this work provide clear evidence for two independent relaxation processes. In principle there exist several possibilities for the assignment of these processes. Since it is generally accepted that there are a large number of long chains present in a-Se as normally prepared,[14] one might be tempted to conclude that the step in the correlation functions as presented in Fig. 5 represents the entanglement plateau. which is a well known feature in the mechanical spectra of polymers.[37]

An alternative view on the two relaxation processes (and one consistent with the direction of the annealing effect seen in Fig. 3), is the following: An arrangement of ring-like conformations as proposed by Misawa and Suzuki,[16] can be deformed relatively easily under external stress. This is because the bonding between these structural elements is mediated by van der Waals interactions. After application of strain, these merely localized modes may be expected to relax before long ranged deformations of the chains take place. A quantitative confirmation of this interpretation of our obervations comes from the computation of the relaxation strength of the faster process. The relative strength f of this contribution to the stress decay is calculated from Eq. (2) for $t = 0$ and gives $f = 1 / (1+z)$. It reflects the fraction of elastic modes originating from relaxations of ring-like conformations in the atomic level structure of a-Se and approaches unity at low temperatures.

In Fig. 8 we compare the fraction f from the present study with the predictions of the rotational isomeric state model. At temperatures above the calorimetric glass transition our

experimental data are close to the theoretical results of Misawa and Suzuki. Below T ≈ 307 K strong deviations are noticed. For non-equilibrated samples one would expect the fraction of ring-like conformations f to be no larger than its value at the glass transition. The relative ring relaxation strength from the viscoelastic experiments in which we have carefully annealed to equilibrium before taking the data on which this discussion is based, become systematically larger with decreasing temperatures than that predicted from the calculations for the disordered chain model, see Fig. 8. The effect is reversed (z increases) on re-equilibration at higher temperature, see Fig. 3. Our findings therefore suggest that a sulfur-like cooperative transition, which is kinetically inaccessible to most measurements, takes place in supercooled selenium at around 305 K as conjectured by Moynihan.[9]

We now examine the relation between relaxational and thermodynamic characteristics of a-Se and in particular the relation between the relaxation time and the Kauzmann temperature T_K.[4,9] This is the temperature at which the extrapolated configurational entropy of the supercooled liquid equals that of the crystal. For selenium it was estimated from calorimetric data that T_K is (240 ± 10) K.[33] T_K may be viewed as the glass transition temperature that would be measured if the liquid were cooled infinitely slowly. Therefore this quantity has also been estimated from the temperature dependence of the relaxation time τ (or the viscosity η)

$$\tau = \tau_0 \exp [DT_0 / (T - T_0)], \qquad (6)$$

by identifying T_0 and T_K. The Vogel-Fulcher Eq. (6) is a generalization of Eq. (5). By evaluating Eq. (6) at T_g one finds for the liquid "strength" index $D = \delta(T_g/T_K - 1) \ln(10)$. The parameter $\delta = \log \tau_g/\tau_0$ (or $\log \eta_g/\eta_0$) is found to be ≈ 16 for many glassformers. By evaluating the derivative of Eq. (6) at T_g one finds that the slope m in a scaled Arrhenius representation is given by[29]

$$m_{VF}(T_g) = [D/\ln(10)] (T_K/T_g) (1-T_K/T_g)^{-2}. \qquad (7)$$

Trivially, the slope of the Arrhenius law [Eq. (5)] when plotted vs T_g/T is given by $m_A = E_a/[RT_g \ln(10)]$. By using $m_A = mv_F(T_g)$ and inserting the above expression for the strength index D one arrives at

$$T_K = T_g (1 - \delta \ln(10) R T_g / E_a). \qquad (8)$$

This relation allows the calculation of T_K from the glass transition temperature $T_g = T(10^{12}$ Pa s) and the apparent activation energy E_a assuming that the process under study has remained coupled to the fundamental enthalpy relaxation. From the viscosimetric experiments of Ref. 29 one finds for a-Se T_K = 245 K while the present relaxation times $<\tau_s>$ yield T_K = 250 K, both in agreement with the calorimetric result.[33]

Note that these reasonable correlations have been made using data in both calorimetric and transport measurements for T > 310 K in which cooperative ring-chain effects are minimal (see Figs. 6 and 8) and z changes smoothly with temperature. Extrapolations which include data in the range 300 - 310 K should give anomalous results for T_K if the ring-chain exchange gives rise to an important enthalpy contribution.

In the following we will comment on the temperature dependence of the fractional exponent β_S. Although from a theoretical viewpoint it is not clear at present whether there exists a minimum $\beta > 0$,[48] has been observed for several supercooled liquids that $T_{\beta \to 0}$ coincides with the Kauzmann temperature T_K.[49] In our case the extrapolation of the data in Fig. 6 yielded at $T_{\beta \to}$ of 270 K, greater than T_K, however the basis for the extrapolation included data in the temperature interval 300 - 310 K, hence should be an overestimate.

On the other hand the extrapolations of β could also be unreliable in our case because of the complication that the width of the time dependent Young modulus $Y(t) = 3\ G(t)\ [1 + \nu(t)]$ (where ν is the Poisson ratio) will show a stronger temperature dependence than the shear modulus G(t) [if the spectral width of G(t) is not a constant]. This is because the relaxation of the Poisson ratio $\nu(t)$, if it

takes place on roughly the same time scale as G(t), will lead to an additional broadening of Y(t). The degree of this additional broadening depends on temperature and vanishes as the high-frequency value of ν approaches 0.5 at high temperatures. These effects are hard to evaluate from the present data since it is not quite clear whether the time constants which govern the relaxation of the shear and the bulk moduli (and hence ν) are of similar magnitude (see Sec. II.A).

IV. Summary and conclusions

We have studied the mechanical response of bulk quenched amorphous selenium following two types of external perturbations. Firstly we have used bending strains to measure Young's moduli. The subsequent relaxation of the tensile stress was monitored over a range of six decades in time. The isothermal mechanical spectra obtained that way are composed of two relaxation processes showing up on distinctly different time scales and having different spectral shapes. Secondly by using relatively large temperature steps as perturbations we probed the non-linear structural response. It was shown that the two relaxation processes are governed by different equilibration dynamics. We analyzed the carefully stabilized complex spectra and computed the relative strengths of the two relaxation processes. Their temperature dependence was compared to theoretical predictions. Our results together with the Misawa-Suzuki calculations suggest the occurrence of a sulfur-like polymerization transition near the calorimetric glass point of a-Se.

It appears that our broadband viscoelastic measurements are well suited to mapping out conformational changes in polymeric materials if their structural subunits possess different elastic or relaxational properties. It would be most interesting to extend our studies to supercooled liquids the average coordination of which differs from two in order to suppress or enhance the one or the other of the relaxation processes observed in selenium. Possible candidates for the doping of a-Se are halogens,[50] which decrease the average length of the polymeric chains and should lead to a weakening of the

long time relaxations and higher coordinated atoms which should remove the short time processes. For instance we recently[51] found that the degree of crosslinking introduced by replacement of 6 at% Se by Ge and As is sufficient to lead to an almost complete suppression of the faster processes. This encourages further investigation of relaxation phenomena in alloys with even smaller doping levels.

Acknowledgments

We are indebted to B. L. Halfpap for providing us with the high-quality melt quenched selenium. This work has been supported by the Office of Naval Research under Agreement No. N00014-84-K-0289 (selenium studies) and the Department of Energy under DE-FG02-89ER45398 (technique development).

References

1 *Gmelin Handbuch der Anorganischen Chemie*, Selen, Ergänzungsband A2 (Springer, Berlin, 1979), p. 239

2 S. B. Berger, R. C. Enck, M. E. Scharfe, and B. E. Springett, in *The physics of selenium and tellurium*, edited by E. Gerlach and P. Grosse (Springer, Berlin, 1979), pp. 256-266

3 A. T. Ward and M. B. Myers, J. Phys. Chem. **73**, 1374 (1969) and references cited therein.

4 G. Brieglieb, Z. Phys. Chem. **A144**, 321 (1929).

5 L. J. Graham and R. Chang, J. Appl. Phys. **36**, 2983 (1965).

6 G. Gee, Trans. Faraday Soc. **48**, 515 (1952).

7 A. Eisenberg and A. V. Tobolsky, J. Polym. Sci. **46**, 19 (1960).

8 R. C. Keezer and M. W. Bailey, Mat. Res. Bull. **2**, 185 (1967).

9 C. T. Moynihan and U. E. Schnaus, J. Am. Ceram. Soc. **54**, 136 (1971).

10 G. Lucovsky, A. Mooradian, W. Taylor, G. B. Wright, and R. C. Keezer, Solid State Commun. **5**, 113 (1967).

11 M. Gorman and S. A. Solin, Solid State Commun. **18**, 1401 (1976).

12 A. J. Bradley, Phil. Mag. **48**, 477 (1924).

13 R. D. Burbank, Acta Cryst. **4**, 140 (1951).

14 G. Lucovsky, in Ref. 2, pp. 178-192.

15 M. Misawa and K. Suzuki, Trans. Jpn. Inst. Metals **18**, 427 (1977).

16 M. Misawa and K. Suzuki, J. Phys. Soc. Jpn. **44**, 1612 (1978).

17 Rotational isomeric state models have widely been used to describe conformational transitions of polymeric materials. See e. g. I. Bahar and W. L. Mattice, Macromolecules **24**, 877 (1991) and refs. cited therein.

18 S. Brawer, *Relaxation in viscous liquids and glasses* (American Ceramic Society, Columbus, OH, 1985).

19 The rate dependent calorimetric glass transition temperature of a-Se is $T_g = 310 \pm 7$ K, see e. g. M. Abkowitz and D. M. Pai, Phys. Rev. Lett. **38**, 1412 (1977); R. B. Stephens, J. Appl. Phys. **49**, 5855 (1978); and in particular Ref. 9 and papers cited therein. Samples prepared from the batch used for the present

study gave a T_g of 310 K when heated with 10 K/min, see M. Tatsumisago et al., Phys. Rev. Lett. **64**, 1549 (1990). At T the enthalpy relaxation time is of the order of 200 s.

20 R. B. Stephens, J. Non-Cryst. Solids **20**, 75 (1976).

21 R. B. Stephens, J. Appl. Phys. **49**, 5855 (1978).

22 E. Kittinger, Phys. Stat. Sol. (a) **44**, K35 (1977).

23 S. Etienne, G. Guenin, and J. Perez, J. Phys. D: Appl. Phys. **12**, 2189 (1979).

24 E. Kittinger, J. Non-Cryst. Solids, **27**, 421 (1978).

25 E. Kittinger, Z. Naturforsch. **32a**, 946 (1977).

26 M. Abkowitz, D. F. Pochan, and J. M. Pochan, J. Appl. Phys. **53**, 4173 (1982).

27 A. Eisenberg and A. V. Tobolsky, J. Polym. Sci. **61**, 483 (1962).

28 S. Etienne, J. Y. Cavaille, J. Perez, R. Point, and M. Salvia, Rev. Sci. Instr. **53**, 1261 (1982).

29 M. Tatsumisago, B. L. Halfpap, J. L. Green, S. M. Lindsay, and C. A. Angell, Phys. Rev. Lett. **64**, 1549 (1990).

30 R. Böhmer, H. Senapati, and C. A. Angell, J. Non-Cryst. Solids (1991), in press.

31 see the review given in Ref. 23.

32 S. Etienne, J. Perez, S. Peytavin, and M. Ribes, preprint (1990).

33 S. S. Chang and A. B. Bestul, J. Chem. Thermodyn. **6**, 325 (1974) and S. S. Chang (private communication).

34 It is known that exposure of a-Se to electromagnetic radiation promotes its structural equilibration, S. Etienne, J. Y. Cavaille, J. Perez, E. Bonjour, and R. Calemczuk, J. Phys. (Paris) **43**, C9-599, (1982).

35 F. Kohlrausch, Ann. Phys. (Leipzig) **119**, 337 (1863).

36 For a recent example in a crystalline orientationally disordered glass see e. g. J. Hessinger and K. Knorr, Phys. Rev. Lett. **65**, 2674 (1990).

37 J. D. Ferry, *Viscoelastic properties of polymers*, 3rd ed. (Wiley, New York, 1980).

38 The changes in the non-equilibrium relaxation time τ_n over a small temperature interval can always be parametrized as $\tau_n =$

A exp (E / RT_F) [see also Eq. (5)]. Evaluating this expression for T_1 and T_2 with $T \approx (T_1T_2)^{1/2}$ gives $\Delta \log \tau_n = - \Delta T_F (E/T)^2$.

39 C. T. Moynihan et al., Ann. N. Y. Acad. Sci. **279**, 15 (1976).

40 H. G. K. Sundar and C. A. Angell, in *Collected papers of the XIVth International Congress on Glass*, New Delhi (Indian Ceramic Society, Calcutta, 1986), vol. II, pp. 161-168; C. A. Angell, J. Non-Cryst. Solids **102**, 205 (1988).

41 M. Abkowitz, D. F. Pochan, and J. M. Pochan, J. Appl. Phys. **51**, 1539 (1980).

42 C. P. Lindsay and G. D. Patterson, J. Chem. Phys. **73**, 3348 (1980).

43 J. Lamb, Rheol. Acta **12**, 438 (1973).

44 Y. Tsuchiya, J. Non-Cryst. Solids **122**, 205 (1990)

45 M. Cukierman and D. R. Uhlmann, J. Non-Cryst. Solids **12**, 199 (1973) and references cited therein.

46 C. A. Angell, Solid State Ionics **18&19**, 72 (1986).

47 U. G. Volkmann, R. Böhmer, A. Loidl, K. Knorr, U. T. Höchli, and S. Haussühl, Phys. Rev. Lett. **56**, 1716 (1986).

48 M. H. Cohen and G. S. Grest, Phys. Rev. B **24**, 4091 (1981); I. A. Campbell, J. M. Flesselles, R. Julien, and R. Botet, J. Phys. C **20**, L47 (1987); P. K. Dixon et al., Phys. Rev. Lett. **66**, 960 (1991).

49 P. K. Dixon and S. R. Nagel, Phys. Rev. Lett. **61**, 341 (1988); M. Oguni, H. Hikawa, and H. Suga, Thermochim. Acta **158**, 143 (1990); P. K. Dixon, Phys. Rev. B **42**, 8179 (1990).

50 S. Hamada, N. Yoshida, and T. Shirai, Bull. Chem. Soc. Jpn. **42**, 1025 (1969).

51 R. Böhmer and C. A. Angell, Phys. Rev. Lett. (submitted).

Figure Captions

FIG 1. Tensile moduli Y(T) and shear moduli G(T) of amorphous selenium. Open circles are results from the present investigation. They have been normalized to match Youngs modulus of Y = 9.8 GPa as determined from ultrasonic measurements at ambient temperature (closed circle).[31] Elastic shear constants taken at 1 - 20 MHz (closed square, Ref. 31) and at a very low frequency from Ref. 27 ("five second moduli", displayed as a solid line) have been included for comparison. The dashed line is a guide to the eye only.

FIG. 2. Time dependence of normalized tensile stress $Y(t)/Y(t=0)$ of amorphous selenium which has previously been quenched from above the glass transition. The labels indicate the times at which the measurements have been started relative to the first run. The solid lines are fits using Eq. (1) with $\beta = 0.47$ and $Y_0 = 0$. The variations in the relaxation times are given in Fig. 4.

FIG. 3. Tensile autocorrelation functions $\log[-\ln(Y/Y)]$ of a-Se as a function of log t. In this representation Eq. (1) yields a straight line with slope β. Temperatures T and annealing times t_a (in hours after starting the first run) are indicated near the curves. Measurements at 304.6 K preceded those at 307.5 K. Note that the strength of the slow process increases with time as structural equilibrium is approached from below.

FIG. 4. Variation of the relaxation times with annealing time. The lines are guides to the eye only.

FIG. 5 Double logarithmic plot of stress versus time. For clarity the spectra taken at T = 307.5 K and T = 314.1 K were shifted downwards by 0.25 and 0.5 respectively. Solid lines represent fits using Eq. (1) [for T = 300.5 K] and Eq. (2). The inset shows the

derivative -d[Y(t)/Y]/d[log t/s] of the fit to the data taken at 307.5 K. A two peak structure is clearly seen.

FIG. 6 Temperature dependence of the fractional exponent β_S and the weighting factor z from the fits to the tensile autocorrelation functions of a-Se. Lines are guides to the eye only.

FIG. 7 Arrhenius plot of amorphous selenium relaxation times obtained using creep measurements[21] (solid line) internal friction measurements[28] (+) and tensile stress relaxation measurements (• for $<\tau_S>$, ▲ for $<\tau_L>$ from the present work). Note that the results from the creep compliance measurements[21] have been transformed into modulus relaxation times using the procedure described in the text. The dashed line was calculated using the E_S value given in the text. The dash-dotted line is drawn to guide the eye only; its slope corresponds to an apparent activation energy E_L of 530 kJ/mol and prefactor log A = -86.

FIG. 8 Fraction f of eight membered rings in amorphous selenium. From the weighing factors z shown in Fig. 6, the fraction was calculated as f=1/(1+z). The results from the rotational isomeric state model are shown as solid line.[16] The thermodynamic model by Eisenberg and Tobolsky predicts the fraction f to vary according to the dash-dotted line.[7] Open circles represent the experimental results from the dissolution studies by Brieglieb.[4]

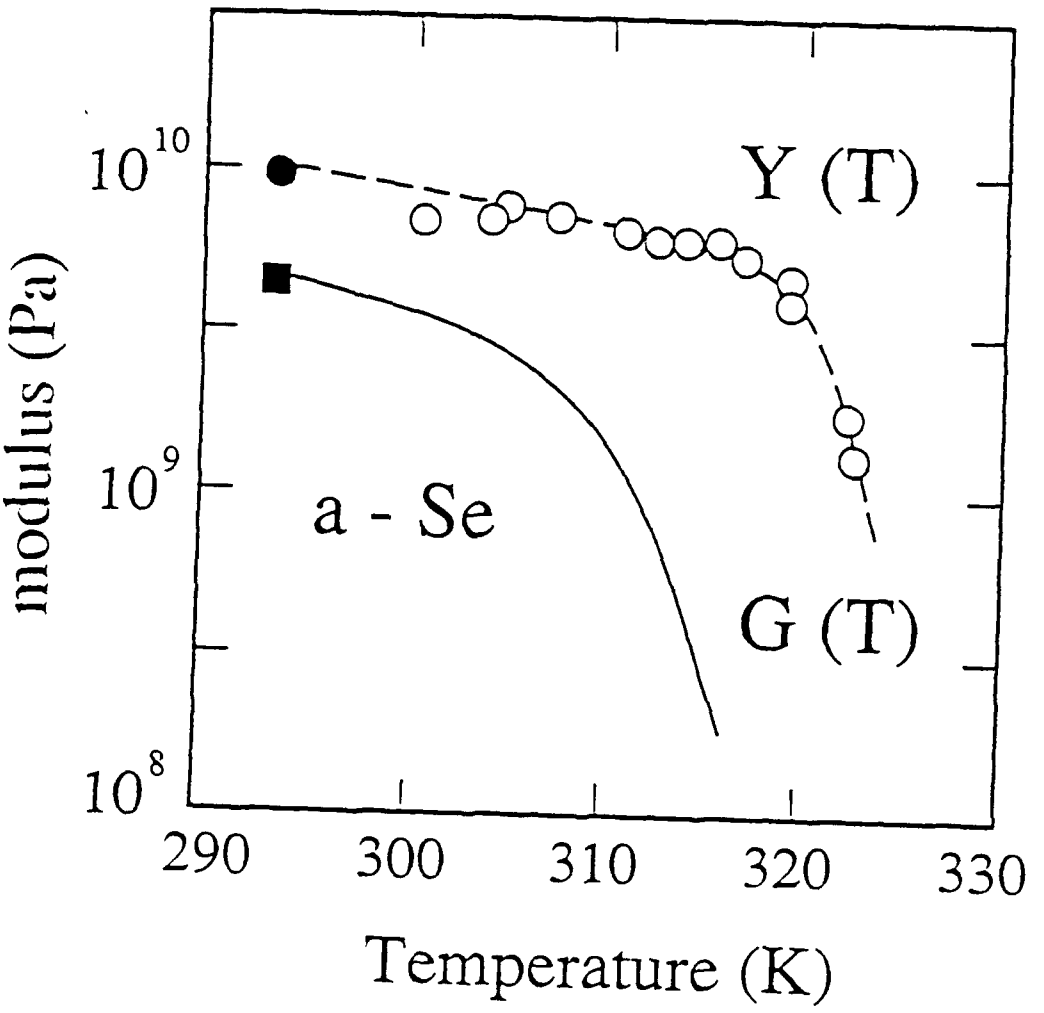
modulus (Pa)
10^{10}
10^{9}
10^{8}
Y (T)
a - Se
G (T)
290
300
310
320
330
Temperature (K)

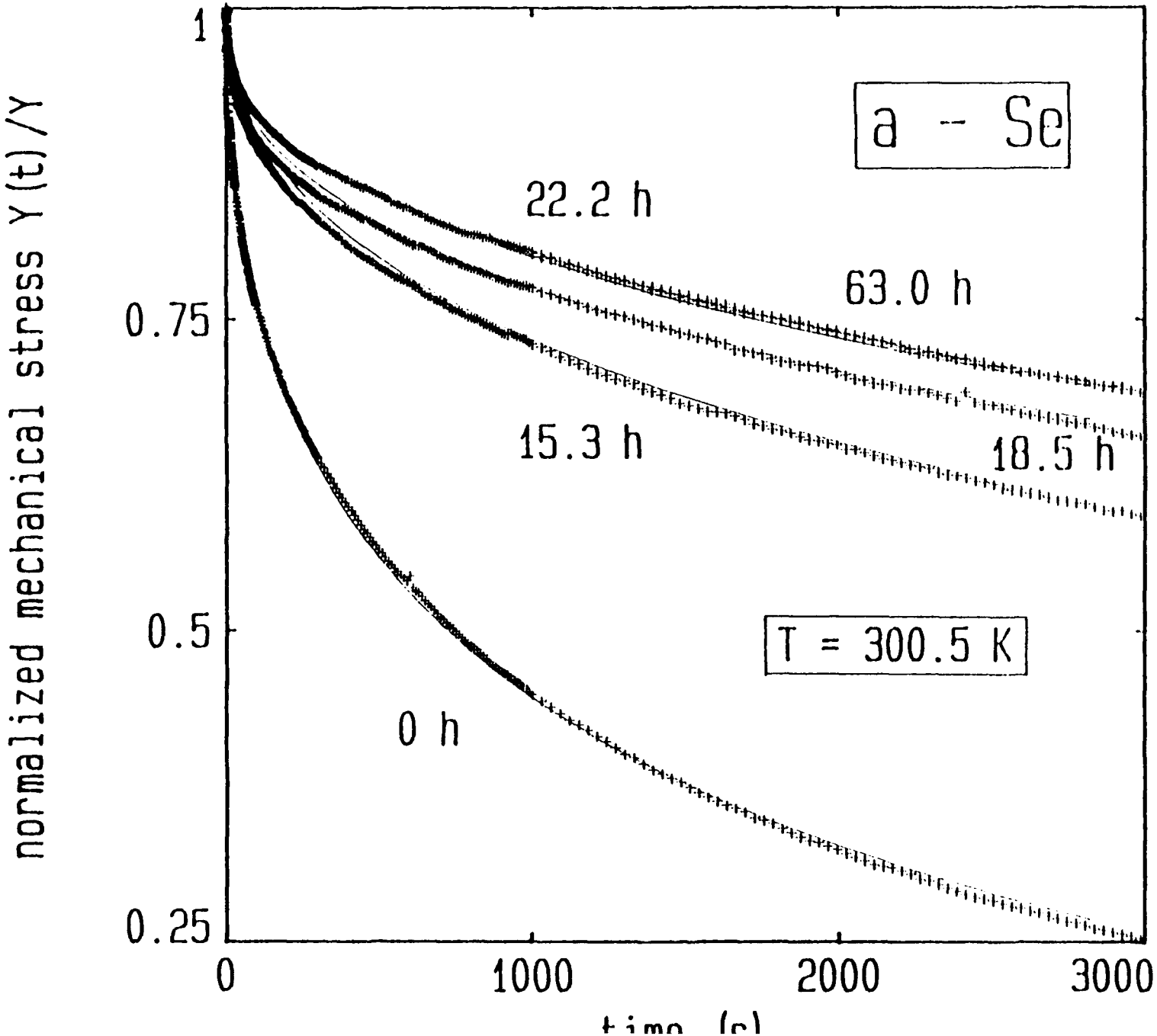
a -- Se
22.2 h
63.0 h
15.3 h
18.5 h
T = 300.5 K
0 h
normalized mechanical stress Y(t)/Y
1
0.75
0.5
0.25
0
1000
2000
3000
time (s)

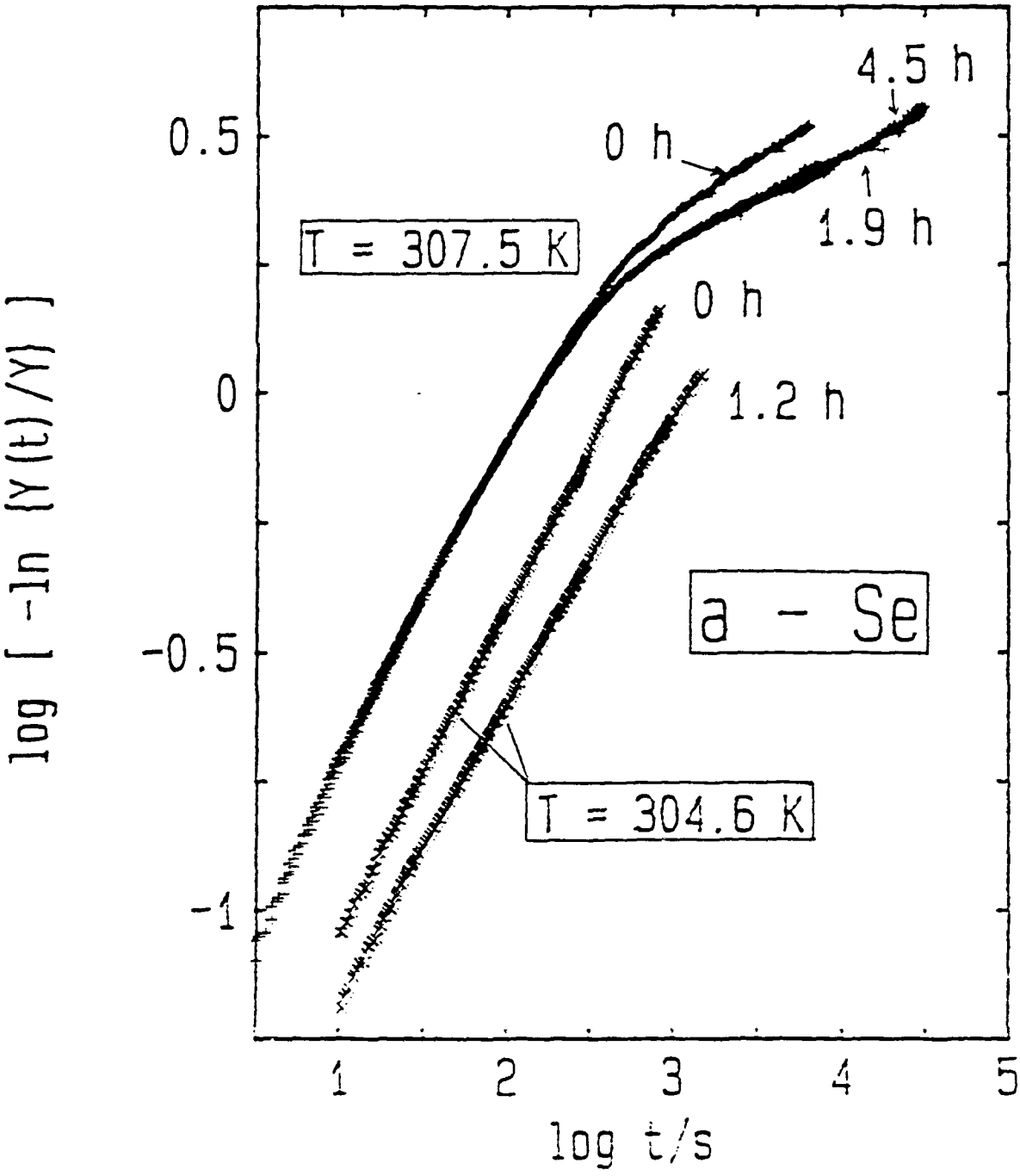
4.5 h
0 h
1.9 h
T = 307.5 K
0 h
1.2 h
a - Se
T = 304.6 K
0.5
0
-0.5
-1
1
2
3
4
5
log [-ln (Y(t)/Y)]
log t/s

FIG. 3

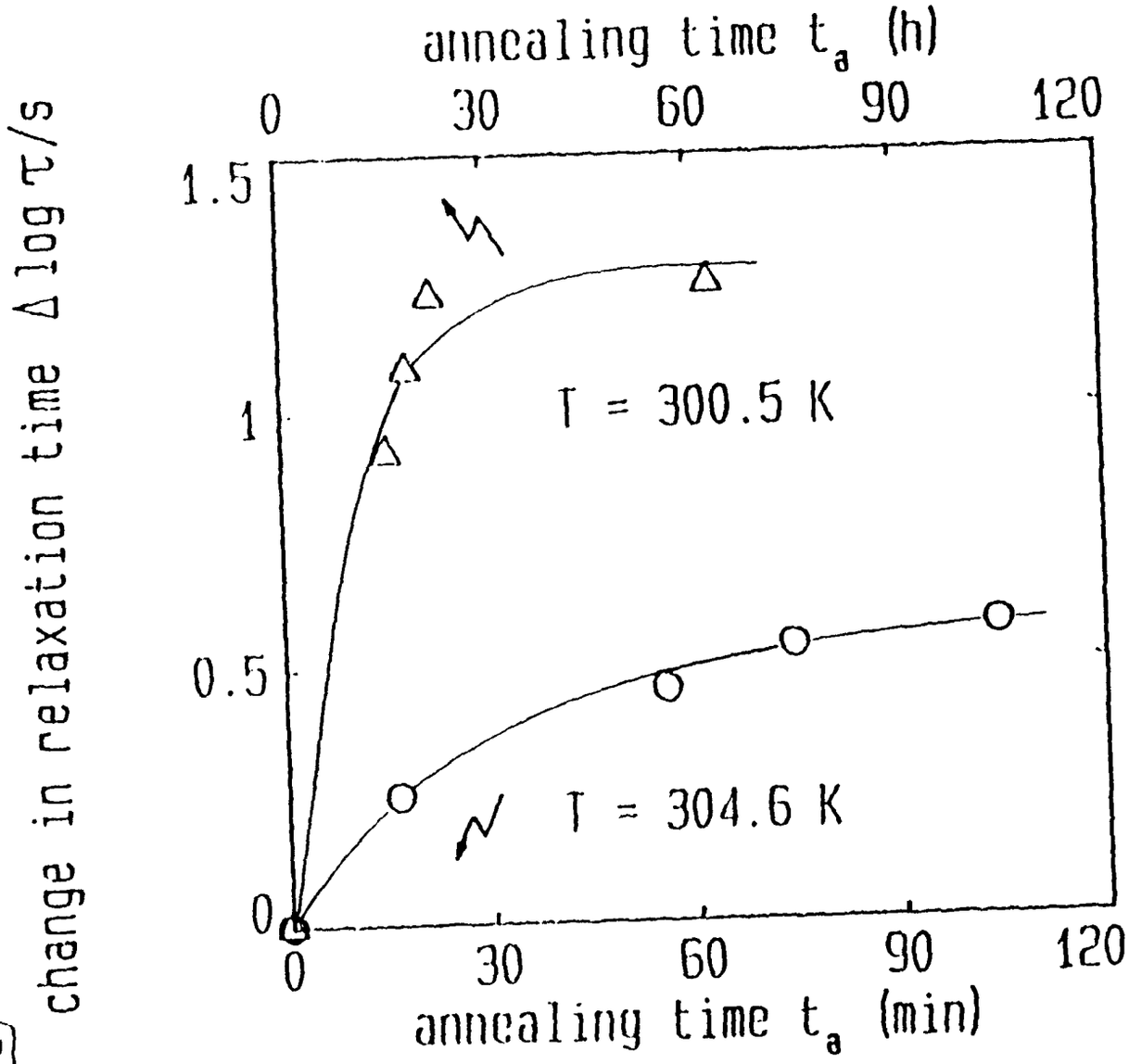
annealing time t_a (h)
0
30
60
90
120
1.5
1
0.5
0
change in relaxation time $\Delta \log \tau/s$
T = 300.5 K
T = 304.6 K
0
30
60
90
120
annealing time t_a (min)

FIG. 4

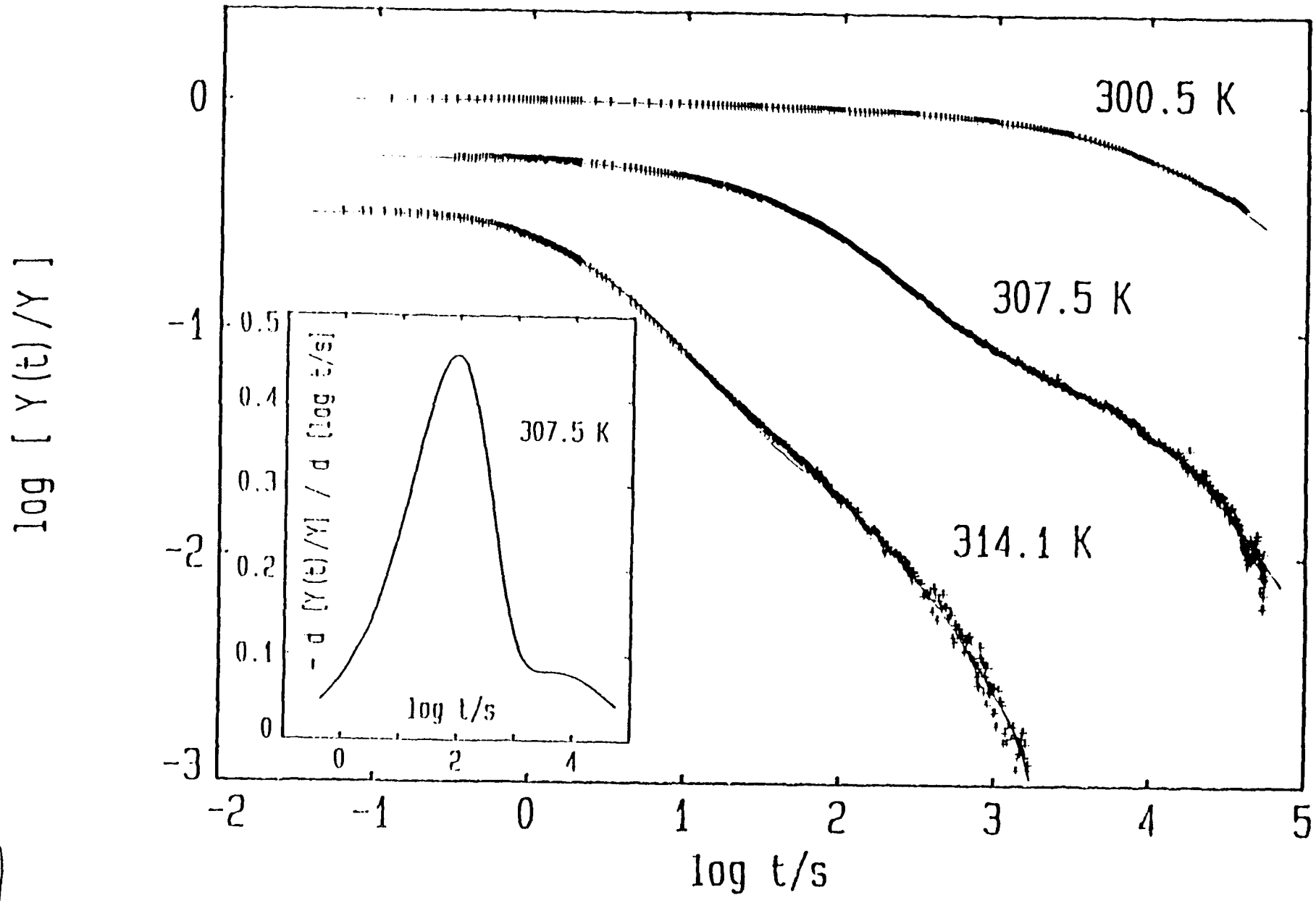
300.5 K
307.5 K
314.1 K
log [Y(t) /Y]
log t/s
- d [Y(t)/Y] / d (log t/s)
307.5 K
log t/s

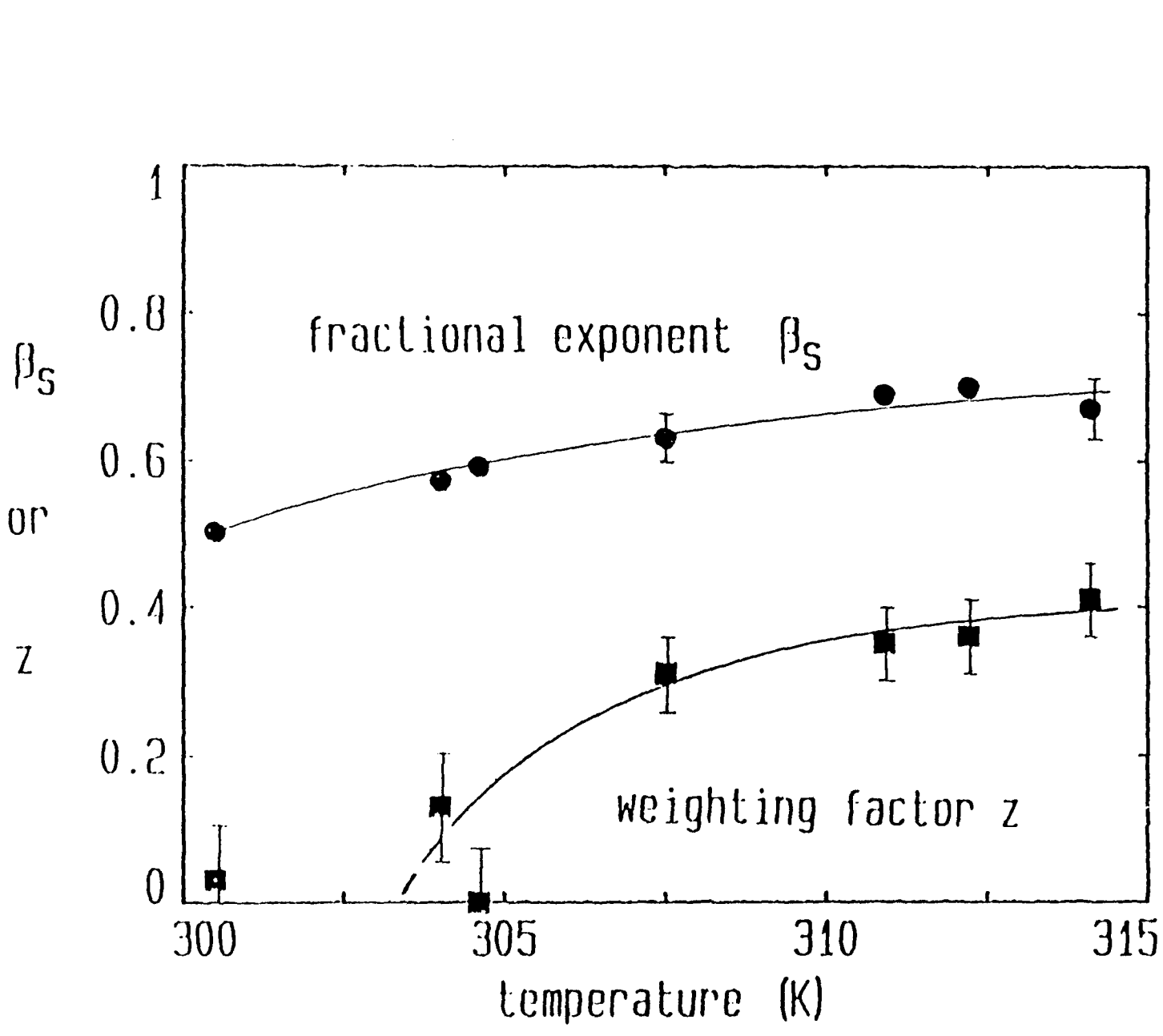
1
0.8
0.6
0.4
0.2
0
β_S
or
z
fractional exponent β_S
weighting factor z
300
305
310
315
temperature (K)

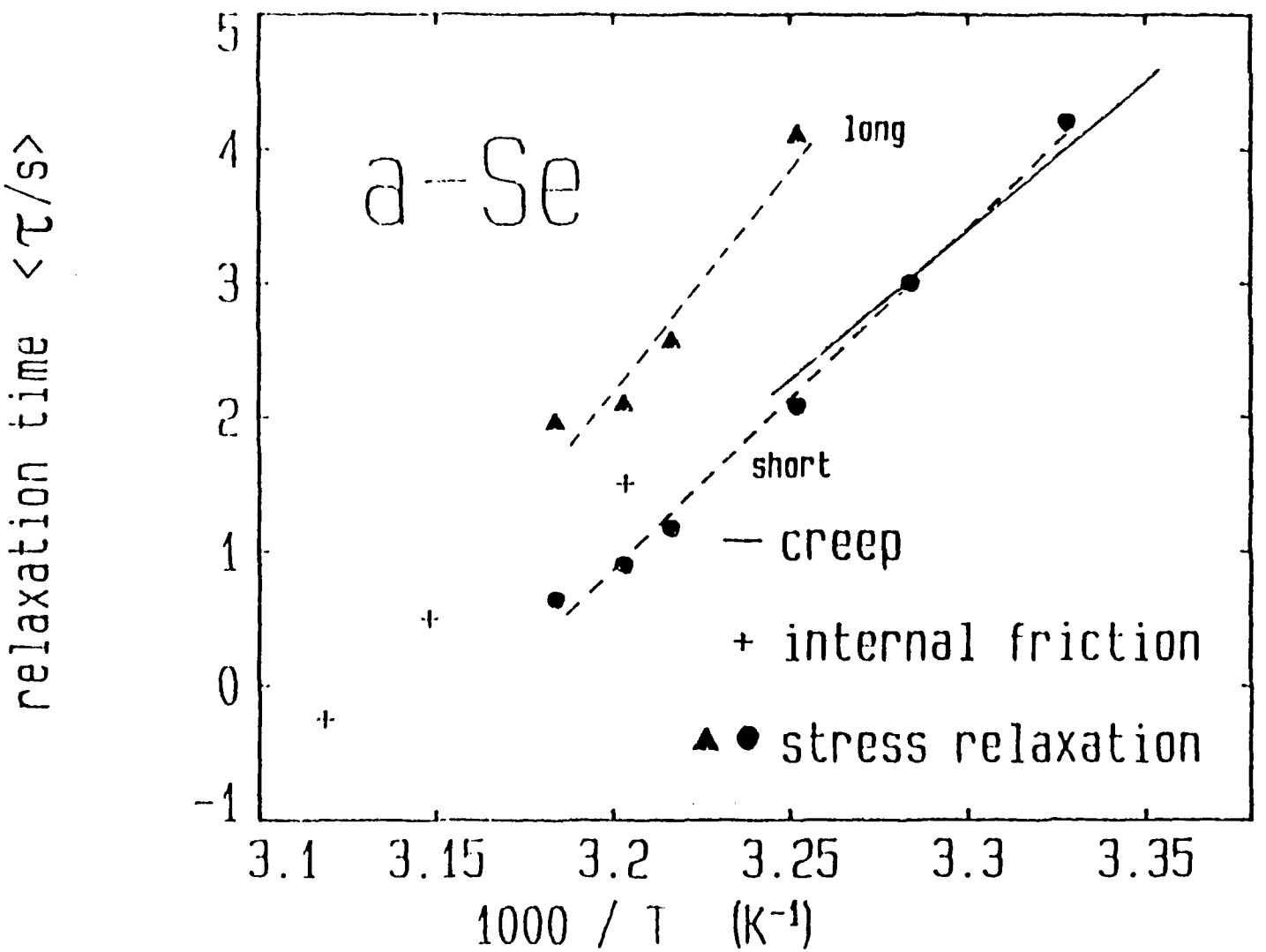
a-Se
long
short
creep
internal friction
stress relaxation
relaxation time <τ/s>
1000 / T (K⁻¹)
5
4
3
2
1
0
-1
3.1
3.15
3.2
3.25
3.3
3.35

FIG. 7

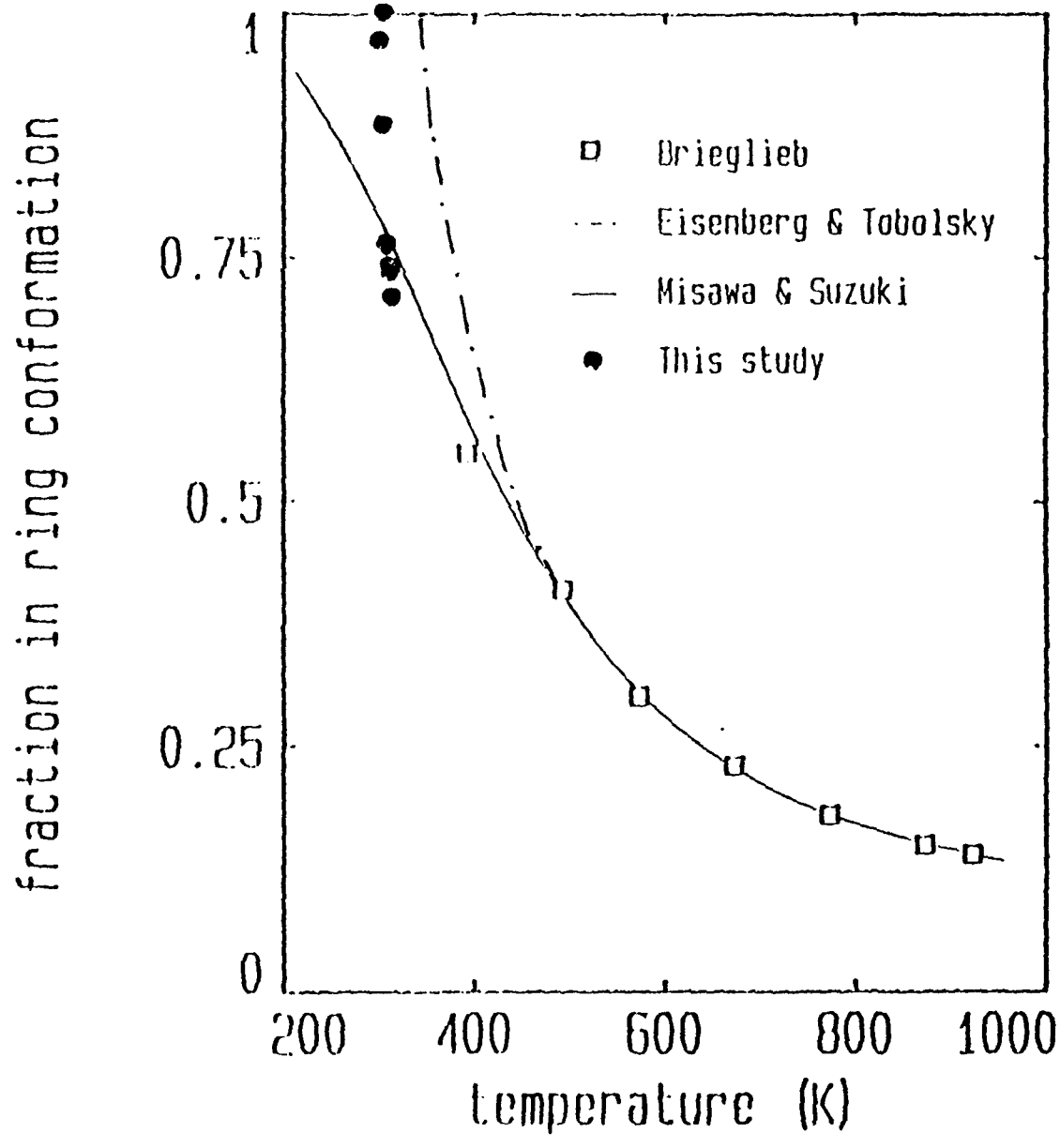
fraction in ring conformation
1
0.75
0.5
0.25
0
200
400
600
800
1000
temperature (K)
Brieglieb
Eisenberg & Tobolsky
Misawa & Suzuki
This study

Fig. 3

Subject index: rigidity percolation, mechanical spectroscopy, glass transition
Running heading: Fragility and non-exponential mechanical relaxation
(drop *mechanical* if too long)

(20)

Connectivity, fragility, and non-exponentiality of mechanical relaxations in covalently bonded glassformers

R. Böhmer
Institut für Physik, Johannes Gutenberg-Universität, D-6500 Mainz, Germany

C. A. Angell
Department of Chemistry, Arizona State University
Tempe, AZ 85287-1604, USA

ABSTRACT
Using a broadband transient viscoelastometer we have studied the stress relaxation of supercooled Ge-As-Se liquids after exposing them to flexural strains and temperature steps. This allowed us to monitor the linear mechanical response as well as the non-linear structural response. The departures from exponential stress relaxation correlate with the variations in fragility in the chalcogenide system. The structural state dependence of the mechanical relaxation, observed in pure and weakly crosslinked Se, is suppressed at the percolation threshold where the liquid fragility is minimum.

1. INTRODUCTION
The notion that the connectivity of covalently bonded glasses should correlate with their stiffness has stimulated numerous ultrasonic investigations.[1] However the onset of rigidity at the theoretically predicted threshold,[2] i. e. at the average coordination of $\langle r \rangle = 2.4$ has not been detected in elastic experiments on various chalcogenide alloys. Recently however, it was recognized that the concept of connectivity is useful in understanding the composition dependences of various low temperature ($T < 2K$) properties [3] as well as of characteristics of the glass transformation range, viz. the fragility and configurational thermodynamic properties of Ge-As-Se liquids.[4] The interrelation between these key aspects of the vitrification process finds an explanation in the characteristic topologies of the potential energy hypersurfaces for different compositions.[5] Following these arguments it has been suggested that an increase in fragility should be accompanied by

increases in the non-exponentiality and non linearity (state dependence) of the dynamical behavior in the glass transformation range.[6]
Despite the wealth of experimental data on the relaxational behavior of glass formers,[6,7] a systematic investigation of these questions is still missing. Therefore we have studied the time dependent stress relaxation of Ge-As-Se glassformers after exposing them to flexural strains and temperature steps.

2. EXPERIMENTAL

The melt cooled $Ge_aAs_bSe_c$ samples used for this study were taken from batches which had been prepared and characterized previously.[4] From the mole fractions a, b, and c the average coordination number can be calculated by $\langle r\rangle=4a+3b+2c$. At constant connectivity the composition is further specified by the fraction $y=a/(a+b)$. The experiments have been performed on samples along pseudo-binary cuts in the ternary system with either $\langle r\rangle$ (=2.4) or y (=0.5) being constant.
Most measurements were taken on bar samples cut to identical sizes (1x1x5 mm^3). The tensile stress relaxation at constant strain was monitored in the flexural (three point bending) conformation for seven compositions at constant $y=0.5$, and for two at $\langle r\rangle=2.4$ but $y\neq0.5$. Data were recorded automatically [8] in the time range $10^{-1}s < t < 10^5s$ and for temperatures between 300 and 600K. Since the relaxation time for a liquid in the glass transformation range usually depends on its structural state (fictive temperature) as well as the actual temperature,[9] we have repeated the runs after various equilibration times both to ensure equilibration is reached and to acquire data on this non-linear aspect of the phenomenon.

3. RESULTS AND DISCUSSION

3.1 FRAGILITY AND STRESS RELAXATION

The stress relaxation data obtained for the chalcogenide alloys are similar in quality to those previously reported.[8] For $\langle r\rangle > 2.1$ all spectra on the equilibrated specimen could be described [10] using the Kohlrausch function [11]

$$Y(t) = Y(t=0)\exp\left[-(t/\tau)^{\beta}\right]. \qquad (1)$$

Here β characterizes the broadening and $\langle\tau\rangle=\tau\Gamma(1+1/\beta)$ the average relaxation time of the tensile stress autocorrelation function. For pure and weakly crosslinked amorphous selenium (a-Se), i. e. $\langle r\rangle < 2.1$, the stress decay was composed of two contributions with distinctly separated average time scales. The relative strength of the two relaxation processes was found to be temperature dependent for a-Se.[12] In the vicinity of the glass transition the faster process, which was ascribed to localized modes,[12] relaxed more than 50% of the initial stress. For the $\langle r\rangle=2.1$ sample the short time relaxation was responsible for no more than 5% of the total stress decay. In each case the slower relaxations could be parameterized satisfactorily using equation (1).
The temperature dependences of $\langle\tau\rangle$ from all our samples within experimental uncertainty were found to comply with the Arrhenius law $\langle\tau\rangle=\tau_0\exp[E/(RT)]$

but with unphysical τ_o. In figure 1a we present the connectivity dependence of the fragility (or steepness index [13]) defined by

$$m = d \log \langle\tau\rangle / d\,(T_g/T) = E/[\ln(10)\ R\ T_g] = \log \tau_g/\tau_o. \qquad (2)$$

The fragilities m obtained from the present tensile stress relaxation experiments are in good agreement with those from previous shear viscosity measurements.[4] The mean relaxation time τ_g used in equation (2) was chosen to be 200s which is the typical time scale of the enthalpy relaxations at $T_{g,cal}$ as determined in differential scanning calorimetry experiments.[9] The glass transition temperatures from the present work [$T_g=T(\langle\tau\rangle=\tau_g)$] are in agreement with those from numerous calorimetric investigations.[4,14] As shown in figure 1a we find that the fragility of the Se rich alloys decreases with increasing crosslinking. The minimum of m at <r>=2.4 is very shallow and the increase of this figure is very slight towards larger <r>. Note that the minimum value m can reasonably have with the above definition of τ_g is when τ_o is the inverse of a vibration frequency, whence m≈16.

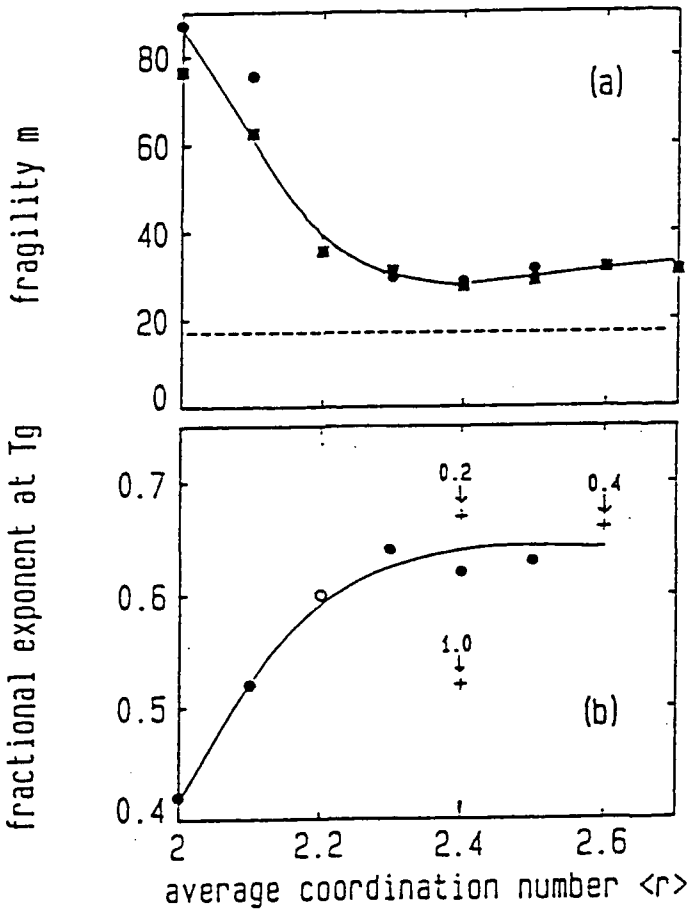

FIGURE 1. Connectivity (<r>) dependence of (a) fragilities m, and (b) fractional exponents β as determined at their glass transition temperatures T_g. The squares represent results from measurements of the viscosity on samples with y = 0.5 (taken from [4]). The present stress relaxation experiments yielded data on alloys with y=0.5 (circles) and off that pseudo-binary cut with y given near the plusses. The fractional exponent at <r>=2.2 was extrapolated from a measurement of a thicker (2.5x2.5x5 mm^3) sample. The dashed line indicates the minimum fragility. The solid lines are guides to the eye.

In the lower part of figure 1 we present the variations of the Kohlrausch exponent β with the average coordination as determined at T_g of various samples with y=0.5. The relaxation of a-Se is the most non-exponential. With

increasing crosslinking β assumes larger values and for <r> ≥ 2.3 is roughly constant at 0.63. Figure 1b also shows that $\beta(T_g)$ for several compositions at <r>=2.4 is not universal, probably due to chemical effects.[15] The results presented in figure 1b demonstrate that the increase in the fragility m is accompanied by an increase in β.

In figure 2 we have replotted the results from figure 1 as fractional exponent β versus fragility m. Also included are results from mechanical spectroscopy on polymers as compiled by Plazek and Ngai.[13] This plot reveals an interesting correlation between m and β. It should be interesting to include even more data from mechanical relaxation studies in order to check whether the correlation suggested in figure 2 can be further substantiated. We note that recently this matter has been discussed controversely.[6,7,16]

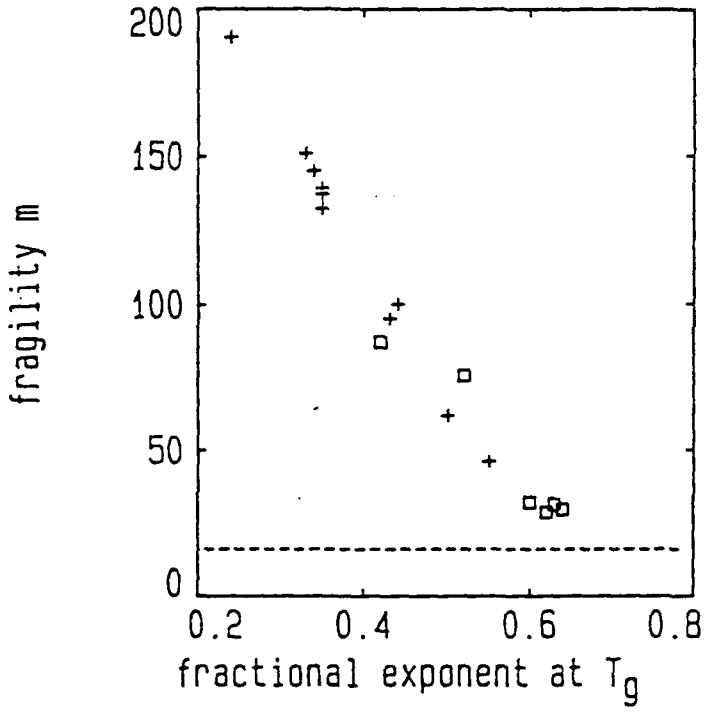

FIGURE 2. Fragility m versus fractional exponent β at the glass transition for polymers (circles, taken from Plazek and Ngai [13]) and chalcogenides (squares, this work). The broken line indicates the minimum fragility.

It is important to note that the detailed shape of the β versus <r> curve (figure 1b) depends on the definition of T_g, which is arbitrary. By requiring the glass transition to correspond to a much longer relaxation time than τ_g, a slight maximum at <r>=2.4 would show up in figure 1b, which by extrapolation would become more pronounced as the Kauzmannn temperature [5] is approached. This is because the fractional exponents necessary to describe the relaxational spectra of our samples show a temperature dependence with $d\beta/dT$ being smallest for $Ge_{15}As_{15}Se_{70}$ (<r>=2.4, y=0.5), i. e. the least fragile sample.

3.2 FRAGILITY AND STRUCTURAL RELAXATION

The results discussed so far have been taken on structurally equilibrated samples, i. e. those which within experimental uncertainty yielded identical stress relaxations in successive runs. It is well known however, that after

changing the temperature of a supercooled liquid it may take some time for its structure to reach thermal equilibrium. For instance, the time constant characterizing this stabilization process was found to be roughly ten times larger than the equilibrium stress relaxation time $\langle\tau\rangle$ in a fragile nitrate melt [17] and $(7\pm2)\langle\tau\rangle$ in a-Se.[12] In those experiments the samples were quenched from well above T_g to a temperature at which (for experimental convenience) the average relaxation time is larger than 10^3s. The temperature steps employed in those studies (and also in the present work) typically were as large as some tens of degrees. Under these circumstances the structural equilibration times should depend on the sign as well as the magnitude of the perturbation, i. e. the temperature step.[18] These are the hallmarks of the non-linear response regime.

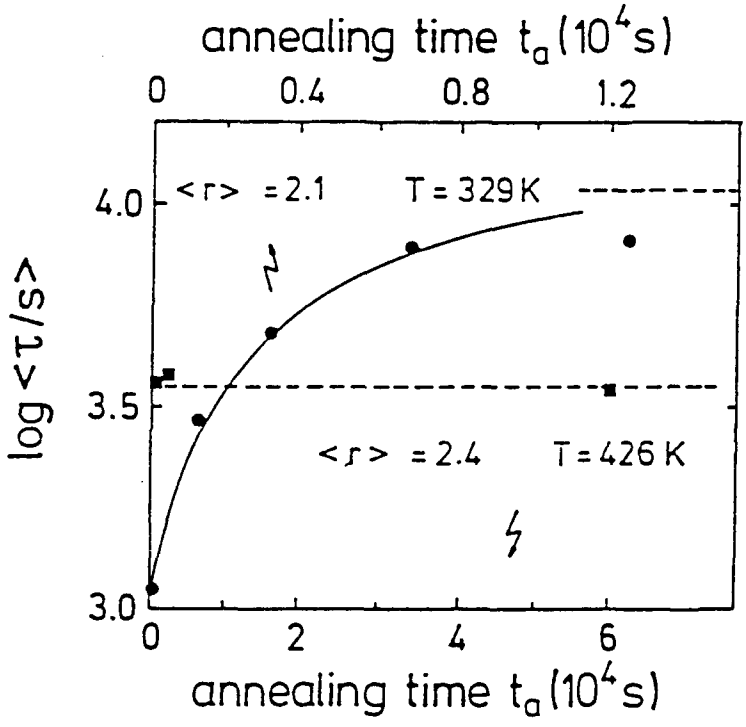

FIGURE 3. Evolution of the mean relaxation time on annealing for two different samples with y = 0.5. Prior to taking these data the samples were cooled with rates of several degrees per minute to the temperatures given near the curves. The dashed lines indicate the equilibrium relaxation times calculated using the parameters given in Fig. 2. The solid line is a guide to the eye only.

The evolution of the average non-equilibrium stress relaxation times $\langle\tau_n\rangle$ recorded during the isothermal stabilization of $(Ge_{0.5}As_{0.5})_{1-x}Se_x$ samples with $\langle r\rangle$=2.1 and 2.4 is depicted in figure 3. For the latter sample no change of $\langle\tau_n\rangle$ could be detected. Note that in these experiments it is not possible to record the initial part of the structural relaxation, i. e. the one which occurs before the stabilization of the final temperature (about 15min) is complete. The absence of pronounced changes during the annealing of the strong $\langle r\rangle$=2.4 liquid is compatible with its weak calorimetric anomaly at T_g.[4] In the fragile $\langle r\rangle$=2.1 sample large changes in $\langle\tau_n\rangle$ were observed. However in contrast to the $\langle r\rangle$=2.0 case the structural equilibration, surprisingly, now proceeds faster than the relaxation following a bending strain. Therefore the first few $\langle r\rangle$=2.1 points in figure 3 are based on stress relaxation curves which have only been recorded down to 30-50% of the initial stress. We observed that the spectral width of the autocorrelation functions broaden on annealing (as seen earlier

[17]). However no quantitative analysis of this effect was attempted because it is very likely that the effective spectral width was not even constant during each single run.

4. SUMMARY

We have shown that supercooled Ge-As-Se alloys with low connectivity, typical of fragile liquids, show very non-exponential and state-dependent mechanical stress relaxations. Conversely at the percolation threshold <r>=2.4 the non-exponentiality is small and a state dependence cannot be detected.

5. ACKNOWLEDGEMENT

We thank B. L. Halfpap for providing the glass ingots and Q. Zheng for helping with sample preparation. Stimulating discussions with R. V. Chamberlin, C. R. Kurkjian, and S. M. Lindsay are also acknowledged. This work has been supported in part by the Office of Naval Research under Agreement No. N00014-84-K-0289 and the Department of Energy under DE-FG02-89ER45398.

REFERENCES

1. K. S. Gilroy and W. A. Phillips, Phil. Mag. B 47, 655 (1983); J. Y. Duquesne and G. Bellessa, J. Physique. 46, C10-445 (1985); K. Tanaka, Solid State Commun. 60, 295 (1986); B. L. Halfpap and S. M. Lindsay, Phys. Rev. Lett. 57, 847 (1986); Y. Ito, S. Kashida, and K. Murase, Solid State Commun. 65, 449 (1988); J. Y. Duquesne and G. Bellessa, Europhys. Lett. 9, 453 (1989); S. S. Yun, H. Li, R. L. Cappelletti, R. N. Enzweiler, and P. Boolchand, Phys. Rev. B 39, 8702 (1989); S. Etienne, J. Perez, S. Peytavin, and M. Ribes (unpublished).
2. J. C. Phillips, J. Non-Cryst. Solids 34, 153 (1979); M. F. Thorpe, J. Non-Cryst. Solids 57, 355 (1983).
3. J. Y. Duquesne and G. Bellessa, J. Physique. 46, C10-449 (1985). S. P. Love, A. J. Sievers, B. L. Halfpap, and S. M. Lindsay, Phys. Rev. Lett. 65, 1792 (1990). O. Brand, H. v. Löhneysen, and R. Blachnik, Physica B 169, 567 (1991).
4. M. Tatsumisago, B. L. Halfpap, J. L. Green, S. M. Lindsay, and C. A. Angell, Phys. Rev. Lett. 64, 1549 (1990).
5. C. A. Angell, J. Phys. Chem. Sol. 49, 863 (1988).
6. C. A. Angell, in *Relaxations in Complex Systems* edited by K. L. Ngai and G. B. Wright (Naval Research Laboratory, Washington, DC, 1984) p. 3-11.
7. K. L. Ngai, J. Non-Cryst. Solids 95&96, 969 (1987).
8. R. Böhmer, H. Senapati, and C. A. Angell, J. Non-Cryst. Solids (in press).
9. C. T. Moynihan *et al.*, Ann. N. Y. Acad. Sci. 276, 15 (1976).
10. Excellent fits were also obtained with the model described in R. V. Chamberlin and D. N. Haines, Phys. Rev. Lett. 65, 2197 (1990).
11. F. Kohlrausch, Pogg. Ann. Phys. 119, 337 (1863).
12. R. Böhmer and C. A. Angell, Phys. Rev. B (submitted).
13. D. J. Plazek and K. L. Ngai, Macromolecules 24, 1222 (1991).
14. P. J. Webber and J. A. Savage, J. Non-Cryst. Solids 20, 271 (1976); U. Tille, G. H. Frischat, and K. J. Leers, in *Non-Crystalline Solids* edited by G. H. Frischat (Trans Tech Publications, Aedermannsdorf/Switzerland, 1977), pp. 631-638; Z. U. Borisova, *Glassy Semiconductors* (Plenum, New York, 1981) pp. 261-274. L. Ferrari, W. A. Phillips, and G. Russo, Europhys. Lett 3, 611 (1987). S. Asokan, M. V. N. Prasad, G. Parthasarathy, and E. S. R. Gopal, Phys. Rev. Lett. 62, 808 (1989).
15. A. Feltz, H. Aust, and A. Blayer, J. Non-Cryst. Solids 55, 179 (1983); J. C. Phillips, Phys. Rev. B 31, 8157 (1985).
16. L. M. Torrell, L. Börjesson, and M. Elmroth, J. Phys. 2, SA207 (1990).
17. C. A. Angell, J. Non-Cryst. Solids 102, 205 (1988).
18. e. g. R. W. Rendell, K. L. Ngai, G. R. Fong, and J. J. Aklonis, Macromolecules 20, 1070 (1987).